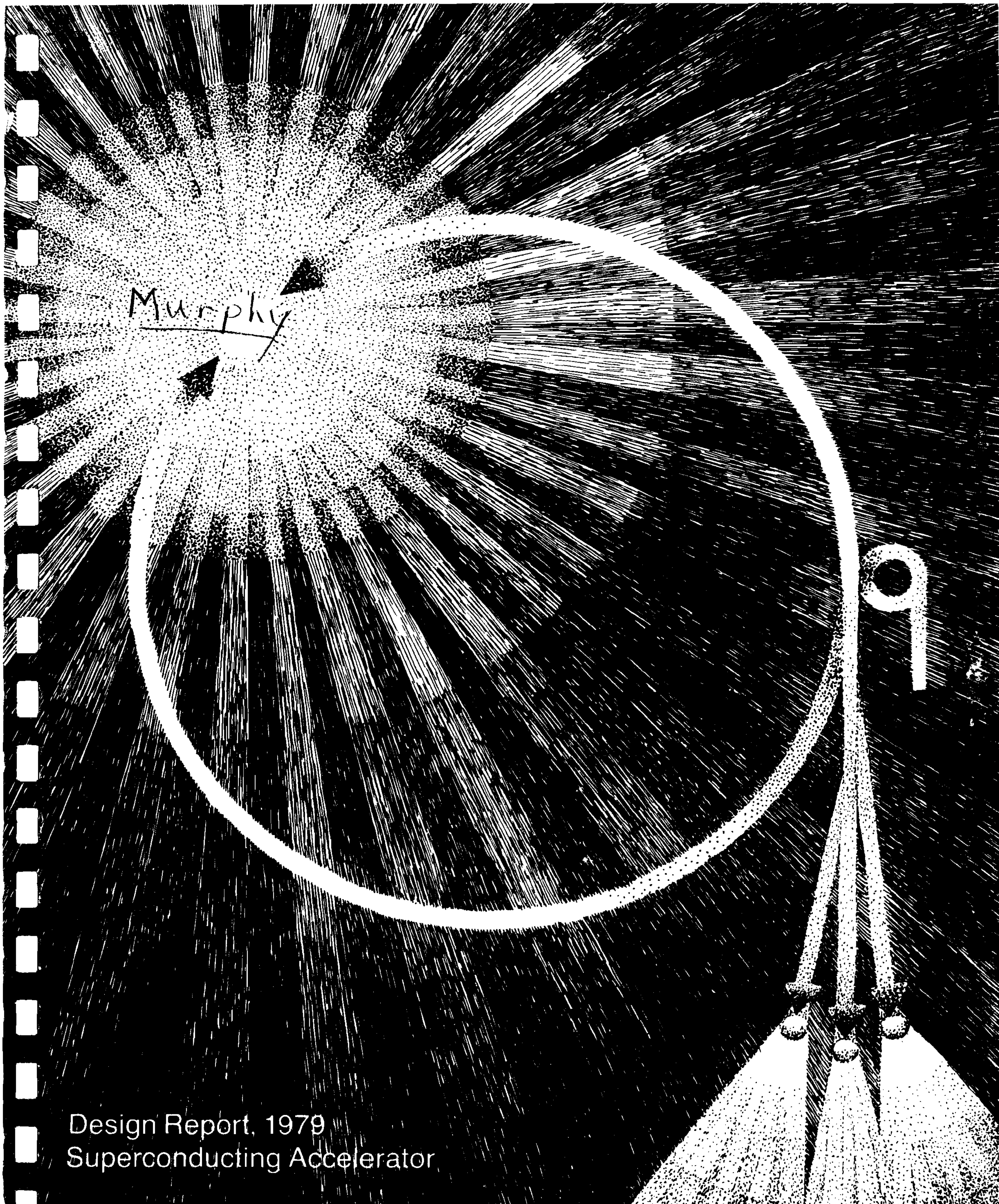
Murphy
Design Report, 1979
Superconducting Accelerator

A REPORT ON THE DESIGN

OF THE

FERMI NATIONAL ACCELERATOR LABORATORY

SUPERCONDUCTING ACCELERATOR

MAY, 1979

Fermi National Accelerator Laboratory
Batavia, Illinois

Operated by Universities Research Association
for the United States Department of Energy

FOREWORD

This report represents the cumulative work of many Fermilab people, both present and past. In past years, emphasis was primarily on magnet and refrigerator development. In this work members of the Magnet Section have shown great ingenuity, perseverance, and patience. During the past year, design emphasis has also been directed toward a consistent accelerator - collider design and has been diligently pursued by many members of the staff, in the Accelerator Division and throughout other sections of the Laboratory. The report covers this work, describing what we believe to be a clean, consistent, and economical design. Continuing effort in design will of course be necessary, with emphasis directed toward more detailed technical points.

Leon M. Lederman

The report was assembled and edited by F. T. Cole, M. R. Donaldson, D. A. Edwards, H. T. Edwards, and P. F. M. Koehler.

TABLE OF CONTENTS

LIST OF FIGURES

LIST OF TABLES

1. GENERAL DESIGN AND LAYOUT

1.1 Scope of This Report

The aim of this Design Report is to present as complete a design as possible of the superconducting accelerator to be built at the Fermi National Accelerator Laboratory. There have been many significant advances in design of the accelerator in the last year and it is useful to record these advances in order to put these problems behind us and continue the work. It is also useful to make a coherent presentation of the plans in order to integrate the design.

In addition, in the last few years, the possible long-range scope of the accelerator has enlarged greatly with its suggested applications for colliding beams, either proton-antiproton or proton-proton. These new applications have prompted considerable new design effort, the details of which will be documented here. Finally, it is our hope that this report will have some value for reference by the Fermilab people working on the project.

All these aims can best be met by a report in considerably greater technical depth than has been exhibited in most previous design reports on the Fermilab superconducting-accelerator work. Our objective in this report is to lay out the design in as much detail as possible. The history of the Fermilab effort in this field and the use of this accelerator for high-energy physics research have been discussed in adequate detail in the previous reports and are not included in this report.

1.2 Design Goals

The ultimate goal of the superconducting ring is to extend research at Fermilab to higher energy. The field strength that has been achieved in superconducting-magnet development implies a fixed-target physics program at twice the energy now available. The potential exists for colliding-beam experiments at very high energy, either with the new ring itself for antiprotons on protons or with the new accelerator and the Main Ring for protons on protons. A significant interim goal is to reduce the power demands and costs of present operation in the 400-GeV range by sharing the acceleration cycle between the two rings.

This will be the first large superconducting-magnet synchrotron-storage ring to be completed. The development work has broken new technical ground in a number of ways. Real gains have been made in the areas of superconductive stability, quality control of superconducting materials, the engineering of large cryogenic systems, and production of extremely precise magnetic fields in the face of large Lorentz forces on conductors and of large temperature variations.

At this time, there are still questions outstanding concerning production of high-quality superconducting magnets in large quantity, concerning operation of very large cryogenic systems, and concerning quenching of magnets by particle beams. There have been successes in the Fermilab work on these problems, but continued effort is required.

Specifications of the superconducting accelerator as a fixed-target accelerator, as a $\bar{p}p$ collider, and as a pp collider are given in Tables 1-I, 1-II, and 1-III respectively.

Table 1-I. Fixed-Target Accelerator Specifications.

Peak energy	800-1000 GeV
Intensity	$> 2 \times 10^{13}$ ppp
Injection energy	150 GeV, single turn
Repetition rate	1-2 cycles/min
Acceleration rate	50-75 GeV/s
Flattop time	Variable to dc
Extraction	Slow: 1 to 10 s Fast: 1 ms
Beam abort system	Single - turn extraction

Table 1-II. $\bar{p}p$ Collider Specifications.

Peak energy	(800-1000 GeV) × (800-1000 GeV)
No. of bunches in each beam	1-12
Luminosity/bunch	$1-8 \times 10^{28} cm^{-2} sec^{-1}$
No. of interaction region	1-2
Longitudinal space for detector	> 10 m
Vacuum in warm regions	$< 10^{-8}$ Torr
Storage time	> 3 h
Injection	Forward and backward, single bunch
RF	Independent phase adjustments on $\bar{p}$ and p bunches
Abort	Forward and backward

Table 1-III. pp Collider Specifications.

Peak energy	Main Ring: 150-200 GeV Superconducting Ring: 800-1000 GeV
Intensity of each beam	$> 2 \times 10^{13}$
Luminosity	$> 2 \times 10^{30} cm^{-2} sec^{-1}$
No. of interaction region	1
Longitudinal space for detector	> 10 m
Storage time	$> \frac{1}{2}$ h
Injection and acceleration in Main Ring	Forward and backward

1.3. Layout

The layout is constrained by the requirement that it should be installed in the Main-Ring tunnel. The ring will be located directly underneath the Main Ring and will have six long straight sections coinciding with those of the Main Ring. Figure 1-1 is a Main-Ring tunnel cross section showing the locations of the superconducting magnets and their utilities.

All beam-manipulation functions must be laid out in the six long straight sections, which will have warm beam pipes. These functions are:

1. Injection; p forward and $\bar{p}$ backward at an energy greater than 100 GeV.
2. Acceleration; in addition to accelerating a forward p beam at more than 50 GeV/s, the rf system is to be capable of accelerating simultaneously a forward p beam and a backward $\bar{p}$ beam with independently adjustable phases for the two beams.
3. Extraction of the forward p beam; a resonant-extraction system that can provide both slow (1 to 10 s) and fast (1-ms) beam spills into the present switchyard.
4. Abort; must be able to abort both the forward p beam and the backward $\bar{p}$ beam with near 100% efficiency.
5. Colliding-beam region; at least one long straight section will be dedicated to colliding beams (both $\bar{p}$p and pp). This will be the location of the principal detector for colliding-beams experiments.
6. Scraper-shield; to obtain the required high efficiency of aborting and extraction, it is necessary that a scraper-shield be interlaced into a local orbit bump generated by conventional magnets that can withstand high radiation levels. Lower-energy charged

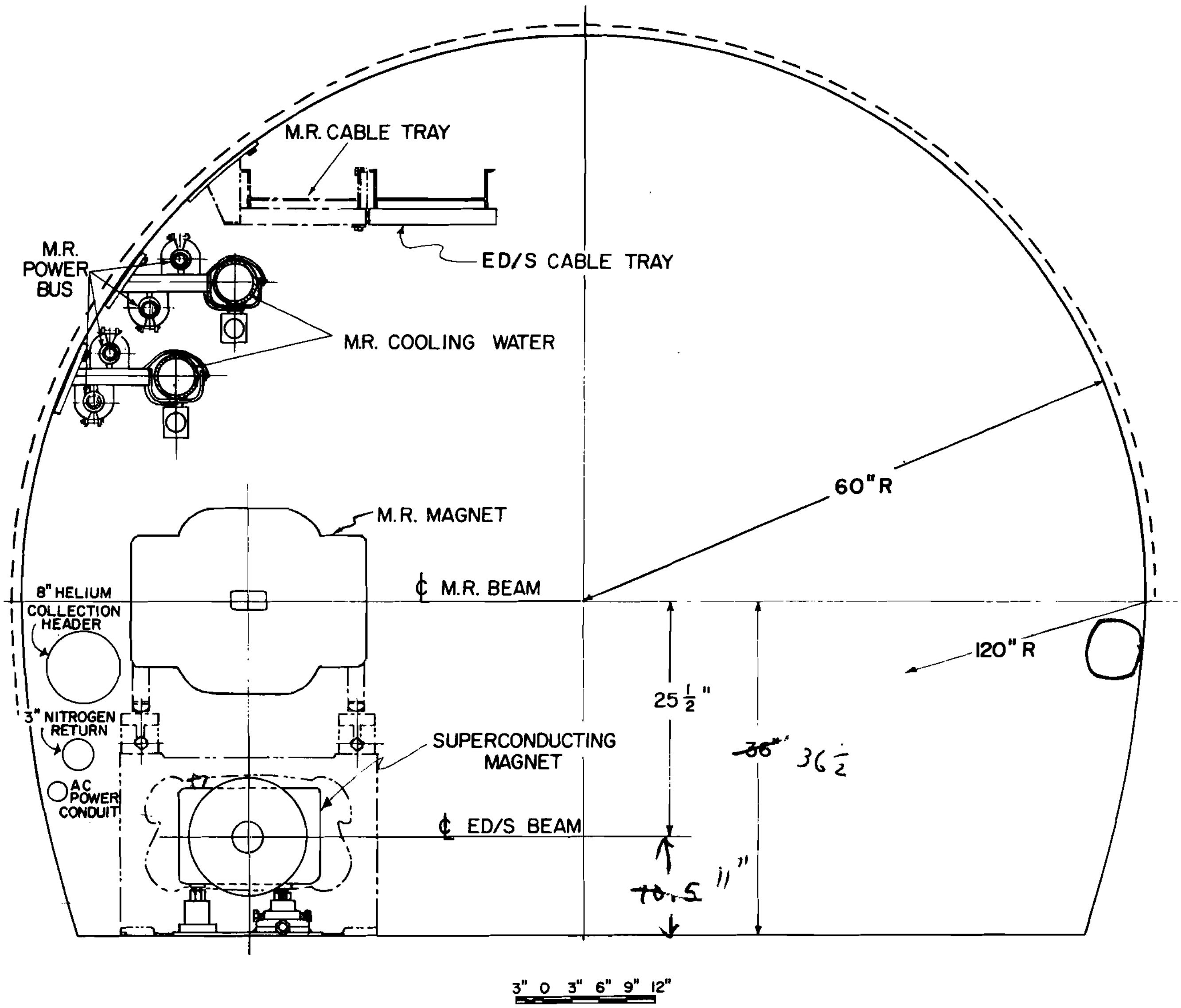

Fig. 1-1. Cross section of the accelerator tunnel.

particles in the nuclear cascade will be swept away by the magnetic field. The two high-radiation regions are the extraction-septum region and the beam-abort region. An elaborate scraper-shield will be installed in each of these two regions. In addition, there will be a simpler scraper-shield installed in mini and median-straight sections at the quadrupole to shield the superconducting coils of the magnets from stray beam.

These functions are arranged in the six long straight sections as shown in the layout drawings of Figs. 1-2 and 1-3.

Long straight-section A - p extraction channel (also injection and extraction for the Main Ring).

Long straight-section B - Colliding-beams region.

Long straight-section C - Abort systems, both p and $\bar{p}$; and a scraper-shield system (also p and $\bar{p}$ abort for the Main Ring).

Long straight-section E - Injection systems, both p and $\bar{p}$, for transfer of beams from the Main Ring.

Long straight-section F - RF accelerating system.

The boundary conditions and reasoning leading to the choice of this arrangement are:

(i) Because of the location of the existing RF Building, F is the natural choice for the r f system. Furthermore, the coupling between the Main-Ring and superconducting-ring rf systems is such that as the demand

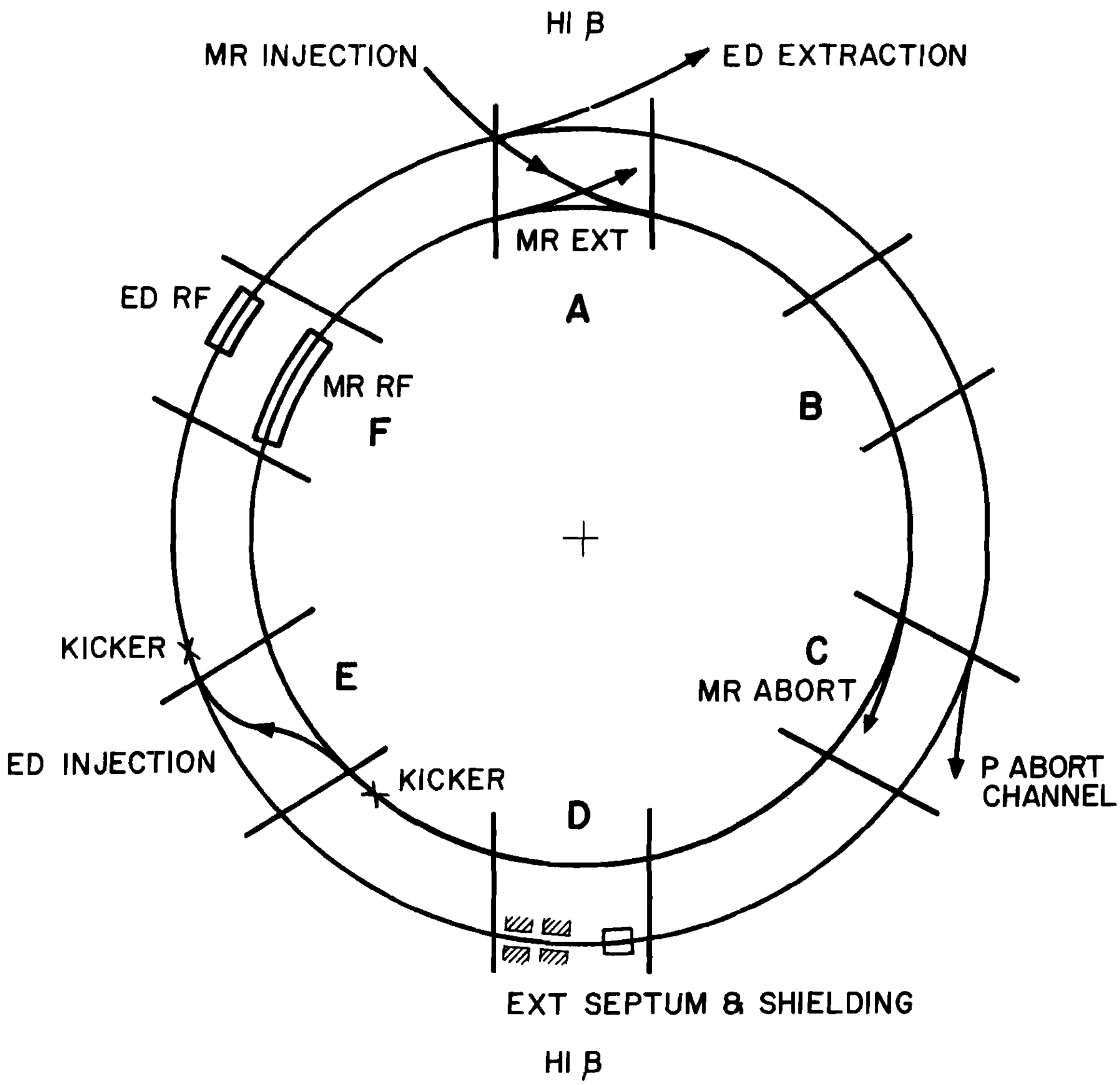

Fig. 1-2. Use of the six long straight sections in the fixed target mode.

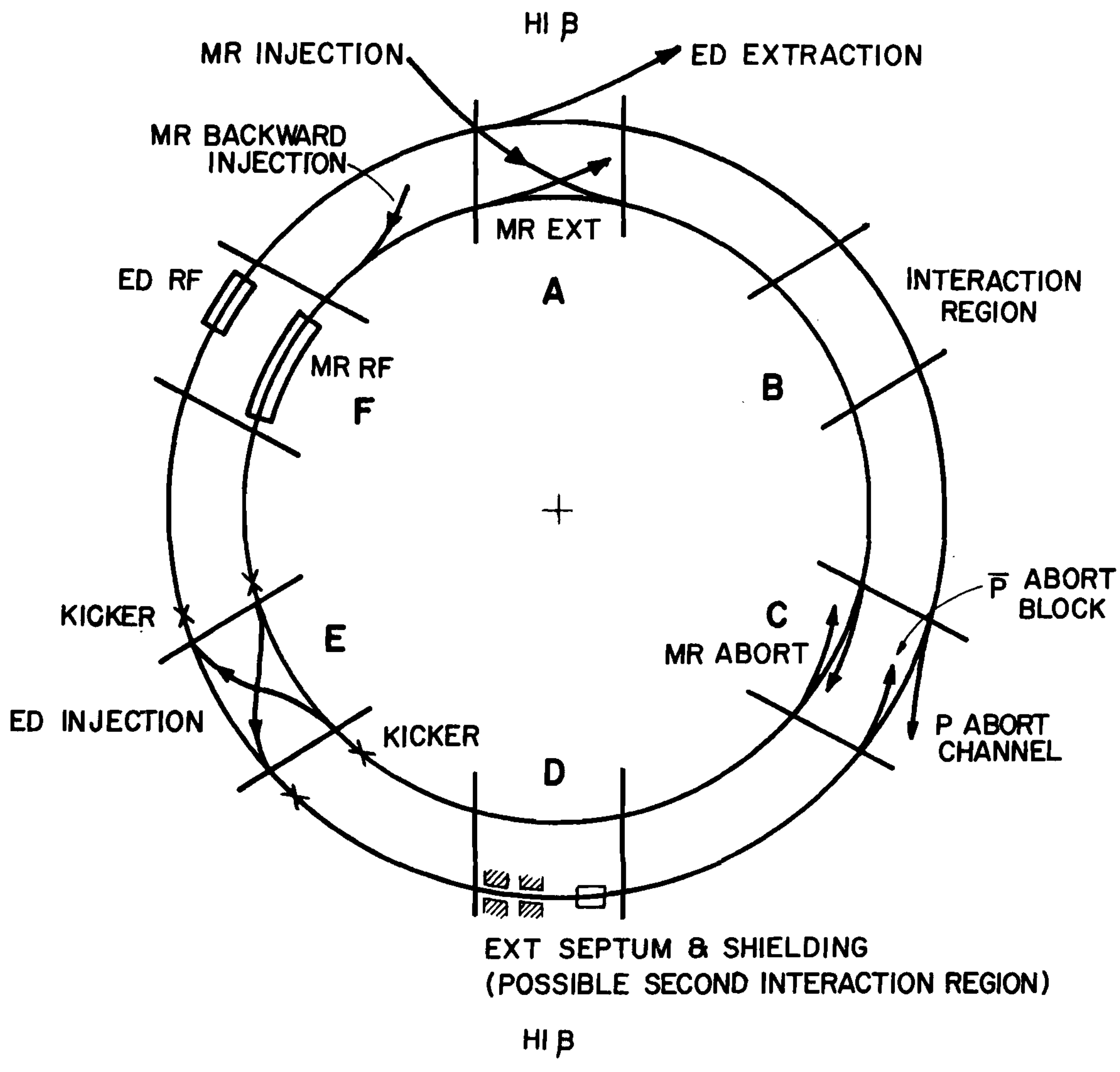

Fig. 1-3. Use of the six long straight sections in the colliding-beams mode.

increases on the superconducting-accelerator rf system, the demand on the Main-Ring rf system will probably reduce, so that putting the two rf systems in the same long straight section will provide optimum use of space for all times.

(ii) Since the extracted p beam has to go to the present switchyard, the extraction channel must be in A.

(iii) The electrostatic extraction septum should be at an odd number of quarter wavelengths of betatron oscillation upstream from the channel entrance in A. This proper phase occurs at F, D, and B. F is already occupied by the rf system; D is the next upstream and we therefore assign the extraction septum, and hence also the associated scraper-shield, to it. Detailed studies indicate that the beam loss on the septum will be about 30% more with the septum in D instead of in F. Nevertheless, the loss can be adequately shielded by the scraper-shield and the placement of the rf system in F is considered to have overriding merits.

(iv) It may happen that the p beam must be aborted during extraction. In this event, it is preferable to have the abort system located an odd number of quarter betatron-oscillation wavelengths upstream of the extraction septum, where the beam is narrower. Thus we place the abort systems in C. In so doing, we have reserved B, which is more easily accessible from the control room, for other functions needing more immediate and frequent access. The abort systems should not require as much access, at least during normal operation.

(v) Whether the easily accessible long straight-section B should be assigned to injection or colliding beams is largely a matter of choice.

We have chosen to locate the injection systems in E, leaving B for colliding-beams experiments. It would not cause any serious problem if the two functions were interchanged.

For a long period of colliding-beams operation with no fixed-target physics, it is conceivable that the extraction septum and scraper-shield at D could be removed and the straight section used as a second colliding-beams region. As will be evident later from the detailed discussions of the designs of beam-manipulating systems, there is no obvious way of shoehorning two of these functions into one long straight section to leave two straight sections permanently available for colliding-beams experiments.

In addition to these "lumped" systems in the long straight sections, there are "distributed" systems, each consisting of a large number of identical elements distributed around the ring, roughly one element to each mini-straight section. These are (1) the correction-magnet system, (2) the beam-detector system, and (3) the general scraper-shield system. These systems will also be described in detail in the following sections, as well as the major systems of the accelerator.

Parameters of the accelerator are collected in Appendix I for reference.

2. LATTICE

2.1 Ring Location and Normal Lattice

The design of the lattice of the superconducting ring is constrained by the requirement that it fit in the existing Main-Ring tunnel beneath the Main Ring. It is not realistic to consider any lattice that is not very similar to the Main Ring. The lattice designed therefore has 6 superperiods with 6 long straight sections and normal cells with 8 dipoles and 2 quadrupoles. There have been difficulties with magnet installation in the sector test because the superconducting dipole ends were directly under the Main-Ring ends and work space was extremely cramped. The bend magnets in this new lattice have therefore been moved 15.5 in. upstream. Figures 2-1a and 2-1b sketch the position of the quadrupole in the lattice and the position of a normal cell relative to the Main-Ring lattice. The beam center line will be 25.5 inches below Main-Ring center line.

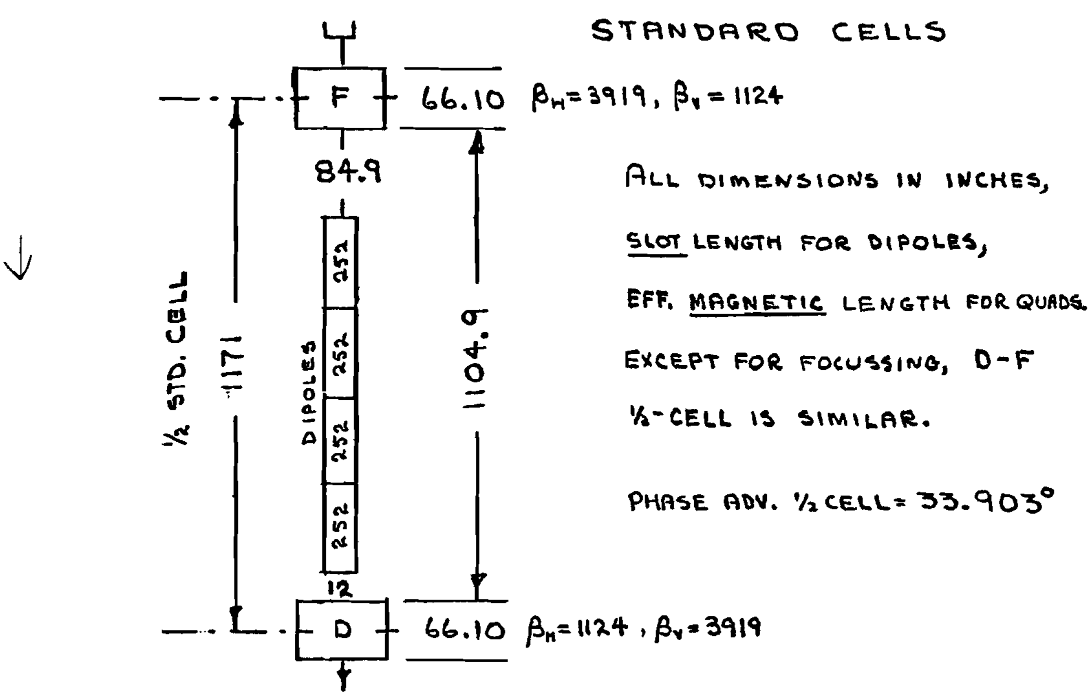

Fig. 2-1(a). Locations of elements in standard cell.

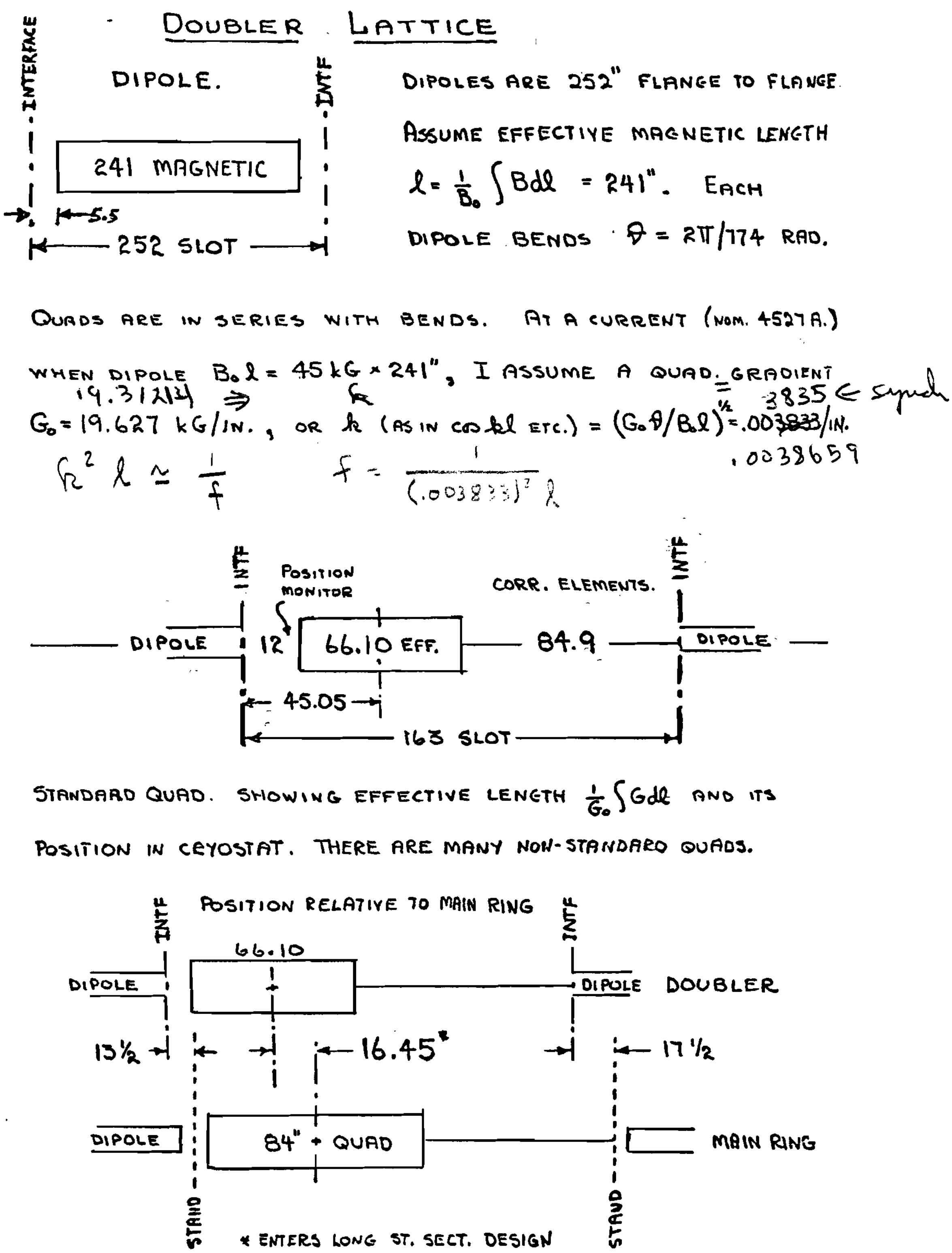

Fig. 2-1(b). Locations of superconducting magnets relative to main ring.

Like the Main Ring, the present lattice has a medium straight section at location 17 formed by omitting two dipoles. Its layout is shown in Fig. 2-1(c) below.

Fig. 2-1(c). Medium straight section. A std. $\frac{1}{2}$-cell with two dipoles omitted. A space of $16\frac{1}{2}$ inches must be inserted at downstream end to close the geometric orbit in the shifted Doubler.

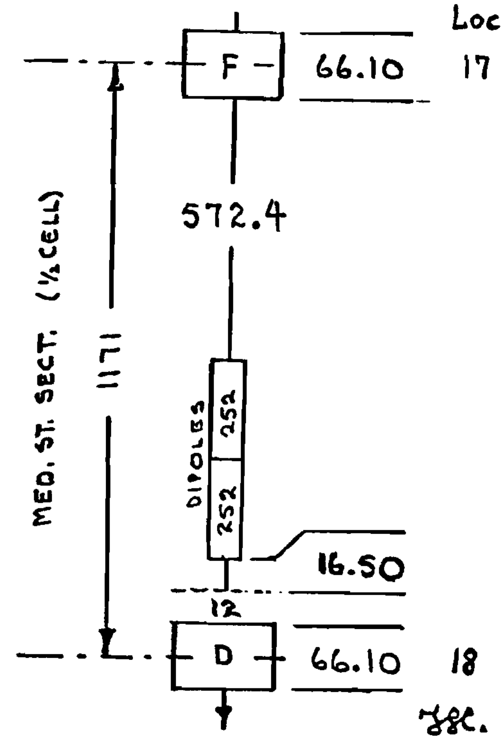

There are also long straight sections of "normal" configuration, ones with high beta function for extraction, and ones with low beta for colliding-beam interactions. These will be discussed separately. Table 2-I summarizes the warm straight-section lengths available in the lattice. This table gives the drift lengths between "effective" magnetic ends of the elements, the available warm length and the space allotted for the cryogenic bypasses of cold-to-warm transitions and vacuum isolation. These bypasses will be discussed in Sections 4 and 5. All medium straight sections at 17 and 48 locations, as well as all long straight sections, will be warm. The space between the long straight-section doublets will be warm only where necessary.

2.2 Normal and High-Beta Long Straight Sections

Figure 2-2 is a sketch of the normal long straight section, giving lengths and amplitude functions. This design is very similar to that of the Main Ring, with the exception that two, rather than four, quadrupoles are

Table 2-I. Warm Straight-Section Lengths.

Location of Warm Region	Drift Length[a] (In.)	Available Warm Length (In.)	Hot-Cold Transition (In.) Upstream	Downstream
Median location 17 (standard quadrupole with corrections)	577.9	414.5	39	34
Normal-β median location 48	322.5	250.5	36	36
High-β median location 48	320.3	248.3	36	36
Normal-β doublet space 49, 11	150.36	78.36	36	36
High-β doublet space 49, 11	151.65	79.65	36	36
Long straight section	2094.25	2022.25	36	36
Low-β long straight section Type I	2046.25	1974.25	36	36
Low-β long straight section Type II	629.59	557.59	36	36

[a]Magnetic lengths used throughout to define drift lengths.

used at either end of the straight section. Normal geometry will be used at C0, E0, and F0. It will also be used initially at B0 before the low-beta quadrupoles are installed. Matching for injection between the Main Ring and the new ring can be easily accomplished with this geometry.

The high-beta long straight section is illustrated in Fig. 2-3. Here the order of focusing in the doublets has been reversed and lengths of all six quadrupoles changed slightly. A large horizontal beta is produced at the upstream end of the straight section. High-beta regions will be used at A0 and D0 to facilitate resonant extraction. The good-field aperture of the superconducting magnets is not large and the use of a high beta at the location of the extraction electrostatic and magnetic septa reduces the aperture required for extraction in the rest of the magnet ring.

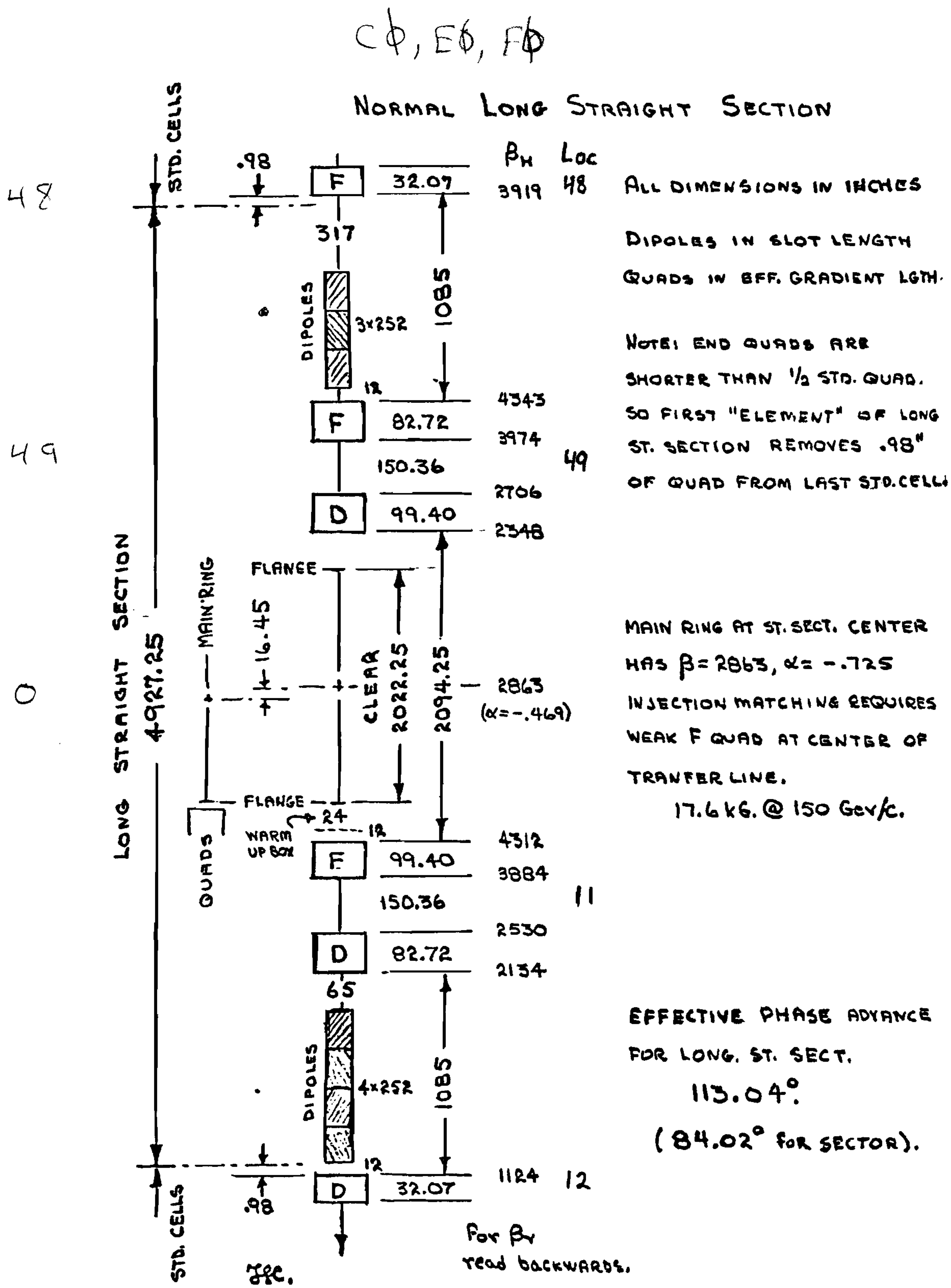

Fig. 2-2. Normal long straight section.

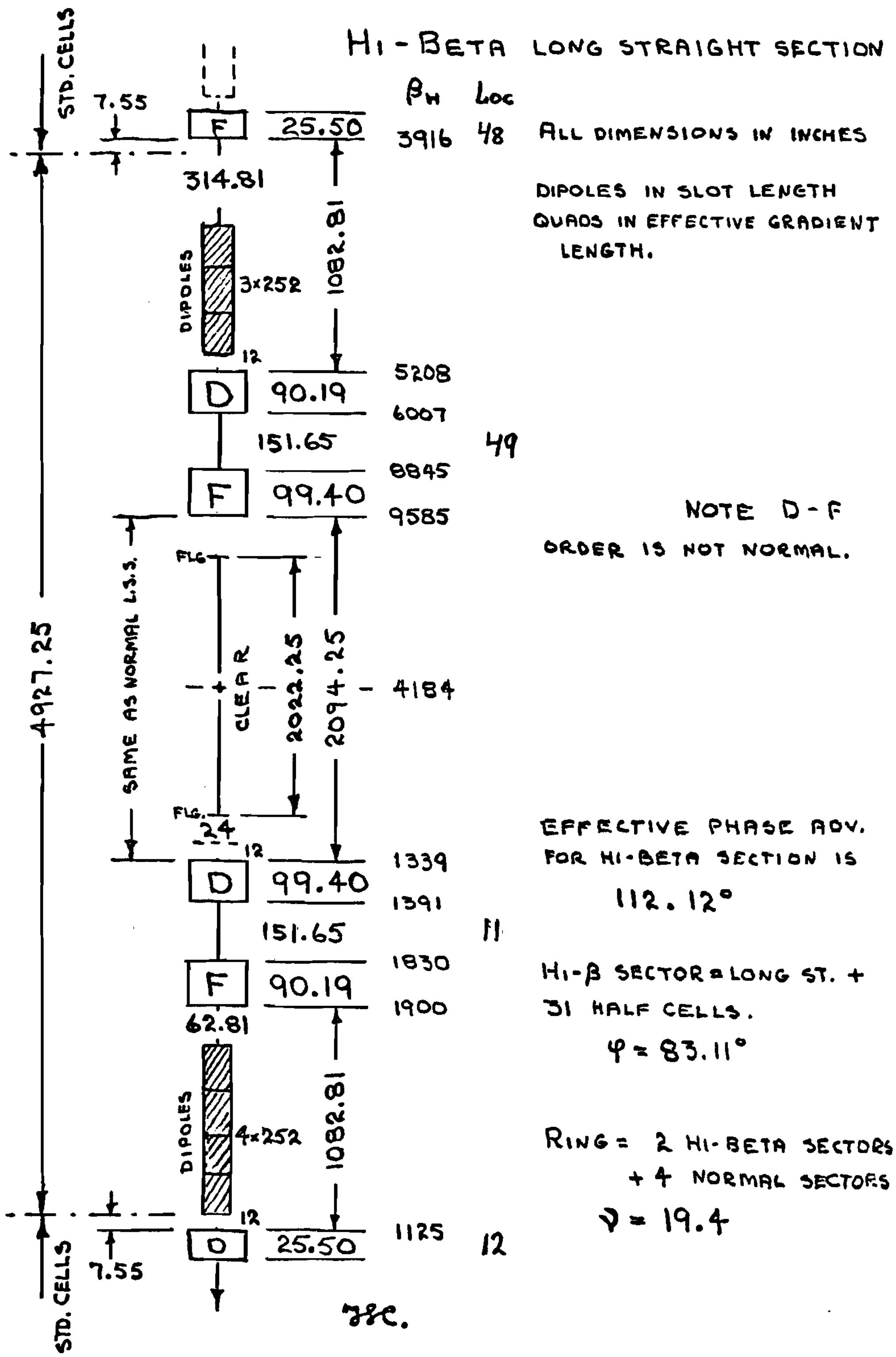

Fig. 2-3. High-beta long straight section.

We include in Appendix II a SYNCH output and geometrical drawings describing the lattice in detail without the low-beta section, which is treated separately in Section 2.5 below.

2.3 Circumference

In order to equalize the revolution times of unequal energy protons in the Main Ring, and the new ring for 150×1000 GeV pp colliding-beam physics, a slight increase in the path length of the higher energy beam is necessary. An effective change in path length could be made only using off-momentum orbits, but in view of the somewhat limited aperture in both rings, we have chosen to minimize the momentum offset necessary either at injection or during storage by making an increase in the circumference of the new ring of 4.4 cm. This value corresponds to an average $\Delta r/r$ increase of 7×10^{-6} relative to the Main Ring's 1 km radius.

This difference in radii will require the following operating conditions:

	Main Ring ($\Delta p/p$)	New Ring ($\Delta p/p$)
Injection	+0.25%	0.0%
150×1000 GeV pp	-0.32%	+0.10%

2.4 Lattice Elements

Table 2-II lists the various lattice elements required for a ring incorporating two high-beta long straight sections and four normal long straight sections. The lengths shown are magnetic lengths in inches.

2.5 Low-Beta Long Straight Section[1]

By replacing the two inner pairs of quadrupoles in the normal long straight section with considerably longer, independently powered, three-

Table 2-II. Lattice Elements.

Element	Magnetic Length (In.)	Number	f (inches) (m)
Dipole	241.0	774	
Standard quadrupole	66.1	180	1029.7 / 26.15
Long straight inner quadrupole	99.4	12	
Normal long straight short quadrupole (48, 12 location)	32.07	8	
Outer quadrupole	82.72	8	
High beta long straight short quadrupole (48, 12 location)	25.5	4	
Outer quadrupole	90.19	4	

shell quadrupoles, as shown in sketch (b) in Fig. 2-4, a pp colliding insertion can be produced. With the four outer quadrupoles running normally and the inner ones set at rather weak values, the lattice functions across this insertion can essentially duplicate those of the normal straight sections. By leaving quads #1 and #12 connected in series with the regular magnets, turning off quads #2 and #11, and repowering the inner quads, a β^* of approximately 10 m can be obtained. Quadrupole settings for these cases are listed in Table 2-III and some dynamic parameters are listed in Table 2-IV. Figure 2-5 illustrates the Type I interaction region. By adding additional power supplies to the other two pairs of quadrupoles, one can obtain lower values of β^*, although β_{max} starts to increase rapidly.

With the insertion of four more long, strong, and independently powered quadrupoles, one can produce a β^* of the order of 1 m. This is the Type II low-β shown in Fig. 2-4 and Fig. 2-6. Table 2-III lists quadrupole settings for minimum beta values of 1 and 2 m. Parameters for these cases are again listed in Table 2-IV. A few arbitrary decisions have been made at this point and should be mentioned.

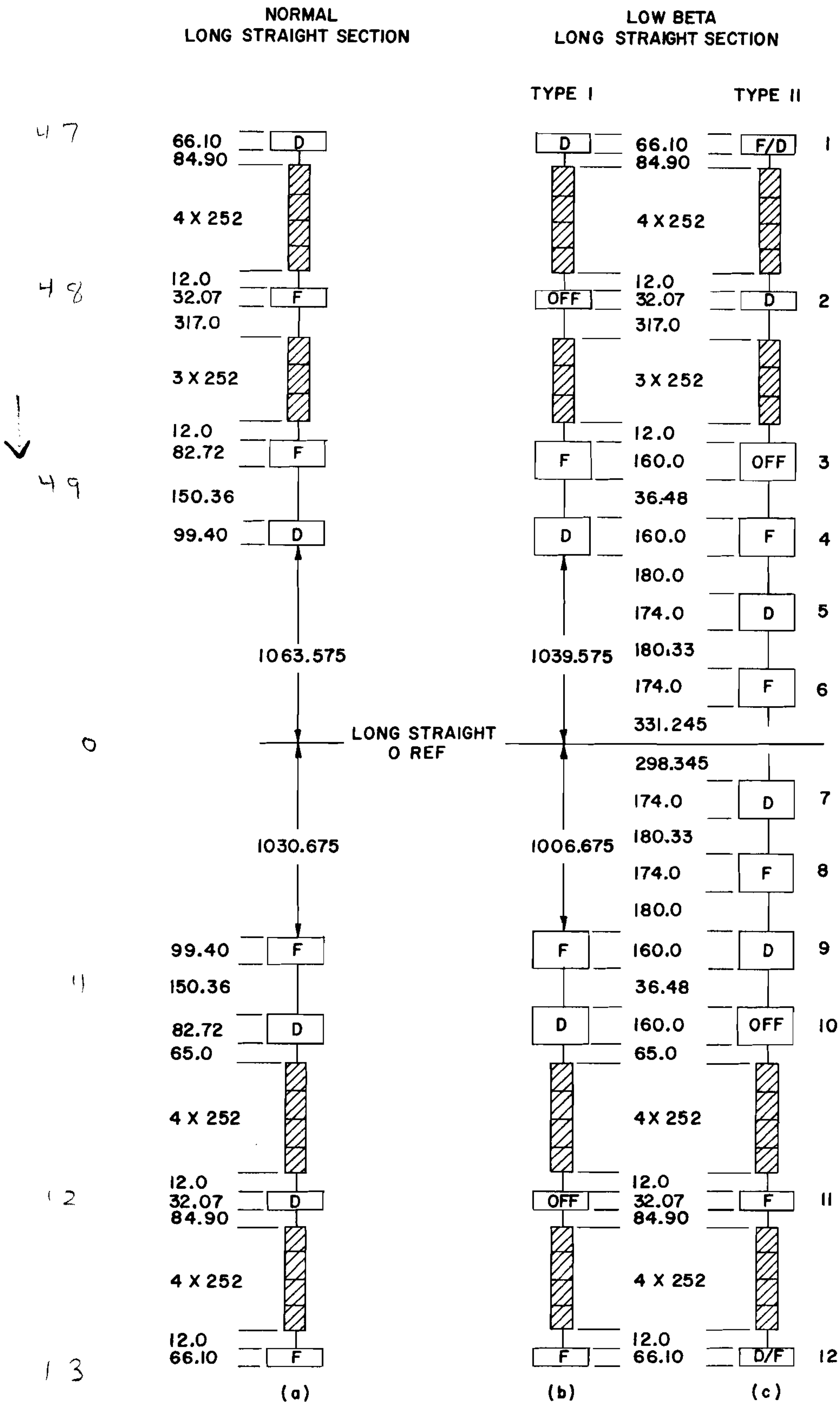

Fig. 2-4. Layout of normal and two types of low-beta long straight section.

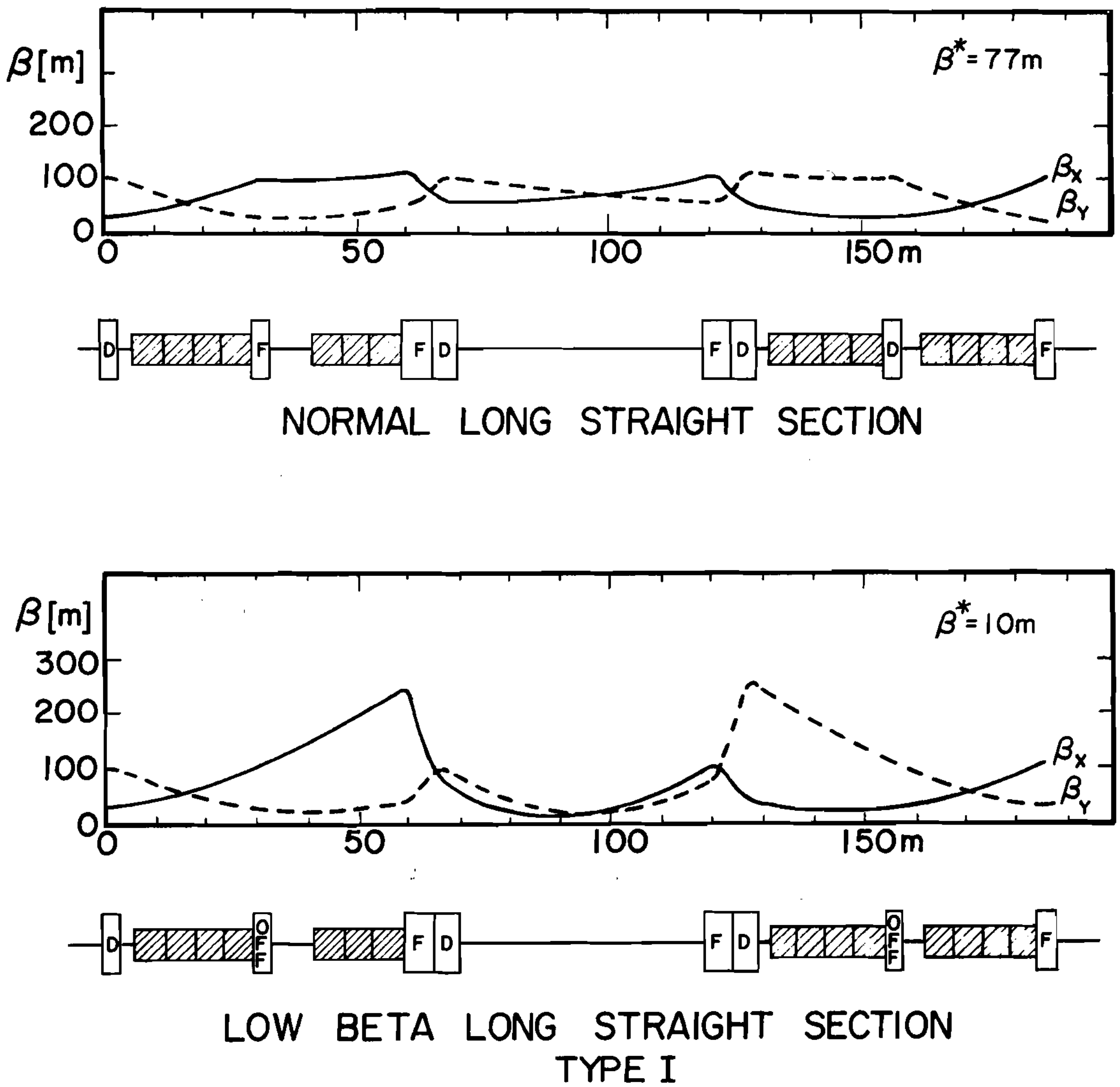

Fig. 2-5. Lattice functions for normal and for type I low-beta long straight sections.

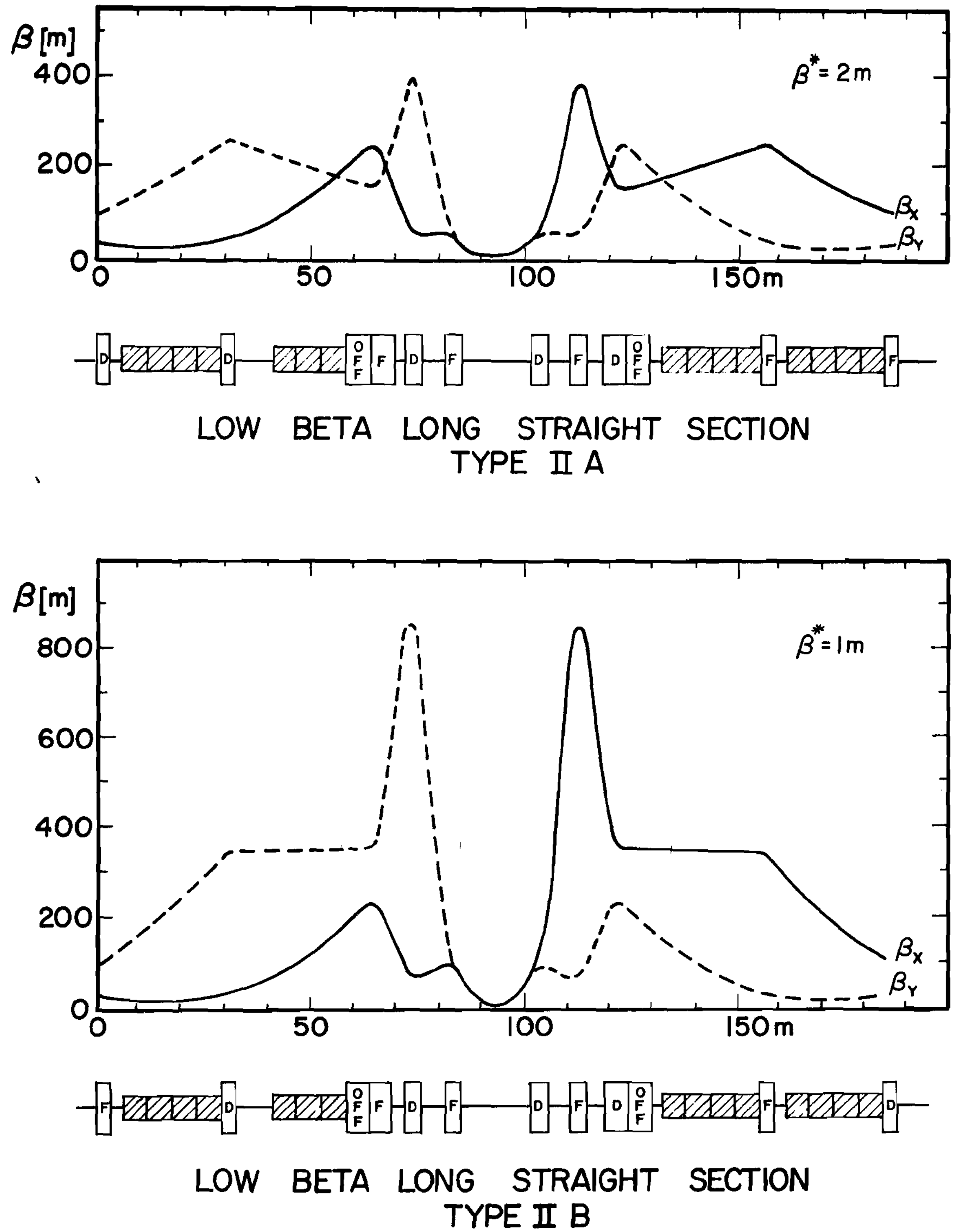

Fig. 2-6. Lattice functions for type II low-beta long straight sections.

Table 2-III. Quadrupole Settings (Values in kG/m for 1 TeV).

	Type I		Type II		
	Case A	Case B	Case C	Case D	Case E
Quad #	"normal"	β* = 10 m	β* = 2 m	β* = 1 m	β* = 2 m, η* = 0
1	-760.3206	-760.3206	-159.4277	195.9240	-326.7387
2	760.3206	0	-530.2842	-690.3435	181.1120
3	481.9685	931.4100	0	0	-302.2334
4	-561.0630	-1023.1598	696.6825	677.6592	908.8754
5	-	-	-1032.4382	-1056.4156	-1039.4206
6	-	-	885.3317	1040.3000	932.9205
7	-	-	-885.3317	-1040.3000	-466.9477
8	-	-	1032.4382	1056.4156	1038.6460
9	561.0630	1023.1598	-696.6825	-677.6592	-654.7409
10	-481.9685	-931.4100	0	0	-75.5129
11	-760.3206	0	530.2842	690.3435	346.6425
12	760.3206	760.3206	159.4277	-195.9240	812.9308
13	normal	normal	normal	normal	-634.0335
14					702.6145
Correct. Quads	0	±28.3963	±25.3289	±29.9300	±29.9300

1. Quadrupoles #3 and #10 are turned off. These could be missing, but it seemed easier to leave them and add new ones. They are useful to return to normal, fixed-target operation, and, at least in the 1-m case, are not long enough to serve as one of the inner quads.

2. The lengths of the strong quadrupoles may have to increase slightly depending on the maximum gradient obtainable. A maximum value of approximately 26.8 kG/in. at 1 TeV has been used. Slight differences could be accommodated, perhaps down to around 25 kG/m, but certainly not as much as if one went to two-shell quadrupoles.

Table 2-IV. Lattice Functions.

	Normal lattice	Case A	Case B	Case C	Case D	Case E
Free Space (m)	53.194	51.974	51.974	15.992	15.992	15.992
β_x^* (m)	72.7	73.9	10.3	2.0	1.0	2.0
η^* (m)	2.24	2.26	0.21	0.40	0.48	-0.08
$\eta^{*'}$ (mrad)	18.1	18.2	-6.4	144	298	4.7
β_x max (m)	243	243	247	378	851	240
β_y max (m)	243	243	252	380	868	618
η_{max} (m)	6.0	6.0	8.6	9.5	10.5	7.5
η_{min} (m)	1.1	1.1	-0.5	-3.3	-5.2	-0.1
Q_x	19.395	19.393	19.394	19.393	19.400	19.632
Q_y	19.434	19.432	19.434	19.432	19.441	19.205
ξ_x	-22.5	-22.5	-23.2	-25.2	-29.1	-24.6
Δ Q of correction used	-	-	-0.317	-0.283	-0.334	-

Most of the objections raised with the previous low-β designs have been overcome in these designs. The maximum values of beta and dispersion have been brought down to believable sizes, and the dispersion mismatch throughout the ring is also relatively small. Further investigations of these designs show them to be quite reasonable. The tune corrections needed, from 30 correcting quads per sector, are easily handled, and the chromaticity corrections are also rather simple. Table 2-V lists the effect of momentum on various machine parameters for the low-β cases. The one parameter that could present a problem is the change in β_{max}. The percentage change of β_{max} as a function of $\Delta p/p$ is plotted in Fig. 2-7. Although this change in β_{max} is rather large, the correction system is the simplest possible, two independent sextupole families. By going to a larger

Table 2-V. Accelerator Parameters vs $\Delta p/p$.

$\beta^* = 2$ m,		$(B''\ell)_F = 429$ kG/m,		$(B''\ell)_D = -733$ kG/m	
$\Delta p/p$ (%)	β^* (m)	η^* (m)	η_{max} (m)	Q_x	Q_y
-0.375	1.76	0.36	9.3	19.394	19.434
-0.250	1.84	0.37	9.4	19.393	19.433
-0.125	1.92	0.39	9.5	19.393	19.433
0	2.01	0.40	9.5	19.393	19.432
0.125	2.10	0.42	9.6	19.393	19.433
0.250	2.20	0.43	9.7	19.393	19.433
0.375	2.30	0.44	9.7	19.394	19.434
$\beta^* = 1$ m,		$(B''\ell)_F = 492$ kG/m,		$(B''\ell)_D = -842$ kG/m	
-0.375	0.77	0.40	10.5	19.405	19.449
-0.250	0.84	0.43	10.4	19.402	19.444
-0.125	0.92	0.46	10.2	19.401	19.442
0	1.01	0.48	10.5	19.400	19.441
0.125	1.11	0.51	10.8	19.401	19.442
0.250	1.24	0.53	11.0	19.402	19.444
0.375	1.38	0.55	11.2	19.405	19.449

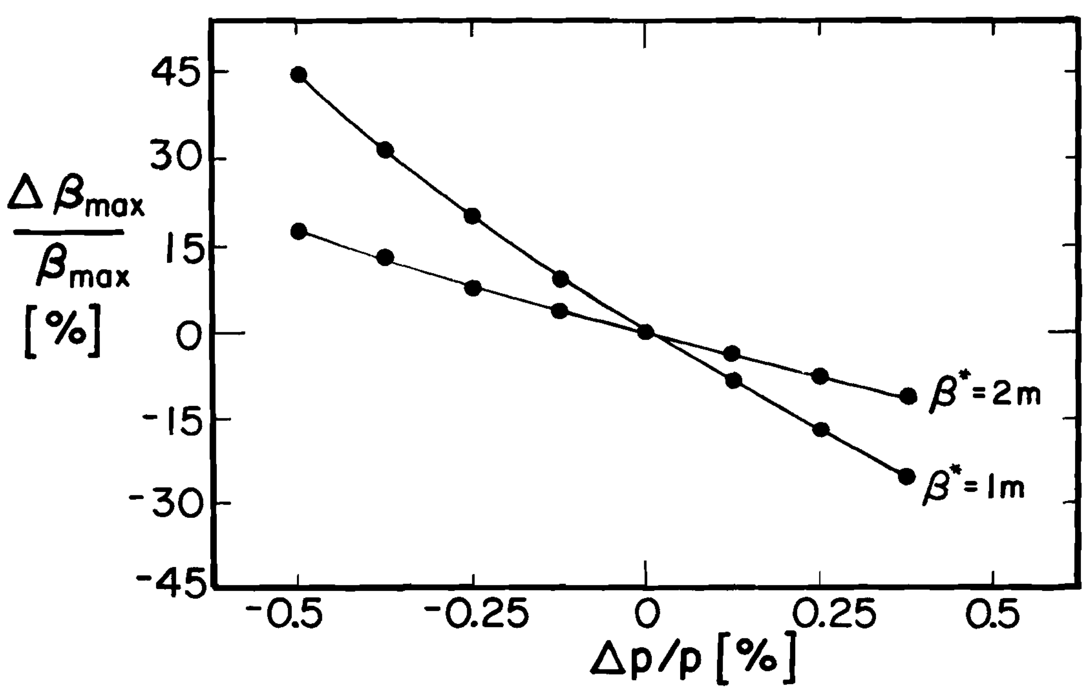

Fig. 2-7. Change in β_{max} as a function of $\Delta p/p$ for β^*=1m and β^*=2m.

number of circuits, a much smaller variation could be obtained. It should be noted that the momentum aperture discussed herein is for perfect magnets. Putting in design field distributions shrinks the available aperture considerably.

Finally, the question of non-zero dispersion at the collision point has been considered and a solution to overcome this problem has been found. This has not yet been studied in depth, but rather is presented as an existence proof. It consists of separately powering 14 quadrupoles, the 12 of Type II plus the next two downstream of the straight section, that is, those at stations 14 and 15. A plot of lattice functions for this case is shown in Fig. 2-8, and this is described in Tables 2-III and 2-IV, There are several points to be noted:

1. This was done for a 2-m β^*. An initial attempt to do it for 1 m failed.
2. The quadrupole at station 15 is definitely needed. Perhaps the one at station 14 could be run normally.
3. Quadrupole #12 is running too hard for a two-shell quad.
4. The tunes have not been properly rematched to 19.4. Completely making the dispersion zero is an extremely difficult process and may not be possible for other tunes.
5. The dispersion at the crossing point is shown as 8 cm. It can be made to be zero.

Finally, Fig. 2-9 is a layout of the interaction region at B0.

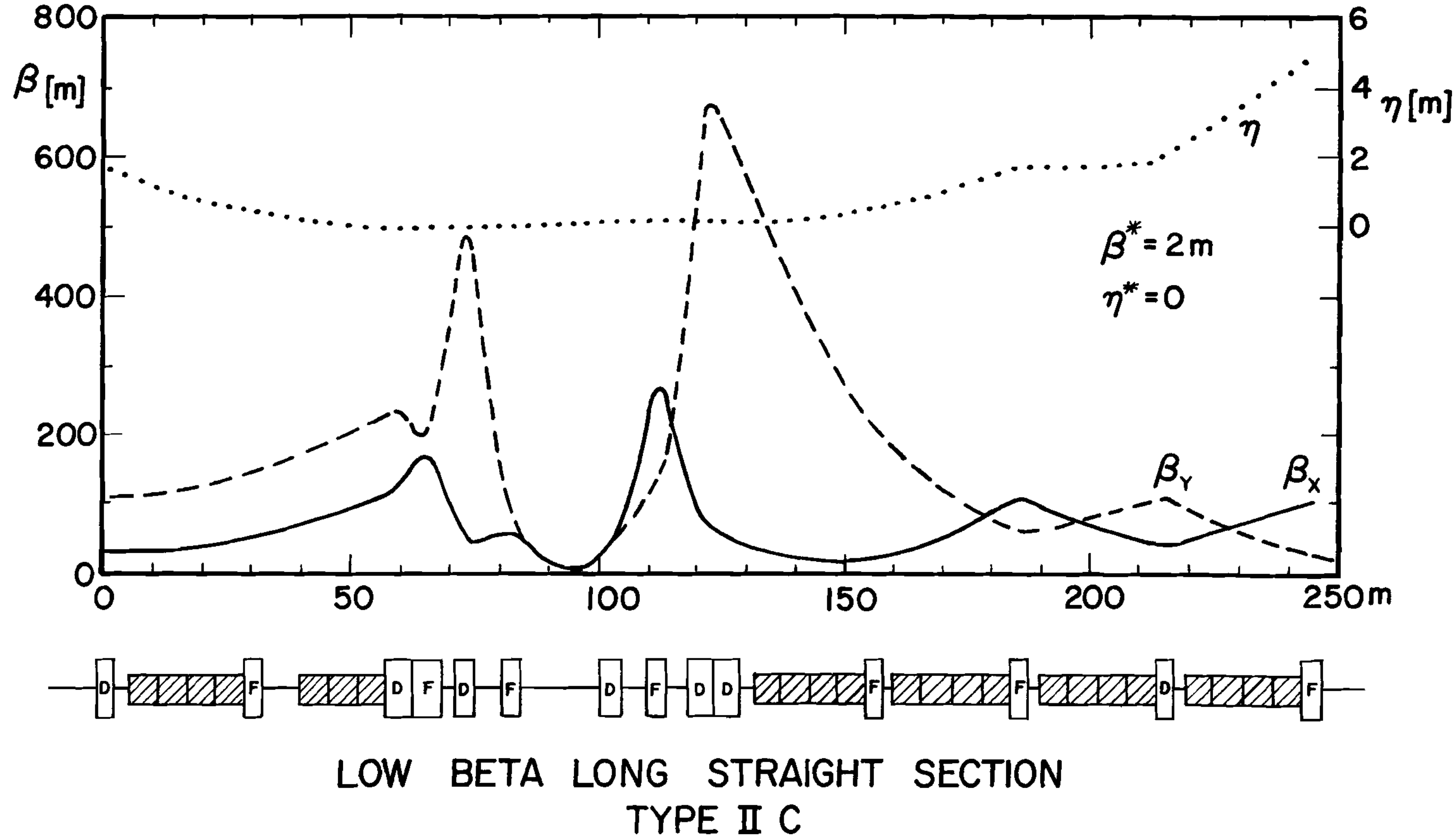

Fig. 2-8. Lattice functions for type IIC low-beta long straight section.

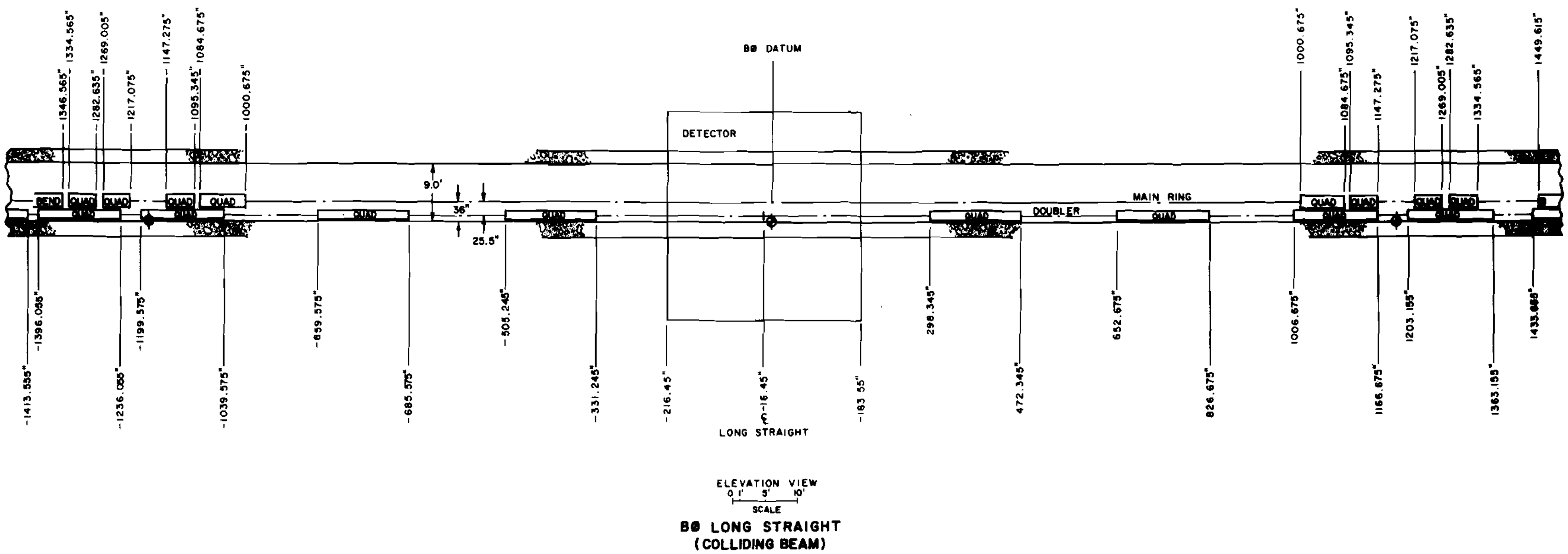

Fig. 2-9. Layout of the B0 long straight section.

Reference

[1] High Luminosity pp and $\bar{p}p$ Colliding Beam Straight Section Designs, D. E. Johnson, Fermi National Accelerator Laboratory Internal Report TM-876, April, 1979.

3. MAGNETS

3.1 Acceptance Criteria

The confluence of test results on more than 170 full-scale magnets[1] that have been built and tested at Fermilab and the accelerator-design work discussed in the remainder of this report, especially the correction and adjustment elements discussed in Section 7, has led to a set of acceptance criteria for dipole magnets. These criteria are given in Table 3-I on the next page.

Both dipole and quadrupole designs are based on extensive computer studies of the magnetic field. We include as Appendix III computer-generated magnetic-field data for both dipoles and quadrupoles.

3.2 Dipole Design

Parameters and specifications of the dipole magnet are given in Table 3-II. Figures 3-1, 3-2, and 3-3 are cross-section views of the dipole, 3-1 showing the over-all magnet, 3-2 the detail of the collared-coil assembly, and 3-3 the end of the cryostat, in particular the helium and nitrogen connections and the helium-pressure relief system. Figure 3-4 is an elevation view, showing the details of the beam tube and cryogenic-fluid connections.

The magnet is a cold-bore, warm-iron design with a two-shell $\cos\theta$-type coil around a circular bore. The beam tube is slightly flattened into a four-sided cross section, as can be seen in Fig. 3-1. This gives better helium flow where needed between the beam tube and the coils.

The superconducting cable is formed into a keystone cross section during winding. The inner coils are wound flat, then pressed into a saddle shape around a mandrel. The outer coils are saddle wound. The return

Table 3-I. Dipole Acceptance Criteria.

Quench Current	> 4350 A @ ≥ 200 A/s
AC Loss	< 500 J/cycle @ 4000 A and 300 A/s
Relative Variation of Integral Field	$<\pm 10^{-3}$ about mean @ 2000 A
Magnetic Vertical Axis rms = 1 mrad ⇒ 6.4 mm	$<\frac{1}{2}\times 10^{-3}$ rad from vertical measured and marked absolute accuracy @ 2000 A
Outside Physical Dimensions	
Curvature	±15 mil from nominal
Flatness and Twist	within 30 mil envelope
Relative Twist	2 mr

Integral Multipole Fields (B_n/B_o at 1 in.) at ≥ 2000 A

	Normal	Skew
Quadrupole	$\pm 2.5\times 10^{-4}$	$\pm 2.5\times 10^{-4}$
Sextupole	$\pm 6.0\times 10^{-4}$	$\pm 2\times 10^{-4}$
Octopole	$\pm 2\times 10^{-4}$	$\pm 2\times 10^{-4}$
Decapole	$\pm 2\times 10^{-4}$	$\pm 2\times 10^{-4}$

Hipot		
Coil, bus, heater to ground	< 5 μA @ 5 kV	
Electrical Parameters		
(acceptable tolerance about mean)	R ± 0.3%	(dc)
	C ± 10%	
	L ± 2%	(at 1 kHz)
	Q ± 10%	(at 1 kHz)
Vacuum (maximum leak room temp.)	5×10^{-9} atm-cc/s	

Table 3-II. Dipole Parameters and Specifications.

COIL SUPERCONDUCTOR:

Cross Section (In.):
Width - $0.307^{+0.001}_{-0.000}$

Thickness - $0.055^{+0.000}_{-0.001}$ Outer Edge, $0.044^{+0.001}_{-0.000}$ Inner Edge

Strand Diameter: 0.0268±0.0003 in.

No. Strands/Cable: 23

Filaments: 8 μm diameter Ni-Ti alloy
2100 filaments/strand

Copper to Superconductor Ratio: 1.8/1 by volume

Strand Twist Pitch: 0.5 in.

Cable Twist Pitch: 2.25 in.

Cable Short-Sample Current (min.): 5350 A @ 50 kG and 4.2 K

Strand Short-Sample Current (min.): 244 A @ 50 kG and 4.2 K

Copper Resistivity Ratio: R(9.5K)/R(273K) = 0.023 ± 0.002

Insulation: (In.) 0.001 thick × 0.375 wide Kapton, spiral wrap, 7/12 lap, plus
0.007 thick × 0.250 wide B-stage/fiberglass, spiral wrap, 1/8 in. gap

RETURN BUS SUPERCONDUCTOR: (Same parameters as above except as follows):

Cross Section: (In.) 0.286 wide
0.058 outer edge thickness
0.049 inner edge thickness

Insulation: 4 layers - 0.001-in. thick × 0.375-in. wide Kapton, spiral wrap, 7/12 lap plus
0.007-in. thick × 0.250-in. wide fiberglass, spiral wrap, butted (no gap) (alternate spirals dry and B-staged)

COILS: Conductor placement computer printout reference:

SNOWDON 041979-1030

Inner Coil: No. Turns: 2 ×35 Inner Radius: 1.500 in.

Outer Coil: No. Turns: 2 × 21 (including bus ½ turn)
Inner Radius: 1.835 in.

Cable Lengths/Magnet:

Inner: 2900 ft
Outer: 1756 ft
Bus: 25 ft

Coil collaring preload requirements 15000 lb/linear in.

YOKE DIMENSIONS (In.):

Inner Radius: 3.765
Width: 15
Height: 10
Maximum Twist: ±1/32
Sagitta: 0.26

LENGTHS (In.):[a]

Yoke: 235
Inner Coil:
To Inner Radii: 238.5
To Outer Radii: 245.115
Outer Coil:
To Inner Radii: 241.474
To Outer Radii: 244.635
Cryostat (to interface): 252

COOLING:

Helium:

1ϕ capacity:	15 ℓ/magnet
2ϕ capacity:	7.1 ℓ/magnet
1ϕ inlet: (1st magnet)	4.5 K
1ϕ outlet: (22nd magnet)	4.6 K
2ϕ inlet: (22nd magnet)	4.47 K
2ϕ outlet: (1st magnet)	4.42 K
Helium flow rate:	20.55 g/s

Nitrogen:

LN capacity:	6.7 ℓ
Max. temp.: (outlet)	85 K

WEIGHTS:

Collared Coil Assembly	1050 lb
Cryostat	550
Yoke	6800
Total	8400

[a] See drawing 1620-MB 103657A

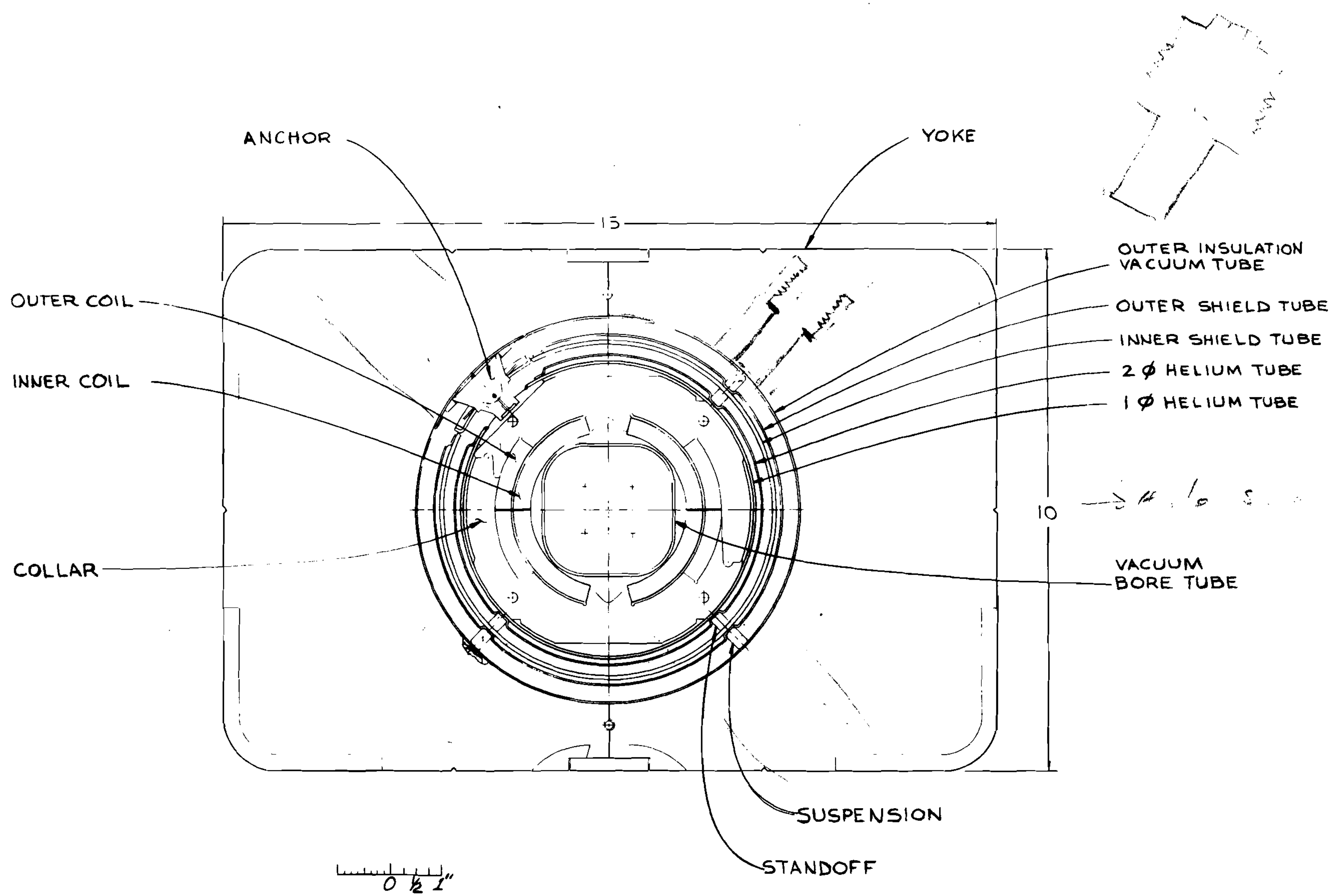

Fig. 3-1. Cross section of dipole magnet.

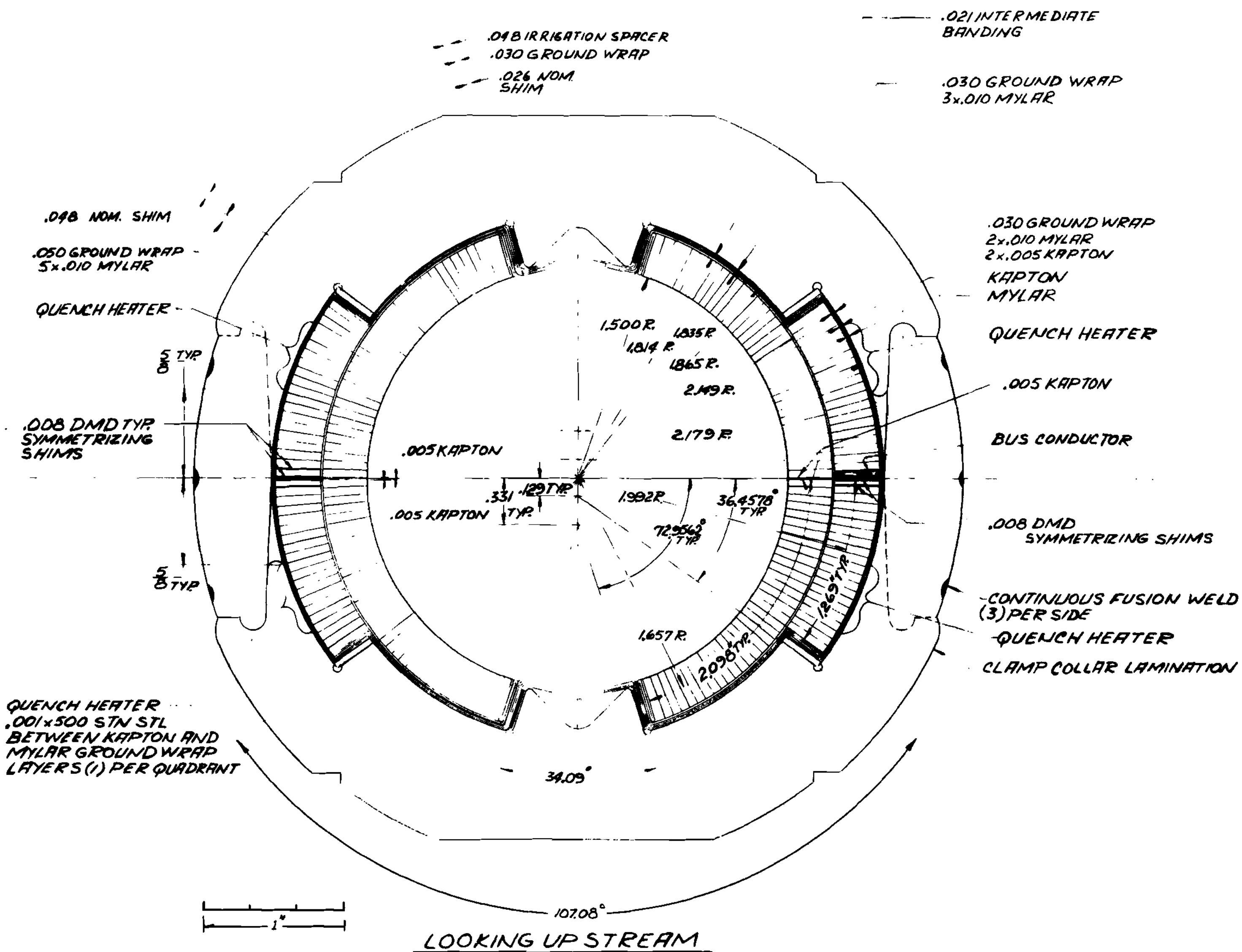

Fig. 3-2. Cross section of dipole collared coil.

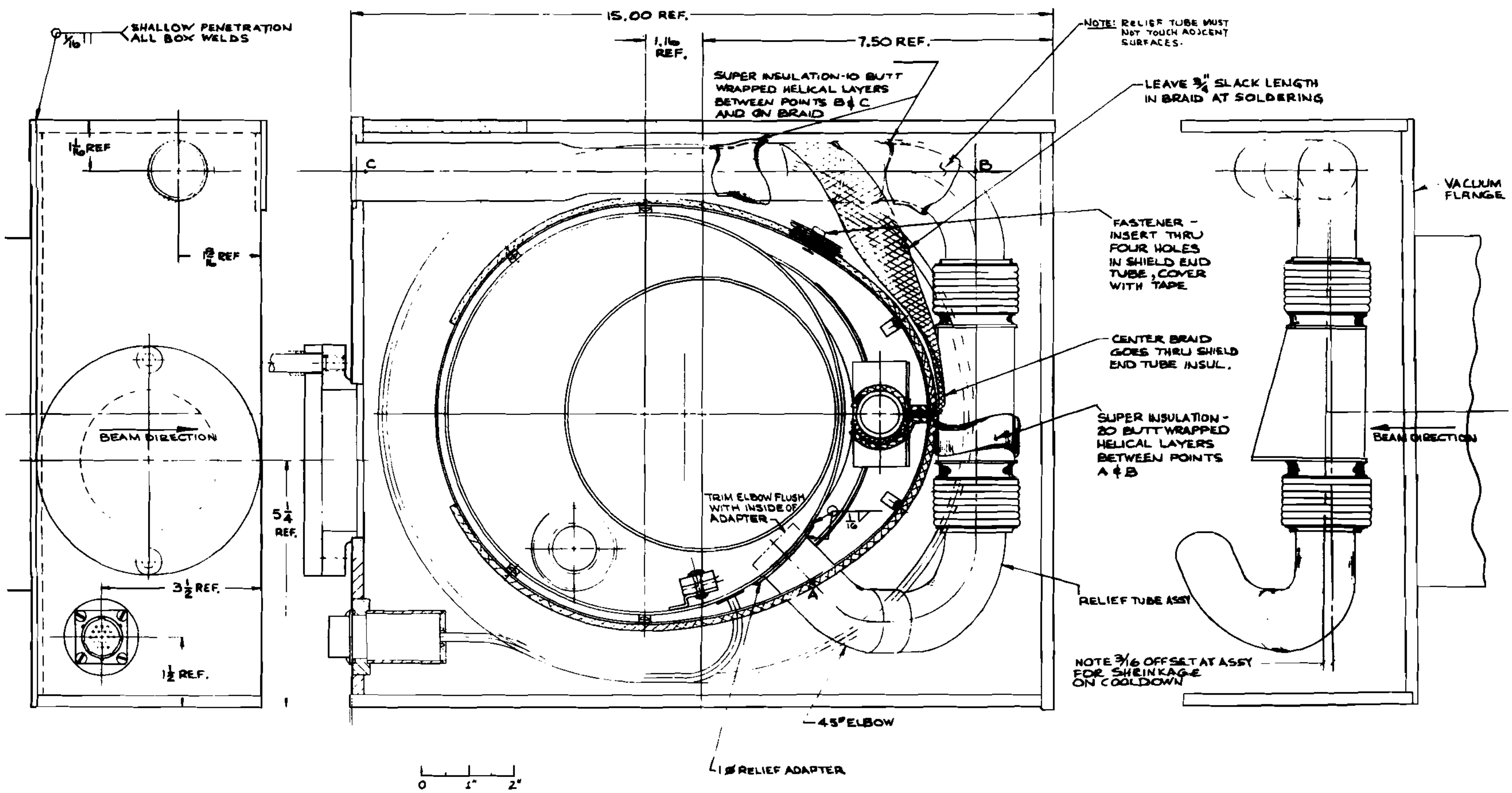

Fig. 3-3. Cross section of dipole cryostat.

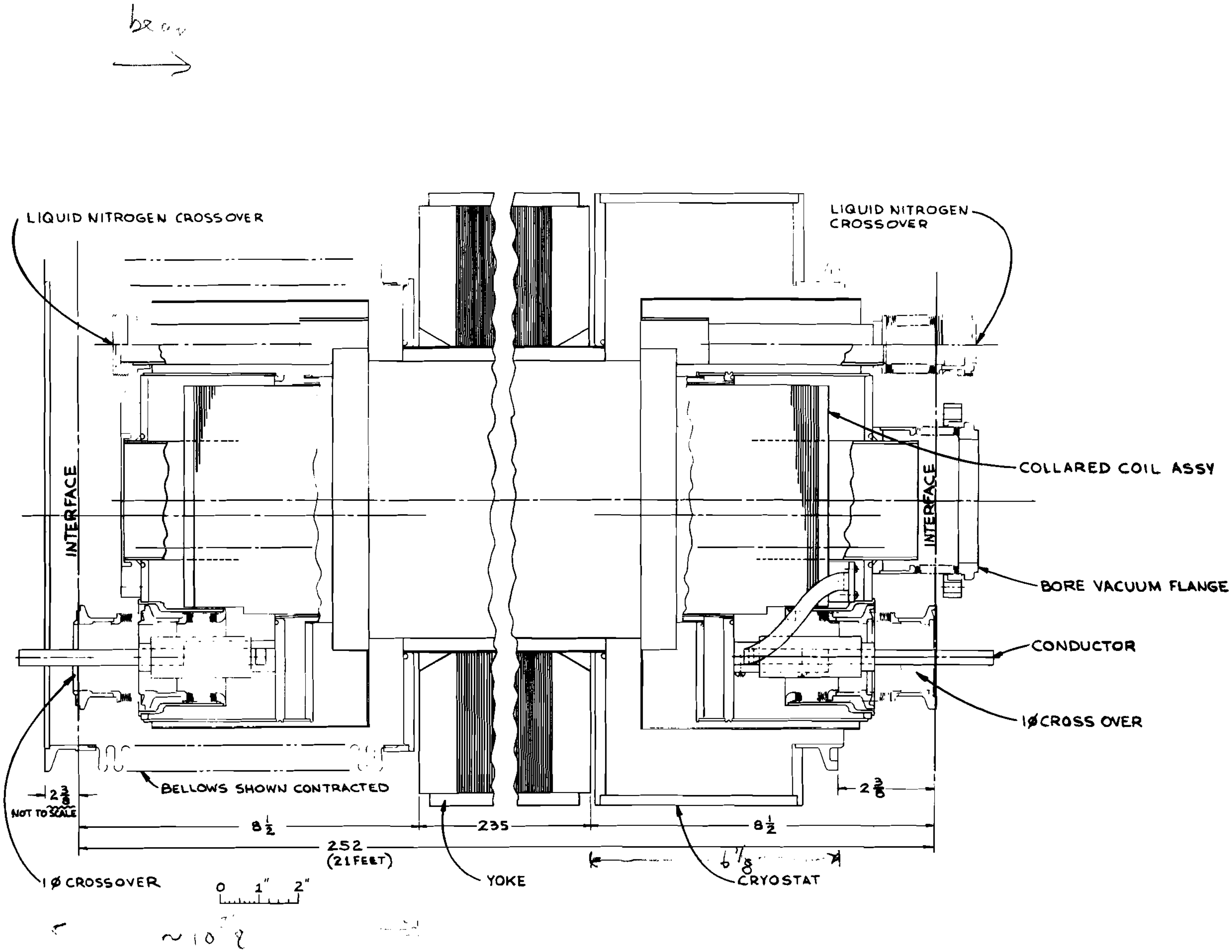

Fig. 3-4. Longitudinal cross section of dipole magnet.

bus and stainless-steel heater coils are wound integrally with the coils. The heater coils are fired when a quench is detected, as discussed in Section 6, to quench all the magnets in a half-cell as a unit and distribute the stored energy of the field to avoid damage.

The coils are held tightly in place against their own magnetic forces by the laminated two-piece stainless-steel collars shown in Fig. 3-2. The individual collars are formed into separate 4-in. upper and lower packs, which are assembled around the coils, then compressed in a press to give the pre-loading. The compressed collars are welded to complete the collared-coil assembly.

Room-temperature magnetic-field measurements are carried out on this assembly, using approximately 10 A in the coils, a multiple-loop stretched-wire pickup coil and a lock-in amplifier system to measure the normal relative multipoles of the coil.[2] The values measured in this way are not identical to those measured in the full-scale superconducting measurements discussed below in Section 3.4. The steel yoke adds a little more than 20% to the dipole field and also makes a change in the sextupole component. The quadrupole, octopole, and decapole components agree in the two systems to reasonably good accuracy. With this correspondence understood, the room-temperature measurements can be used to provide rapid feedback to monitor the production process.

Cooling is by single-phase liquid helium with two-phase counterflow heat exchange. Subcooled liquid helium is delivered to the coil space at 24 feed points around the ring and flows away from the feed points in both directions. Halfway to the next feed point, the liquid passes through a Joule-Thomson valve and flows back through the magnets as boiling helium in thermal contact with the outgoing liquid-helium stream. Heat generated by the coils is transferred to the single-phase liquid, which has relatively high specific heat and heat transfer, and is transferred by it to the colder two-phase reverse flow. Both streams remain at near-constant temperature throughout their paths; heat is absorbed by changing liquid to gas. The refrigeration system external to the magnets is discussed in Section 4 below. Figure 3-1 shows the cryostat in cross section. The standoffs shown are of G-10. The heat leak is measured to be approximately 7 W per dipole.

The complete cryostat is installed in a laminated steel yoke. A wire-loop pickup coil built into the yoke is used to align the cryostat in the yoke, using small currents at room temperature. The yoke assembly has a 0.26-in. sagitta (barely visible) to curve the magnets to fit the orbit.

Considerable experience has been gained by now in fabrication and assembly of all the components of a magnet. One of the important lessons has been the necessity for the strictest quality control at every stage of the process and we have instituted rigorous 100% inspection procedures. It is only by following such procedures faithfully that it is possible to build superconducting magnets with reproducible fields.

The dipole bore is 1.5 in. in radius, with a slightly smaller constriction arising from the squared-off beam tube. The field drops off rapidly beyond a radius of 0.8 in. Such a field is of course rich in multipoles. In particular, the sextupole and decapole are relatively large and opposite in sign. The magnet ends also contribute significantly to these two harmonics and this contribution is difficult to compute precisely. Adjustment of the angles subtended by the inner and outer coils in the collars, using shims, is used to cancel the body and end sextupole and decapole fields.[3] Significant quadrupole fields, both normal and skew, can arise from misalignment of the coils within the yoke and special care is required in assembly.

3.3 Quadrupole Design

Figure 3-5 is a cross-section view of the quadrupole.[4] Figure 3-6 is an assembly drawing and Fig. 3-7 is a sketch showing the complete quadrupole "spool" assembly with correction coils and the beam detector. Parameters and specifications of the quadrupole are given in Table 3-III. Table 3-IV gives parameters of the spool package and Table 3-V gives parameters of the correction-element package.

The quadrupole is a cold-bore, two-shell design of 3.5-in. bore. This diameter is chosen to ensure that the quadrupole is not the limiting aperture of the accelerator. There are two coil sections, separated by a spacer, in the inner shell and one section in the outer shell, as shown in Fig. 3-5. The spacer improves the 20-pole of the quadrupole to a negligible value, at the cost of a 10% increase in length to maintain the required integrated gradient. The thickness of the spacer also controls the 12-pole. A change in thickness of the spacer by ten mils (0.010-in.) changes the 12-pole/quadrupole ratio by about 5×10^{-4} at 1 in.

The following comments concern the design of the ancillary features:

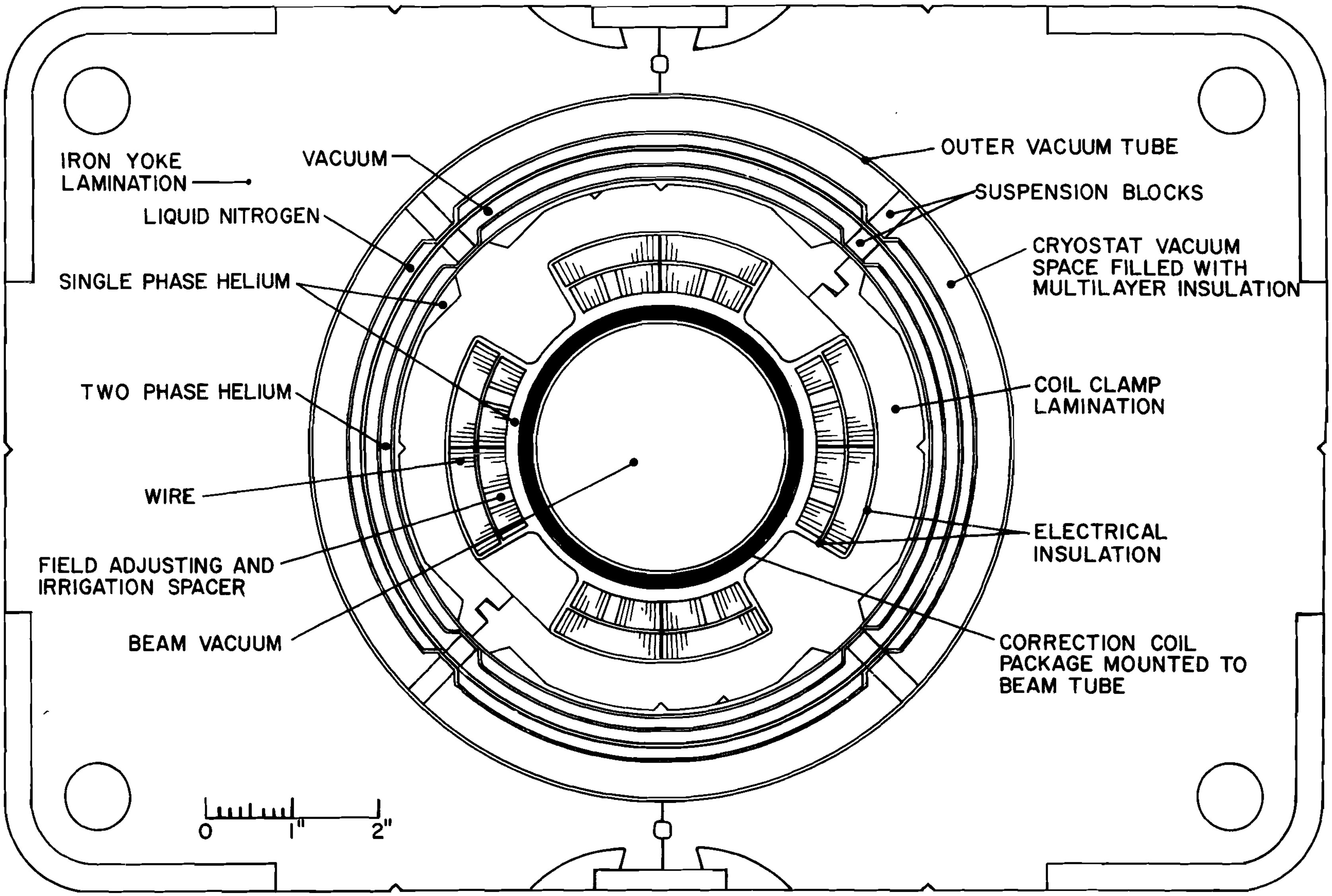

Fig. 3-5. Cross section of quadrupole magnet.

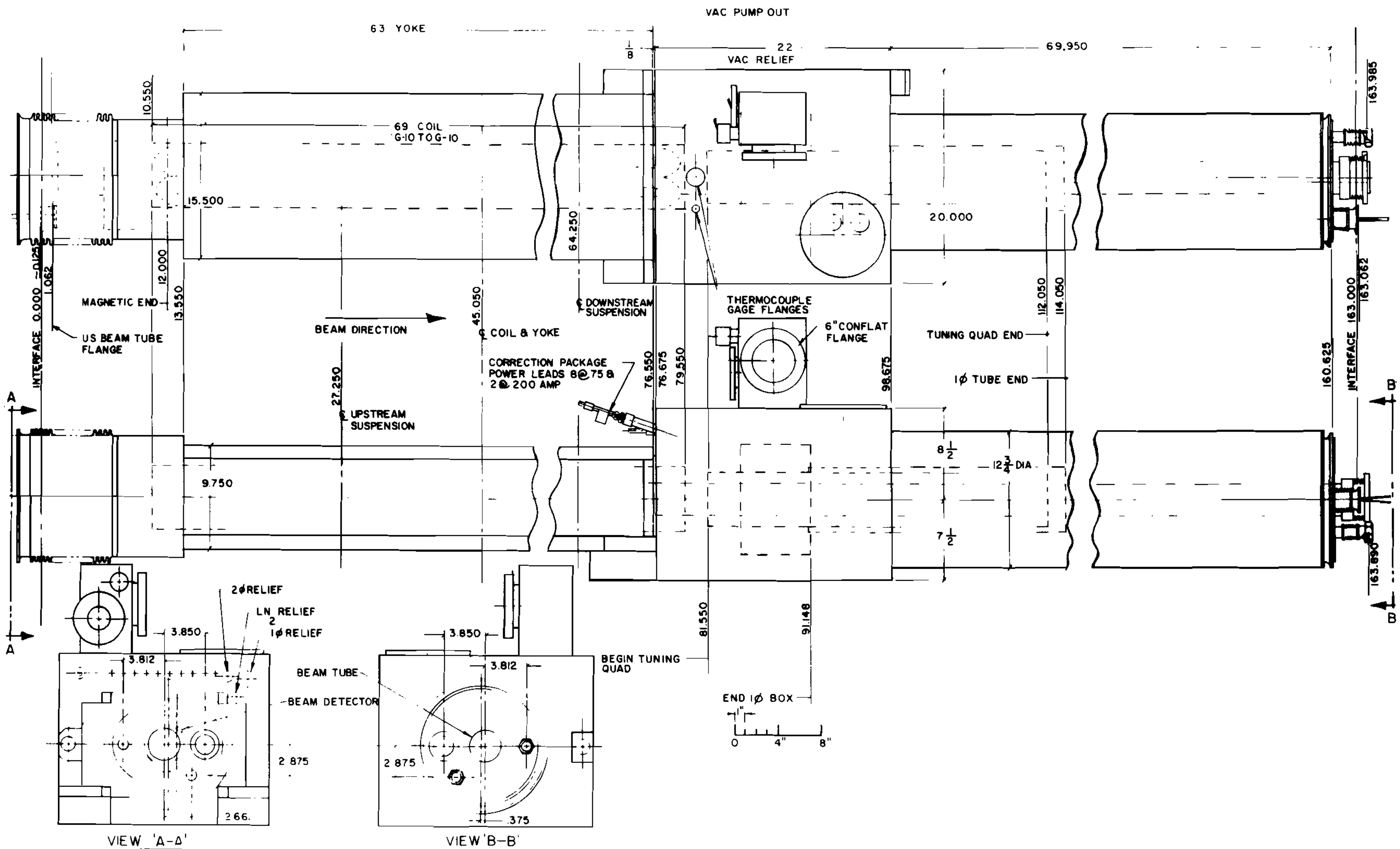

Fig. 3-6. Cross sections of quadrupole and spoolpiece assembly.

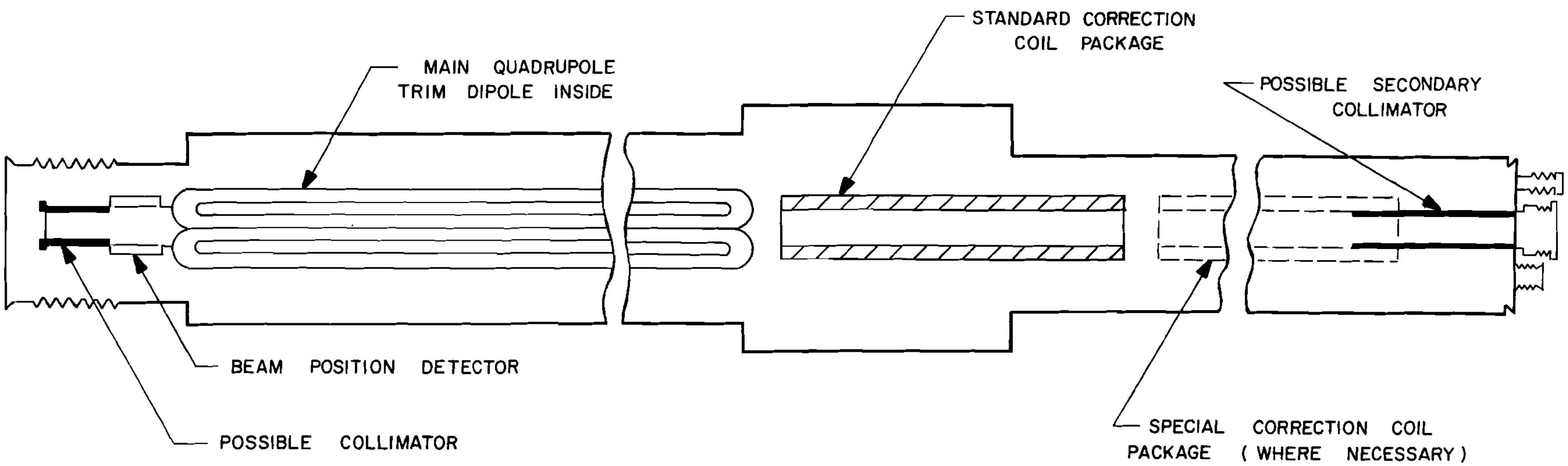

Fig. 3-7. Longitudinal cross section of quadrupole and correction coil assembly.

Table 3-III. Type Q Quadrupole Coil/Cryostat Parameters and Specifications.

	Inner Coil	Outer Coil	
Inner Radius	1.750	2.088	in.
Outer Radius	2.067	2.405	in.
Key Angle	30.1194	30.7839	deg
No. Turns	14	20	
Conductor Required	210 (×4)	280 (×4)	ft

Assembly Dimensions (all in in.):

Outer Collar Radius:	2.933
Ground Wrap Material/Thickness:	Kapton/0.028
Coil Length (Actual):	69
Coil Length (Magnetic):	66.1
Yoke Length:	63
Yoke Inner Radius:	4.000
Yoke Outside Dimension:	9.750 × 15.478
Overall Slot Length:	163

	Inside Radius (In.)	Material Thickness (In.)
Beam Tube	1.372 (3.485 cm)	0.065
1 Phase Tube	3.040	0.036 (20 GA)
2 Phase Tube	3.177	0.036 (20 GA)
Inner Shield Tube	3.389	0.049 (18 GA)
Outer Shield Tube	3.552	0.036 (20 GA)
Vacuum Tube	3.963	0.036 (20 GA)

(i) Vacuum Break. A preliminary design for a vacuum-isolation scheme has been completed as it relates to internal spool components. An external manifold is required to connect upstream and downstream insulating-vacuum regions, assuming redundancy of pumping systems is desired. Although cumbersome, this manifold facilitates the upstream-downstream connection with the proposed break. This external pipe (with valve) is not shown on the assembly drawing.

Table 3-IV. Spool Service Package Parameters and Specifications.

1 Phase Relief:	1 @ 1-½ in.
2 Phase Relief:	1 @ 1 in.
LN_2 Relief:	1 @ 3/4 in.
Insulating Vacuum Relief:	1 @ 1-½ in. 1 @ 5.4 in.^{2}
Insulating Vacuum Pumpout:	6 in. Conflat
Thermocouple Flanges:	1 - KF - 10 1 - KF - 40
Beam Vacuum Sniffer:	2-3/4 in. Conflat termination
Beam Position Monitor:	1 @ 6 in. length, upstream end
Safety Lead:	1 lead, Constantan, 0.3916 in.^{2} cross section, 8 ft length, connected to quadrupole coil lead
1 Phase Instrumentation:	100 Ω carbon resistor for temperature measurement, bus/coil voltage taps
Correction Element Power Leads:	10 vapor-cooled leads @ 75 A for correction packages

Table 3-V Correction-Element Package Parameters and Specifications.

	2P	4P	6P	8P
Inner Diameter	2-7/8 in.	3-7/8 in.	3-7/16 in.	3-1/16 in.
Outer Diameter	3-1/32 in.	4-1/16 in.	3-3/4 in.	3-5/16 in.
Coil Length (maximum)	65 in.	30 in.	30 in.	30 in.
Magnetic Length	62 in.	27 in.	27 in.	27 in.
No. Layers	4	4	7	6
No. Turns	330	220	220	120
Nominal Current	50 A	50 A	50 A	50 A
Self Field	0.32 T	0.44 T	0.45 T	0.47 T
% Field Due to Iron	a	42	23	5
Nominal Strength @ 1 in.	175 kG-in.	61 kG-in.	50 kG-in.	30 kG-in.
Estimated Inductance	250 mH	200 mH	200 mH	130 mH
Iron Length	a	30-½	30-½	30-½
Iron Outside Diameter	a	5 in.	5 in.	5 in.

[a] Steering dipoles are wound as an integral part of the beam-tube subassembly.

(ii) Beam Detectors. The present design of the type Q quadrupole contains one beam detector at the upstream end. It is of the electrostatic type, 6-1/8 in. long, 3-3/4 in. diameter, with a plate separation of 2.557 in. (6.49 cm). A device 8 in. long with a plate separation of approximately 3 in. (7.6 cm) could be accommodated.

(iii) Beam-Loss Shielding. A shield of the kind discussed in Section 13 on the upstream and/or downstream end of the quadrupole package can be easily accommodated. Devices of 3.3 cm o.r. or less and 12-in. length or less should pose no significant problems.

(iv) Feed and Turnaround Region. The single-phase region housing the 30 in. correction package (4P, 6P, 8P) terminates approximately 114 in. from the upstream interface. At regular quad locations 1ϕ, 2ϕ, LN_2, insulating vacuum and beam tube span the remaining 49 in. to the downstream interface (@ 163 in.) at established end-view coordinates. At feed or turnaround locations these lines can be terminated as required in either welded or flange sealed connections.

3.4 Measurements and Results on Dipole Magnets

3.4.1 Training and maximum quench currents. In these measurements, a quench is detected by monitoring the resistive voltage across the magnet. The inductive voltage drop is bucked out by a toroidal coil coupled to the current bus. When a quench is detected, most of the stored energy is dumped by a thyristor switch into an external water-cooled resistance. At full current, only 0.1 MJ of the full 0.5 MJ stored energy is dissipated in the magnet. We have separately studied dumping the full 0.5 MJ in magnets to test the pressure-relief tube. We have also measured the field changes with quenching and found them to be very small.

With the tight restrictions of the interlocking Type V collars, very little training is needed to reach full field. Magnets usually reach more than 4300 A (4.29 T) at a 200 A/s ramp rate after a few quenches. Figure 3-8 on the next page shows ramp-rate dependence of maximum quench fields.

3.4.2 AC loss. Most of the eddy-current loops have been eliminated by the use of Ebonol-treated strand. The ac loss is now consistently smaller than 500 J/cycle in Ebonol magnets, which is low enough to allow operation with the refrigeration system of Section 4.

3.4.3 Integral fields. The integral fields are measured as a function of excitation by a stretched-wire system. The integral field is approximately 6.409 T-m/kA. Figure 3-9 shows the dependence on excitation and it can be seen that the hysteresis is quite small. The hysteresis is approximately 14 G and saturation of the steel is noticeable above 3000 A. The total effect reaches 20 G at 4000 A.

The stretched-wire system is a difficult measurement and we have therefore recently developed equipment that scans the field through the magnet with a NMR probe and a NMR-calibrated Hall probe for the fringe fields. This system is providing a more accurate absolute integral field as well as the longitudinal structure of the field. An example is shown in Fig. 3-10.

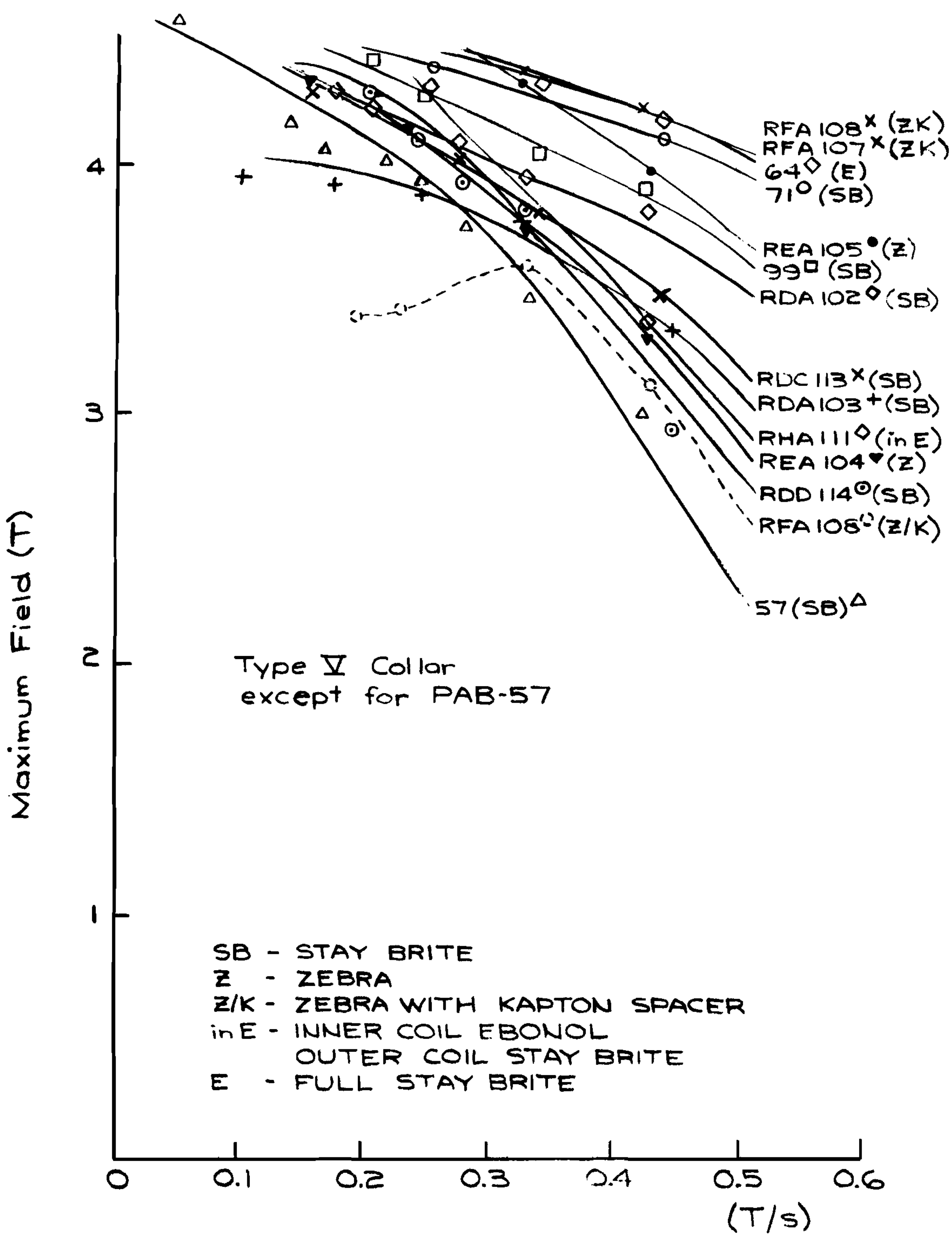

Fig. 3-8. Ramp-rate dependence of maximum quench fields.

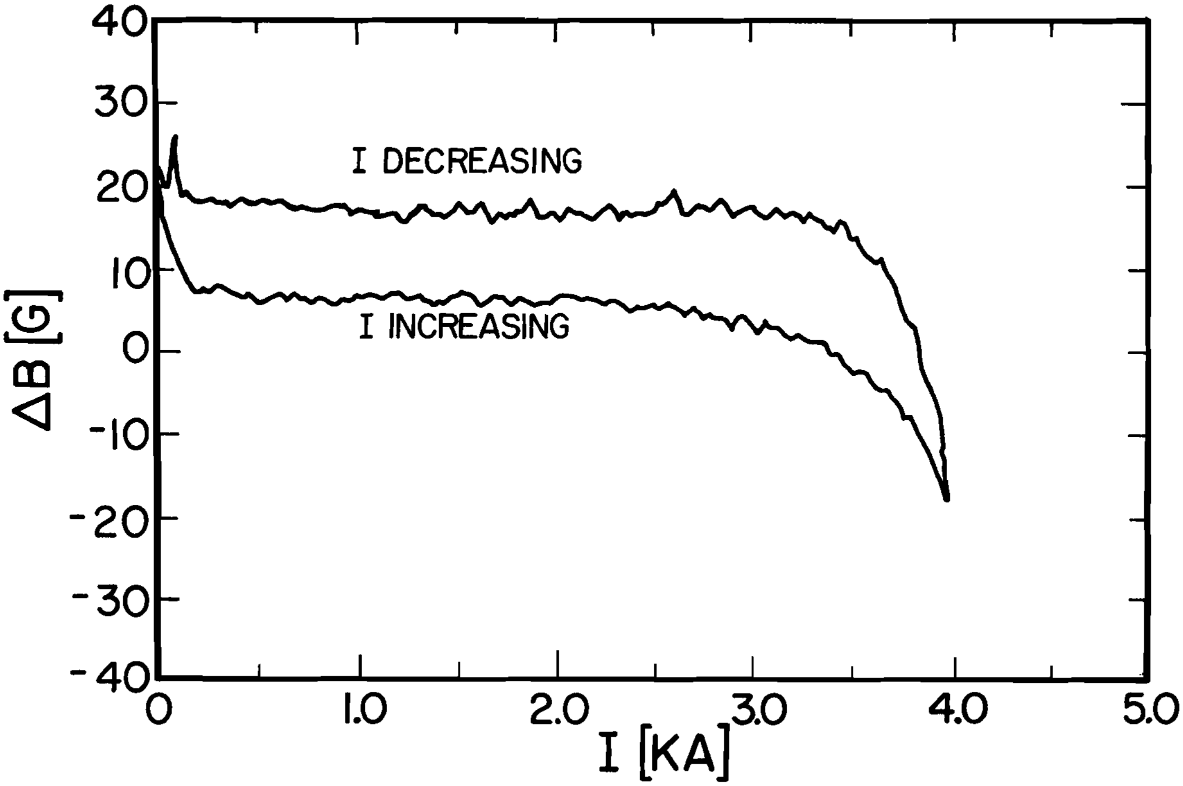

Fig. 3-9. Nonlinearity of magnetic field as a function of current.

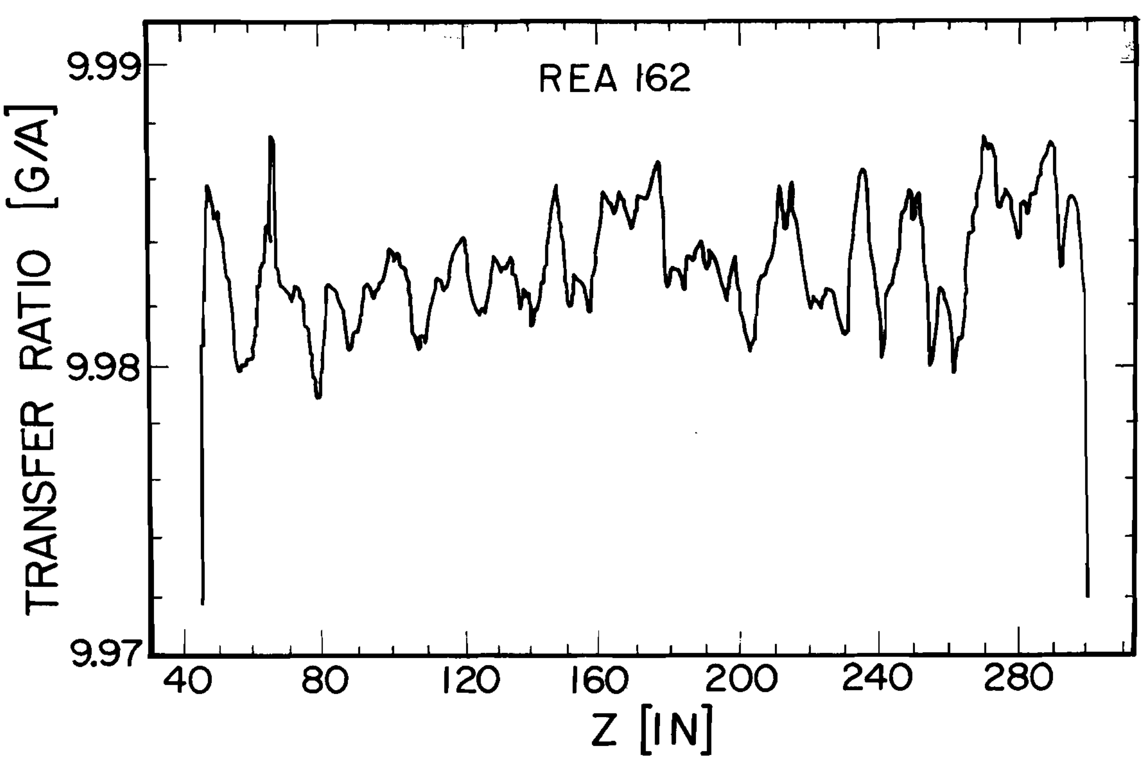

Fig. 3-10. Scan of the transfer ratio of a dipole magnet along its longitudinal axis.

3.4.4 Multipole fields. The field in the beam bore is measured by a harmonic coil. Harmonic components up to the 30th pole are required to give an accurate description of the field.

Our coil is 8 ft long and therefore three measurements are required to cover an entire magnet. Signals are analyzed in real time and transformed to normal (b_n) and skew (a_n) harmonic components, defined as

$$B_y + iB_x = B_o \sum_{n=0}^{\infty} (b_n + ia_n)(x + iy)^n,$$

where the pole number is $2(n + 1)$. The sextupole and decapole values are used to adjust the key angles of the coils.

There were some difficulties with overpressures in the collaring process partially crushing the small helium irrigation channels located next to the inner-coil keys. The resulting changes in coil dimensions were mirrored in changes in the sextupole. With careful attention to quality control, we are now building production magnets whose multipole components are close to the tolerances of Table 3-I.

Because of persistent currents in superconductors, some multipole components have large hysteresis effects, as shown for the sextupole component in Fig. 3-11, but they are quite reproducible. They are, of course, less important at higher excitations. There are no observable saturation effects on the multipole components, because the steel is far from the coils.

Harmonic components are also measured dynamically with ramping current. Figure 3-12 is a comparison of the sextupole fields at different ramp rates.

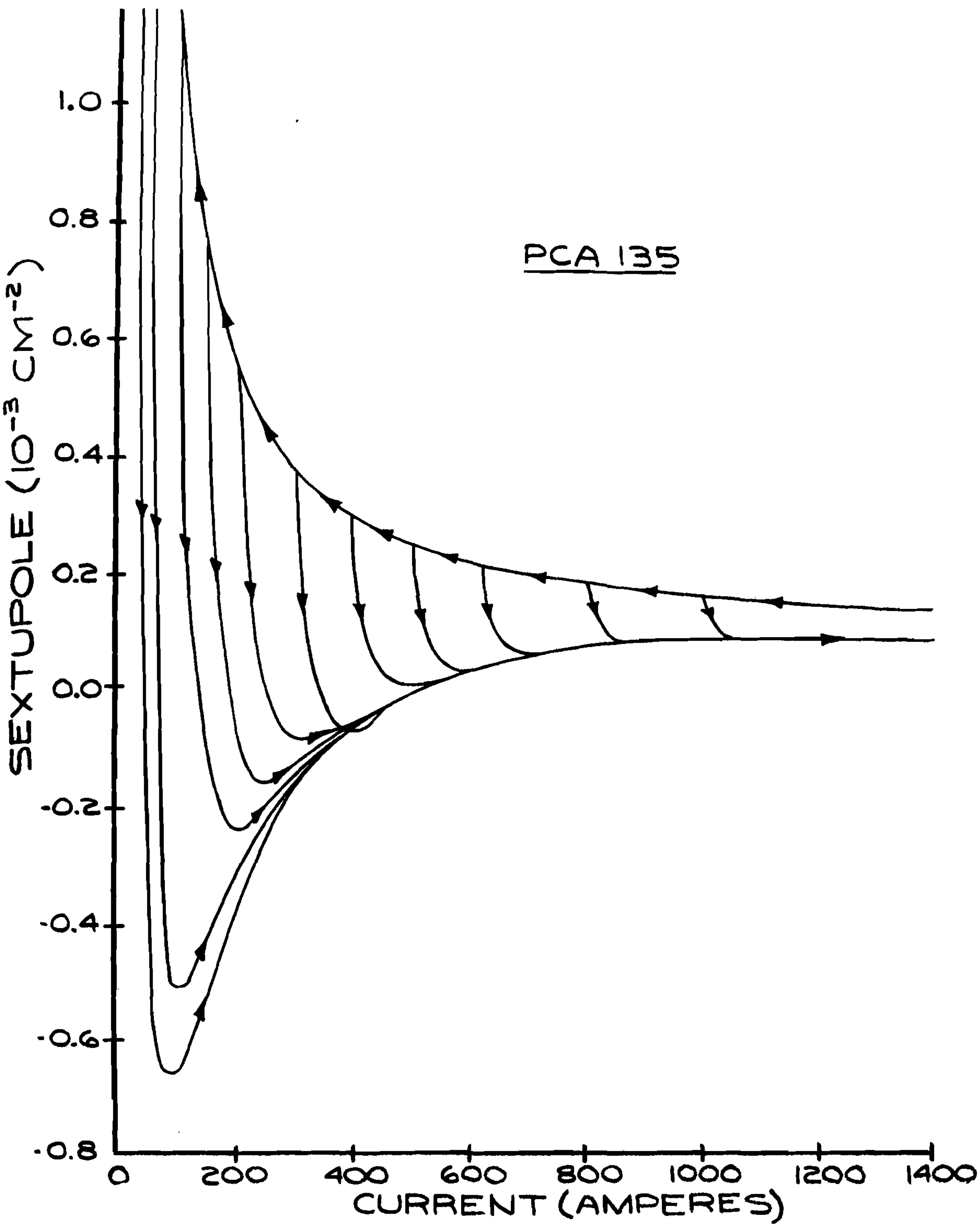

Fig. 3-11. Hysteresis behavior of the sextupole component in a dipole magnet.

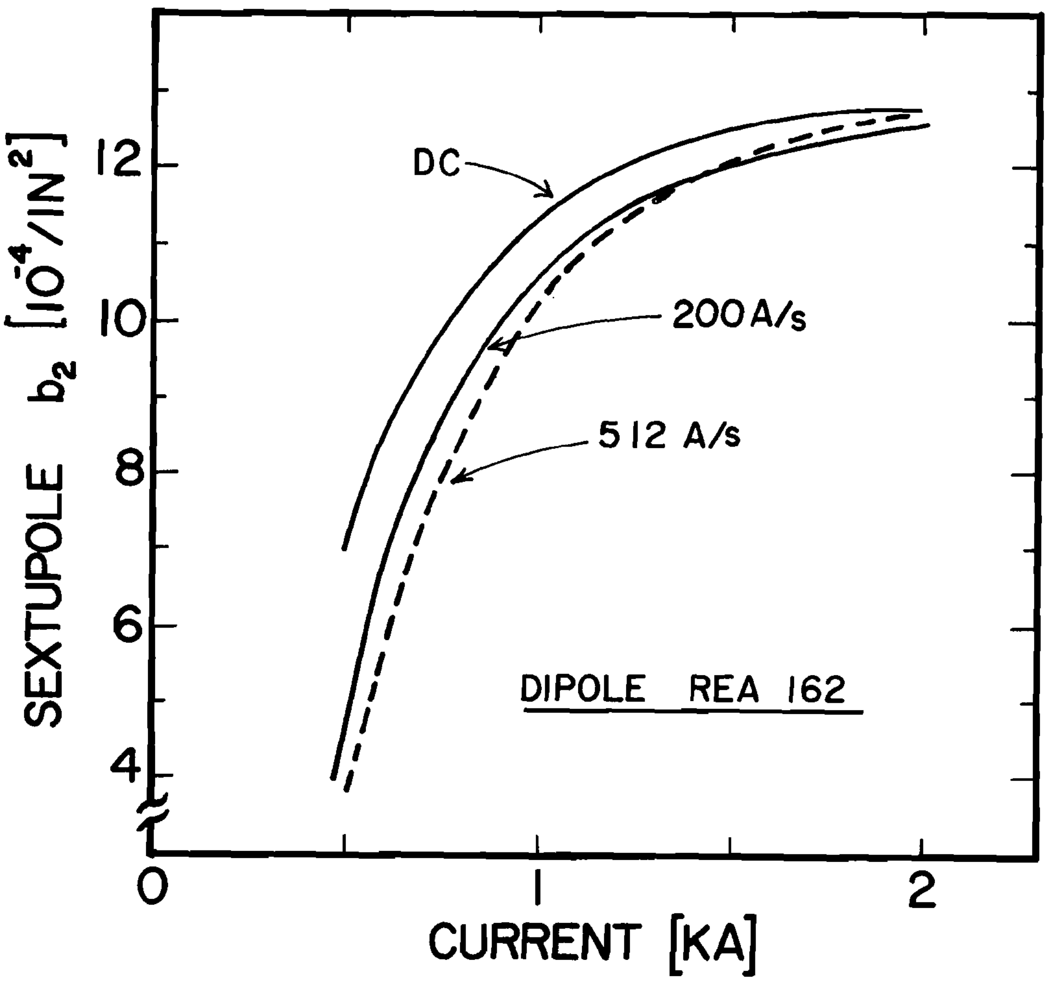

Fig. 3-12. Ramp-rate dependence of the sextupole component in the body field for dipole magnet REA 162.

Here the DC sextupole component is large because the data include only the body field. It has a large positive sextupole, which is to be cancelled by negative sextupole in the end fields.

3.4.5 Field orientation. The cryostat is aligned with the magnet yoke at room temperature during assembly as discussed above. The vertical plane is then measured in the superconducting state by a stretched-wire technique.

The magnitude of the deviation of magnetic from yoke vertical has been of concern to us, because it has major consequences on the sizes planned for correction dipoles. Results are covered in the statistical discussion of Section 3.6. We are still refining our techniques in this measurement.

3.5 Measurements and Results on Quadrupole Magnets

3.5.1 Quench current. Maximum quench currents are large (4.57 kA at a ramp rate of 670 A/s on QB2) and one can only make the magnet quench at the maximum ramp rate of our Test Facility power supply.

3.5.2 Integral gradient. The integral quadrupole strength is measured with twin wire loops stretched through the magnet. The relative difference in area of the two loops is approximately 2×10^{-3}. The integral gradient strength in QB2 is 121.6 T, whereas the design value is 119.6 T.

3.5.3 Multipole fields. The harmonic coil is composed of two main coils and four supplementary bucking coils. A dipole component arises from off-center positioning of the harmonic coil and this dipole component, as well as the quadrupole component, must be suppressed in order that the harmonic coil give workable sensitivity for higher multipoles. Rough reductions of the dipole and quadrupole are done by the two main coils and further reduction to the order of 10^{-4} is achieved with two orthogonal dipole and two orthogonal quadrupole bucking coils.

The harmonic components at 4000 A are given in Table 3-VI below.

Table 3-VI. Harmonic Components of Integral Field Relative to the Normal Integral Quad Field ($\times 10^{-4}$/In.$^{1-13}$) in Magnet QB2.

Pole	Normal	Skew
6	6.33	6.01
8	-0.44	-1.70
10	0.59	-1.83
12	-0.95	0.84
14	0.88	0.31
16	0.01	0.00
18	0.51	0.59
20	-1.63	0.26
22	0.11	-0.03
24	-0.04	-0.11
26	-0.38	-0.50
28	0.60	-0.06
30	0.11	0.08

The deviation from a pure quadrupole field is shown in Fig. 3-13 on the next page. The normal sextupole component can be seen to dominate. There are also skew 8- and 10-poles and a normal 20-pole. The excitation dependence of the 12-pole is shown in Fig. 3-14, also on the next page. The center line of the hysteresis has become much flatter than in older quadrupoles. This means that the new collars have almost completely eliminated coil motion. The 12 pole is also measured with a Morgan coil and the two methods give similar results.

3.6 Statistical Analysis of Magnet Data

3.6.1 Dipoles. We have made 100 individual measurements on about 70 magnets. A statistical overview of the data is presented here.

Figure 3-15 is a histogram of quench currents in Magnet Test Facility measurements. The cooling conditions are all similar. The typical

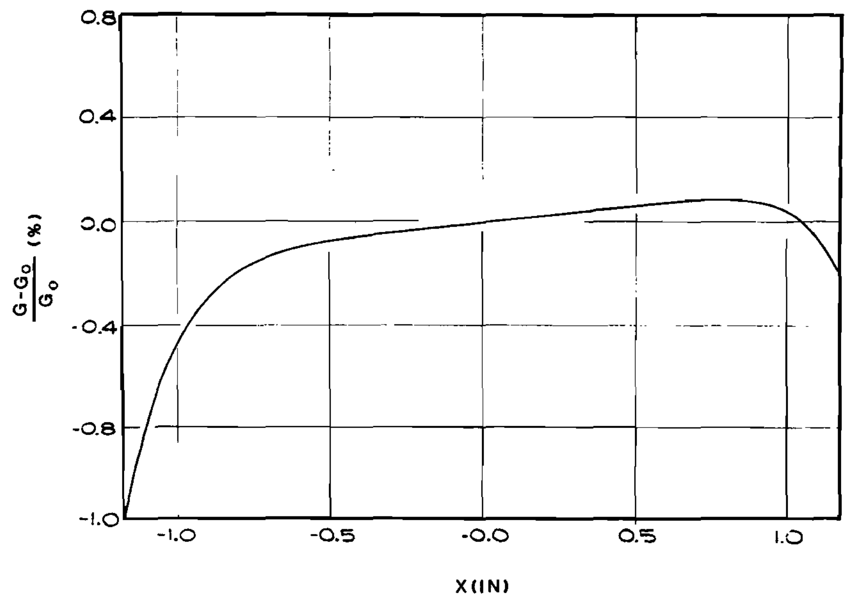

Fig. 3-13. Measured gradient distribution in QB2.

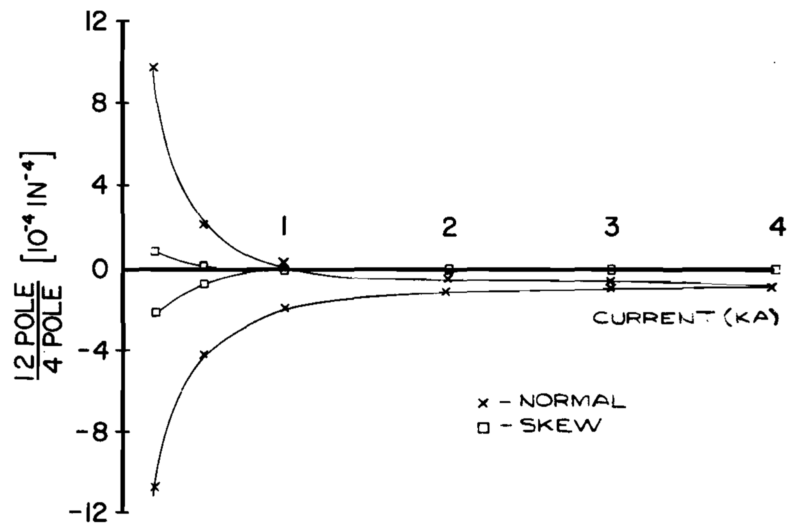

Fig. 3-14. Ratio of 12-pole to 4-pole field at 1 in. as a function of current in QB2.

temperature in the single phase is 4.7 K (±0.1 K) and 4.55 K in the two-phase return. Usually the subcooling of the single phase is 3 psi and the mass flow is 20 to 30 g/s.

There have been noticeable changes in transfer ratios (G/A) with various collaring schemes, as shown in Fig. 3-16. The FWHM is

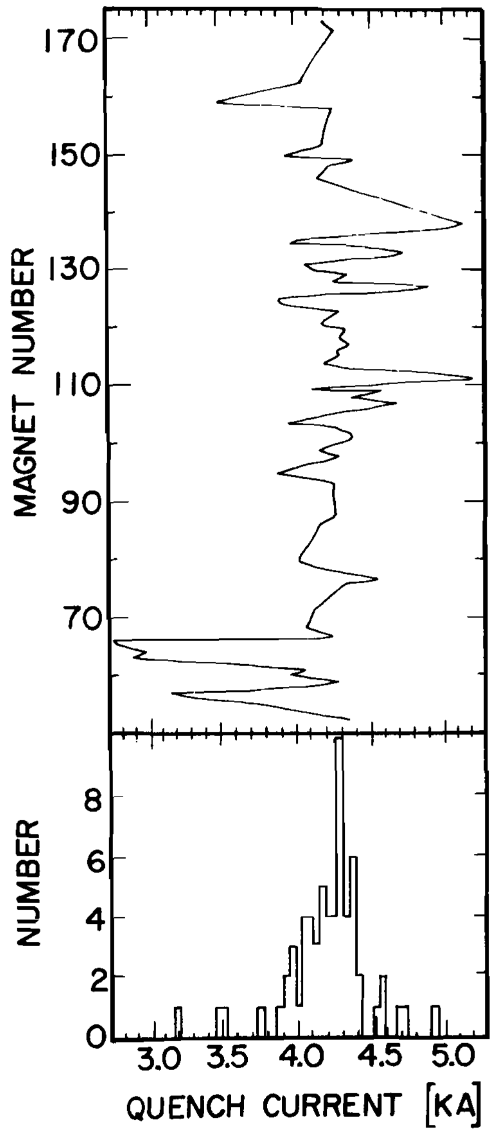

Fig. 3-15. Quench-current distribution over dipoles.

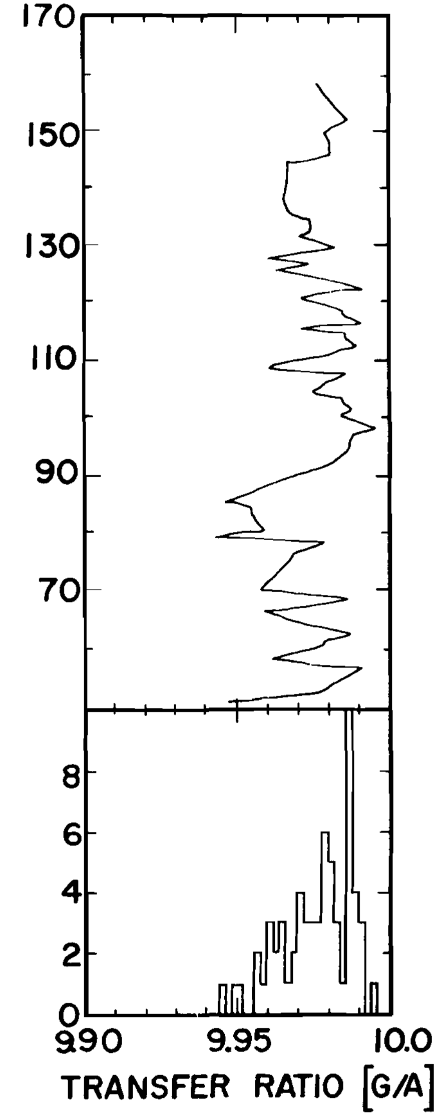

Fig. 3-16. Transfer-ratio distribution over dipoles.

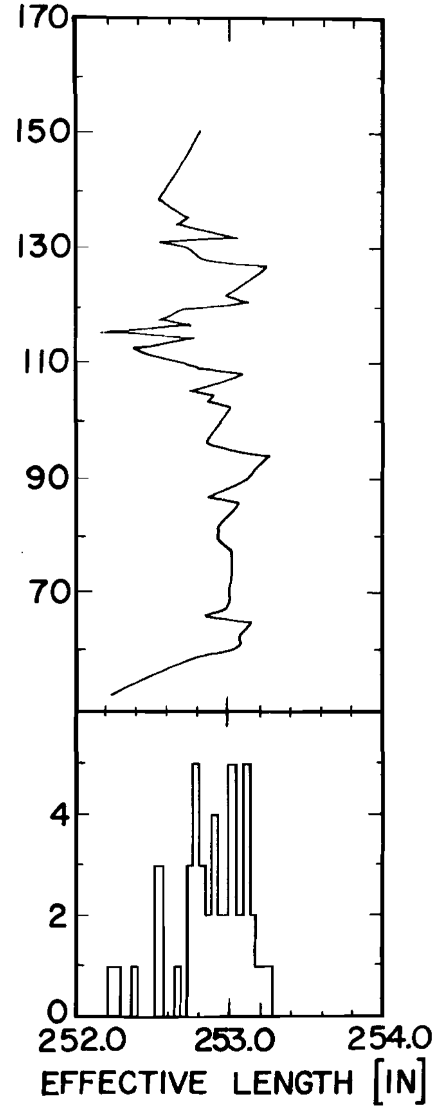

Fig. 3-17. Effective-length distribution over dipoles.

approximately 0.1% over all magnets measured, but bunching with smaller width can be perceived as a function of magnet number.

The integral field is difficult to measure in a 22-ft dipole by stretched-wire techniques and until recently some data were inadequate. Nevertheless, at the 0.1% level, the magnets are clearly reproducible in effective length, as shown in Fig. 3-17.

We have made detailed studies of the rotation of the dipole field with quench history and also with warmup-cooldown cycles, a more violent change. There are indications that the field orientation rotates randomly over a heat cycle, but it is within ±0.2 mrad at its maximum. Harmonic components were also measured, but the changes observed were very small.

3.6.2 Quadrupoles. A number of quadrupoles have been built and tested. Four of the nine quadrupoles were built with a spacer of nominal thickness and five with the spacer undersized by 10 mil. The missing 10 mil was shimmed in on the other side of the coil shown in Fig. 3 - 5. A histogram of the values of the 12-pole for the nine quadrupoles is shown in Fig. 3-18(a) (body component) and Fig. 3-18(b) (end component). The peak at 4.6×10^{-4} at 1 in. corresponds to the nominal thickness of the spacer and is approximately the correct body value to compensate the end value to zero for the integrated 12 pole. The 20-pole harmonic is shown in Fig. 3-18(c). The -1.1 value corresponds to the 4.6 12 pole in Fig. 3-18(a). The curves shown are Gaussians at the values indicated, with standard deviations as

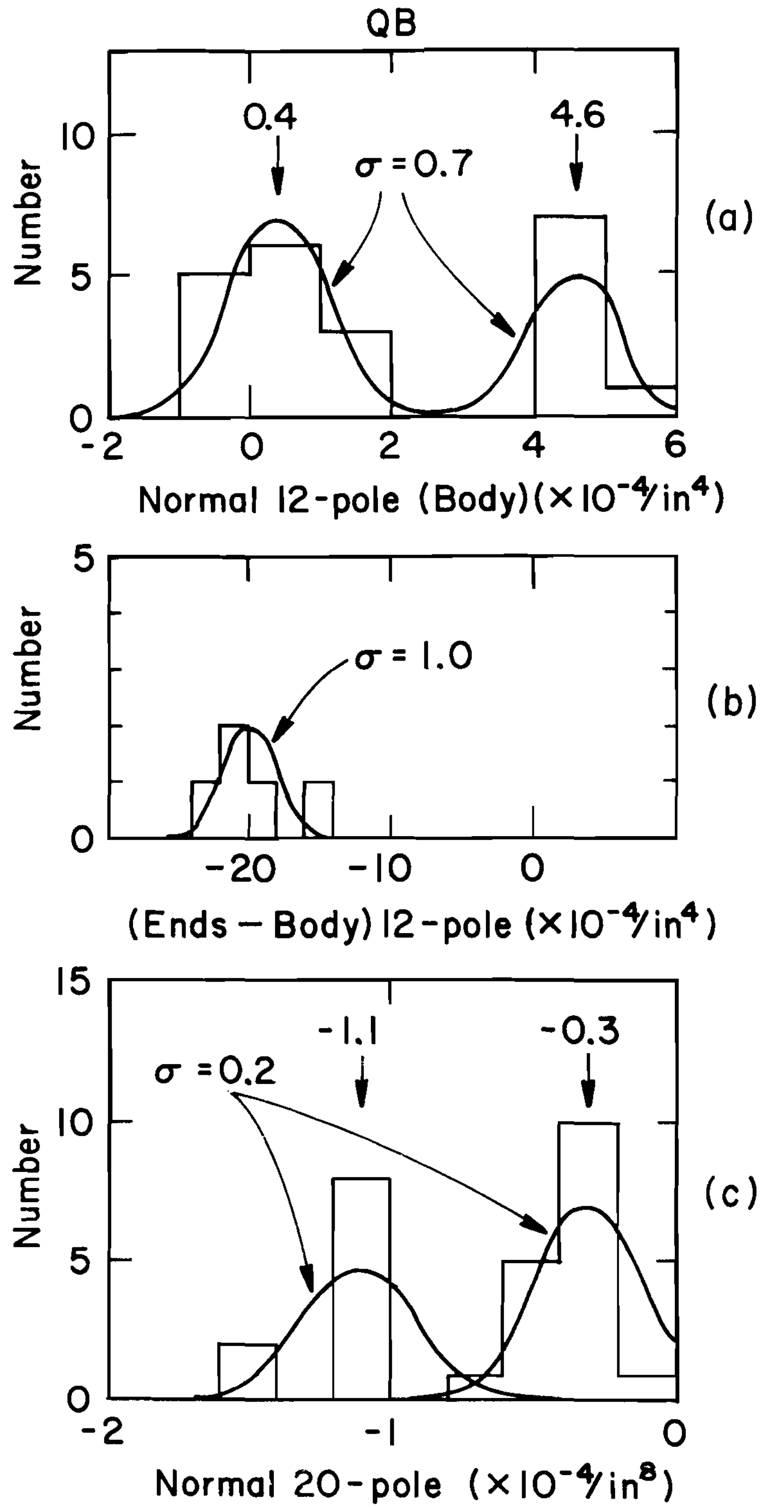

Fig. 3-18. Normal 12-pole and 20-pole distribution of quadrupoles. (Multipole field relative to quadrupole field at 1 in.)

shown. Thus we see that we can build quadrupoles with an integrated 12-pole of $(0\pm1)\times10^{-4}$ at one in. [corresponds to a body value of 5 in Fig. 3-18(a)] with a standard deviation of 1×10^{-4}. The 20-pole will be -1 and the 28-pole 0.6×10^{-4}. The 28-pole has been measured on one complete magnet to be about 0.7×10^{-4}; it cannot really differ from the design, and it does not.

All other harmonics should be absent, apart from construction errors. We show these other harmonics in Fig. 3-19 (skew 12- and 20-pole), Fig. 3-20 (normal and skew 6-, 8-, and 10-pole), and in Fig. 3-21 (the integrated values of Fig. 3-20). Table 3-VII summarizes the harmonics expected in the final production quadrupoles.

Table 3-VII. Expected Quadrupole Harmonics.
Multipole field relative to quad field at 1 in. ($\times10^{-4}$/in.$^{n-1}$)

	Value	σ (per Q)
Integral 12-pole	0±1	< 1
Integral 20-pole	-1	0.2
Skew 12-pole	0	0.25
Skew 20-pole	0	0.05
Average 6-pole	0	< 4
Average 8-pole	0	1.7
Average 10-pole	0	1.0
28-pole (measured)	~0.6	-

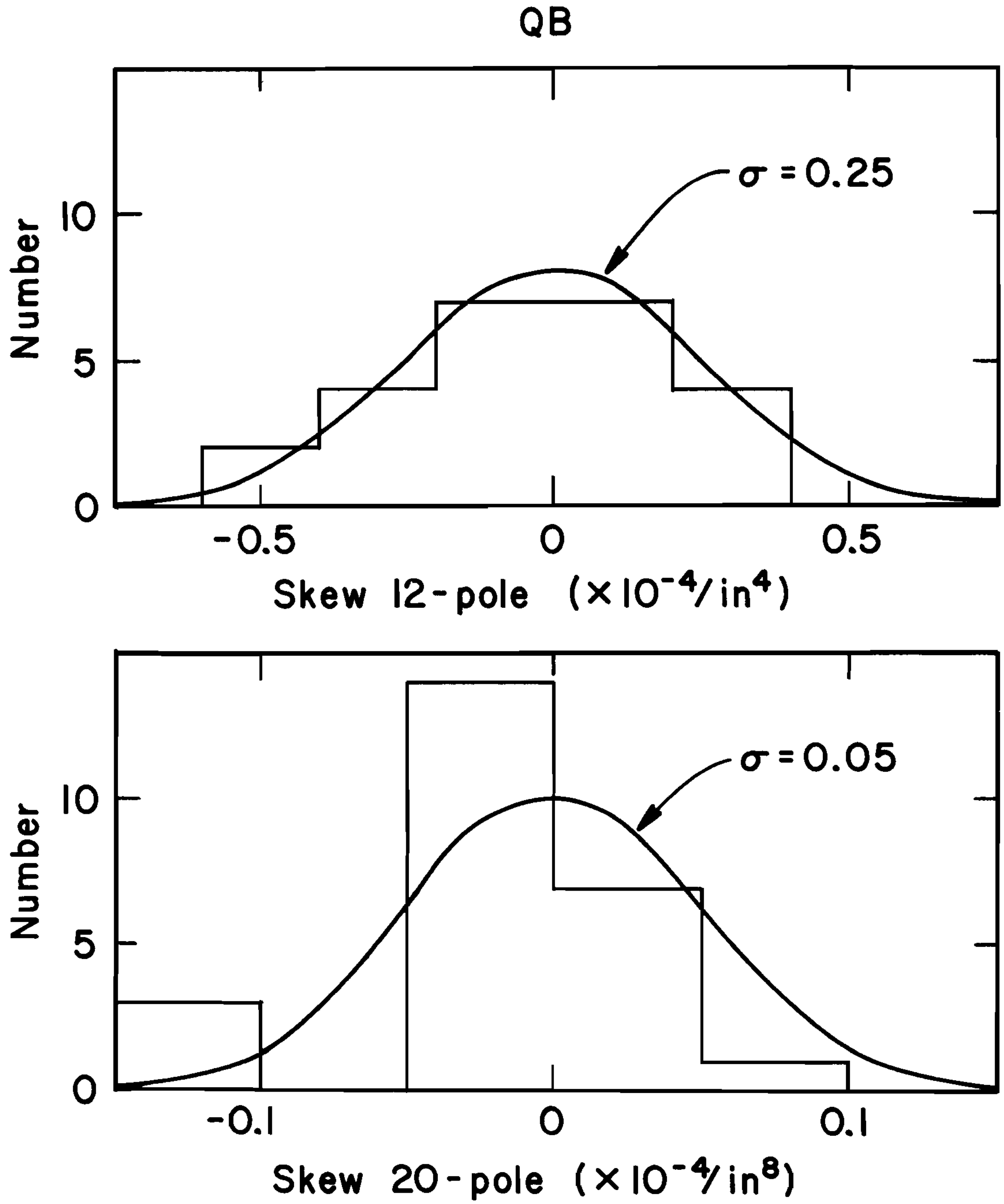

Fig. 3-19. Skew 12-pole and 20-pole distribution of quadrupoles. (Multipole field relative to quadrupole field at 1 in.)

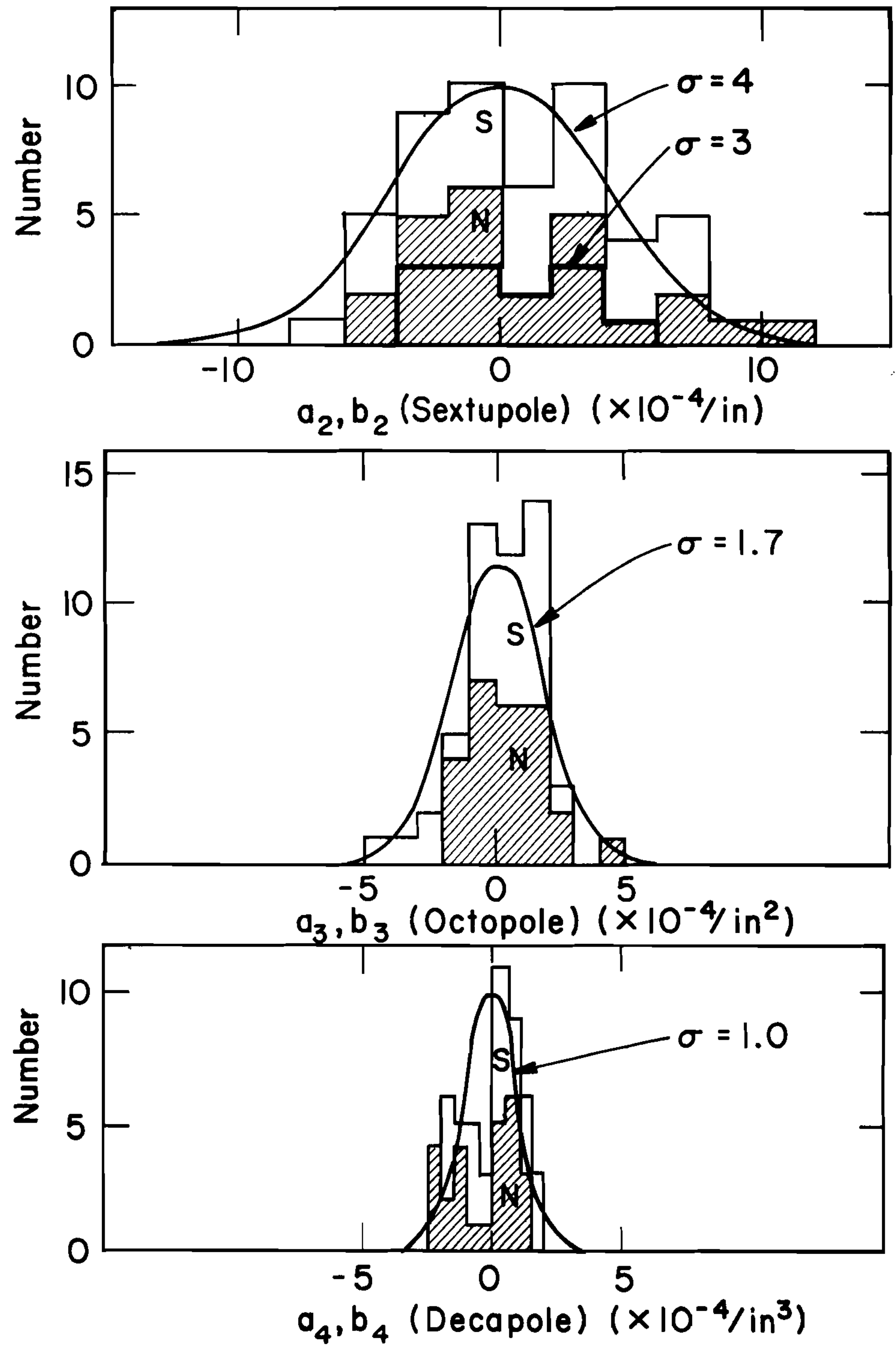

Fig. 3-20. 6-pole, 8-pole, and 10-pole distribution of quadrupoles. (Multipole field relative to quadrupole field at 1 in.)

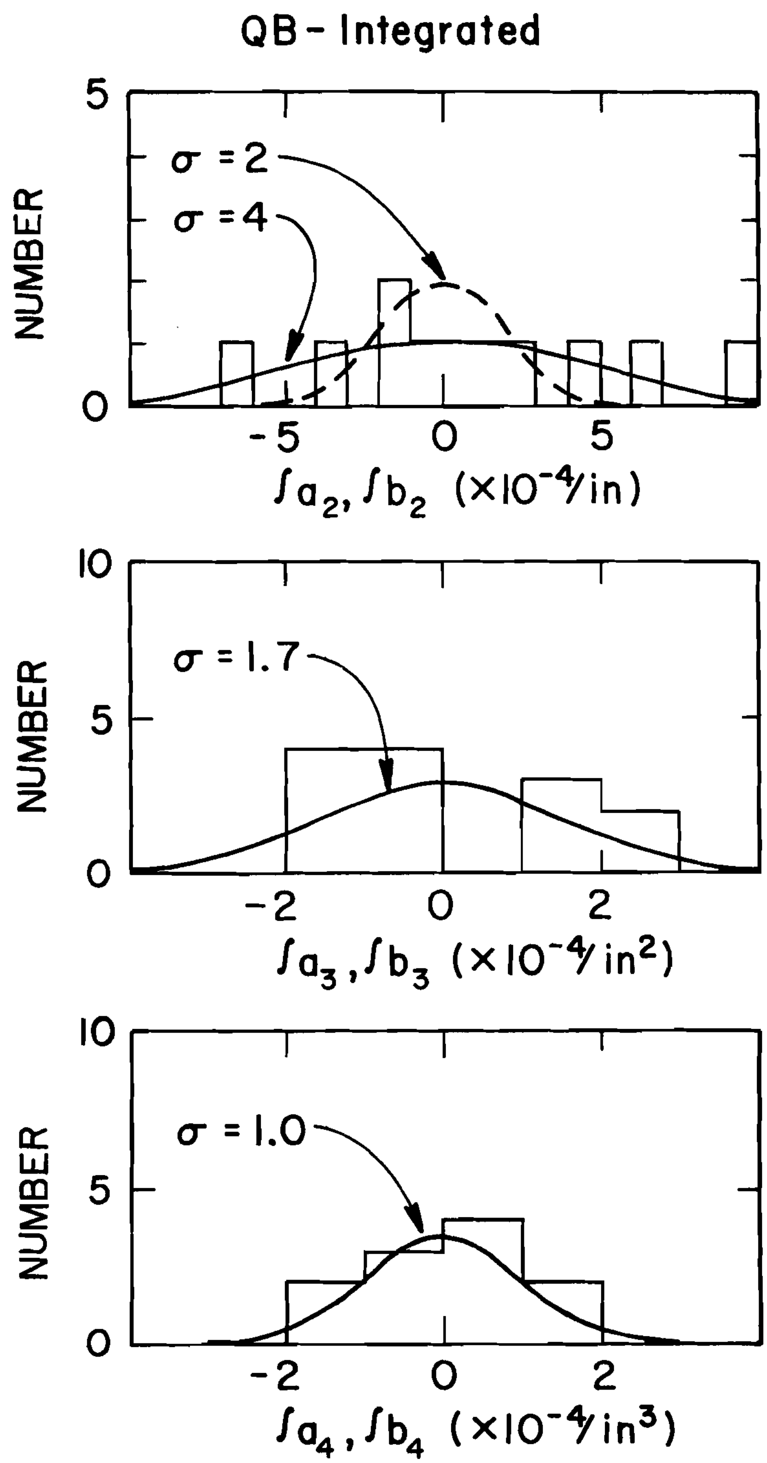

Fig. 3-21. Integrated 6-pole, 8-pole, and 10-pole distribution of quadrupoles. (Multipole field relative to quadrupole field at 1 in.)

References

[1] Recent Measurement Results of Energy Doubler Magnets, M. Wake et al., Proc. 1979 Particle Accel. Conf. (to be published) and Fermi National Accel. Laboratory Report UPC-95 (March 1979).

[2] R. E. Peters, IEEE Trans. Magnets 15, 135 (1979).

[3] The Amateur Magnet Builders Handbook, A. V. Tollestrup, Fermi National Accelerator Laboratory Report UPC-86, Feb. 22, 1979.

[4] Quadrupoles, G. R. Kalbfleisch and R. E. Peters, Fermi National Accelerator Laboratory Report UPC-42, January, 1979.

4. REFRIGERATION

4.1 Description of the Refrigeration System

Refrigeration is provided by a central plant (the CHL) with nitrogen and helium liquefiers and 24 satellite refrigerators in service buildings. This arrangement combines advantages of a single central facility with those of individual stand-alone units stationed around the ring. The central liquefiers have the high efficiency associated with large components, but requirements for distribution of cryogenic liquids and electric power to the service buildings are reduced. The likelihood of continued operation in the event of equipment failure is also significantly improved.

The total power to run the system is 11.33 MW. This provides 2,550 ℓ/h of liquid nitrogen, which in turn is used in the liquefaction of 4,000 ℓ/h of 4.6 K helium. The helium is then used in the 23 kW of 4.6 K refrigeration produced by the satellites.

The nitrogen reliquefier produces liquid into a 14,000-gallon dewar which supplies the needs of the CHL, the satellite system and the magnet shields. It operates in a closed cycle, collecting warm nitrogen gas from the magnet shields, the transfer lines, the helium cold box, purifiers, and satellites. The liquid is transported in vacuum-insulated transfer lines from the dewars to all use points.

Liquid helium from the central liquefier is collected in a 5000-gallon dewar and pumped through the feed line to each of the 24 satellites and subsequently distributed to the ring. Each satellite uses 144 ℓ/h for lead cooling and satellite "boosting." The boosting action results in 966 W of 4.6 K refrigeration being delivered to the magnet string. In this process, the liquid from the CHL is warmed to ambient temperature and recompressed for delivery back to the CHL and use in the high-pressure stream to the cold box. This system has the advantage of extracting the available refrigeration from the stream at each satellite location, reducing the size and cost of the necessary transfer lines.

Figures 4-1 and 4-2 show schematically the major components of the helium-refrigeration system. Figure 4-1 on page 65 shows the components located at the central helium-liquefaction facility. These are:

a) Two parallel helium compressors A and B.

b) A single oil-removal system C serving both compressors.

c) A medium pressure helium gas storage facility D which removes or adds gas to the system upon demand.

d) A compressor-seal gas-cleanup system E to repurify helium gas leaking from the compressor piston-rod packings.

e) The helium-liquefier cold box F.

f) A liquid-gaseous helium separator G in which the gas of the liquefier JT stream is separated from the liquid and returned to the liquefier.

g) A 5,000-gallon liquid-helium storage tank H.

h) A liquid-helium pump I followed by a subcooler to drive liquid helium from the CHL to the distribution system.

Figure 4-2 on page 66 shows the major components of one of the 24 satellite stations along the ring. Liquid helium circulates through the distribution line, which parallels the magnet ring. Excess liquid is returned to the storage dewar H of Fig. 4-1. Each satellite station refrigerator cold box M requires liquid in an amount sufficiently large to cool two strings of magnets. Liquid from M flows to the magnet string through a subcooler L. At the end of each magnet string the pressure of the

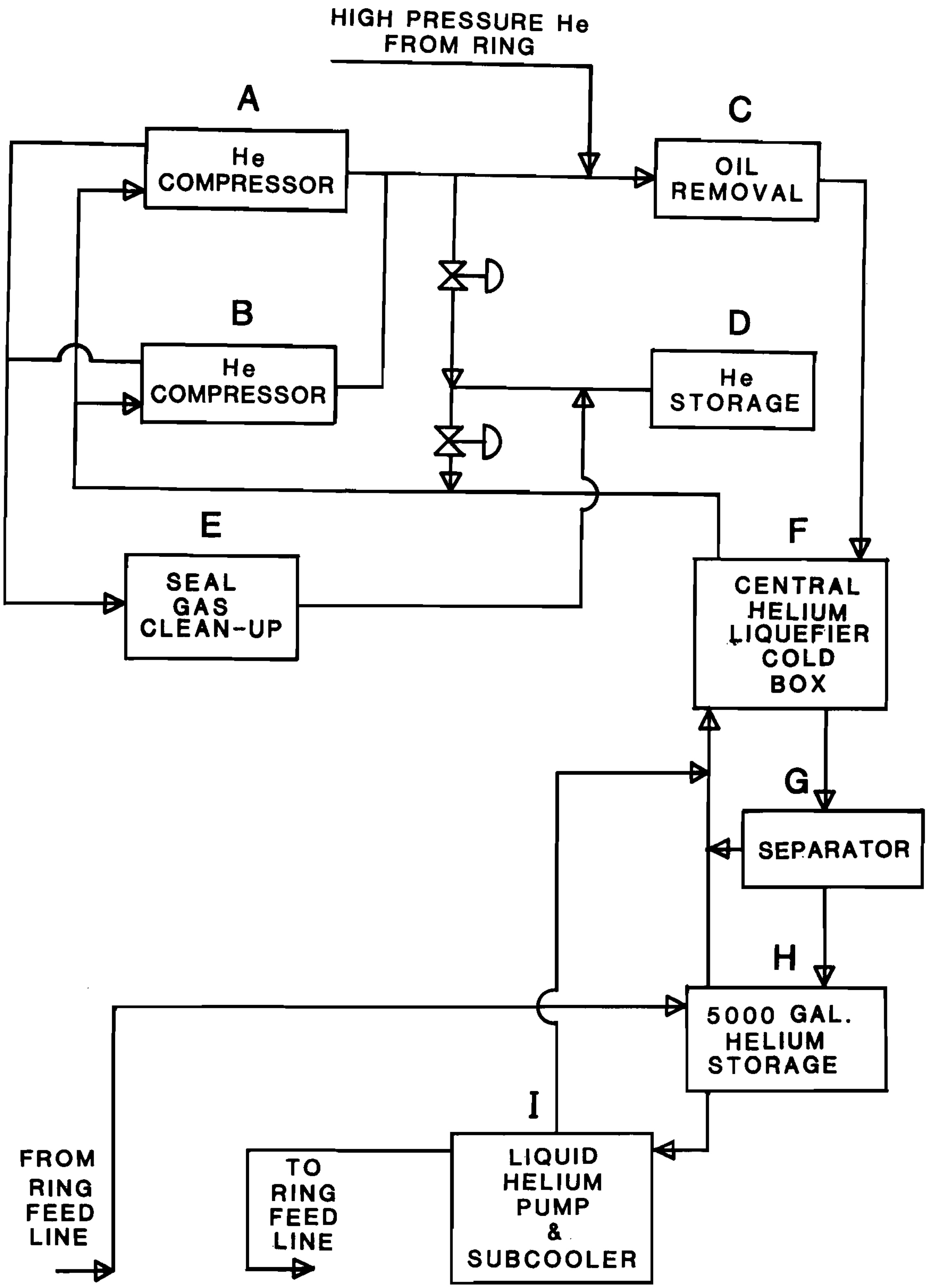

Fig. 4-1. Central helium liquefier.

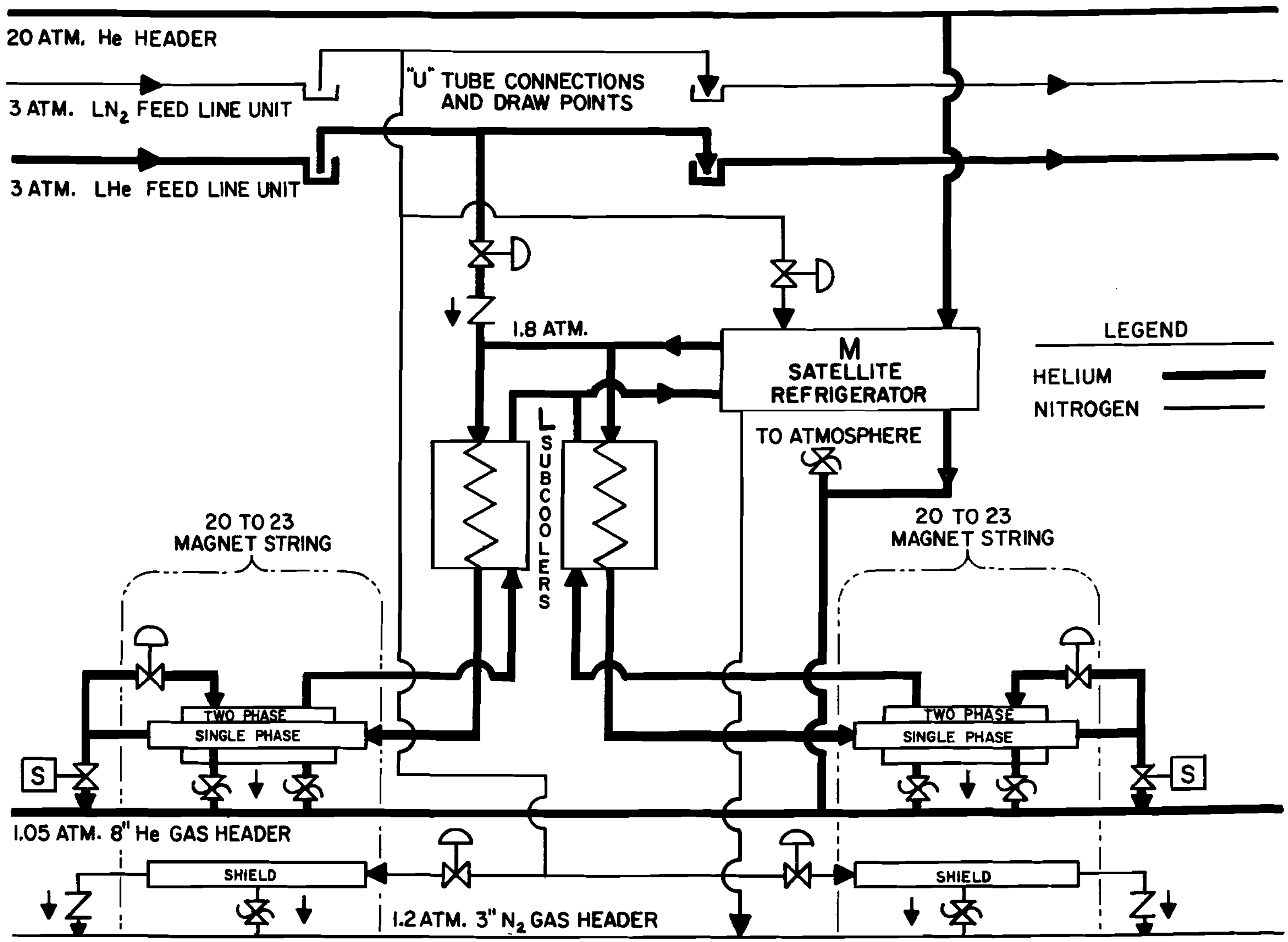

Fig. 4-2. Satellite refrigerator.

single-phase liquid is dropped in a JT valve and it is returned as two-phase liquid. This two-phase fluid cools the magnets and is returned to the satellite-refrigerator cold box M, after passing through the low-pressure side of the subcooler L.

An overall layout of the helium refrigerator system is shown in Fig. 4-3 on page 68, illustrating the relative location of the major refrigeration components, helium-transfer line and warm piping. Compressors of the satellite refrigerator are located in six service buildings along the ring. Low- and high-pressure gas is distributed through 8-in. and 3-in. pipes, respectively. The 8-in. pipe also serves to receive the low-pressure gas flow from the electrical leads and cooldown flow during the time when the ring is cooled from ambient temperature. Helium gas is returned to the CHL after compression by the satellite refrigerator compressors through the 3-in. high-pressure header.

4.2 System Requirements

The static heat load of a dipole magnet has been measured to be approximately 7 W at 4.6 K. AC eddy current and hysteresis losses are approximately 450 J per magnetic cycle. Quadrupole-package heat loads at 4.6 K are estimated to be approximately equal to those of a dipole. Tables 4-I and 4-II list the calculated load for the dipole and quadrupole magnets. The dipole numbers differ slightly from those measured from a string of magnets.

Each of the 24 satellite refrigerators supply subcooled single phase helium to typically 32 dipoles and 8 quadrupoles in the two parallel

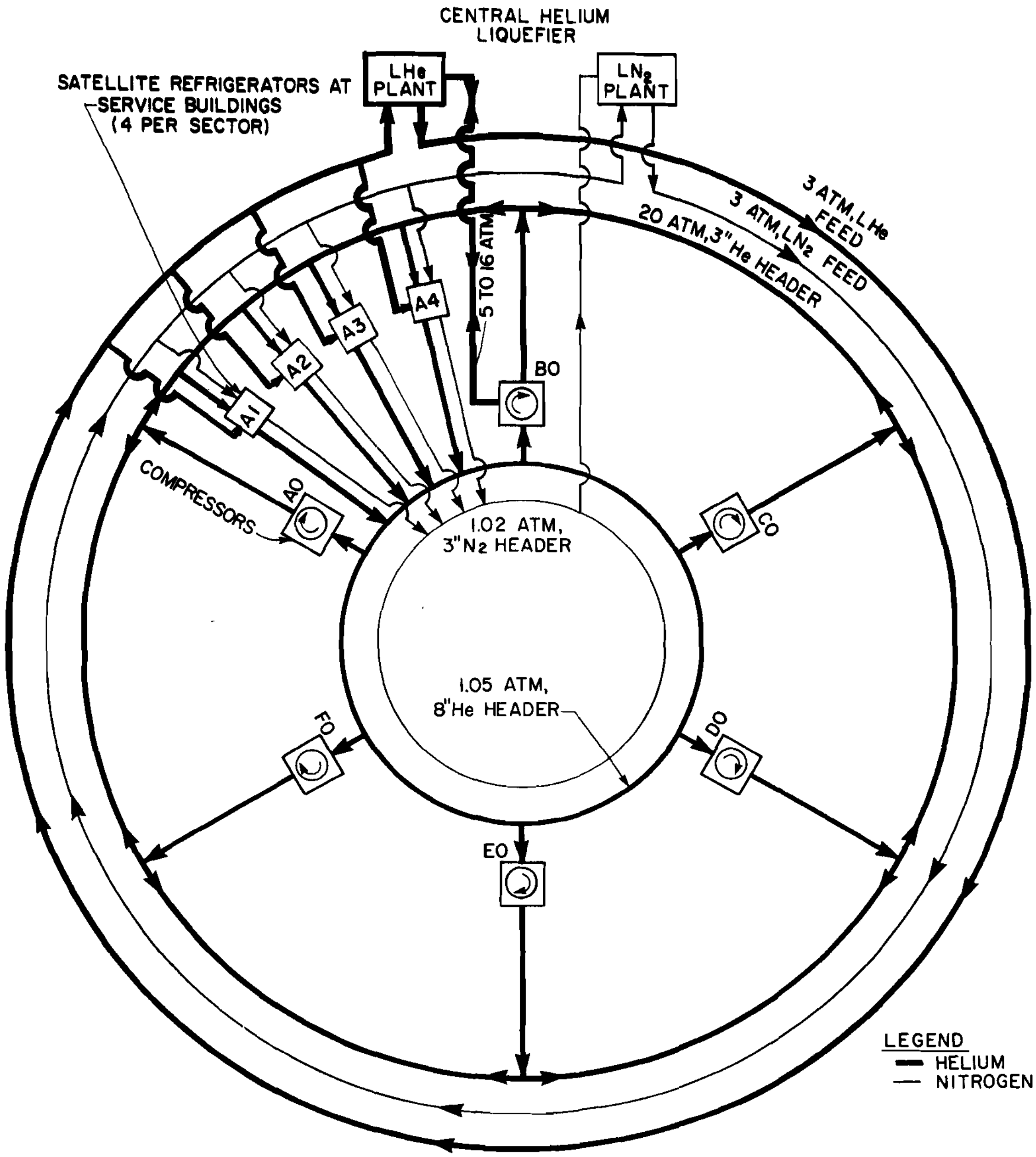

Fig. 4-3. Layout of the refrigeration system.

Table 4-I. Calculated Dipole Heat Loads.

Dipole Model 135 Cryostat	80 K W	4 K W
Infrared (main body)	10.08	0.381
Supports conduction	13.30	3.028
Anchor	1.00	0.164
Vent pipe (Mark 1 Model)	1.66	0.108
Instrumentation leads		0.156
Infrared (junction)	0.38	0.155
4 K cooling	-3.99	
Totals	22.43 W	3.992 W

Table 4-II. Calculated Quadrupole Heat Loads.

Quadrupole	80 K W	4 K W	Evap. ℓ/h
Infrared (main body)	6.41	0.210	
Infrared (junction)	0.19	0.008	
Supports conduction	3.04	0.680	
4 K cooling	-0.90		
Vent pipe for LN_2	0.27		
Vent pipe for 1ϕ	1.91	0.496	
Vent pipe for 2ϕ	1.57	0.325	
1 safety lead (5 kA)		1.000	
5 pairs of correction leads (75 A)		0.75	1.05
Instrumentation leads		0.156	
Totals	12.49 W	3.63 W	1.05 ℓ/h

cryogenic loops. The heat deposited in the liquid is exchanged with the return two-phase counterflow helium. The entire helium system is shielded by a two-phase nitrogen system. These systems are labeled in the dipole cross section of Fig. 3-1 on page 33. Table 4-III gives the distribution of loops in a sector with the location of the feed and turn-around points and the number of magnets per loop. Table 4-IV gives the heat loads and refrigeration and helium requirements of a worst-case

Table 4-III. Magnet Cooling Loops.

Building	Feed Station	Four Satellites per Sector: Turn-Around Station	Loop	Dipoles	Quads	Special Quads
1	15	11	1	16	3	3
		21	2	18	5	-
				34	8	3
2	25	21	3	16	4	-
		29	4	16	4	-
				32	8	-
3	35	29	5	16	4	-
		39	6	16	4	-
				32	8	-
4	45	39	7	16	4	-
		49	8	15	2	3
				31	6	3
Totals				129	30	6

Table 4-IVa. 4.6 K Refrigeration Loads (Worst Building).

	Each W	Each ℓ/h	1000 GeV DC W	1000 GeV DC ℓ/h	1000 GeV W	35 s cycle ℓ/h
34 dipole magnets	7.0	-	238.0	-	238.0	-
34 dipole ac losses[a]	13.0	-	-	-	442.0	-
11 quad magnets	7.0	1.05	77.0	11.55	77.0	11.55
11 quad ac losses[a]	11.0	-	-	-	121.0	-
1 pair 5000-A leads[b]	10.0	14.0	10.0	14.0	10.0	14.0
Set end boxes	20.0	-	20.0	-	20.0	-
Totals			345.0 W	25.55ℓ/h	908.0 W	25.55 ℓ/h

[a] 35-s cycle time
[b] 7 out of 24 buildings

Table 4-IVb. 80 K Nitrogen Requirements (Worst Building).

	Each W	1000 GeV DC W	1000 GeV 35-s Cycle W
34 dipole magnets	22.4	762	762
11 quadrupole magnets	13.5	138	138
Totals		900	900

service building. In the standard mode of operation the satellite refrigerator uses liquid helium from the Central Helium Liquefier to produce the necessary refrigeration in a building. In addition, the CHL must supply the liquid for the power leads. Specifications for the satellite are given in Table 4-Va and b and those for the Central Helium Liquefier and Nitrogen Reliquefier in Tables 4-VI and Table 4-VII respectively, shown immediately following.

Table 4-Va. Satellite-Refrigerator Parameters.

Mode	Consumption	Production
Satellite	129 ℓ/h He	966 W
Refrigerator	52 ℓ/h N_2	623 W
Liquefier	84 ℓ/h N_2	126 ℓ/h He
Accelerator standby	59 ℓ/h N_2	490 W + 26.6 ℓ/h He

Table 4-Vb. Mycom Satellite-Compressor Parameters.

Type	Screw
Stages	2
Power	350/261 Bhp/kW
Suction pressure	1.05 atm
Discharge pressure	20 atm
Throughput	57.54 g/s

Table 4-VI. Central Helium Liquefier Specification.

Inlet pressure	1.05 atm
Discharge pressure	12.3 atm
Flow rate (two compressors)	8,573 lb/h
Power required (two compressors)	2,470 kW
Power required (He air cooler)	52 kW
Liquid helium production (9,900 lb/h of He at 11.9 atm to the cold box)	≥ 4,000 ℓ/h at 4.6 K
Liquid nitrogen consumption per liter of liquid He produced	≤ 0.6 ℓ/ℓ

Table 4-VII. Nitrogen Reliquefier Specifications.

Nitrogen reliquefier	2,550 ℓ/h 54 tons/day
Production rate based on	
a compressor flow rate of	37,500 lb/h
suction pressure	1.05 atm
discharge pressure	123.5 atm
power requirement	2,540 kW

A summary of the total system requirements, consumption, and production specifications is given in Table 4-VIII, together with power requirements.

Table 4-VIII. Summary of Refrigeration Requirements. and Production Figures

Requirements	1000 GeV, dc W	1000 GeV, dc ℓ/h	1000 GeV, 35-s cycle W	1000 GeV, 35-s cycle ℓ/h
Helium				
Magnet system helium, 4.6K	7,480	350	19,918	350
Helium transfer line pump, 4.6 K	200		200	
Satellite consumption		≃1,548		3,096
Total	7,680 W	≃1,898 ℓ/h	20,118 W	3,446 ℓ/h
	W	Equiv. ℓ/h	W	Equiv. ℓ/h
Nitrogen				
Magnet system nitrogen, 80 K	21,600	490	21,600	490
Helium transfer line	4,500	100	4,500	100
CHL at 3,446 ℓ/h				2,068
Total at 3,446 ℓ/h He				2,658 ℓ/h
Total at max. operation				3,590 ℓ/h
Power				
		kW		
24 satellites		6,270		
Central Helium Liquefier		2,552		
Nitrogen Reliquefier		2,540		
Total		11,332 kW		

Production	W	ℓ/h
Helium		
Satellite refrigerators	23,000	
Central Helium Liquefier	200	≥4000
Nitrogen		
Reliquefier (Additional liquid nitrogen can be purchased at approximately $140 for 2400 ℓ)		2,550

4.3 Central Helium Liquefier

The central liquefier consists of three large compressors, a helium liquefier, nitrogen liquefier, purification equipment, and storage tanks. The compressors are surplus compressors from an air-separation plant. Two of the three have been modified for helium service, while the third will operate for nitrogen service. Nitrogen production is rated at 2550 ℓ/h. The liquid helium is fed from the storage dewar to a pump dewar, where it is compressed from 1.4 to 3.0 atm. The flow is then cooled to 4.65 K by heat exchange with liquid in the pump dewar. The dewar boil-off is returned to the liquefier as 5 K gas. The 4.65 K, 3-atm output of the exchanger feeds the ring transfer line.

4.4 Satellite Refrigerators

Each unit consists of a 35-ft long heat-exchanger column, a liquid expansion engine, two flow-splitting subcoolers, and a stand-by 30 K gas expansion engine. The unit has four modes of operation, as illustrated in Table 4-Va and shown schematically in Fig. 4-4. The primary mode, which will be used for the accelerator operation, is the satellite mode. The unit is continuously supplied 4.48 g/s liquid helium (plus 0.5 g/s power-lead flow) from the CHL. This causes an imbalance in the heat-exchanger flow (53.06 g/s supply vs 57.54 g/s return) giving a double pinch at 25 K and 5 K. The liquid engine expands from 20 atm to 1.8 atm, producing slightly subcooled liquid. The cold-end refrigeration comes from three sources: 44% from the heat exchangers flow imbalance, 48% from the liquid expander, and 8% from the central liquefier flow.

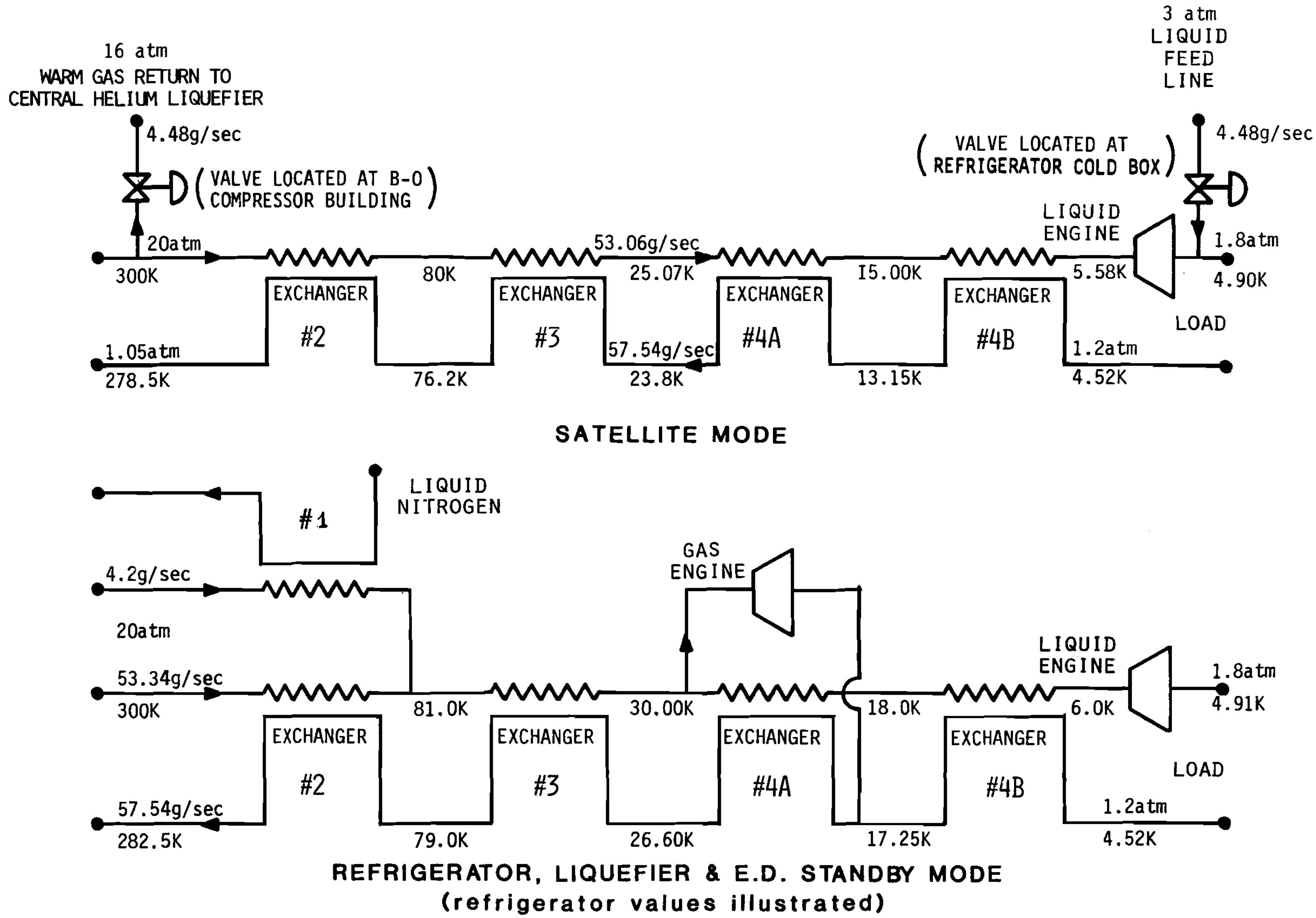

Fig. 4-4. Satellite refrigerator modes.

In the other three modes, liquid nitrogen is used instead of liquid helium. The stand-by gas engine is now operated at 30 K for these modes, while the liquid engine produces a two-phase liquid-gas mixture. We have tested the cold box and expanders in the first three modes and exceeded design in both the liquefier and refrigerator modes and 90% of design in the first attempt in the satellite mode. The stand-by mode is a mixture of refrigeration modes and liquification with a trade-off ratio of 5.0 W to 1.0 ℓ/h. This mode is designed to cool strings of magnets without the aid of the CHL both during initial construction and later during failures of the CHL. This mode was used for both the 10- and 25-magnet A1 runs. There are many additional mixtures of satellite and refrigeration modes that could be used if the CHL were operating at reduced efficiency.

4.5 Feed System

The liquid He and N_2 will be fed to the ring by a 25-section, 4-mile long vacuum-jacketed loop. The loop runs from the CHL to A4, around the ring in the proton-beam direction to A3 and then back to the CHL. The N_2 that is used to cool the shields of the magnets also provides the shield for the feed line. The sections are coupled by two rigid vacuum-jacketed U-tubes, each with a branch tee to feed the local satellite refrigerator. This will permit us to install, test, and cool down one section at a time without interfering with the operation of the rest of the system. With the connection of the last service building, A3, back to the CHL, we can take any section out of service for repair, if needed, by feeding the return line in reverse. We estimate a maximum 4.6 K heat load of 150 W and maximum 80 K load of 4500 W for the entire line.

The satellite gas piping consists of three gas header loops. On the wall of the tunnel behind the magnet, there is an 8-in. low-pressure He pipe and a 3-in. low-pressure N_2 pipe. The He pipe is the suction line for the compressors, as well as the main magnet relief and manifold for lead and cooldown flow. The N_2 pipe is the collection header for all shield flow, precooler flow, and also N_2 reliefs. The third header is a high-pressure He pipe that is located on the Main Ring road side of the berm. These are shown in plan in Fig. 4-3 and in elevation in Fig. 4-5 and Fig. 1-1.

Two 3-in. gas headers which connect to the CHL are located at A4. The first is a 10- to 18-atm bidirectional He gas line. Normally it is used as the gas return for the liquid supplied by the CHL, dumping gas into the discharge of the CHL compressors (13 atm). During startup and in accelerator standby mode, the line can also supply gas to the 8-in. header. The second header is teed into the 3-in. N_2 loop and is the main N_2 return for the N_2 liquefier.

The compressor system is located in the six "zero" buildings, with four compressors per building for maximum capacity. The compressors are connected across the two He headers with all twenty-four in parallel. The grouping of compressors into a header system totally decouples cold boxes from compressor operation; that is, we can shut down all four compressors at B0 without shutting down any cold boxes (but of course we have lost 1/6 of our total capacity).

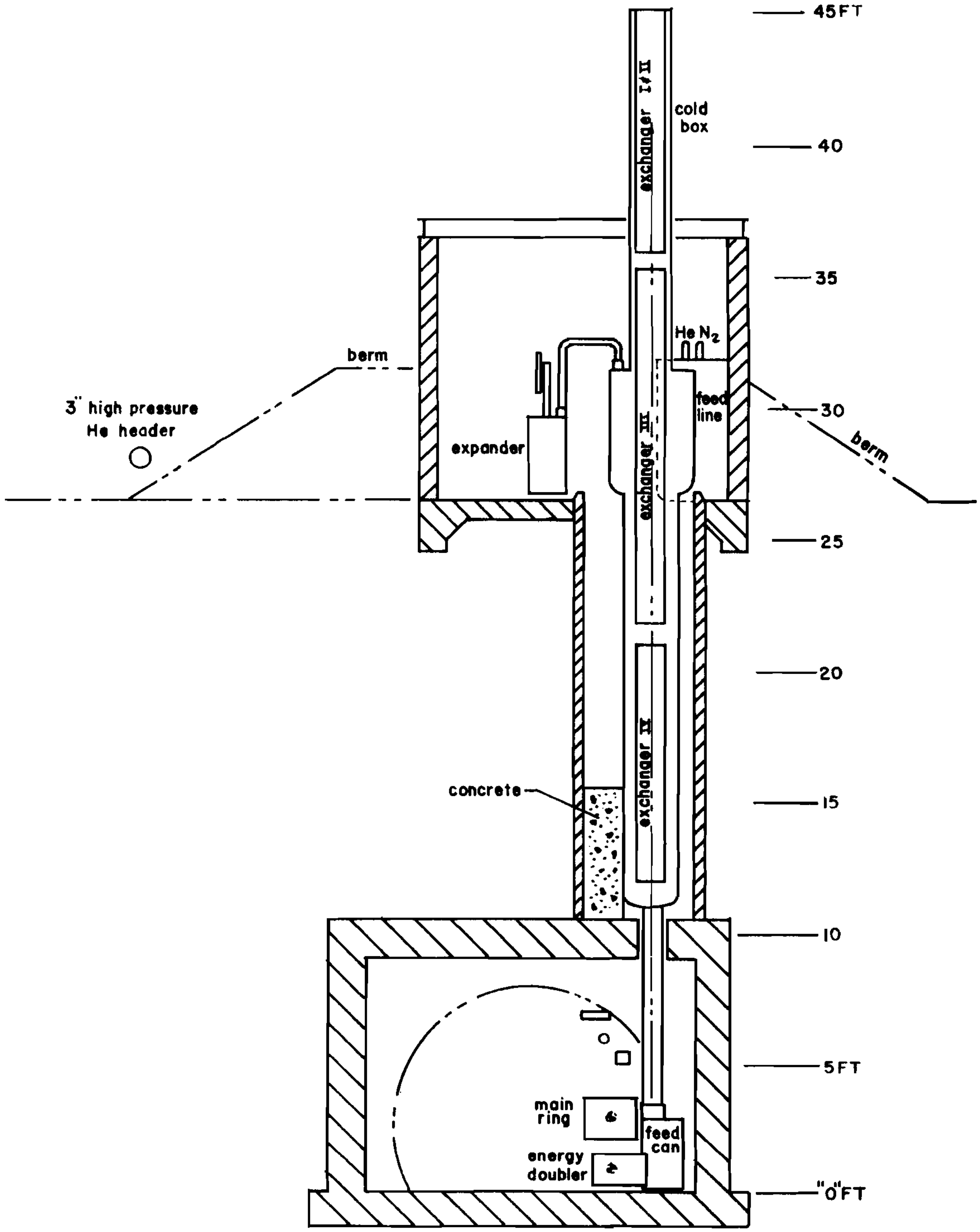

Fig. 4-5. Cross section of satellite refrigerator and cryogenic feed to the superconducting magnets in the tunnel.

4.6 Tunnel Components

The tunnel cryogenic system consists of 48 cryogenic loops. Figure 4-6 is a block diagram of one loop, giving the temperatures at significant points along the flow. The liquid helium is subcooled by a small heat exchanger in the feed box. It reaches equilibrium after the first magnet, at point 3. There is a small temperature rise, 0.05 K, from point 3 to point 4 because of the two-phase pressure drop from point 5 to point 6. The flow is controlled by the Joule-Thompson valve (JT) to maintain point 8 at 0.1 K of superheat.

The operation of the system at higher capacity is simply a matter of turning on additional compressors, since to first order the ratio of capacity to mass flow rate is constant. It must be noted that the pressure drop in the two-phase cryostat of the magnet plus the shell side of the heat exchanger varies as the square of mass-flow rate, so that the operating temperature of the shell side of the magnets increase with the square of the mass-flow rate.

$$T = T_0 + \alpha \left(\frac{F}{F_0}\right)^2 ,$$

where T_0 = 4.277 K. The parameter α for the shell side of the prototype refrigerator was designed to be as low as possible and was measured to be 0.4 K. We have redesigned the A2 cold box to give a lower value of this parameter.

The extreme importance of α as a design parameter is not generally appreciated. Commercial refrigerators give 0.3 to 0.4 K, but we have been trying to reach less than 0.2 K. Not only does a low α mean that one can

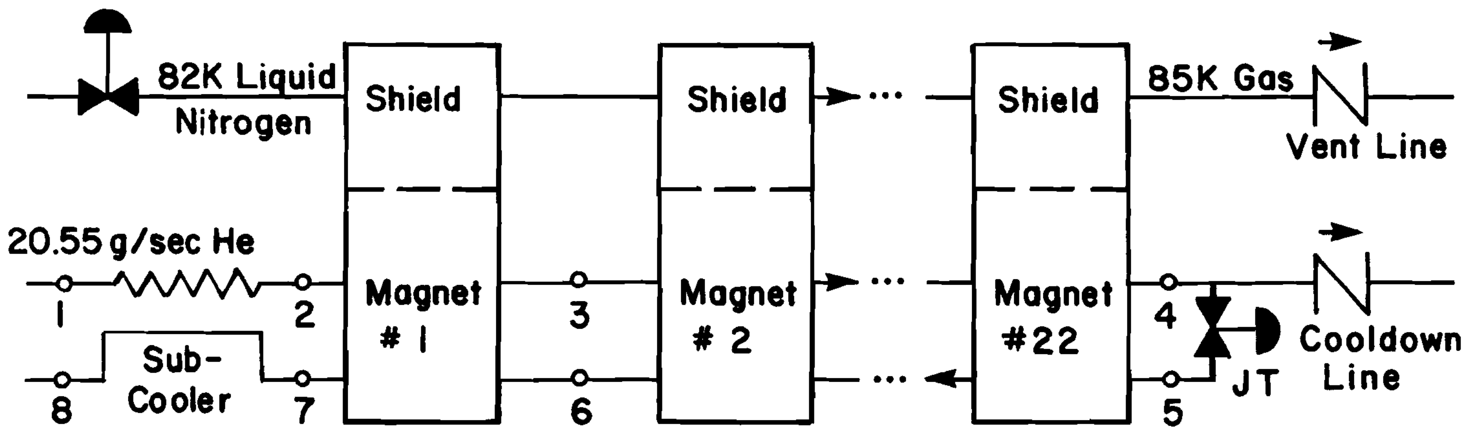

POINT	T(K)	P_{atm}	$H_{J/g}$	% LIQUID
1	4.90	1.8	14.22	100.
2	4.50	1.8	11.20	100.
3	4.55	1.8	11.47	100.
4	4.60	1.8	11.75	100.
5	4.47	1.25	11.75	96.
6	4.42	1.2	27.49	13.
7	4.42	1.2	27.99	10.
8	4.52	1.2	31.01	0.1K Super Heat

Fig. 4-6. Details of the cooling loop for a string of cryogenic magnets (1/48 of the ring).

operate at lower temperatures and, conversely, higher capacities in special areas (low beta, extraction, and injection), but also that one can operate at twice nominal capacity during quench recovery, which means a factor of 3 to 5 in recovery time. In addition, with the control system as installed at A2 we can automatically shift refrigeration from one loop to another or from one sector to another on a pulse-to-pulse basis, as the beam scrapes at different locations.

The main magnet cryogenic, vacuum, and electrical components are unavoidably interwoven. The cryogenic system consists of 48 single phase-two phase loops. Each satellite refrigerator feeds two loops and each loop has a JT valve at its far end. The beam-tube vacuum system (discussed in more detail in Section 5) has warm gate valves that isolate sections of each sector at (typically) ten locations. These valves are located between cryo loops and at the two ends of each warm region (the long straight section and the medium straight sections at locations 17 and 48). The electrical circuit (discussed in more detail in Section 6) for the main magnets consists of all coils connected in series along the coil bus and of foldbacks at the two ends of the B0 straight section bringing current back through the magnets along the return bus. Power-supply feed points are located once per sector at the same locations as one of the cryogenic feeds. Thus cryogenic feedthroughs of the two electrical buses are necessary at the end of every cryogenic loop except at B0. The interrelation between the three systems is illustrated for a typical sector in Fig. 4-7.

The feed box contains a pair of power leads where necessary, one or two cryogenic feedthroughs, a pair of subcoolers and instrumentation for

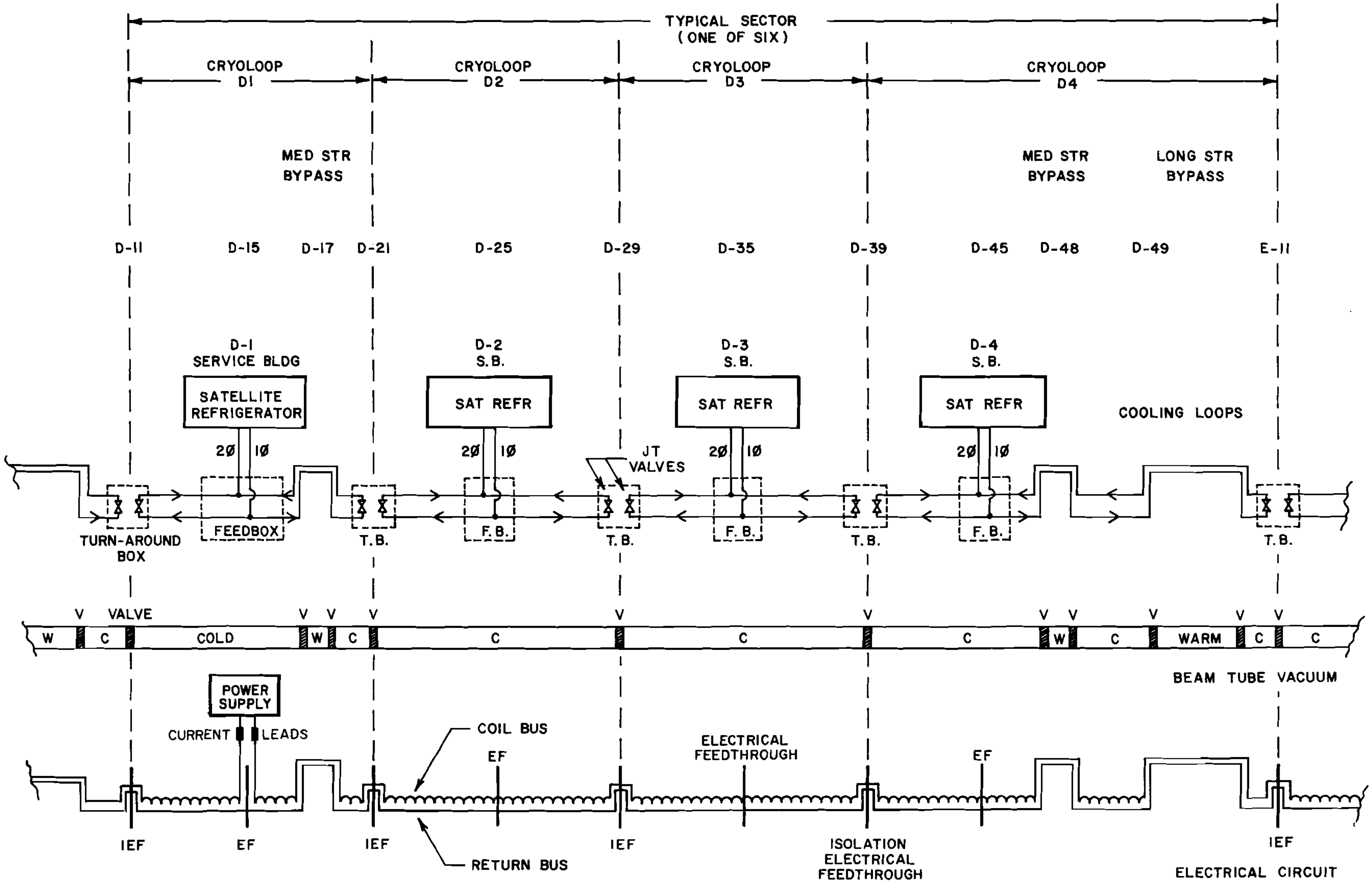

Fig. 4-7. Schematic of cryogenic components in the tunnel for a typical sector.

cryogenic control of the refrigerator and magnets. Figure 4-8 is a simplified engineering drawing of a feed box. These boxes are welded into the downstream ends of normal quadrupole cryostats at locations 15, 25, 35, and 45 and use 20 in. of available mini-straight space.

The turnaround box, shown in Fig. 4-9, has a cold-warm-cold transition for the beam-tube vacuum isolation valve, a pair of JT values for the turnaround of the two cryogenic loops, a pair of He cooldown vents, a pair of N_2 vents, and instrumentation for the cryogenic control of the refrigerator and magnets. In addition, it contains the special feedthroughs for the electrical circuits, which must be maintained at helium temperatures.

The design requirements on this electrical feedthrough are:

(i) During normal operation, it must make a 5000-A superconducting connection. Heat load per cryo loop is $\frac{1}{2}$ ℓ/h plus $\frac{1}{2}$ W maximum.

(ii) When one pair of cryoloops is cold and the adjacent pair is warm:

(a) The heat load into the cold loop shall be less than 5 ℓ/h plus 10 W.

(b) No surface in the warm loop shall be less than 0°C.

(iii) During warmup of a pair of cryo loops, the feedthrough must be able to carry current starting at 1000 A, decreasing to 10 A over a 4-h period. During this period, there is no heat-load limit on the cold loops.

The turnaround boxes are also welded into the quadrupole cryostats and use 20 in. of mini-straight space. They occur at locations 11, 21, 29, and 39.

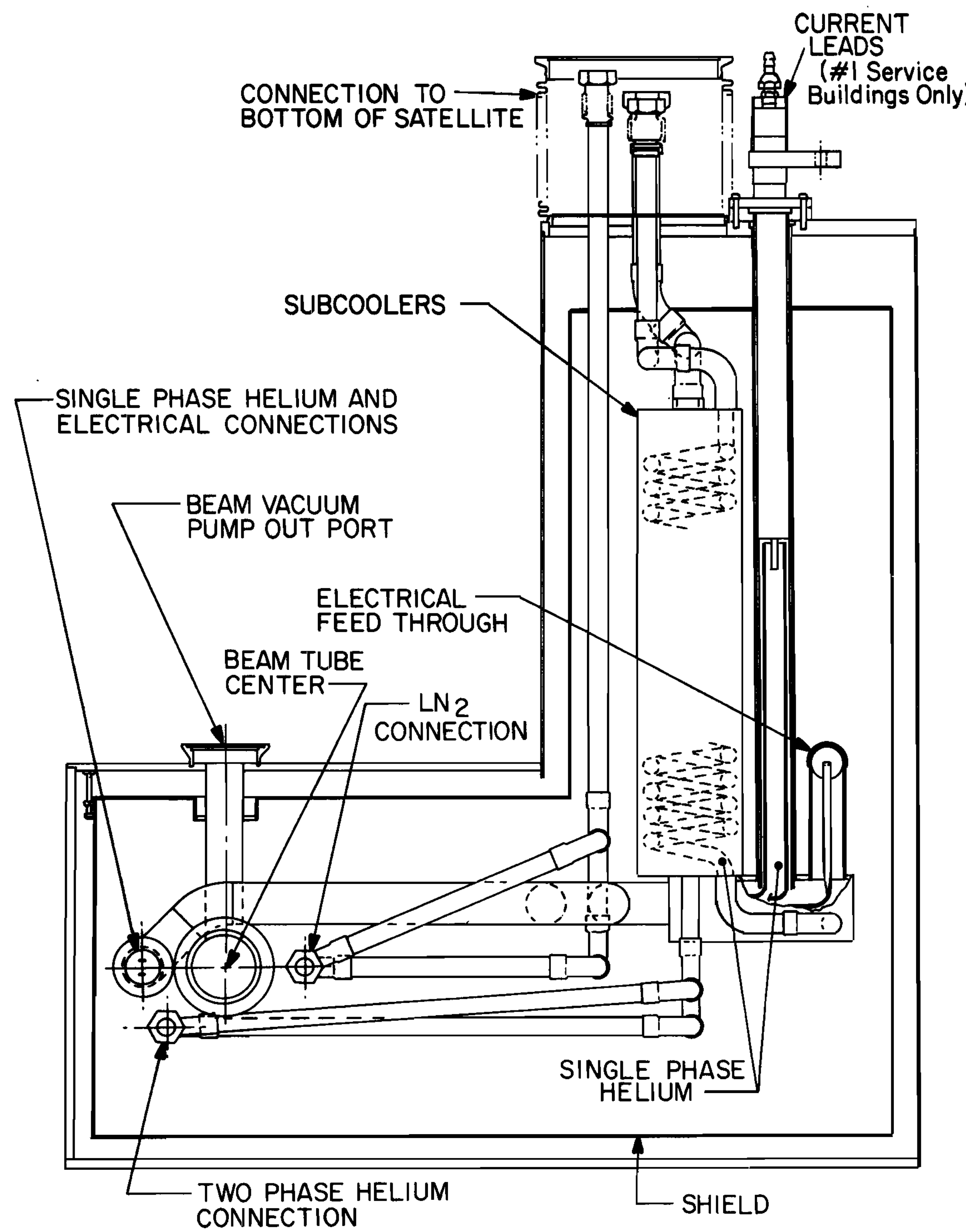

Fig. 4-8. Feed box.

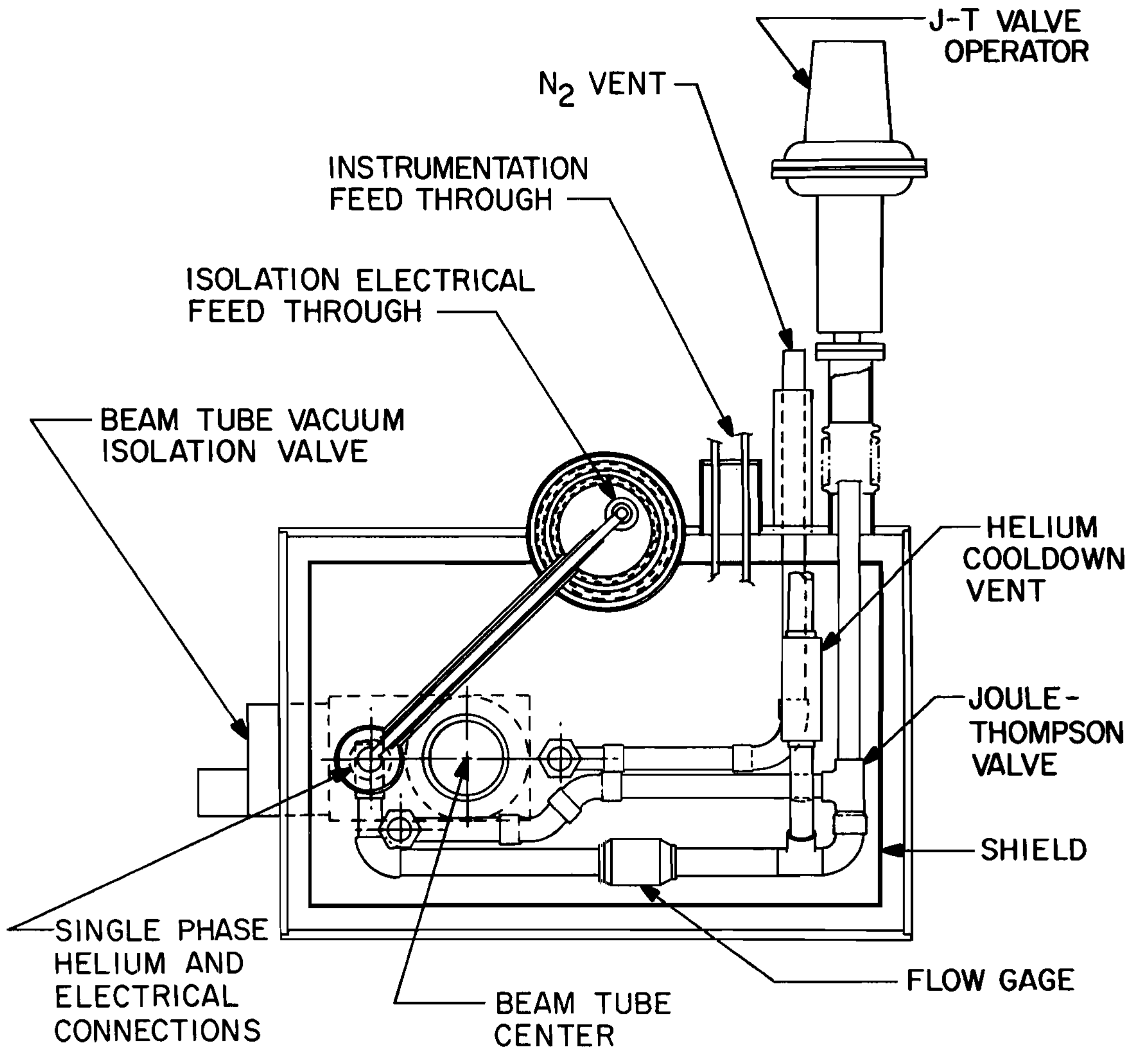

Fig. 4-9. Turnaround box.

The straight section bypasses occur at the long straight sections and at locations 17 and 48. At these locations a helium-transfer line containing the two power leads is brought out parallel to the beam tube for the length of the straight section. Straight-section space required for the bypass and cold-warm transitions is a total maximum of 25 in. for both ends. Isolation vacuum valves and sublimation pumps will require an additional 24 in. of straight-section space at each end. Figure 4-10 illustrates a typical bypass.

4.7 Cooldown and Warmup

If one attempted to cool down long strings of magnets in the normal operating mode, it would take several months or might be altogether impossible, because the magnets are heat exchangers and therefore most of the refrigeration that is supplied is heat exchanged with the return line and then vented. We therefore use single-pass cooling of the single-phase rather than loop flow, with the two-phase deadheaded. The wave front is very steep and travels through the magnet string much like a step function through a transmission line; the discharge remains at room temperature during almost the entire cooldown cycle.

Cooldown with the CHL operational is very straightforward. The satellite is tuned up in the liquefier mode, producing 126 ℓ/h, which is added to the 200 ℓ/h from the central (if one is cooling only one service building this might be as high as 2000 ℓ/h, stress, pressure drops, and thermo-acoustic oscillations permitting). This helium is run through the single phase of the magnets, returning to compressor suction by way of the cool-down lines, where it recompresses to 20 atm. The excess gas is then

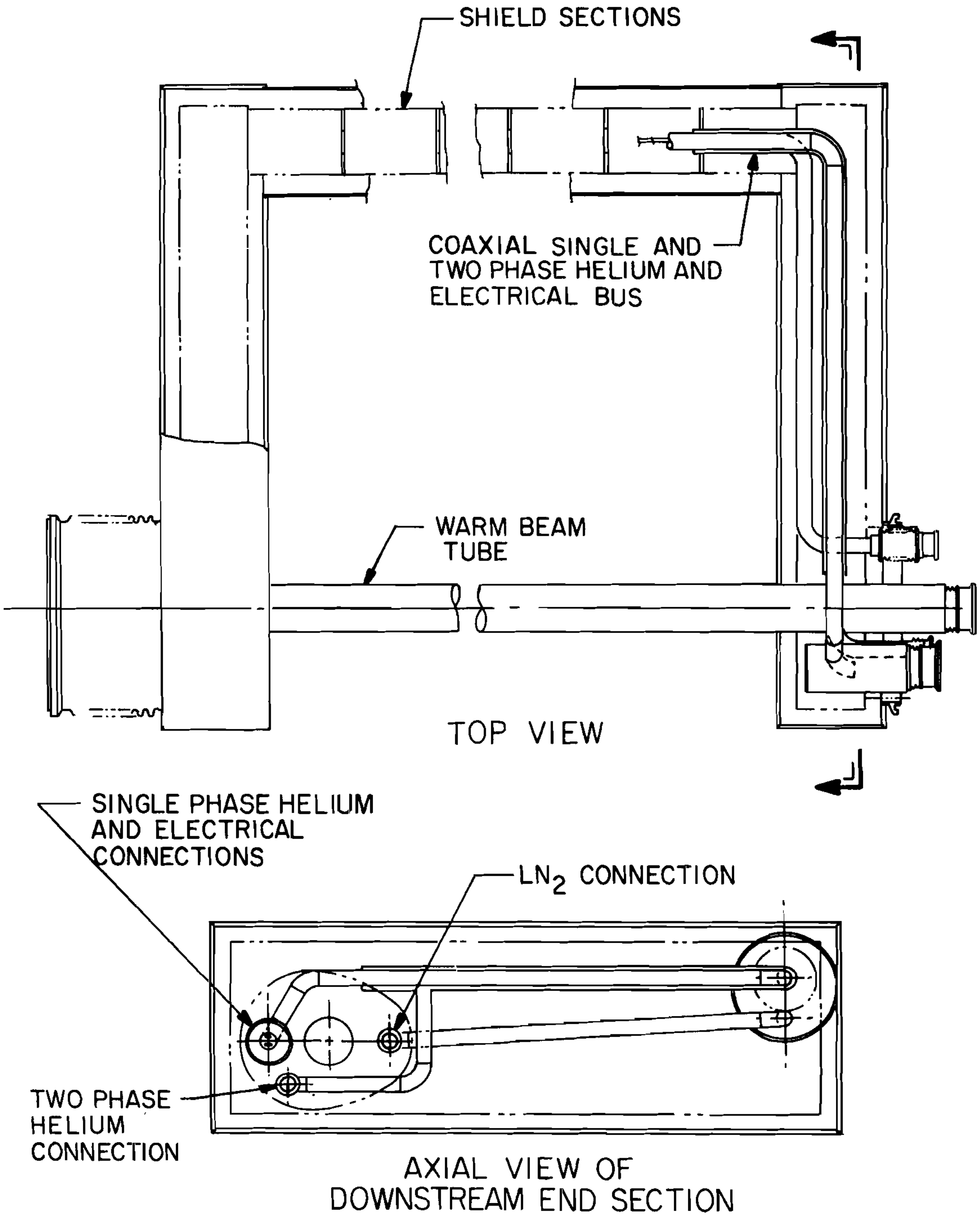

Fig. 4-10. Bypass.

returned to the discharge of the CHL compressor (13 atm), where it is reliquified. When the wavefront reaches one of the cool-down lines, it is shut off and the magnet JT is opened. When it reaches the second one, the same is repeated, 1000 ℓ are transferred from the central to fill the magnets, the dry engine is turned off and the satellite is tuned for the satellite mode.

If the CHL is not operational, cooldown is slightly more complicated, but can be carried out using the liquefier mode followed by the standby mode of the satellites. Since the CHL was not complete, this mode was used to cool the 25-magnet string in the A1 tests.

Cool down after a quench is a function of the energy dissipated in the magnet. For a quench during injection, recovery time should be less than 100 s. During the 25-magnet A1 test, the system recovered much faster than the length of time it took to turn on the power supply.

For fast recovery at high power levels we require a fast electronic valve control circuit which does the following:

(i) Fire relief or auxiliary cool-down valves at both ends of quenched half-cell in a time $\Delta t < 50$ ms.

(ii) Close JT valve in $\Delta t < 2$ s.

(iii) After 5 seconds, close valve on quad closer to refrigerator.

(iv) Run in cool-down mode, venting into suction header at the quad further from refrigerator until T_{out} equals 10 K.

(v) Close second quad valve and open JT valve.

(vi) Refrigerate and fill.

Warmup is a function of the electrical status of the magnets. If there is continuity in the electrical circuit, the string can be warmed up in 4 hours using either the main power supply or a special warmup supply.

If electrical continuity is lost, several heater supplies can be installed across the safety leads so that, combined with hot gas from the compressor, a heating rate of 50 kW can be achieved (10-20 h warmup).

If both electrical continuity is lost and there are large holes in the single-phase He cryostats, hot N_2 at 3 atm is connected and warmup takes several days.

4.8 Failure Modes

Because of the complexity of the system, it is highly probable that at any one time, one component may be down and several may be operating at reduced efficiency. The system must be designed to continue to cool the magnets with at most a reduced ramp rate. Table 4-IX gives projected replacement and beam-off times for various component failures. Times do not include an allowance for troubleshooting the system and travel time for the repair crew; troubleshooting in many cases can be longer than replacement times. The extremely rapid replacement time is possible because of our concept of separate cryostats and quick-disconnect vacuum U-tubes.

Table 4-IX. Operation in Failure Modes.

Defective Component	Consumption Times Replacement (ℓ/h)		Beam Off (h)	Replace-ment (h)	Ramp Rate (min)	Action Taken	Comments
	He	N_2					
Normal operation	144	20	-	-	1		
Central Helium Liquefier	0	79	-	as needed	5	start gas engines	
Central Nitrogen Liquefier	144	20	-	as needed	1	buy N_2	\$105/h for total ring
Feed line	144	20	1.0	168-336	1	reverse flow	
Magnet	-	-	48	48	beam off		
Satellite Cold Box	-	-	48	48	beam off		
Satellite Compressor	144	20	-	as needed	1	turn on standby com-pressor	each comp. is 4% of total re-frigeration
Satellite Wet Expander	400	20	2×0.1	2	1	sat. JT valve	
Satellite U-Tube	as needed	20	0.1	0.1	beam off		
Feed U-Tube	as needed	-	0.5	0.5	beam off		

5. VACUUM SYSTEM

5.1 Description

The vacuum system consists of three different systems, each with its own particular characteristics and requirements:

1. Cold beam tube, vacuum sections in which the beam tube is at cryogenic temperature (about 4.6 K).
2. Warm beam tube, vacuum sections in which the beam tube is at room temperature.
3. The cryostat insulating vacuum which is completely separate from the two systems above.

The beam tube is, of course, continuous around the ring, approximately 6 km in length. The beam-tube vacuum around the ring is conveniently divided into 24 sections which coincide with the 24 cryoloops. Each section terminates in a turnaround box at either end. At each of these points there is a short (about 10 cm) warm section of the beam tube with isolation valve (section valve).

The beam tube is cold except in the six long straight sections and the twelve medium straight sections at locations 17 and 48. Additional warm space will be provided between the quadrupole doublets at the ends of the long straight sections where necessary. Each of these warm sections of the beam tube has an isolation valve at each end. Vacuum barriers built into the superconducting quadrupoles subdivide the insulating vacuum into approximately 200 sections, each about 30 m long. The following is a separate description of the details for each of the three vacuum systems.

5.2 Cold Beam Tube

5.2.1. Pumpdown. Prior to cooldown the beam tube is pumped out via "sniffer" ports located near each section valve and at each cryogenic feed box, which is approximately mid-way between section valves. The pumping is done with a slightly modified version of the standard pump station. (A description of the standard pump station is given in Sec. 5.5) Assuming normal surface phase contamination for clean but unbaked stainless steel, it should take a few hours to reach a pressure of 10^{-5} torr. This roughing is done with the section valves closed. When the beam tube is cold external pumping is no longer required and the pump stations are valved off. Calculations and measurements show that at 4.6 K there are essentially no gas phenomena in the tube. This is true even for helium if the coverage of helium on the beam tube wall is a small fraction of a monolayer. Assuming a pressure of 10^{-5} torr at the start of cooldown and assuming that the gas is condensed on the wall more or less uniformly during cooldown, the resulting wall coverage would be about 10^{-3} of a monolayer. If the residual gas were all helium (the worst case, and very unlikely), this would result in an equilibrium pressure of less than 10^{-11} torr at 4.6 K.[1]

Furthermore, if there is a small leak, the helium admitted into the beam tube through that leak would also be pumped onto the wall very near the leak. As the buildup of helium on the wall increases, the equilibrium pressure in that region also increases and the gas migrates to a previously clean region close by and is again pumped onto the wall. This phenomenon is very slow, taking hours or perhaps even days for leaks as large as 10^{-7} torr·liters/sec to move the distance of a half cell. In other words, it is impossible to give a practical definition of the conductance for the cold tube and very difficult to pump the cold tube effectively with lumped or periodic pumps.

5.2.2. Pressure measurements. The pressure in the beam tube is difficult to measure for at least three reasons, first, for the same reason that it is difficult to pump the cold beam tube, second, because any penetration into the tube will have a high pumping speed of its own, since it is also cold and probably has a higher wall-area to cross-sectional area ratio than the beam tube itself, and third, because the measurement will be dominated by the outgassing of the warm parts of the measuring device.

We have tried to solve some of these problems by the use of what is called the "sniffer" shown in Fig. 5-1. During the beam-tube pumpdown, the sniffer is baked at 200° C to decrease the surface contamination. When the magnet is cold, the copper sleeve in the sniffer is at 80 K so that it is not pumping helium or hydrogen. To decrease the background further, the warm parts of the sniffer are outgassed in a vacuum furnace at 900° C before assembly into the cryostat. The conductance of the sniffer is about 10 liter/sec for hydrogen.

Sniffers will be located at each quadrupole, as shown in Fig. 5-2. Every sniffer will be equipped with a Bayard-Alpert gauge, capable of measuring pressures down to about 2×10^{-11} torr. The sniffers used for pump-out will have low and medium vacuum gauges useful for monitoring the pumpdown. All connections are made with Conflat type copper gasket flanges. All the devices connected to the beam tube except the gate valve are all-metal.

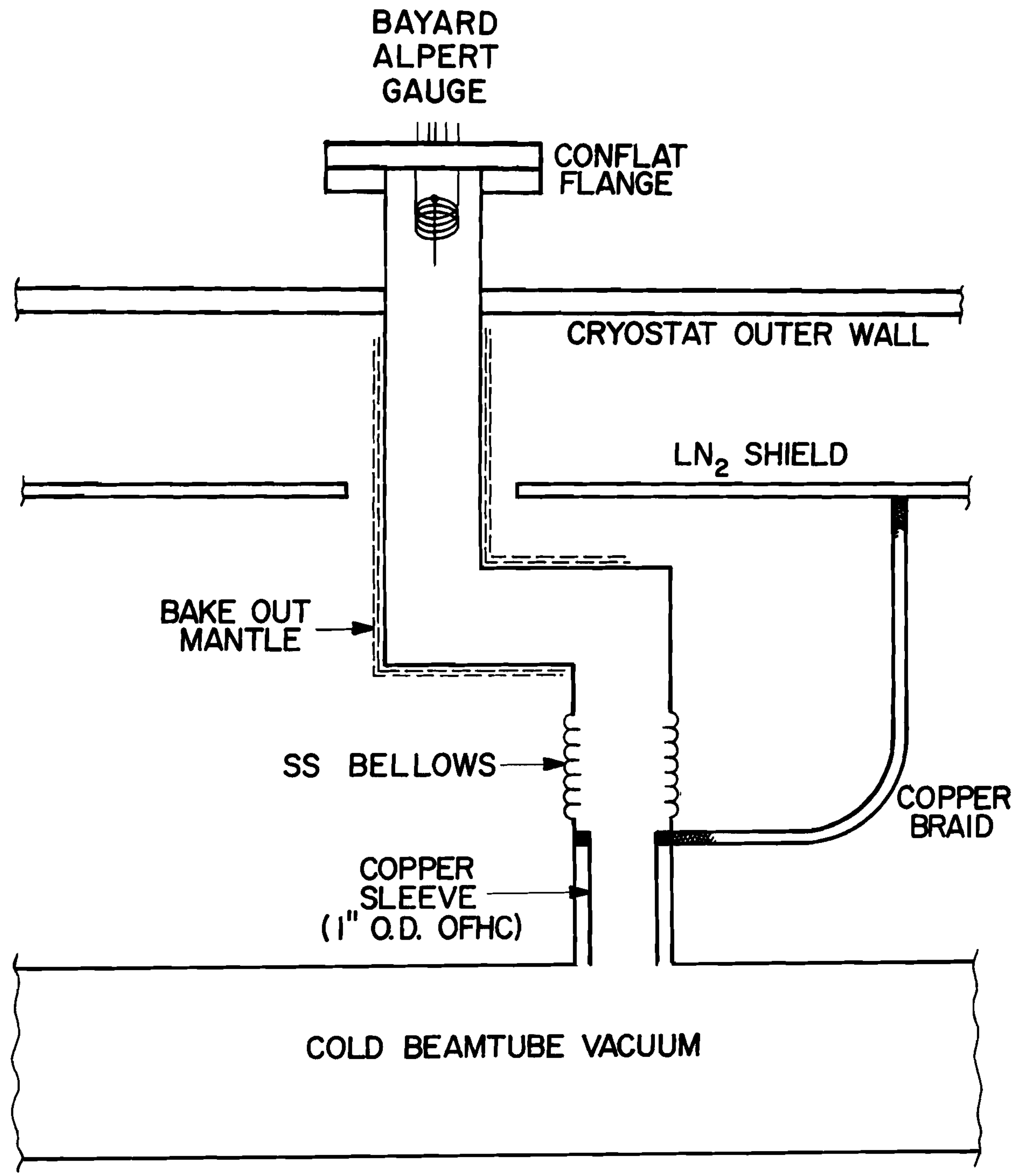

Fig. 5-1. Schematic of the "sniffer" port to the cold beamtube vacuum.

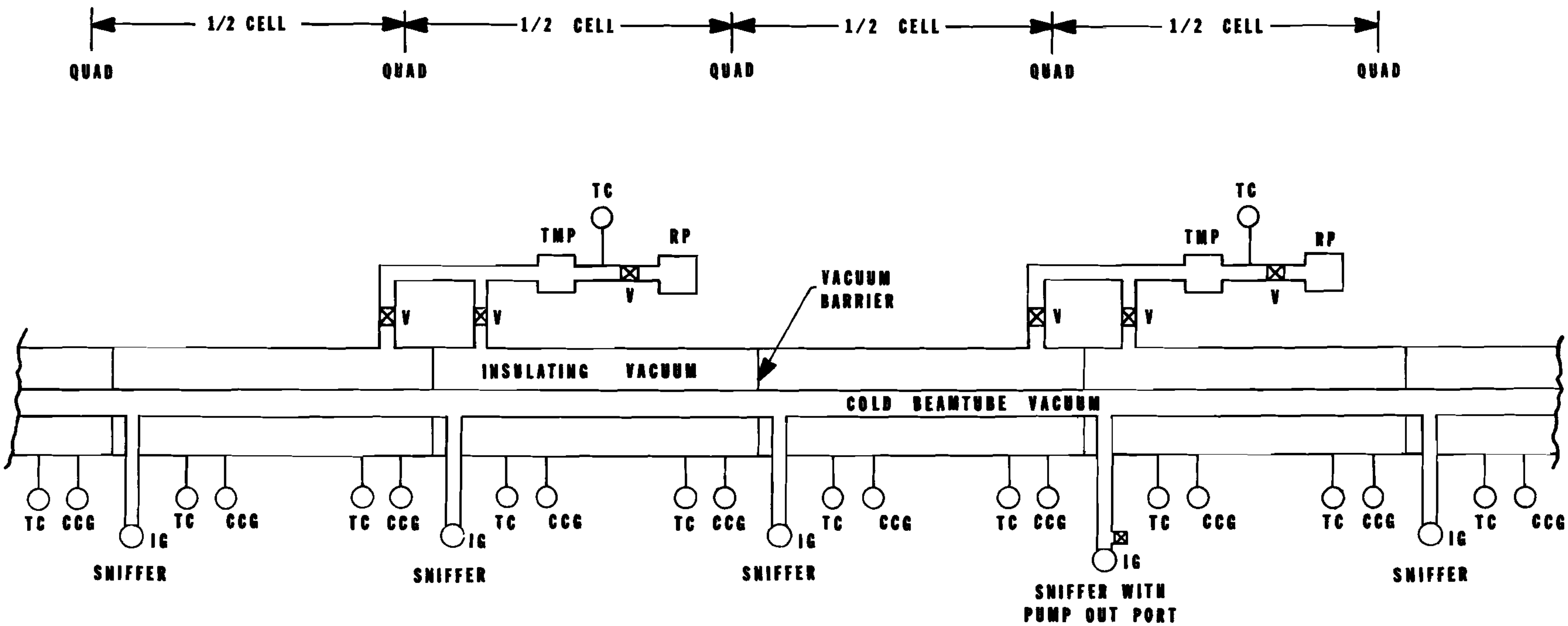

Fig. 5-2. Typical section of cold beamtube and insulating vacuum.

At a later time, if it proves necessary to have more pumping capacity for the beam tube vacuum, the sniffers can be fitted with small sputter ion pumps.

5.2.3. Section gate valves. The section gate valves all operate at room temperature. They have a 4-in. diameter nominal bore and are made of stainless steel, sealed with bellows, and operated electropneumatically. The valves between two cold sections have elastomer seals, probably of ethylene propylene. This material has reasonable outgassing properties, takes a minimum set, and has very good radiation resistance. Reliability, space limitations, and cost dictate the use of elastomer gate seals. They are open almost all the time and our experience in the Main Ring has been that they stand up very well. Ethylene propylene seems to be still flexible enough to seal after a dose of 10^9 rads. Because of the high pumping speed of the cold bore, there will be very little, if any, pressure rise in the vicinity of the valve. The gate valves in the warm sections of the beam tube vacuum will probably be all-metal, including the gate seals.

5.2.4. Interlocks. In order to prevent a cold section from pumping on a warm section, thus contaminating the beam-tube wall, the section gate valves are interlocked to the Bayard-Alpert gauges. They cannot be opened unless the pressure on both sides of the valve is less than some specified pressure, perhaps 10^{-8} torr. The exact value of the set points will be determined from operating experience, but there will be no manual override of the interlock. The valves are closed automatically upon pressure rise, or loss of power, after a beam abort has been generated.

5.2.5. Beam-tube design and quality control. Because of the difficulty of pumping on a cold beam tube, it is extremely important that there be very few leaks. On the other hand, because there is no outgassing of the tube when it is cold, it seems unnecessary to bake the tube in situ or otherwise degas it. The only treatment is to wash the tube in a caustic degreasing agent and a nitric acid pickling bath and maintain a clean environment for it.

The tube material is 316 L stainless steel sheet with a matte 2-D finish. This finish is chosen because it has a high ratio (>3) of real surface area to apparent surface area and thus a high capacity to pump helium and hydrogen on its surface. The tube is rolled to approximate shape, machine TIG welded, drawn to final shape, and annealed.

A key point in the design of the cryostat is that, apart from the seam weld, there are no welds made on the beam pipe that face liquid helium. All the welds, bellows, and seals are in the insulating vacuum. This means, for example, that a leak in a beam tube seal must be very large to be of any consequence because the insulating vacuum is usually better than 10^{-7} torr. The seal between the beam tubes of adjacent magnets is made with a lead-coated C-seal, trapped in a rotatable, bolted flange set.

In addition to the final leak check of the completed cryostat, each magnet is to be leak-checked cold during and after field measurement at the Magnet Test Facility. When the magnet is connected in the tunnel, the seal and bellows are again checked with a helium leak detector by evacuating the beam tube and bagging and flooding the seal area with helium gas. The leak check is then completed by pressurizing the single-phase helium loop.

5.2.6. Miscellaneous points relating to beam stability.

(i) The pressure-bump instability. This instability is due to runaway of gas desorption from the beam tube walls. It is a function of beam current, geometry, pumping speed, temperature, and pressure, at least. Calculations and measurements[2, 3] indicate that the ring could circulate 5 to 10A before wall desorption would be a problem. This is true even for large wall coverage of hydrogen or helium and arises from the very high pumping speed of the cold wall. We conclude that the pressure-bump instability will not be a problem in the cold sections of the ring.

(ii) Trapped electrons in the beam. Ionization electrons produced by the beam can be trapped in its potential well and cause beam instabilities. We do not consider this a serious problem because of the large gap (1.9 μs) in the circulating beam, which must be there to accomodate the risetime of the abort kicker. This gap, together with rf bunch structure, should give sufficient time for electrons to be swept from the beam region.

5.3. Warm Beam Tube

The warm sections of the beam tube vacuum are the six long straight sections (50m long) and the twelve medium straight sections at locations 17 (approx. 14 m long) and 48 (approx. 8 m long). These sections must contain all devices not incorporated in the main magnet system such as kickers, injection and extraction magnets, dampers, separators, and so on. The vacuum system in these regions will be an integral part of this equipment. The average pressure required in these warm regions is 10^{-8} torr. At the interfaces between the warm pipe and the cold pipe, we must provide high pumping capacity in order to prevent the cold region from pumping gas from the warm sections and contaminating the walls. Titanium getter (sublimation) pumps will be added at these interfaces. The sublimation pump plus gate value assembly will use 24 in. of drift space at each interface, as shown in Fig. 5-3.

5.4. Cryostat Insulating Vacuum

In order to decrease the static heat load, the insulating vacuum should be better than 10^{-5} torr. Below this pressure, heat transfer by radiation and conduction across the layers of superinsulation dominates. Our experience has been that in a good leak-tight system the vacuum is much better than that; in fact, it is usually less than 10^{-7} torr. The major difficulty in achieving a good insulating vacuum is the location and elimination of leaks. To facilitate this task, the insulating vacuum has been subdivided into approximately 200 sections by permanent vacuum barriers in each of the quadrupoles, as shown in Fig. 5-2.

5.4.1. Pumpdown. We have chosen to use turbo-molecular pumps to pump out the insulating vacuum (see Section 5.5). Even though the conductance in the insulating space is extremely low, if there are leaks it is advantageous to pump on the space even when the magnets are cold, because a large number of layers of the superinsulation are relatively warm and gas which migrates to those areas can be effectively pumped. Pump stations will be placed at every other half-cell boundary, each station pumping on two half-cells. The number of pumps (approximately 100) can be increased as experience warrants.

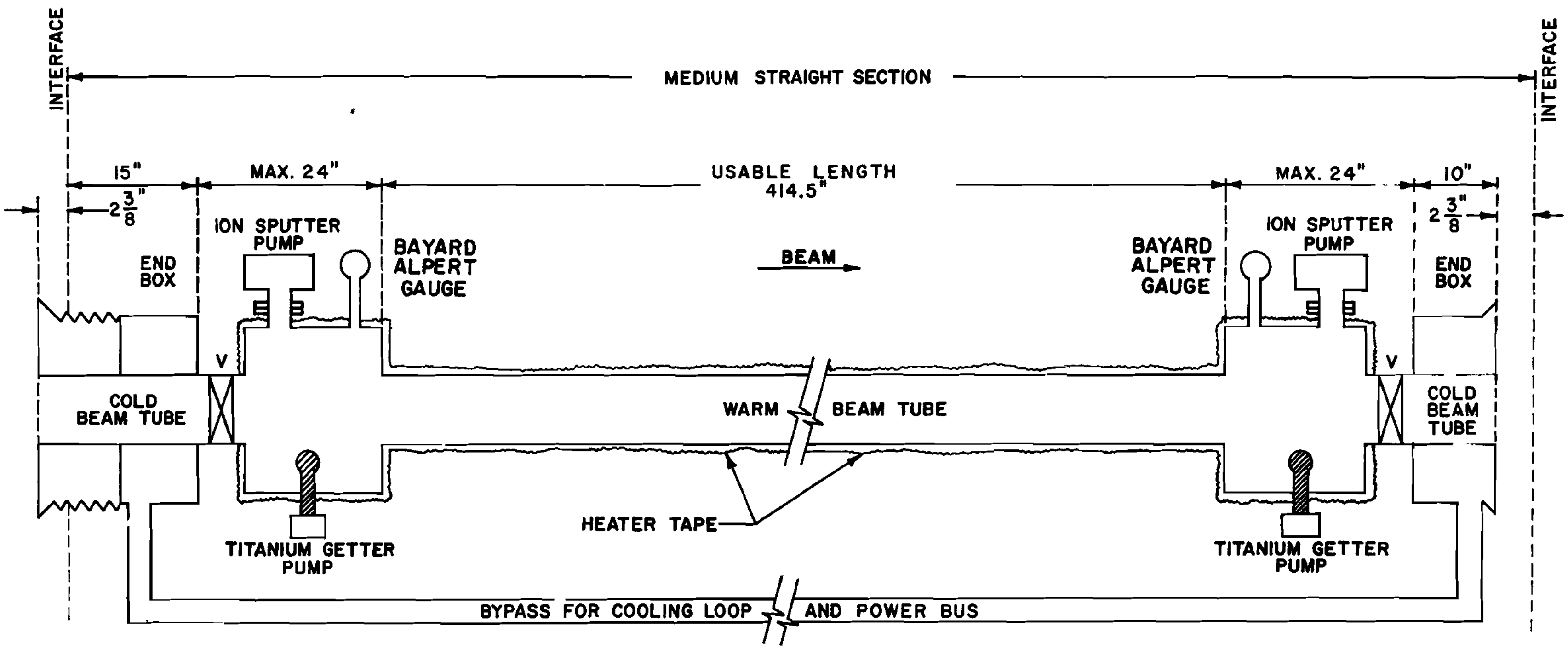

Fig. 5-3. Warm beamtube with cryogenic bypass in medium straight section.

When roughing begins, the turbopumps are started at the same time as the rotary-vane pumps, with the gate valve open. In this mode the turbopump acts as a trap for oil vapor backstreaming out of the rotary-vane pump. (The first time a region is pumped it is advisable to purge it a few times with dry nitrogen to remove water vapor.) Cooldown is started after a final leak check with the pressure less than 10^{-3} torr. If there are no leaks the pumpdown takes about 6 to 8 hours. If the superinsulation has been pumped previously and let up to dry nitrogen, the pumpdown time is much faster, taking only 1 or 2 hours. If the cooldown is started at too high a pressure, water vapor and other gasses condense on the superinsulation, degrading the emissivity and thereby increasing the heat load.

5.4.2. Pressure measurement. The pressure gauges are shown in the diagram of Fig. 5-4 and explained in Section 5-5 along with valves and interlocks.

5.5 Pump Stations

All the pump stations are essentially identical. A standard insulating vacuum pump station is shown schematically in Fig. 5-4.

5.5.1. Pumps. The pumps are a small turbo-molecular pump of approximately 100 liters/s capacity, backed by a direct-drive two-stage rotary vane pump of approximately 5 ℓ/s capacity.

The turbo-molecular pump is mounted with its axis in the horizontal direction by means of a 4 in. ID Conflat flange. The roughing pump is mounted near the pump and connected with a flexible stainless-steel hose.

5.5.2. Valves. Each pump station has two electropneumatic gate valves of 4 in. ID with Conflat flanges. These are all-stainless bellows-sealed valves with elastomer O-rings of ethylene propylene. In addition, there are two hand-operated valves between the roughing pump and the turbopump. They are used during leak checking, when the leak detector is used as the roughing pump for the turbopump and the normal roughing pump is valved off. This gives very good pumping speed to the leak detector and increases the sensitivity.

5.5.3. Pressure measurements. There are five gauges at each roughing station:

1. A thermocouple gauge with fast response (Pirani gauge) monitors the roughing line.

2. A Pirani gauge and a cold-cathode high-vacuum gauge, sensitive to pressures down to 10^{-6} torr, measure the insulating vacuum on each side of the vacuum barrier.

5.5.4. Interlocks. The gate valves automatically close when power is lost. In addition, they are interlocked to each Pirani gauge in order to protect against loss of vacuum on either the high-vacuum side or the backing-pump side. This protects the turbo-molecular pump (TMP).

Other interlocks protect against overtemperature of the TMP and power loss to either pump. A sudden rise in the insulating vacuum will also cause a beam abort and closing of the beam section valves, in addition to closing the roughing gate valves and turning off the TMP.

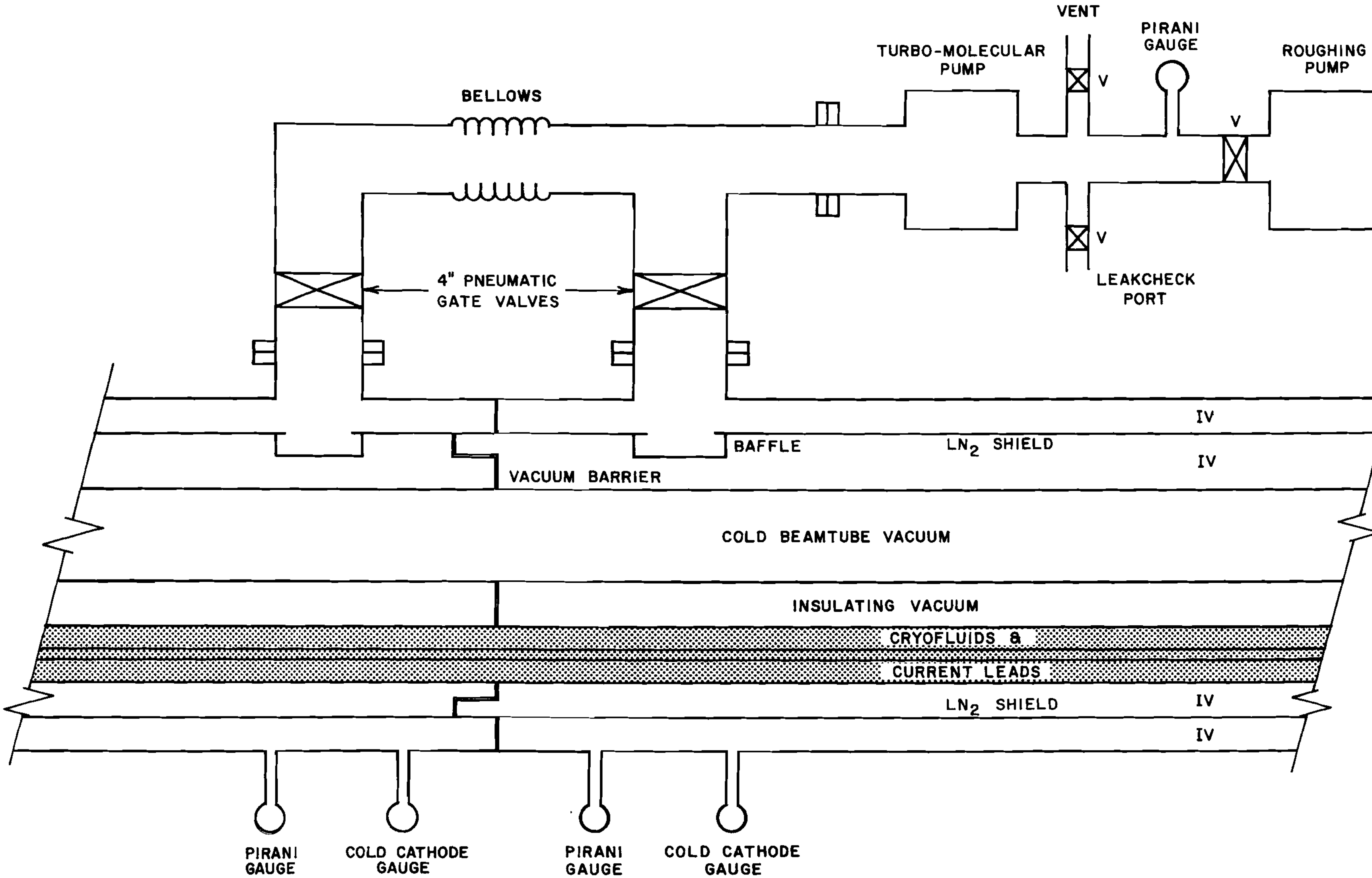

Fig. 5-4. Pump station for insulating vacuum.

When the pumps are turned off they are automatically vented. This stops the TMP from rotating and reduces the chances of damaging the pump.

5.5.5. Power requirements. Each TMP is powered from the service building by a frequency converter unit which requires 10A at 208V, 3 ∅. Each rotary-vane pump uses 20A at 208 V, 3 ∅; its contacts are controlled from the service buildings.

References

[1] Pressure Measurements in a Cryogenic Environment, D. Edwards, Jr., and P. Limon; Journal of Vacuum Science and Technology, 15 (3), May/June 1978.

[2] A Vacuum Cold Bore Test Section at the CERN ISR, C. Benvenuti, R. Calder, N. Hilleret; CERN ISR-VA/77-19.

[3] Ion Desorption of Condensed Gases, N. Hilleret and R. Calder; CERN ISR-VA/77-33.

6. MAGNET POWER SUPPLY AND PROTECTION

6.1 Requirements

The main magnet system is a single series circuit of 774 dipoles and 216 quadrupoles distributed around the 1-km radius ring. There are also typically ten main quadrupoles in each low-beta section and a large number of correction elements powered separately from the main circuit.

The main power supply must be capable of pulsing the entire series circuit, whose total distributed inductance is 36 H, from 500 A to 4400 A at ramp rates up to 330 A/s. It also must have invert capability so that the 350 MJ of energy stored in the magnetic field can be returned to the power line during de-excitation. The supply must also be capable of dc operation at maximum current. The current regulation needed for slow beam extraction and beam storage is extremely good, on the order of 10^{-5}, and the dc supply must be capable of this.

The cable used in the magnets has a low copper-to-superconductor ratio and is not cryogenically stable. Thus a magnet will quench if a normal region develops. Consequently, a fail-safe mechanism for removing the stored energy from the system must be provided. A reliable quench detector is necessary to trigger this protection system.

6.2 Power Supply

The main power circuit is illustrated in Fig. 6-1 on the next page and parameters of the power supply are listed in Table 6-I. All the magnet coils are connected in series on the coil bus and the current returns through the return bus, which is a superconducting winding adjacent to the main coils

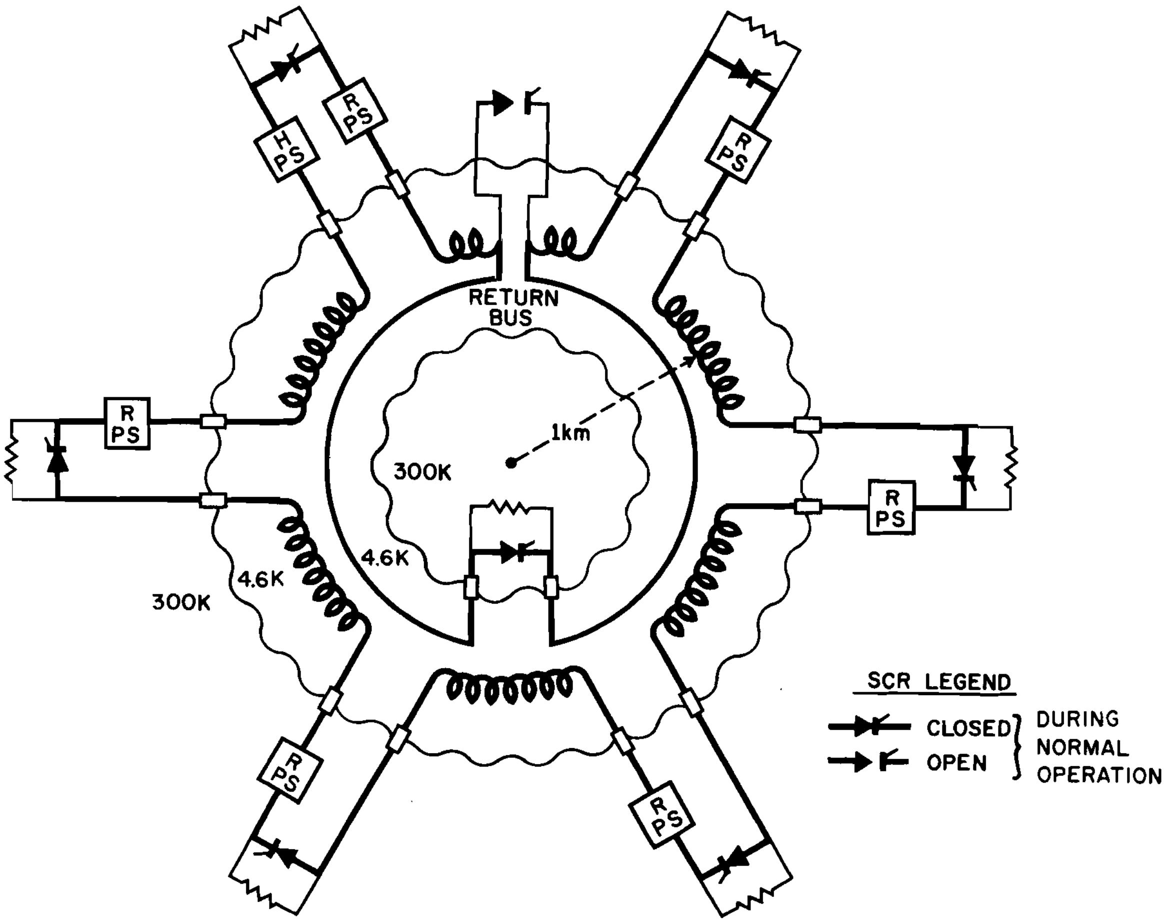

Fig. 6-1. Excitation circuit for superconducting ring.

in the magnets. The return bus contributes to the magnetic field and it is therefore necessary that it carry current at all times during magnet operation.

Six ±2-kV, 4500 A bidirectional converter-inverter energy-transfer supplies are distributed at equal spacing along the coil bus. These six power supplies will be obtained by converting twelve existing Main-Ring power supplies to this use. At each of the A1, B1, C1, D1, E1, and F1 service buildings, the two 1-kV Main-Ring bend-bus power supplies will be removed from the Main-Ring magnet system and connected in series to

Table 6-I. Magnet Power-Supply Parameters.

Power Supply		
No. of rectifier stations (ramping)	6	
No. of rectifier stations (holding)	1	
Peak current	4500	A
Maximum rms current (ramping)	2500	A
Maximum rms current (holding)	4500	A
Peak power (ramping)	54	MW
Peak power (holding)	900	kW
Peak voltage (ramping)	12	kV
Peak voltage (holding)	200	V
Peak voltage to ground	1000	V
Peak coil to bus voltage	1000	V
Current Data - Magnets		
Dipole inductance	0.045	H
Quadrupole inductance	0.006	H
Total inductance (100 cells)	36	H
Total resistance of cables and holding supply components	0.025	Ω
System L/R	1400	s
System stored energy	350	MJ
Nominal Excitation Profile		
Maximum rate of rise	330	A/s (75 GeV/s)
Injection current	660	A
Minimum operating current	500	A
Maximum flattop current	4400	A
Time to flattop (minimum)	12	s
Maximum rate of fall	-330	A/s
Ramping-station ripple	1.5	volt peak
Holding-station ripple	0.15	volt peak
Current Tolerance		
Ramping mode	N.A.	(voltage regulated)
Holding mode	±40	mA
Emergency Energy Dump		
Number of stations	6	
Resistance/station	0.5	Ω
Peak voltage to ground during dump	1000	V
Peak coil to bus voltage during dump	1000	V
Total system L/R in dump mode	12	s

provide a 2-kV energy-transfer station. These power supplies will have a local voltage-regulation loop. The Main-Ring bus will bypass these buildings with a minor modification of the bend buses in the tunnel.

In addition, there is one low-voltage holding supply that is capable of continuous operation at 4500 A. This power supply must be constructed anew and requires a special transformer providing a lower voltage than existing Main-Ring transformers, but capable of continuous operation at 4500 A. This power supply will act as the system current regulator.

The function of the ramping supplies is to change the current of the magnet. The holding supply is used to make up non-superconducting bus losses during constant-current portions of the cycle. All six of the ramping supplies will be programmed to produce equal voltage. Thus the maximum voltage between any coil and ground, or between any coil and the bus, will be one-half the peak voltage of each supply, or 1 kV.

The maximum-performance acceleration cycle is shown in Fig. 6-2. At the start of the cycle, 150-GeV protons are injected from the Main Ring while the current is at 660 A (see Section 10). Previous to injection, the current has been cycled to 500 A in order to compensate for the hysteresis behavior of the main magnets. The ramping stations then increase the magnet current as the beam is accelerated. When the peak current is reached, the ramping stations are removed from the magnet circuit and the current is held constant by the current-regulated holding supply. A current tolerance of ±40 mA is required while the beam is stored or slowly extracted from the synchrotron.

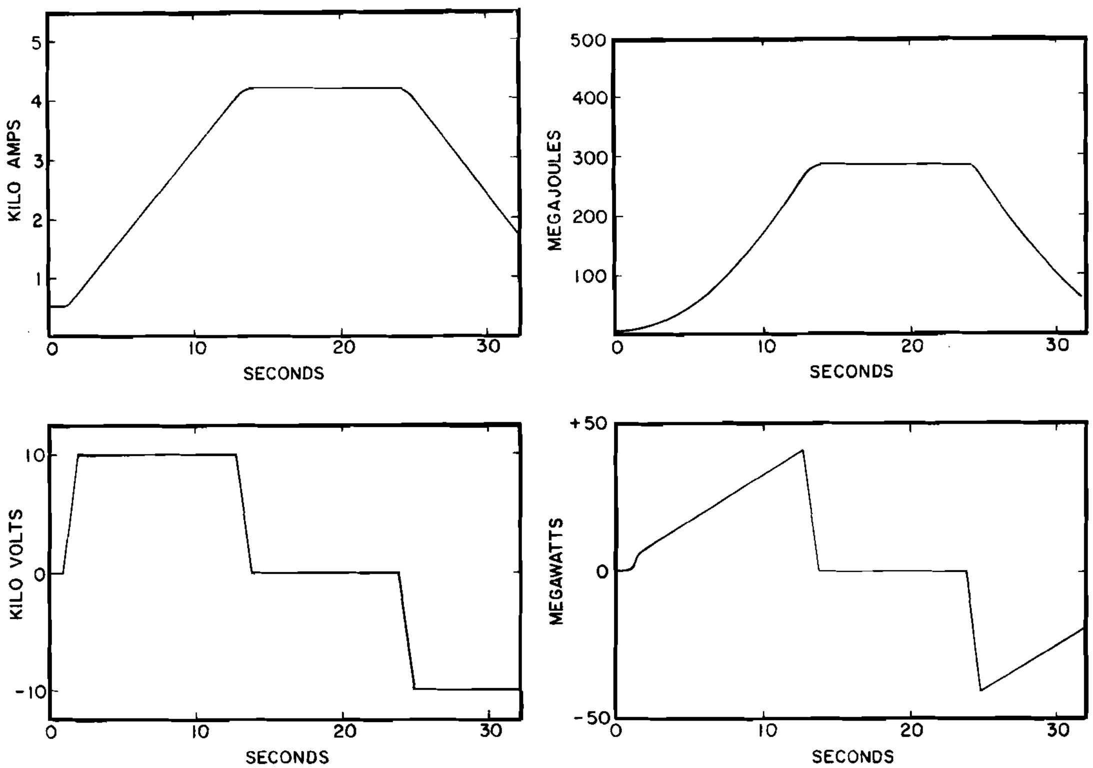

Fig. 6-2. Maximum-performance magnet cycle.

Removal of the ramping stations is accomplished by bringing the power-supply voltage to zero and shorting their outputs with bypass SCR's. A schematic of a ramping station is shown in Fig. 6-3. In order to keep the dc losses made up by the holding supply to a minimum, substantial copper buses must be provided between the tunnel and service buildings at the six power-supply locations and at the bus energy-dump location.

6.3 Filter, Regulation, and Controls

6.3.1 Filter. Each supply consists of a twelve-pulse rectifier system utilizing thyristors. The output of the power supply is variable from 0 to $\pm V_{max}$ by controlling the firing angle of the thyristors. Power supplies of

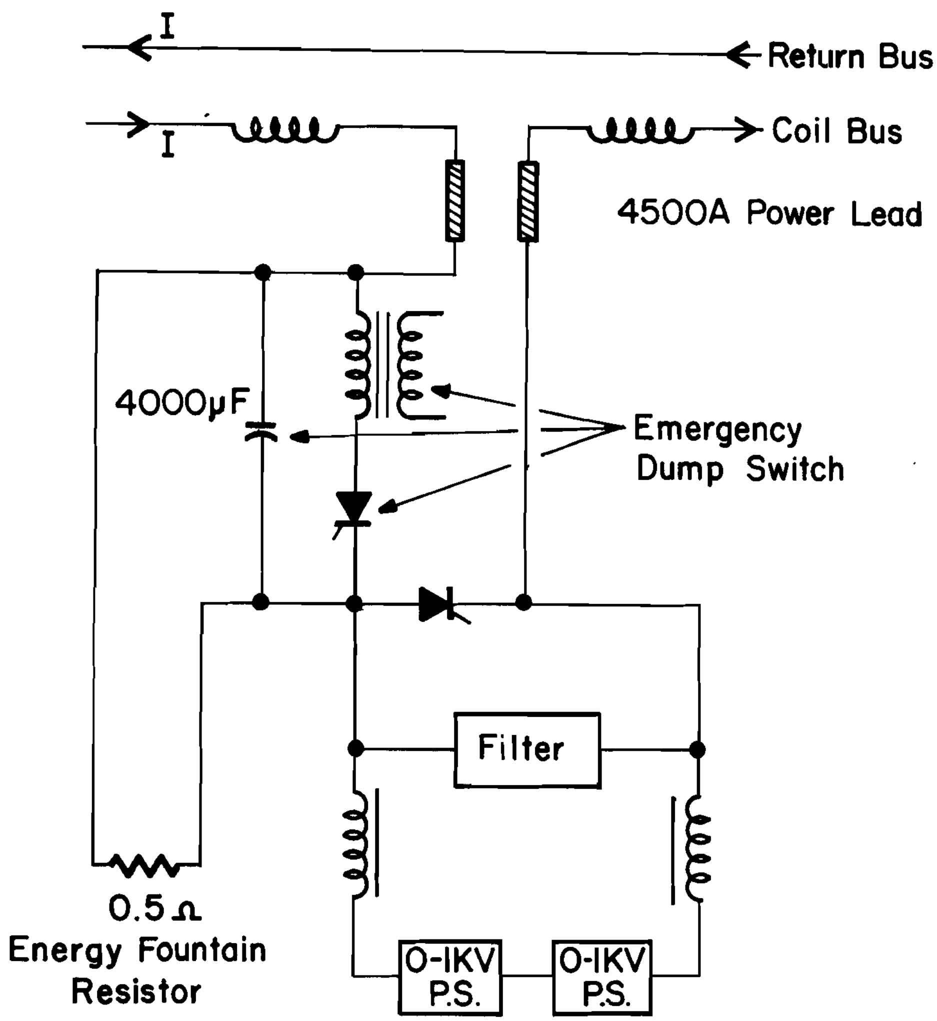

Fig. 6-3. Schematic of a ramping station.

this type produce ripple at a fundamental frequency of 720 Hz with a varying amplitude and harmonic content dependent upon the firing angle. This ripple voltage must be attenuated significantly to ensure that variations in the magnetic field are below the level required for stable operation of the beam.

A passive filter, shown in Fig. 6-4, will be provided at each power supply. It is an underdamped low-pass filter with an added 720-Hz trap to improve attenuation at the fundamental ripple frequency. The voltage attenuation of this filter is shown in the graph of Fig. 6-5 on page 111. The

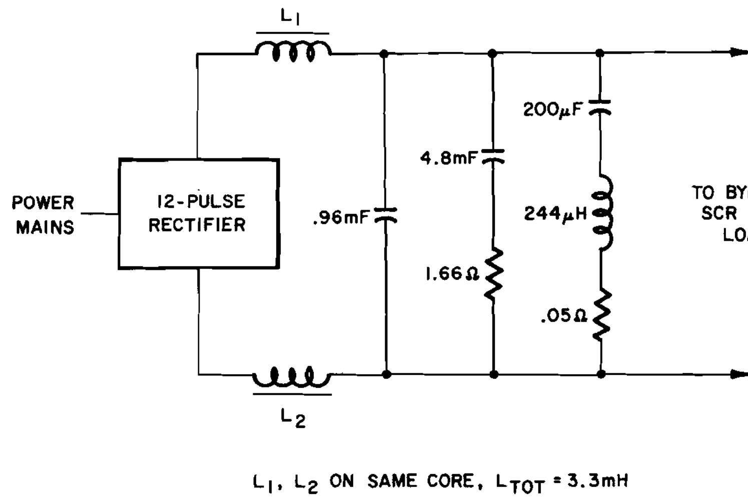

Fig. 6-4. Power supply passive filter.

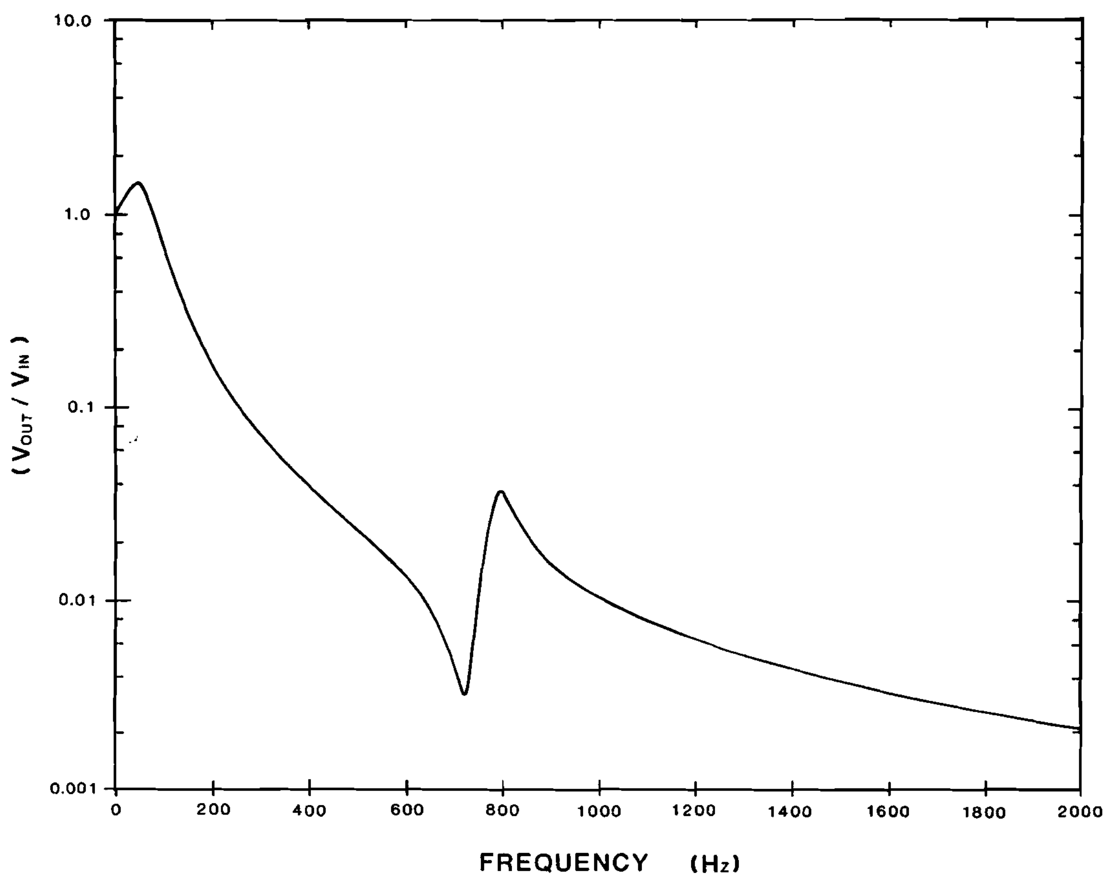

Fig. 6-5. Frequency response of passive filter.

filter provides a ramping supply worst-case ripple of 3 V peak-to-peak, and a holding-supply worst-case ripple of 0.3 V peak-to-peak, ignoring sub-harmonics caused by feeder-line unbalance.

The average ripple current of this voltage should be adequately filtered but, should the final regulation requirement exceed that now expected, the components used in the passive filter could be reconfigured with a shunt active filter of modest voltage and current rating to provide significantly greater ripple reduction. In the interest of simplicity and reliability, only the passive filter is presently planned for use.

At 720 Hz, the expected peak current is about 2 mA, based on a peak voltage at that frequency of 1 V, a damping resistor of 80Ω per half cell, and a characteristic transmission-line impedance of 260 Ω for the dipole string. The purpose of the damping resistor is primarily to damp standing waves in the dipole string, which would otherwise occur at multiples of 12 Hz. The expected attenuation length at 720 Hz is 22 dipoles, and the phase rotation about 3.1 degrees/dipole. Although the dc transfer ratio is 10 G/A, at 720 Hz it is only 0.9 G/A as the damping resistor shunts most of the ripple current around the magnet, and the eddy currents internal to the magnet attenuate the magnetic field effects. Thus the peak fields expected at 720 Hz for a typical supply are about 2 mG, and for a holding supply about 0.2 mG. Hence $\Delta B/B = 3 \times 10^{-7}$ for a normal supply (worst case) and $\Delta B/B = 3 \times 10^{-8}$ for a holding supply.

The most serious subharmonic expected is the 120-Hz component (about 13 V peak), which will produce about 11 mA of ripple current. The transfer ratio is expected to be about 4 G/A and we therefore expect 5×10^{-2}

G (peak) for a normal supply, and 5×10^{-3} G (peak) for a holding supply. The attenuation length and phase rotation at this frequency are 75 dipoles and 1.3 degrees per dipole, respectively. The worst-case $\Delta B/B$ is then about 1×10^{-5} for a normal supply and 1×10^{-6} for a holding supply (at injection). Although these fields seem quite tolerable as far as orbit motion is concerned, tune-change effects on extraction must still be evaluated. Thus some active filtering of the holding supply may be required.

6.3.2 Regulation. The regulation system is shown schematically in Fig. 6-6. Operation and regulation of the power supplies is controlled by an integral microcomputer. A primary function of this microcomputer is to

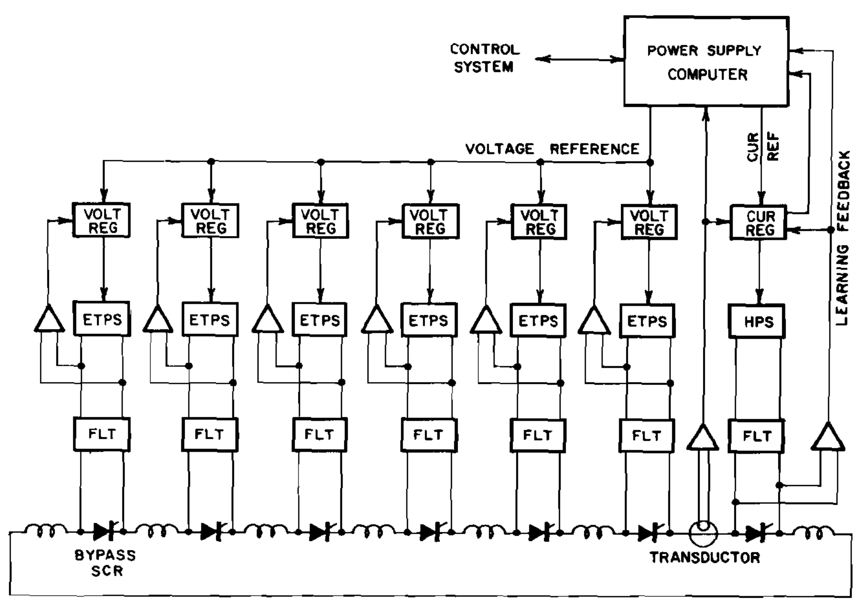

Fig. 6-6. Power-supply regulation system.

generate voltage and current waveforms that command the ramping power supplies and the holding power supply to excite the magnet in the desired manner.

During the ramping portions of the accelerator cycle, the locally voltage - regulated ramping power supplies all receive identical voltage programs from the microcomputer. The voltage capability of the holding supply is extremely small relative to these, so current regulation does not occur during ramping. Magnet-current ripple during this regime must be maintained low, but since the magnet field is the independent variable in the accelerator, lack of current regulation during ramping is acceptable. In order for the holding power supply to provide good regulation during flattop, the ramping power supplies must provide a precise initial flat-top current. Otherwise, the holding power supply will waste its capability correcting this initial error. A learning algorithm in the microcomputer will correct the initial error in the calculated ramping program and provide an acceptable initial condition in a very few cycles after startup. This kind of learning algorithm is well-known from the Main Ring.

During the constant-current portions of the cycle, magnet current will be regulated by the holding power supply. At this time the ramping supplies are switched out of the circuit by the bypass thyristors at their output terminals.

The primary current sensor will be a transductor providing a signal of 2 mV/A of magnet current. Short-term errors and noise in this device are equivalent to approximately 2 mA of magnet bus current at injection and approximately 20 mA at 1000 GeV. Achieving regulation of 1 part in 10^4 at extraction should be easy and achieving 1 part in 10^5 by extra care and sophistication appears possible.

6.3.3 Controls. The power-supply control system is integrated into the total control system discussed in Section 12 of this report. Ramp and safety parameters and commands will be transmitted from the central control room via a serial link. Local microprocessors in the six service buildings with power supplies will directly control the supplies. These microprocessors will be 8-bit Z80 and 16-bit MC68000 devices.

The central accelerator control system will also monitor key operating waveforms directly through analog channels and high-bandwidth binary data links. A B-dot clock signal will be transmitted around the ring by the power-supply system for the benefit of the quench-protection monitors. This signal will also be used for other control functions.

6.4 Quench Detection and Protection

6.4.1 Quench detection. For detection of quenches, we have developed a microprocessor system that sequentially measures the voltage across each half-cell of magnets (4 dipoles and one quadrupole). One microprocessor system, shown in Fig. 6-7, monitors 165 magnets or one-sixth of the entire accelerator.

Each system runs under the supervision of a high-level interpretive BASIC-language program. This program is responsible for setting up parameters, analyzing statistics, and reporting status to the operators.

Every 17 ms, synchronized with the power line, this supervising program is interrupted for a high-priority safety scan of all the analog signals

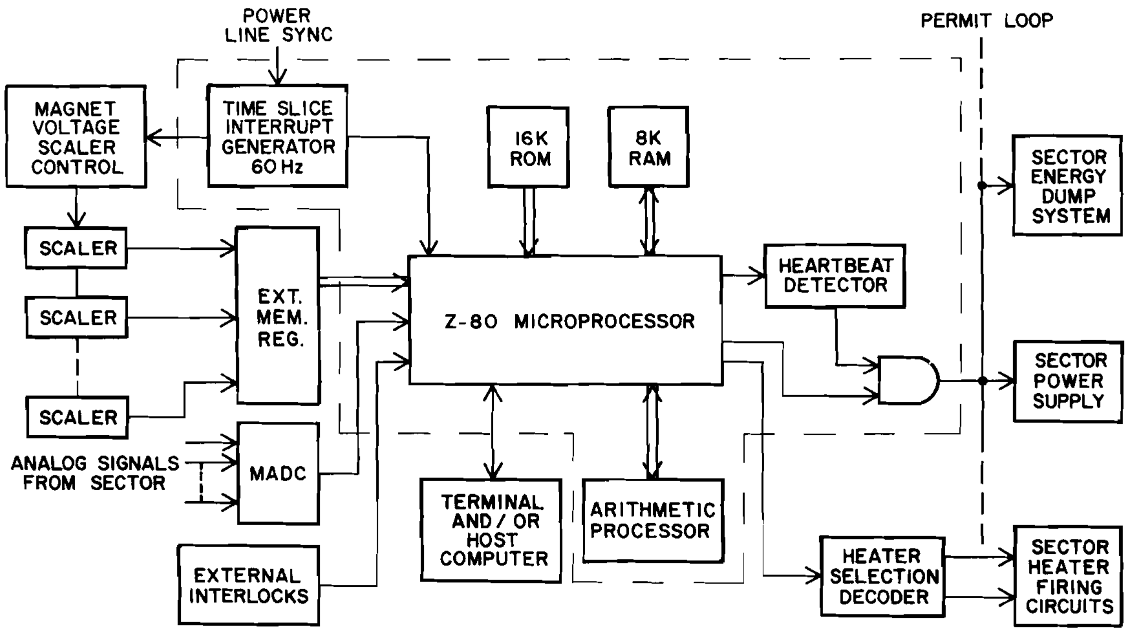

Fig. 6-7. Microprocessor system for quench protection.

from its one-sixth of the accelerator. An auxiliary arithmetic processor is used to enhance the fast on-line safety analysis. If the scan does not reveal any anomalies, the software generates a "heartbeat." If an anomalous condition--quench,overvoltage, lead runaway, overcurrent, etc.--is detected, or if the processor fails to give an indication of activity to the heartbeat detector, the emergency dump system, described below, is activated. The 17 ms between these scans is negligible in comparison with quench-development times. Good voltage-detection sensitivity is critical to insure adequate detection.

The quench-detection algorithm depends on the fact that voltages tapped from the magnets should be distributed according to known inductances. A deviation of a few tenths of a resistive volt indicates the start of a quench.

6.4.2 Coil quench protection. When a quench is detected, the power supply is turned off and a 0.5-Ω air-cooled "energy-fountain" resistor is switched into the coil bus at each of the ramping stations by the emergency dump switch shown in Fig. 6-3. This causes the magnet current to decay with a time constant of 12 s.

In Fig. 6-8 we show schematically the electrical connection of a protection unit containing four dipoles and one quadrupole, a half-cell of the accelerator. After the resistors have been switched into the coil bus, a

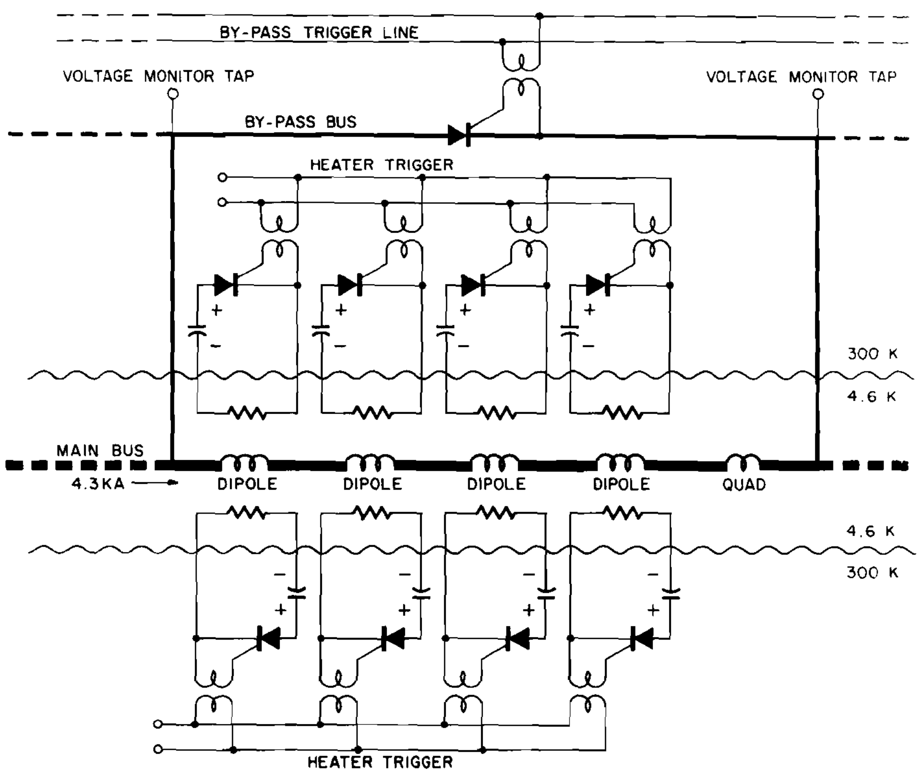

Fig. 6-8. The quench-protection system for one half-cell.

pulse train is applied to the gates of the shunt thyristors all around the magnet ring. If resistive voltage has developed across any protection unit, the associated shunt thyristor will turn on and divert the decaying current around the quenched unit, through two safety leads. These leads are 3/8-in. diameter copper rods designed to carry one pulse of decaying current without damage and to cause a negligible heat leak when passive. They will, of course, have to cool down again before re-use.

In order to protect the thyristors against damage from radiation, they are mounted in a "hole-in-the-wall" module which extends 4 ft through the wall of the tunnel. Surrounding earth provides the shielding. Nevertheless, all shunt thyristors will be regularly tested by gating them on and ramping the magnets fast enough to force current into them. The microprocessor system will scan voltage taps for any open thyristors.

Since the quenched magnets in a protection unit are shorted, they must absorb all their stored electrical energy without damage. To prevent damage, the normal zone must propagate rapidly in the quenched magnet so that the stored energy is not dissipated in a small volume of conductor. To speed the propagation of the quench, we have installed a thin stainless-steel heater strip adjacent to the coil in two high-field regions of the magnet. Results of

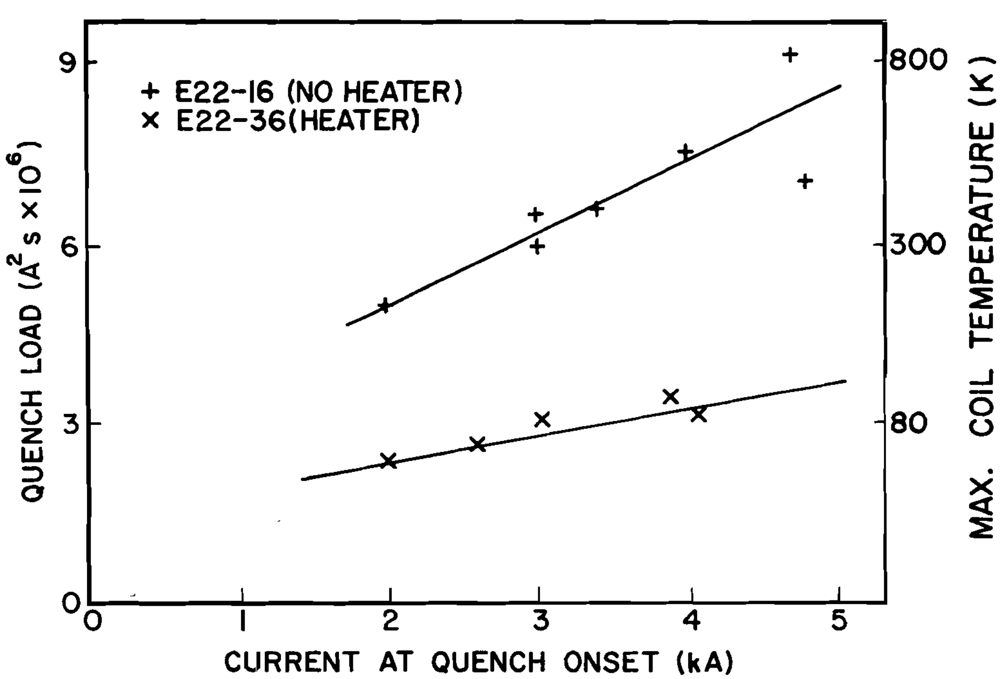

Fig. 6-9. Quench load and maximum coil temperature vs. current for shorted magnets with and without heater protection.

experimental tests of heater strips are shown in Fig. 6-9 on the preceding page. If a quench is detected, then heaters in all the dipoles of the quench unit will be fired.

6.4.3 Return-bus quench protection. The voltage across the bus in each sector (±10 V during ramping, 72 V during dumping) will be monitored via a differential-voltage channel. The total voltage of the entire bus (±60 V during ramping, -1.5 V during dumping) will also be monitored at the fold. It will be possible to detect 0.2 V of normal resistance in the bus.

When a quench is detected, all bypass thyristors will be gated on, including the one at the fold. This will enable the coil current to be bypassed around the entire bus. The bus is dumped through a 0.1-Ω resistor. The bus current falls rapidly at first with a time constant L_{bus}/R_{bus} = 0.15 s, then more slowly with a time constant L_{coil}/R_{coil} = 12 s for 13% of the coil current. The total quench load in the bus gives a maximum temperature rise of 100 K. Figure 6-1 illustrates the bus quench protection elements.

The voltage stress is approximately 200 V if the dump is located opposite the fold. Exact placement is a matter of convenience. The dump must absorb 0.34 MJ at most. It could be made of stainless steel 25 ft long and 0.087 in.^{2} in cross section. The maximum temperature rise in this design would be 350°F (194 K).

Portions of the bus through straight sections will be made of fully stabilized superconductor.

7. CORRECTION AND ADJUSTMENT MAGNETS

7.1 Correction Magnets in a Superconducting Accelerator

If this were a report on the design of a conventional accelerator, there would be little need to discuss this system under a distinct heading. Mention could be made of the corrections required at injection field, adjustments could be treated as aspects of other systems, and free space in the lattice could be identified for later insertion of additional elements if needed.

The situation is markedly different in the case of the superconducting accelerator. Two factors are especially noteworthy. First, error fields are no longer solely a low-excitation phenomenon. Inevitable deviations in superconductor location from the ideal configuration produce significant field distortions that are independent of excitation. Thus, certain corrections are required at all field levels. Second, the beam pipe is relatively inaccessible, buried throughout most of its length inside an essentially continuous cryostat. Elements can no longer be added or shifted about with ease. Rather, it is appropriate to design and construct the correction and adjustment magnets as integral parts of the main magnet system. To be sure, space remains within the lattice to permit introduction of further devices at a later stage, but it is intended that the more numerous element types be installed at the outset.

7.2 Placement of Correction Elements

The magnets of this system are superconducting coils located within the main quadrupole cryostats. A steering dipole is within each main quadrupole coil; other multipoles are immediately downstream of the quadrupole. The latter include a trim quadrupole and sextupole at every normal-cell quadrupole. In addition, either an octopole or a skew quadrupole appears at many of these locations.

Other elements will be required, particularly in and near the long straight sections. At this writing, the design of the normal-cell quadrupole assembly is receiving emphasis, and this discussion will concentrate on the auxiliary magnets to be installed therein. Even with this limitation, the number of devices is large. There are 180 normal cell quadrupoles; steering dipoles, trim quadrupoles, and sextupoles alone represent 540 elements.

7.3 Functions and Strengths

Under this heading the principal roles anticipated for the various elements will be outlined. Strengths will be expressed as field integrals at 1 in. radius, at levels appropriate for 1 TeV.

7.3.1 Steering dipoles.

The primary function of the steering dipoles is correction of the closed orbit at all energies. The rigidity of the superconducting-magnet system and the tight tolerance on orbit centering imposed by extraction argue against a reliance on main-magnet motions for orbit correction. In the case of the present Main Accelerator, the high-energy closed orbit initially exhibited a peak in excess of 1 in. in the horizontal plane. A major reduction was made by moving 25 quadrupoles by displacements of up to 0.25 in. Similar motions of the superconducting quadrupoles are not attractive to contemplate, in view of the stresses engendered on the cryogenic system. For extraction, it is desired that the closed orbit excursions be held within bounds of ±0.1 in. It would be unrealistic to assume that this requirement could be achieved and maintained without high-energy steering.

It is likely that orbit distortions will be large, at least during initial operation. At points in the normal cells where the amplitude function is a maximum, the rms orbit distortion due to dipole field errors and quadrupole misalignments can be written as

$$<x^2>^{\frac{1}{2}} \approx \tfrac{1}{4}[a^2 + \tfrac{5}{9} b^2]^{\frac{1}{2}} \text{ in.},$$

where a characterizes the rms dipole field error in units of 0.1%, and b the rms quadrupole misalignment in units of 0.01 in. In the horizontal plane, a arises from the fluctuation in the field-length product from dipole to dipole; in the vertical plane, a receives contributions from both rotational alignment error and any uncertainty or instability in the dipole field direction. As a specific example, consider the vertical plane, where the magnet aperture is more restricted. The choice a = 1.4 would allow for 1-mrad rotational misalignment during installation and 1-mrad uncertainty or instability in the field direction. The choice b = 2 (0.02 in. placement error), though larger than that normally associated with the conventional accelerator, is not excessive in view of the greater difficulty in referencing the quadrupole magnetic center to external fiducials. Then the rms orbit distortion would be 0.5 in. and, if the errors obeyed a Gaussian distribution, there would be a 60% probability of a peak distortion greater than 1 in.

Horizontal steering will be accomplished by a dipole within each horizontally focusing quadrupole and vertical steering by a "skew" dipole within each vertically focusing quadrupole. The dipole strength required to compensate the deflection generated locally, that is, by the quadrupole misalignment and by the eight neighboring main dipoles, is, for uncorrelated dipole errors

$$\left(\int B d\ell\right)_{rms} = 23\,[a^2 + 0.31\,b^2]^{\frac{1}{2}}\ \text{kG-in.},$$

where a and b have the same significance as above. The choices a = 1.4, b = 2 yield 41 kG-in. at the rms. For Gaussian errors, a steering strength of about 130 kG-in. would be implied in order to have 90% probability of successful correction at 100 locations.

A steering dipole strength of 170 kG-in. has been selected. This figure is considered compatible with the concerns of the preceding paragraphs, with feasibility of construction, and with the desire to reserve some capability for orbit manipulation beyond centering.

7.3.2 Trim quadrupoles. Since the main dipoles and quadrupoles are connected in series, trim quadrupoles must assume the burden of tune correction and adjustment. For half-integer extraction, appropriate quadrupole harmonic terms are needed. In addition, if quadrupole error terms in the main magnets become sufficiently large, compensation of perturbations in the amplitude or dispersion functions could be appropriate.

The dominant single influence on trim-quadrupole strength arises from colliding-beam possibilities. Typical interaction-region designs introduce an added phase advance of close to π in both planes of oscillation; the trim quadrupoles must, in effect, lower both tunes by approximately 0.5 to restore the operating point. The trim-quadrupole strength at 1000 GeV may be inferred from

$$\Delta\nu_H = 0.0214\,(B'\ell)_F - 0.0062\,(B'\ell)_D$$

$$\Delta\nu_V = -0.0062\,(B'\ell)_F + 0.0214\,(B'\ell)_D,$$

where the subscripts indicate the focusing character in the horizontal plane of the adjacent quadrupole. A reduction of both tunes by 0.5 implies a contribution to trim quadrupole strength of 33 kG-in.

Considerably smaller strengths are associated with tune correction. Quadrupole moments in the main dipoles have been a source of concern. A systematic quadrupole term, b_1, in the dipoles would produce tune shifts $\pm 1.1 \times 10^3\, b_1$ in the two planes of motion. The magnet-selection criteria require that b_1 for each dipole lie within the range $\pm 2.5 \times 10^{-4}$/in. If the systematic component were half that value, 5 kG-in. would be required of each trim quadrupole. Recent magnet measurement data suggest that the average value of b_1 will be considerably less.

For half-integer extraction, a typical value of the total strength on the 39th harmonic is 170 kG-in., to be distributed among a suitable distribution of trim quadrupoles. Contributions to this harmonic from quadrupole fields in the dipoles must be compensated. The measurements alluded to in the preceding paragraph indicate a standard deviation for b_1 comparable to the bounds of the magnet-selection criterion. If so, the driving term on either the sine-like or cosine-like phase of the 39th harmonic due to b_1 in the dipoles would be 23 kG-in. at the rms.

At present, there is no cause for alarm concerning disturbances in the amplitude or dispersion functions. For example, if the bound for b_1 established by the magnet-selection criteria is again taken as the standard deviation of the distribution and the distribution is assumed to be Gaussian--an extreme case--then there would be a 20% chance of a peak in the amplitude function 20% in excess of its design value.

The trim-quadrupole strength has been specified at 60 kG-in., safely above the requirement imposed by a single interaction region after allowance for tune correction. Only a few such quadrupoles will be needed for extraction-harmonic generation.

7.3.3 Sextupoles. The principal role envisaged for the sextupoles is control of the chromaticity, although if the third-integer resonance is used as an extraction mode, harmonic generation would be required as well. Only the former application will be considered here.

Thus far, the dipoles have exhibited a substantial systematic sextupole term at high field. Of course, significant sextupole fields due to persistent currents are present at low excitation, but, at present, the average b_2 at high fields is the dominant factor to be considered in chromaticity correction.

The contributions to the chromaticity from systematic sextupole terms in the dipoles and from chromatic aberration in the quadrupoles can be written

$$\xi_H = 2.64 \times 10^5 \langle b_2 \rangle - 22$$
$$\xi_V = -2.45 \times 10^5 \langle b_2 \rangle - 22, \qquad b_2 \text{ in (in.)}^{-2}$$

where the natural chromaticity of -22 is that associated with the basic lattice exclusive of any enhancement from colliding-beam interaction regions. The magnet-selection criteria impose a bound of 6.0×10^{-4} in.$^{-2}$ on the magnitude of b_2; if the average value of b_2 is taken to be one-half of the bound, the chromaticity in one plane or the other would be about 100. Compensation of the effect of the average b_2 requires sextupole strengths of 9 and 15 kG-in. at horizontally focusing and defocusing quadrupoles respectively.

A colliding-beam interaction region can be expected to significantly increase the natural chromaticity (though by less than a factor of two). Provision of an adjustment range of twice the natural chromaticity of the basic lattice adds 9 and 17 kG-in. to the sextupole strengths at focusing and defocusing quadrupoles.

A strength of 50 kG-in. has been adopted for the sextupole located at each normal-cell quadrupole. This value is some 50% higher than the sum of the needs at defocusing quadrupoles as outlined above.

7.3.4 Octopoles. There are two major functions for the octopoles; both are associated with the only process requiring large betatron oscillation amplitude, resonant extraction. In the half-integer case, octopoles provide the nonlinearity that divides the phase plane into stable and unstable regions. Whatever extraction resonance is used, octopoles permit control of the dependence of tune on oscillation amplitude.

The version of half-integer extraction currently preferred employs a 39th octopole harmonic in association with a 39th quadrupole harmonic. The strength of neither harmonic is unique, though specification of one defines the other for fixed values of other extraction parameters. Nevertheless, a total octopole strength of 450 kG-in. on the 39th harmonic for elements placed near focusing quadrupoles is at the upper end of the adjustment range.

Adjustment of the amplitude dependence of tune is useful in its own right. But octopole terms in the main magnets also produce such a tune dependence and correction may be necessary. Of particular concern would be a systematic b_3 in the main dipoles, a possibility that cannot be excluded by measurements to date. The measurements do suggest that it is most unlikely that the average value of b_3 will be as large as one-half the selection criteria bound of 2.0×10^{-4} in.$^{-3}$. As an illustration, if the average value of b_3 were that large, then the tune shifts associated with a 1-in. horizontal-oscillation amplitude and negligible vertical amplitude would be 0.055 and 0.090 in the horizontal and vertical, respectively. Correction by zero-harmonic octopoles implies totals of 260 and 620 kG-in. at focusing and defocusing quadrupoles.

The individual octopole strength has been specified as 30 kG-in. The extraction requirement is satisfied for both sine-like and cosine-like harmonics by octopoles at eight successive focusing quadrupoles at corresponding locations in four adjacent sectors; octopoles are omitted in sectors D and E to minimize amplitude growth between the primary septum and the extraction channel. To correct the zero-harmonic terms in the extreme case of the preceding paragraph, an additional 36 octopoles would be necessary, 12 at focusing quadrupoles and 24 at defocusing quadrupoles. Therefore, the octopoles are at most 68 in number.

7.3.5 Skew quadrupoles. At an early stage of the operation of the Main Accelerator at high energy in 1972, it was observed that a large horizontal oscillation would couple over into the vertical in a single turn. Magnet measurements thus far indicate that an analogous situation will occur here; in fact, a recent analysis of the data on 22 magnets with serial numbers above 100 suggests that the coupling effect may be larger by a factor of two or more than in the Main Accelerator case. In such a circumstance, tune splitting is not effective in ameliorating the effect; rather, skew quadrupoles must be provided.

Skew quadrupoles will be incorporated into the multipole package at locations where octopoles are not necessary. Patterned after the standard trim quadrupole, but rotated by 45°, the skew-quadrupole strength will be essentially the same--60 kG-in. each. At present, it is intended that from 18 to 24 of these elements be installed. The skew-quadrupole coefficient in the main dipoles will be closely monitored in order to review the number and distribution of the skew quadrupoles as construction proceeds.

7.4 Excitation

In this section, comments will be made regarding the tolerances on the currents delivered to the correction and adjustment magnets, and on their arrangement in circuits. Current leads for each magnet are to be brought out of the cryostats. The interconnections among elements can therefore be modified with some freedom. All elements are designed to achieve their nominal maximum strengths at a current of 50 A.

7.4.1 Current tolerances. Because of their role in orbit correction, the steering dipoles inherently require independent bipolar power supplies. Stability and ripple suppression at 0.1% of full scale is needed in order to satisfy the demands of injection and extraction.

The trim quadrupoles and octopoles participate in the half-integer resonant extraction process. The current tolerances that would be associated with a relatively unmodulated slow spill of several seconds duration are unrealistic, but by powering these elements with a limited number of supplies designed at or near the state of the art, the sources of modulation can be held to a minimum in variety and strength, and the usual spill-feedback techniques will have a greater chance of success. Hence, the quadrupoles and octopoles will be wired in functional groups, each powered by a supply providing current stability in the range 0.01% to 0.005% of full scale.

The remarks of the preceding paragraph apply to any sextupoles used to generate third-integer extraction harmonics. The sextupoles also enter any extraction process through the chromaticity correction that they perform, although the tolerances become less severe. It is attractive to adopt the same approach to excitation of the sextupoles as that to be used for the trim quadrupoles and octopoles. But a caveat is in order; it may be necessary to resort to individual sextupole excitation if local compensation of the dipole coefficient b_2 becomes advisable.

7.4.2 Circuits. As noted in the preceding subsection, all steering dipoles are individually powered. Other elements are connected in functional groups.

For the momentum spread associated with single-turn injection at 150 GeV, two sextupole circuits are sufficient for chromaticity adjustment; that is, all sextupoles at horizontally focusing quadrupoles are wired together in the same polarity as are all sextupoles at vertically focusing quadrupoles.

Four trim-quadrupole circuits are required. The two for tune correction and adjustment are assembled in the same fashion as the sextupole circuits, with the exception that eight trim quadrupoles are omitted from the "horizontally focusing" circuit. Four of the latter, at stations B17, B26, C17, and C26 form one of the 39th harmonics for extraction; the other four, at stations B32, B42, C32, and C42 form the other 39th harmonic.

The octopoles will be arranged in four circuits. Octopoles at stations 17, 19, 26, and 28 in sectors F, A, B, and C produce one 39th harmonic; octopoles at stations 22, 24, 32, and 34 in the same sectors produce the other. Specification of the two zero-harmonic circuits can be deferred for the present, awaiting further information on the average value of the coefficient b_3.

7.5 Power Supplies

Two distinct types of power supply will be required - a large number of relatively low-voltage supplies with accuracy at the 0.1% level for the steering dipoles and a much smaller number of high precision supplies for the other elements. There are 180 steering dipoles in the standard cells of the lattice, and at least 4 dipoles will be installed at each long straight section. There will therefore be a need for over 200 supplies of the first variety. That total could increase substantially if individual excitation of sextupoles becomes necessary.

The current requirement is ±50A. The supplies will be designed with load compensation and a conventional roll-off characteristic of 20 db/decade.

7.5.1. Steering dipole supplies. The current stability and ripple limit for these supplies is ± 0.1% of full scale. To complete the specifications, the bandwidth and voltage must be determined. It is reasonable to have a bandwidth which allows the power supply output to follow a constant ramp input within ±0.1% of full scale. The error between programmed input and supply output for a constant ramp is

$$\epsilon \doteq \frac{AB}{2\pi f_0}$$

where

ϵ = lag error (amps)
A = power supply DC gain (amps/volt)
B = input voltage ramp rate (volts/s)
f_0 = power supply bandwith or corner frequency (Hz)

For an error of 0.1% (0.05A) and a ramp from 0 to 50 A in 10 s, a power-supply bandwidth of 20 Hz is adequate. With this 20-Hz bandwidth, the equation above then yields a maximum output ramp rate for 0.1% accuracy of 6.3 A/s.

The supplies will be installed in the existing Main-Ring service buildings. The longest lead from the supply to dipole and back will be 1000 feet. At 50A and 50°C, the voltage drop in that length of #2 wire is 8.8 V. The load inductance will be approximately 0.2 H; at the maximum ramp rate, for 0.1% accuracy, the drop across the magnet would be 1.3 V. A maximum power supply output of 15 V satisfies these requirements and provides a higher slewing capability for current changes under conditions where the accuracy specification can be relaxed.

A block diagram of such a supply is shown in Fig. 7-1. The control system provides a bipolar analog reference waveform from a generator with 12-bit resolution and 8 bits for commands to operate and check each

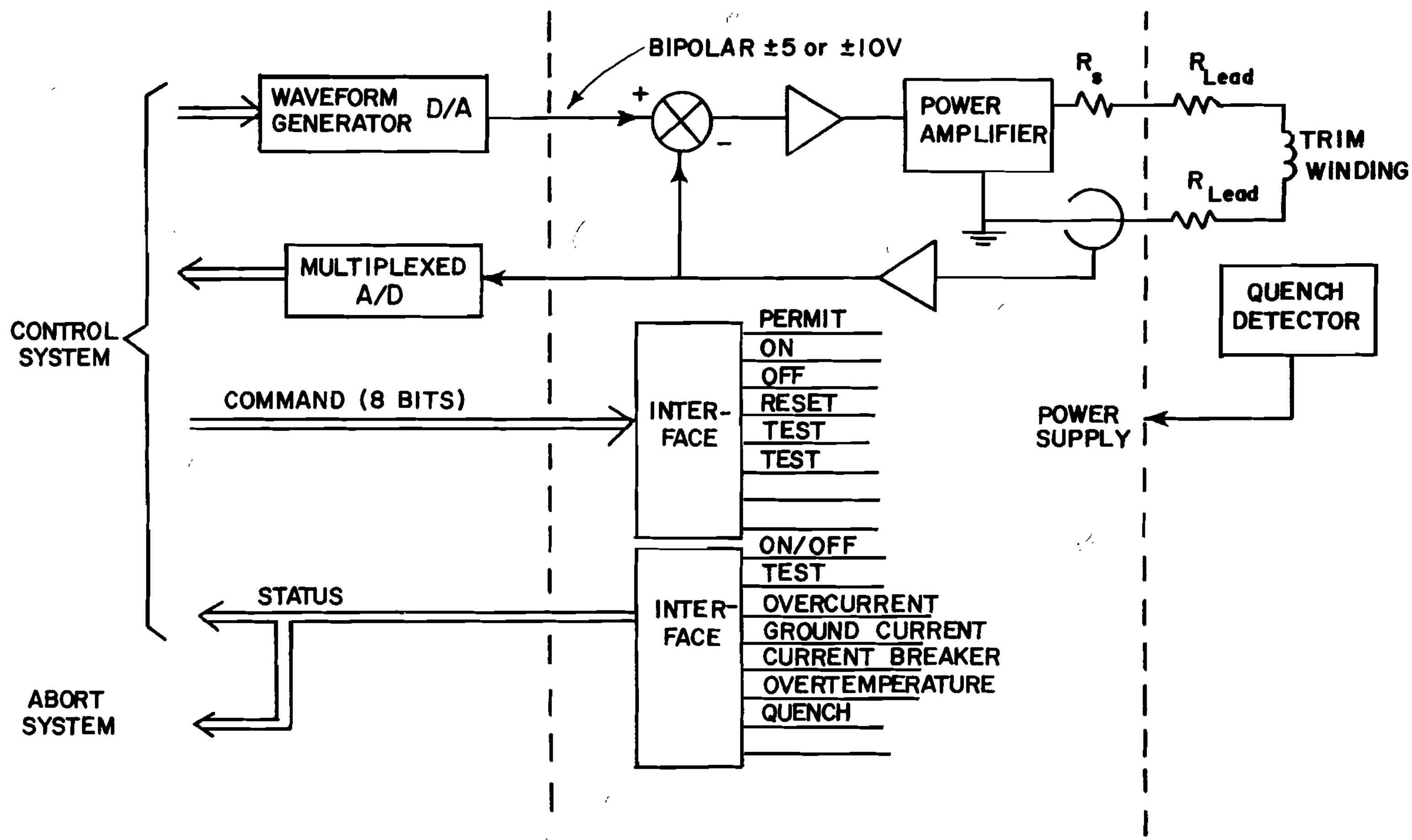

Fig. 7-1. Correction-magnet power supply.

power supply. The current reading is returned to the control system via a multiplexed A/D along with 8 status and fault bits. Isolation is provided between the control system and the power supply for command, status, and faults by means of optical couplers. Isolation of the analog signals is not felt necessary at this time.

The power-supply requirements can be met with either a thyristor-controlled dual converter or a transistorized power amplifier. Either approach would use series output resistors or other techniques to compensate for lead resistance variations, to keep load L/R constant for maximum performance. A preliminary analysis indicates that the costs of the two approaches are about the same.

Quench protection will be provided for each dipole circuit. Several methods are under consideration, but a final design must await system tests that have not been made as yet.

7.5.2. High precision supplies. These supplies are to have a stability and ripple limit in the range 0.005% to 0.01% of full-scale current. To achieve the low ripple current, a transistorized output regulator will be necessary, in which case a bandwidth of 100 to 200 Hz should be obtainable at no extra cost. With this bandwidth, lag error is reduced in comparison to the dipole supplies by a factor commensurate with the increased accuracy.

Although final programmed waveshapes have not yet been established, it is clear that certain of these supplies will have a relatively high output voltage. For the tune adjusting circuits, the requirement can be as high as 250 V. To reduce transistor-bank dissipation, these supplies will use a preregulator to provide variable voltage to the output transistor regulator. The programmable supplies will be operated to keep a nearly constant voltage across the output transistor banks and thus reduce the transistor-bank requirements. By careful design, the transistor-bank regulator for the various high-precision supplies could be the same. The main difference then would be in the choice of the preregulator.

The supplies would be configured much like the steering-dipole supply shown in Fig. 7-1 with a few exceptions. The reference voltage would be provided by a precision 16-bit D/A, and the current sensor would be a high quality current transductor; stability of each at 1 ppm/°C is needed. Suitable components are now available commercially. The waveform generator would be located within the supply to minimize noise pickup. Quench detection and protection will also be provided.

8. EXTRACTION SYSTEM

8.1 Orbit Design

The basic design goals of the extraction system are (i) provision of slow resonant extracted beam with uniform spill over times of 1 to 10 s; (ii) provision of fast resonant extracted beam in the range of 1.0 to 3.0 ms (multipulsed fast extraction is also desirable but presents intrinsic problems in maintaining good extraction efficiencies; the designed extraction system should not be incompatible with this goal); and (iii) the extraction efficiency should be high (losses < 2%) to minimize beam-loss effects on the superconducting magnets.

An accurate estimate of the available effective magnet aperture is essential when considering the extraction process in detail, because extraction will explore fully and be limited by magnet aperture. During the extraction cycle, the maximum-amplitude orbit excursions increase monotonically from turn to turn and each particle will therefore achieve its maximum amplitude on the final turn before being extracted. In order to calculate the effective aperture of a perfectly aligned accelerator with perfect design fields, we must consider a slightly off-momentum orbit, on which the higher-order odd harmonics do not cancel. A momentum offset of 0.05% will give an average orbit offset of approximately 1.5 mm, representative of the operational tolerances that can reasonably be expected. Figure 8-1 shows data resulting from an analysis of this kind. We have plotted the phase-space trajectory for a half-integer extraction separatrix at the upstream ends of the long straight sections sequentially around the ring, starting at B0.

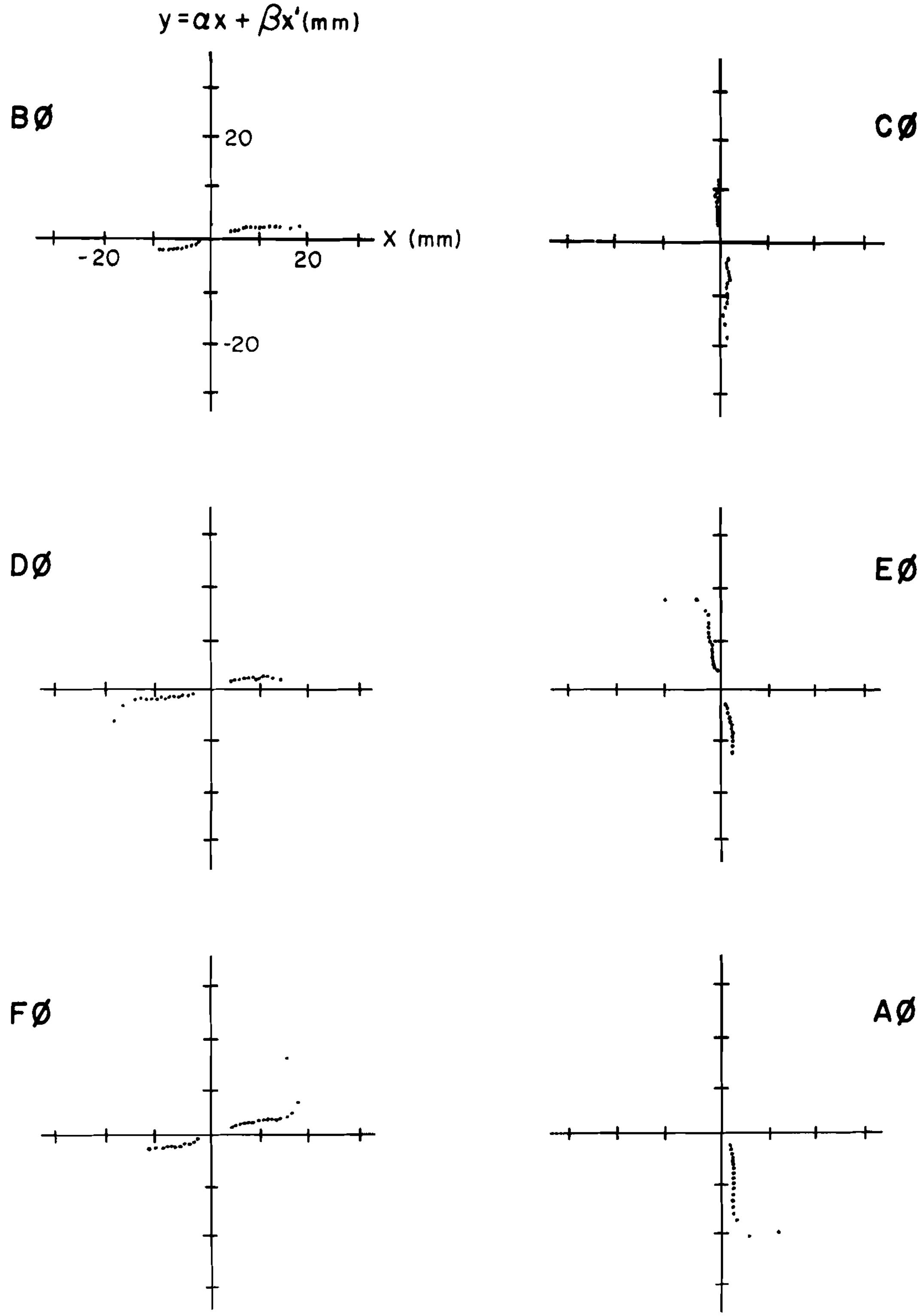

Fig. 8-1. Half-integer slow-extraction separatrix around the ring without high beta.

The growth of the radius vector around the cycle is evident and, starting with the D0 long straight section, we can see the effect of the higher-order terms in the dipole-field harmonics starting to manifest themselves as rotations in the phase-space trajectory; these rotations get progressively larger during the cycle. From a more complete analysis[1,2] we conclude that the horizontal aperture is slightly larger than the vertical aperture and henceforth we shall only consider horizontal extraction. We also find that we need to control the vertical closed orbit to within ±3 mm of the dipole center. With this limitation, the maximum-amplitude orbit oscillations must be within ±2 cm, with the exception of the final few oscillations in the ring, which can grow to approximately ±2.5 cm without any major phase-space distortions. The effect of this 2-cm aperture limitation on the extraction system was too severe and would result in unacceptably high extraction losses if the lattice were the same as that of the Main Ring.

The solution of these problems[3] is to redesign the long straight sections containing the magnetic and electrostatic septa to provide a five-fold increase of the amplitude-function β of the lattice at the upstream end of the long straight sections. The layout of a high-β long straight section is shown in Fig. 2-3. Three different-length quadrupoles are introduced in the 48, 49, 11, and 12 locations, with the polarity of the quadrupole doublets at 49 and 11 reversed from the normal long straight section. The lattice parameters across the high-β

sections are matched to those of the normal lattice. The effect of this lattice modification on resonant extraction has been studied in detail.[1,4] It increases the effective aperture available to the extraction system by a factor of 1.8, which permits a greater extraction efficiency with a more stable extracted beam. The effective strength of the electrostatic septum is increased by a factor of 4.5, which allows the use of a shorter septum than previously and, possibly more important from an operational point of view, allows the extraction septa to be located at the upstream end of the long straight section, permitting the maximum amount of shielding of the downstream superconducting magnets from the primary and secondary products of the extraction losses. The lattice with two high-β long straight sections is discussed in detail in Section 2.

Resonant extraction could be accomplished in either third-integer or half-integer modes. Implementation of both forms is not practical at the outset and consequently a choice between them must be made. A detailed comparison between the relative merits has been done.[5] Slow extraction efficiencies are almost identical for the two cases. Slow spill of the entire beam is easier in the half-integer system. The requirements of fast resonant extraction overwhelmingly indicate a preference for half integer and we have therefore chosen half-integer resonant extraction as the operational system.

8.2 Slow Extraction

We can now begin to formulate the layout of the individual elements and their operational characteristics. The choice of long straight-section A is dictated by the extraction channel to the existing external experimental areas. The magnetic septa (Lambertson magnets) will be located at the upstream end. The presence of the Main-Ring rf cavities at F0 does not leave room for the electrostatic septum and as a result, it will be located at the upstream end of long straight-section D. The appropriate harmonics for the quadrupoles (39th) and the octopoles (39th and/or 0th) needed for slow extraction will be provided by the correction-coil package (discussed in Section 7), which will also allow control over the relative phase of the 39th harmonic. In order to inhibit the growth of the oscillation amplitude between the electrostatic and magnetic septa on the final half turn for the extracted beam, only the correction coils in sectors A, B, C, and F will be used in the extraction system. An analysis of 1/3-integer extraction[4] shows that for fixed phase-space trajectory and available aperture, the optimum extraction efficiency is achieved when the electrostatic-septum offset and the step size across the septum are equal. This sort of criterion can be used to calculate the relative strengths of quadrupole and octopole needed for extraction. Figure 8-2 demonstrates the behavior of the slow-extraction separatrix around the ring, incorporating all of the factors discussed above. The effect of the high-β sections at A0 and D0 is apparent in increasing the beam amplitude at these points. The septum offset at D0 is 12 mm; the step size is adjusted to be 12 mm. This represents the limiting case of the magnet aperture; the average orbit amplitude over the last half turn is approximately 25 mm. The

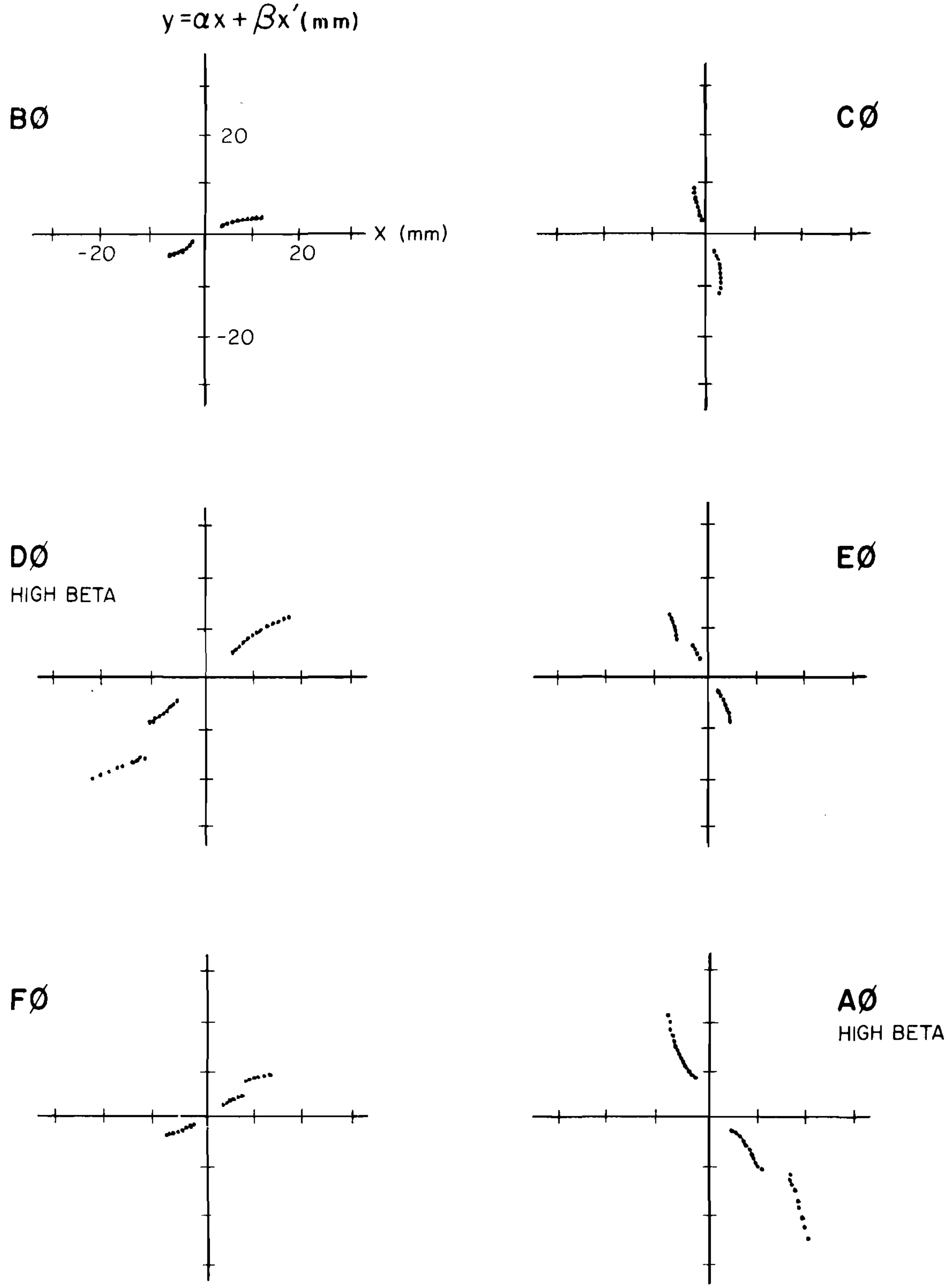

Fig. 8-2. Half-integer slow-extraction separatrix around the ring with high beta.

integrated field strength of the quadrupoles and octopoles in this case is 255 kG-in. and 412 kG-in. respectively at 1 in. The extraction losses of a system with these operational parameters are approximately 1.5%, for a 3-mil effective septum thickness.

8.3 Fast Resonant Extraction

Fast resonant extraction is accomplished by using the slow-extraction elements to bring the beam close to resonance and then firing a series of fast-pulsed quadrupoles to drive the beam into resonance. The strength of the pulsed quadrupoles is determined by the requirements on spill duration. We have studied[6] a fast-extraction system that satisfies the design criteria. The active elements consist of four pulsed quadrupoles located in the warm 48 lattice positions in sectors A, C, D, and F. Work is currently in progress on a Monte Carlo simulation of this fast-extraction system. Figure 8-3 on the next page shows a sample phase-space output at the magnetic septum. The initial results indicate that the required maximum field strength necessary for each element is approximately 25 kG-in. at 1 in. for a 3-ms half-sine-wave pulse. A list of the active extraction elements with their typical operational parameters is given in Table 8-I on the next page.

8.4 Straight-Section Layout

A detailed layout of the D0 long straight section from C49 to D11 is shown in Fig. 8-4 on page 145. The superconducting magnets downstream of D11 are shielded from the extraction losses by a vertical dogleg produced by the bending magnets B1, B2, and B3 and an aperture-limiting scraper downstream of the electrostatic septum. The amplitude of the vertical dogleg is approximately 6 cm. Detailed results of a Monte Carlo study of the loss

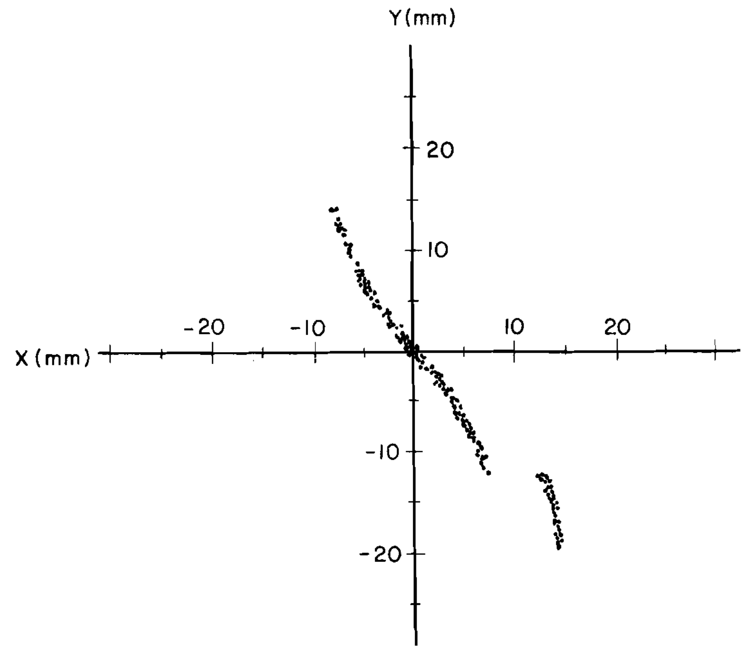

Fig. 8-3. Separatrix for half-integer fast resonant extraction.

Table 8-I. Extraction Elements.

Element	Position	Parameters
Electrostatic Septum	Upstream D0 long straight section	length 6 m gap 16 mm voltage 75 kV
Magnetic Septum	Upstream A0 long straight section	length 95.5 ft field 12 kG
Slow extraction	Correction coils A, B, C, F (28,42) sectors (stations)	255 kG - in. total quadrupole at 1 in.
Slow extraction	Correction coils A, B, C, F (28,42) sectors (stations)	412 kG - in. total octopole at 1 in.
Fast extraction Quads	A48, C48, D48 F48 mini-straight	25 kG - in. at 1 in. (max) per element for 3.0 ms half sine wave pulse

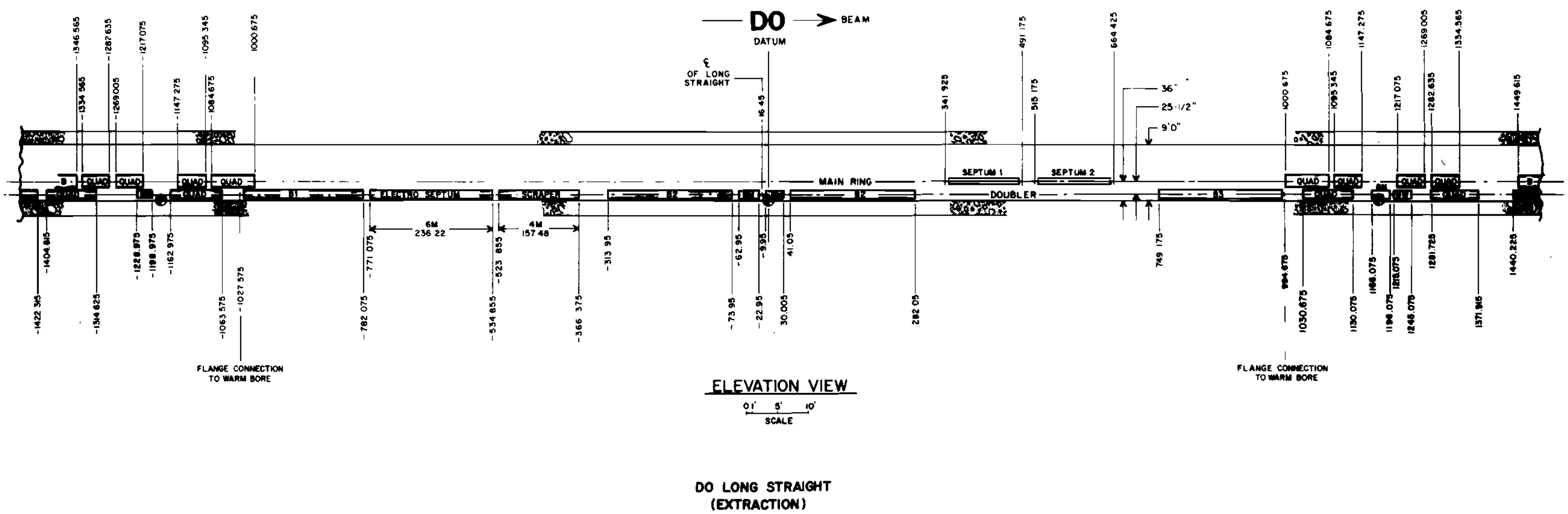

Fig. 8-4. Layout of D0 long straight section.

distributions associated with this design are presented in Section 13 of this report. Local orbit control is provided by the conventional bump magnets located as shown, together with one in the C48 mini-straight section. With this system of bump magnets, we have a maximum spatial offset at the septum of 7 mm and an angular range of 150 μrad.

8.5 Extraction Channel

One of our basic design goals with the extraction channel has been to produce a layout that maintains compatibility with the continued use of the Main-Ring extraction facility. The design we are presenting here fulfills this criterion. The layout of the A0 long straight section is shown in Fig. 8-5. The initial beam separation is accomplished by 5 Lambertson magnets, each 220 in. in length with a 12.5-kG field at 1 TeV, producing a total vertical bend of 10.48 mrad, which results in a vertical displacement of 6.005 in. from the circulating beam at the downstream end of the magnets. The extracted beam is then deflected both horizontally and vertically by a series of three standard superconducting dipoles powered in series with the superconducting ring magnets. This string of magnets, rotated by 19.05° from the horizontal, produces a 23.019-mrad radially outward bend and a downward deflection of 7.948 mrad. A horizontal trim magnet 40 ft further downstream is then used to adjust the beam trajectory to produce a simultaneous horizontal and vertical intercept of the beam with the existing extraction channel upstream of Switchyard Enclosure B. At this point, the beam is deflected into the current extraction channel by a Main-Ring dipole, rotated by 32.06° from the vertical position, on a trajectory similar to the Main-

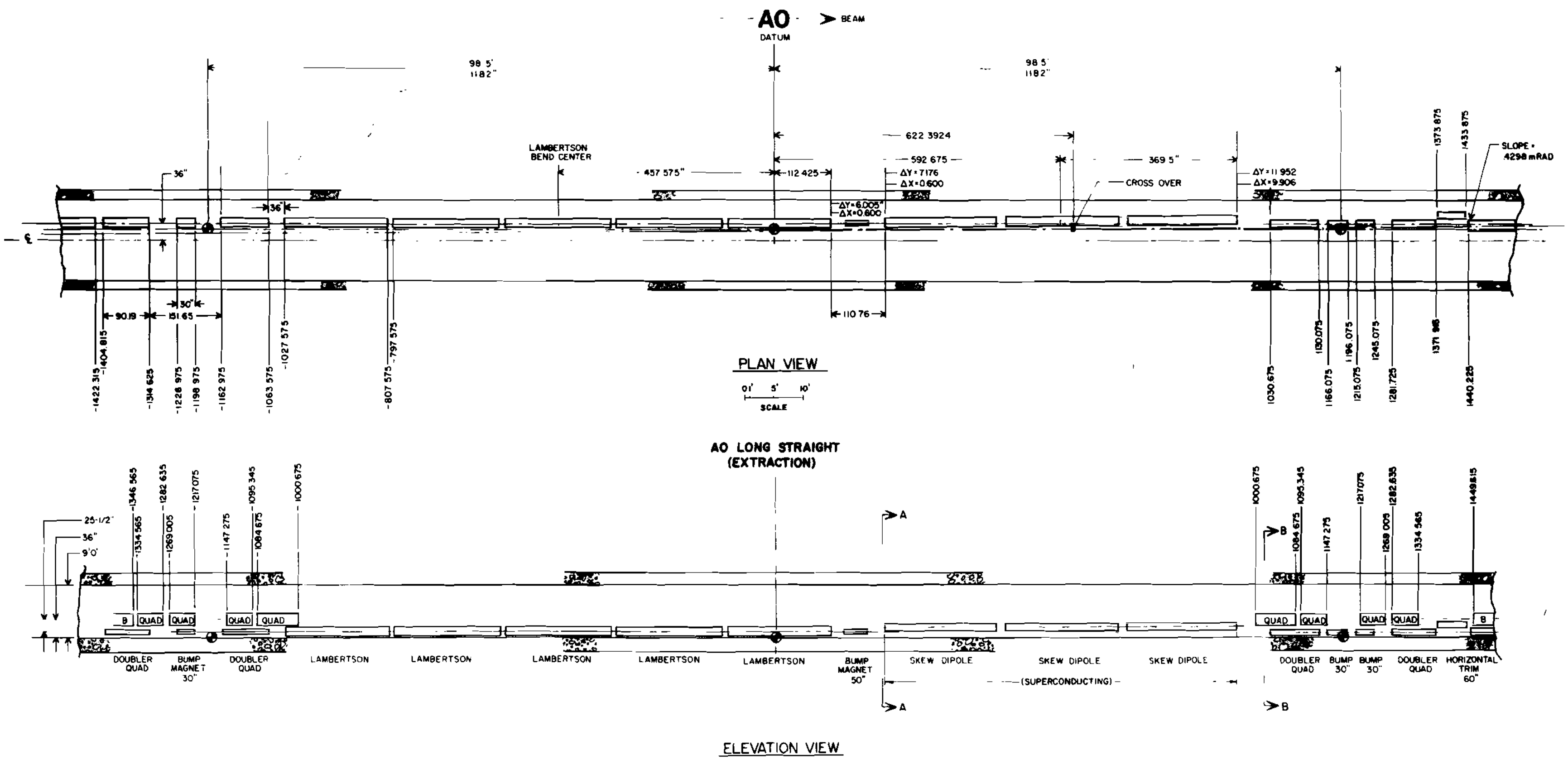

Fig. 8-5. Layout of A0 long straight section.

Ring extracted beam. The detailed horizontal and vertical geometries of the extracted beam are shown in Fig. 8-6.

The phase-space trajectory of the separatrix across straight-section A in Fig. 8-2 shows the extracted and circulating beam converging with a maximum angle of 110 μrad, which corresponds to a reduction in beam separation of 1.2 mm at the downstream end of the Lambertson magnets. In order to correct this somewhat undesirable situation, the upstream Lambertson magnet will be rotated by 85 mrad from the vertical position, causing the two beams to diverge by 100 μrad.

Figures 8-7 and 8-8 give cross-sectional views of the extraction channel at the positions indicated in Fig. 8-5. The minimum clearance between the circulating beam and the extraction elements is 2 in. at the upstream end of the superconducting dipoles. In order to maintain this minimum clearance, a special custom-made turnaround box will be required for these magnets.

Horizontal and vertical steering into the transport line will be accomplished with the horizontal trim magnet and the Lambertson string. The long downstream lever arm ensures ample positional control at the intercept point with the Main-Ring extraction line.

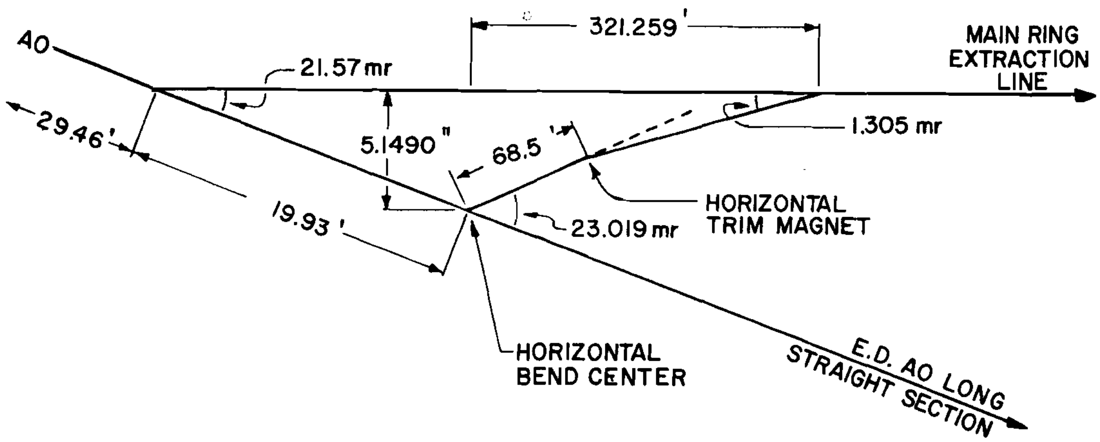

EXTRACTION CHANNEL— HORIZONTAL GEOMETRY

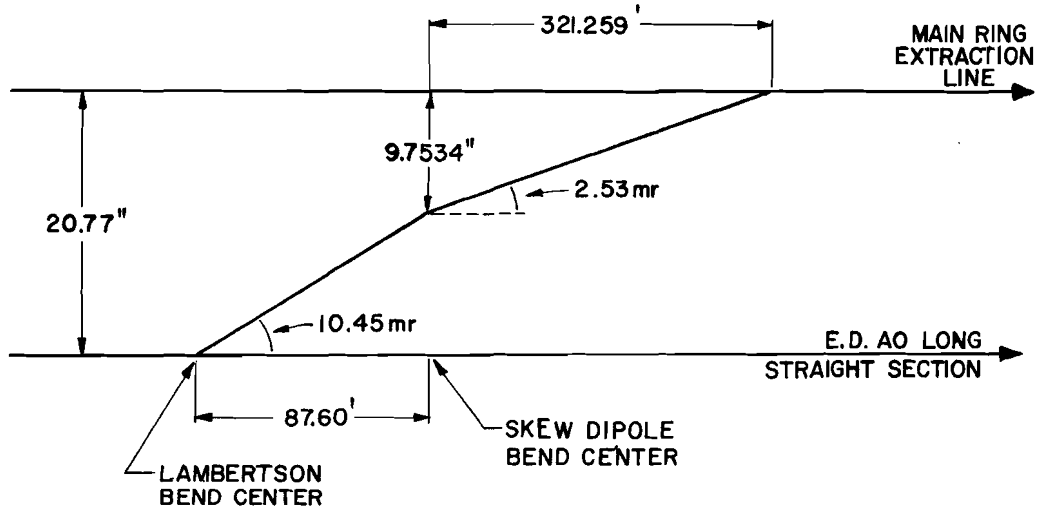

EXTRACTION CHANNEL— VERTICAL GEOMETRY

Fig. 8-6. Horizontal and vertical geometry of the A0 extraction channel.

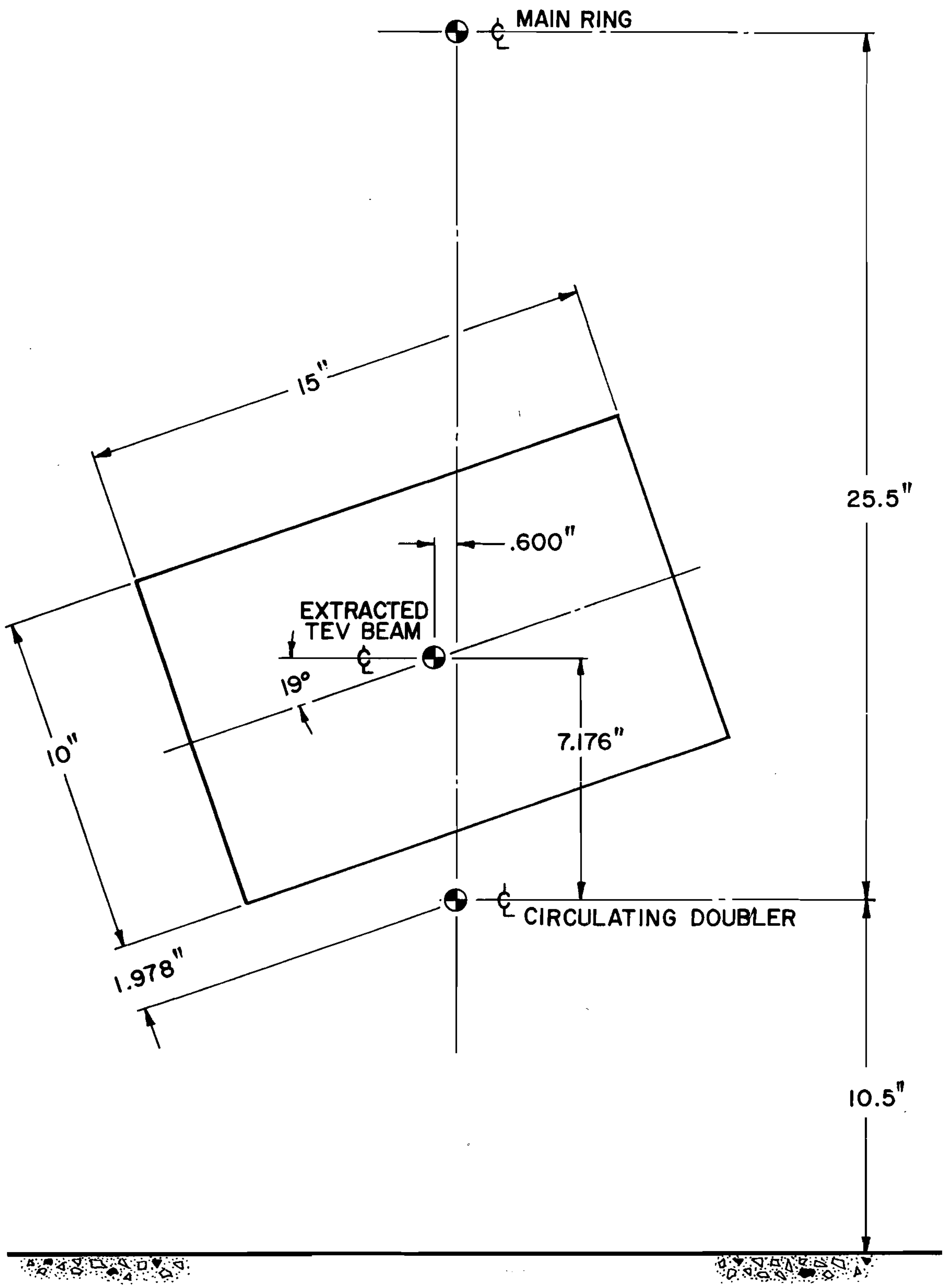

Fig. 8-7. Cross section AA of the extraction channel.

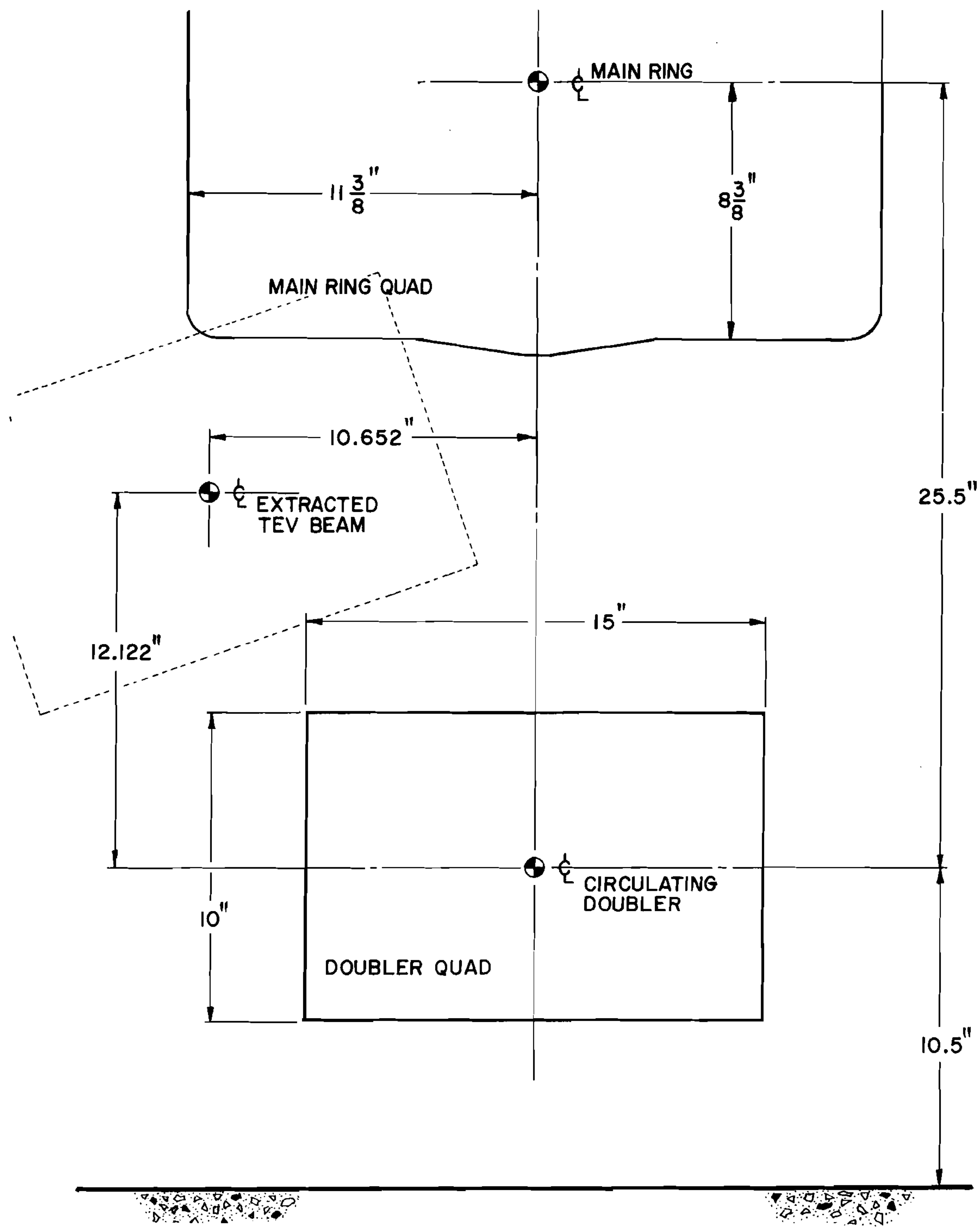

Fig. 8-8. Cross section BB of the extraction channel.

References

[1] M. Harrison, Magnet Aperture and Extraction, Fermi National Accelerator Laboratory UPC No. 16, December 4, 1978 (Revised January 17, 1979).

[2] H. Edwards and M. Harrison, Good Field Region of the Design Bend Magnet and Expected Behavior of Extraction, Fermi National Accelerator Laboratory UPC No. 66, October 19, 1978.

[3] T. L. Collins, High-Beta Straight Sections for the Doubler, Fermi National Accelerator Laboratory UPC No. 14, November 14, 1978.

[4] D. A. Edwards, Effect of a High Beta Insertion on Resonant Extraction from the Energy Doubler, Fermi National Accelerator Laboratory UPC No. 22, December 13, 1978 (revised).

[5] D. A. Edwards, Comparison of Half Integer and Third Integer Extraction for the Energy Doubler: 1. Basic Processes, Fermi National Accelerator Laboratory UPC No. 34, December 1978.

[6] M. Harrison, Extraction III - Fast Resonant Extraction, Fermi National Accelerator Laboratory UPC No. 87, February 27, 1979.

9. ACCELERATION SYSTEM

9.1 Requirements

The first requirement on the system is that it be capable of accelerating a beam of 2.5×10^{13} protons at a rate of 75 GeV/s. It must also provide enough bucket area to contain this beam. Measurements at 400 GeV and 2.5×10^{13} find a longitudinal emittance of approximately 0.3 eV-s, four times that measured at 8 GeV. We will make the conservative assumption that the beam emittance at 150 GeV, the injection energy, will have this larger value, 0.3 eV-s.

The rf voltage and power requirements for proton acceleration of two possible beam intensities are summarized in Table 9-I.

Table 9-I. RF Requirements for Protons.

Beam intensity	2.5×10^{13}	10^{14}	ppp
Average beam current	0.191	0.765	A
Beam power	0.3	1.2	MW
Ramp slope	75	75	GeV/s
Synchronous voltage	1.58	1.58	MV/turn
Bucket area (150 GeV @ 75 GeV/s)	0.9	0.9	eV-s
Synchronous phase	47	47	deg
Peak rf voltage	2.16	2.16	MV/turn
No. cavities	6	6	
Peak cavity voltage	360	360	kV
Total cavity dissipation/station	64	64	kW
Total power per station	126	290	kW
(Beam/total power)/station	0.4	0.7	

There are also special requirements arising from antiproton acceleration. When the ring is to be used only for unilateral acceleration of protons in either direction, the location and spacing of rf cavities is not dictated by any consideration other than available space. For simultaneous bilateral acceleration and subsequent storage of protons and antiprotons, however, some restrictions must be imposed upon cavity spacing. By appropriate spacing and phasing of the rf fields in individual cavities, some aspects of bilateral operation can be optimized. The requirements for $\bar{p}p$ operation are:

(i) The rf system must create sufficient bucket area for simultaneous bilateral acceleration and storage of protons and antiprotons. Because the total number and longitudinal emittance of protons and antiprotons will almost certainly be quite different, the required bucket areas will not necessarily be the same.

(ii) The rf system should provide the capability for moving the bunch collision point azimuthally over some reasonable range (of order 20 m).

(iii) The system may be required to allow for independent control of the phase and amplitude (bucket location and size) of the proton and antiproton buckets.

If requirement (iii) is satisfied, then (ii) is automatically, but it is possible that (ii) may be satisfied in a system that does not meet (iii).

9.2 Cavity Spacing

It is necessary to consider cavity spacing in order to satisfy the requirements listed above for bilateral acceleration. The basic unit is two adjacent cavities placed such that their effective gaps are $3\lambda/4$ apart, where λ is the rf wavelength. A particle moving downstream arrives at the second gap at a time phase $3\pi/2$ radians later than its arrival at the upstream gap.

If the downstream-cavity gap voltage leads the upstream voltage by $\pi/2$, a particle moving downstream will see the gap voltages exactly in phase (modulo 2π), and consequently the two cavities provide maximum voltage and bucket area for such a particle. But a particle moving upstream will see the gap voltages exactly out of phase and, if the gap voltages are equal, will see no net voltage. An additional similarly spaced doublet, with opposite relative phasing, can be placed arbitrarily close to the first pair. There is good reason to space the gaps of the nearest neighbors of adjacent doublets $\lambda/2$ so a pair of doublets (four cavities) will occupy a space of approximately 2.5λ. All three requirements above can be satisfied through the use of such doublets. Upstream and downstream doublets can be driven from separate rf sources and operated at different amplitudes and phases.

As an example, Fig. 9-1 shows three doublets, the two outside doublets providing proton bucket area while the center doublet provides antiproton bucket area. A simple fanout system is shown to demonstrate that the required phasing can be accomplished using easily available components, quadrature hybrid junctions and π radian splitters. In the array shown, with all gap voltages equal, the proton bucket area will be larger than the antiproton area by a factor 1.414 during beam storage. During acceleration, the bucket-area difference will be slightly larger because the antiprotons will require a larger synchronous phase angle because less voltage is available and consequently the moving-bucket factor reduction will be larger.

The cavity spacing described is essentially a series of cavities (1, 4, and 5) with their gaps spaced an integral number of half-wavelengths apart and another group (2, 3, and 6) with the same relative spacing but all

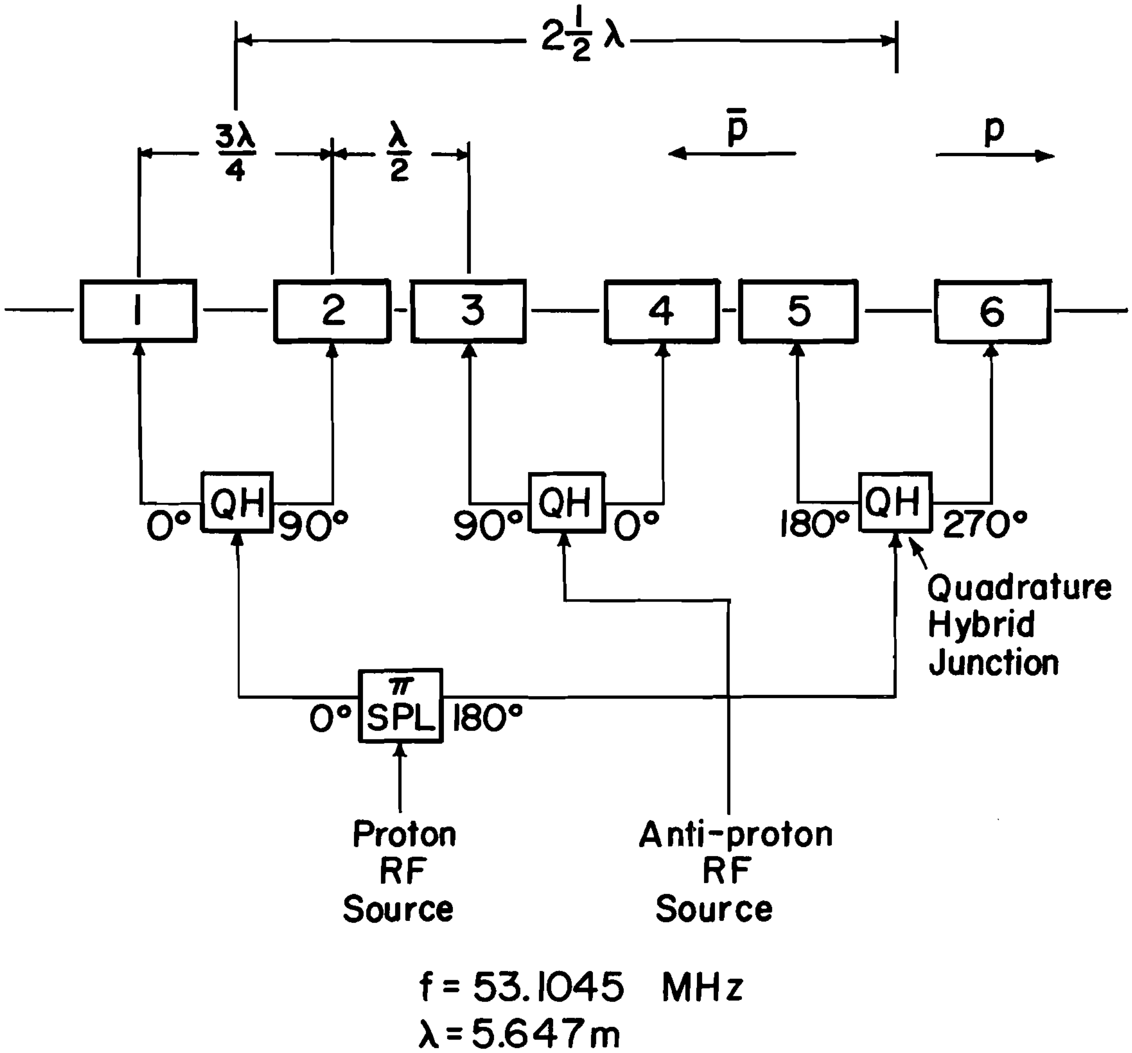

Fig. 9-1. RF cavity spacing and phasing for orthogonal $\bar{p}p$ control.

displaced by $\lambda/4$. Such an array of cavities can be phased in a slightly different manner to provide a greater total bilateral bucket area if requirement (iii) is relinquished. Such a phasing scheme is shown in Fig. 9-2. The proton and antiproton bucket areas are equal and each effective voltage is 0.707 V_{tot}.

With the phasing shown in Fig. 9-2, the intersection point is $\lambda/8$ to the left of the midpoint of the array. If the voltages of cavities 2, 3, and 6 are reduced to zero, the intersection point will move to the midpoint of the array, with a slight reduction in bucket area, and if cavities 2, 3, and 6 are raised to maximum voltage with opposite phase, the intersection point will move to a point $\lambda/8$ to the right of the midpoint.

It is possible that the phasing of Fig. 9-2 could be used during acceleration and the phasing switched to the phasing of Fig. 9-1 to provide orthogonal control after storage energy is reached. Because of the quite different geometry of the two fan-out systems, this phase switching would be difficult and would require great care to avoid phase-space dilution or loss of particles.

9.3 System Design

A frequency of 53 MHz, the same as the Main Ring, is chosen in order to:

(i) give high-efficiency transfer of beam from the Main Ring by means of a synchronous bucket-to-bucket scheme;

(ii) minimize the rf voltage;

(iii) take advantage of an existing 160-kW power amplifier at this frequency;

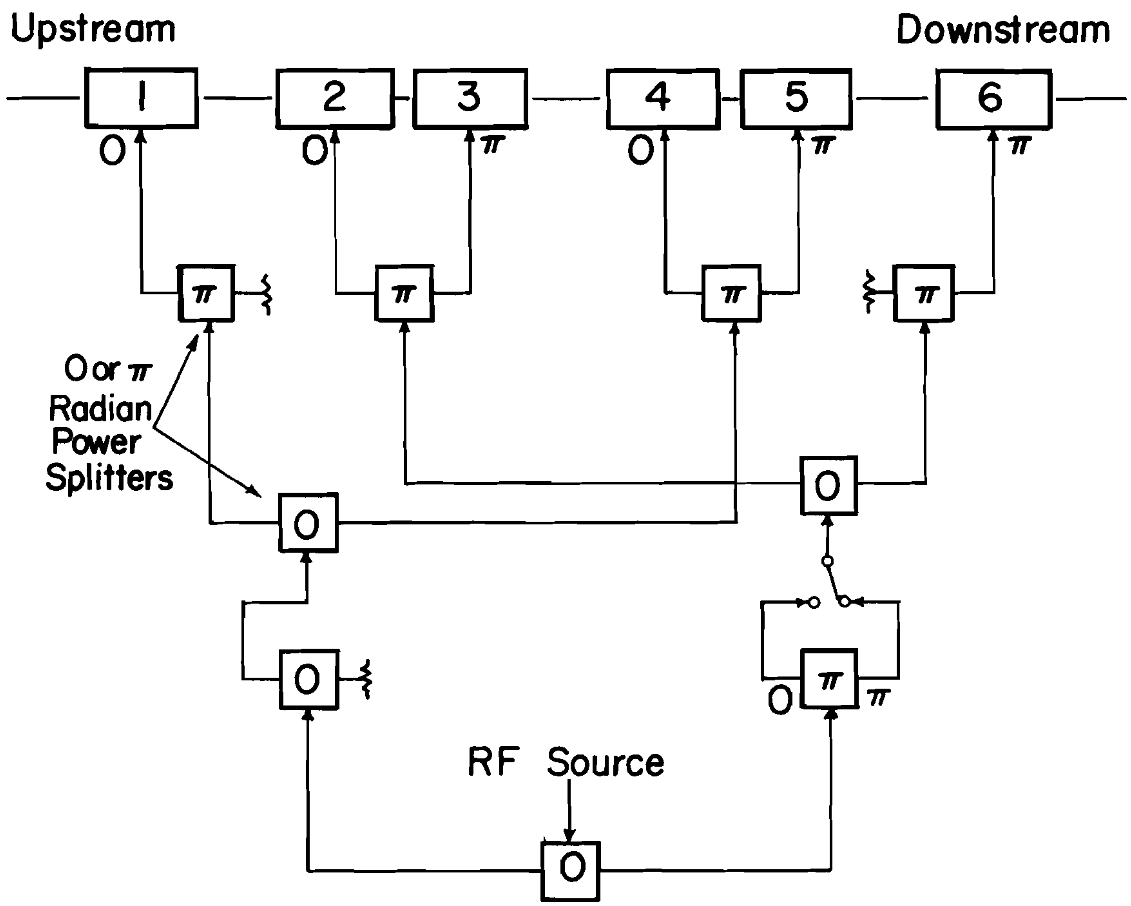

Fig. 9-2. RF cavity spacing and phasing without orthogonal $\bar{p}p$ control.

(iv) have the Main Ring and superconducting ring beams collide in the simplest possible way.

In order to utilize existing facilities and to utilize straight-section space efficiently, it is highly desirable to locate the system in straight-section F. A layout of the six cavities in the straight section is shown in Fig. 9-3. Recent development work has upgraded the voltage and power levels of Main-Ring rf stations. If additional space is needed for the new system, some Main-Ring cavities can be removed without injury to present performance.

The rf power amplifiers will be located in a new ground-level equipment building (65 ft × 28 ft) located directly above the F0 straight section. RF power will be delivered to the cavities by a $3\lambda/2$ long 9-in. coaxial transmission line connecting the equipment room and tunnel. Locating the power amplifiers upstairs has several advantages: less space is required in the tunnel, all the active electronics is directly accessible for repair, and radiation exposure to personnel is reduced. Radiation leakage through the transmission-line penetration should be small.

9.4 RF Station Components

A cross section of an rf station is shown in Fig. 9-4. The components are described below.

9.4.1 Power amplifier. The 160-kW modified Main-Ring power amplifier (PA) is capable of powering a superconducting-ring cavity at levels appropriate for intensities of 2.5×10^{13} ppp (see Table 9-I, column 1) with sufficient power to compensate satisfactorily for beam loading. Above

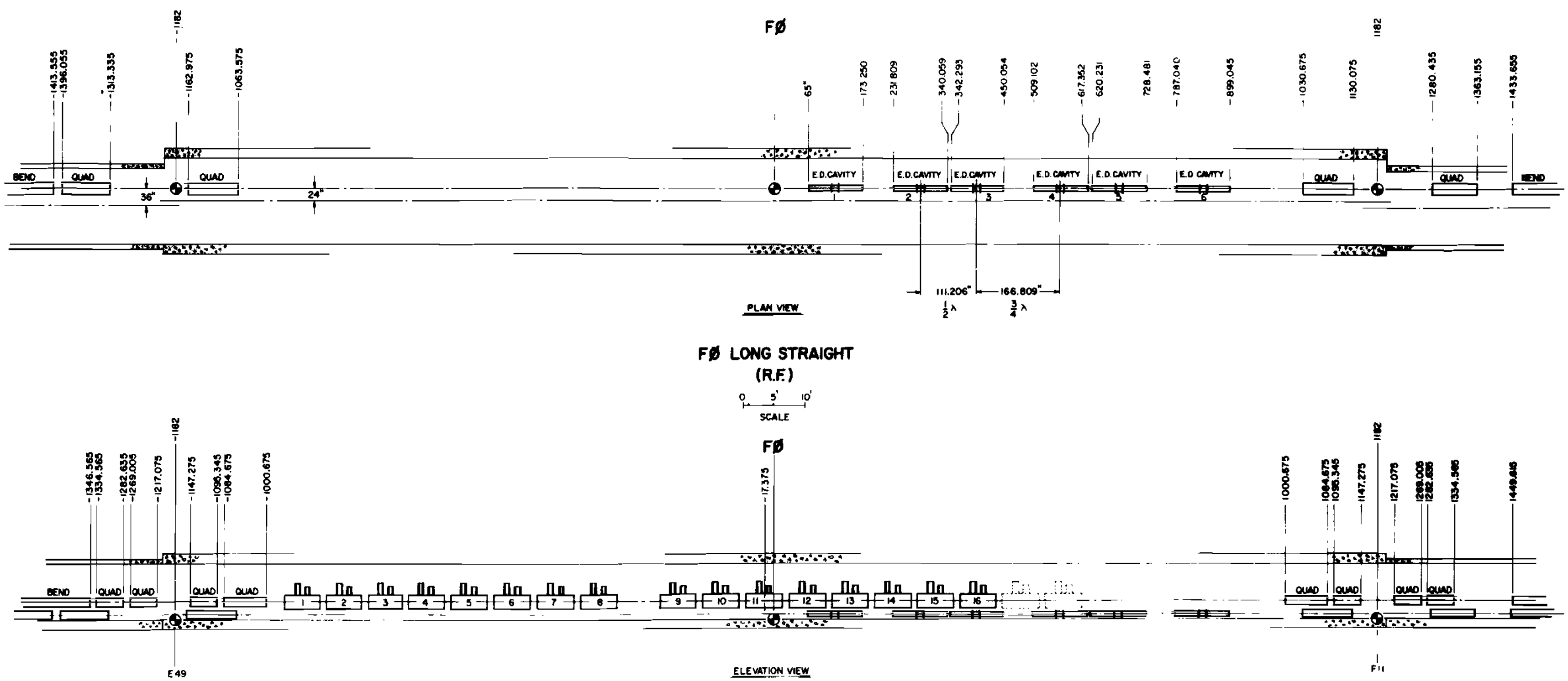

Fig. 9-3. Layout of F0 long straight section.

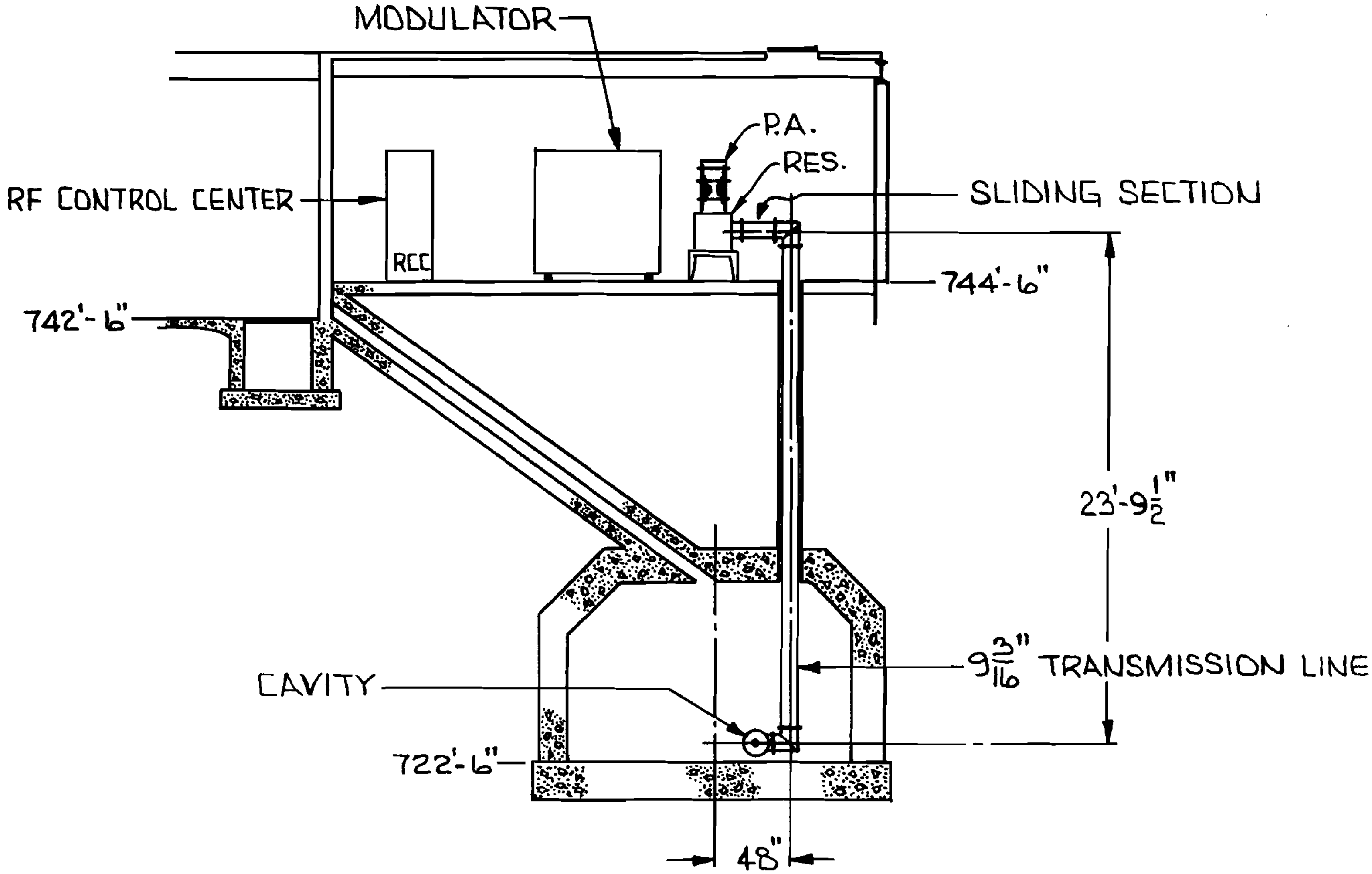

Fig. 9-4. RF station cross section.

intensities of 2.5×10^{13} ppp, it will be necessary to consider additional rf power for both real and reactive beam loading, for example, two PA's per system or a single higher-power PA. Furthermore, by the time beam intensity necessitates increased power requirements, a new PA design could be available. The parameters in column 2 of Table 9-I (10^{14} ppp) can be met with higher-power amplifiers plus fast beam-loading feedback.

9.4.2 Resonator. A tunable resonator is used to match the PA output impedance into a 50-Ω transmission line. A newly designed blocking capacitor of the type used in the Fermilab Booster will be used to couple the PA into the resonator. Figure 9-5 shows a cross-section view of the PA, resonator, and impedance-matching tap arrangement.

A prototype resonator has been constructed for testing the 160-kW PA. A means of automatic tuning of the resonator over a frequency range of a few kHz will be worked out to adapt the test resonator to the rf system. Power is coupled out of the resonator into a $3\lambda/2$ transmission line.

9.4.3 Transmission line. The coaxial line will be 9-3/16-in. rigid 50-Ω line with Rexolite insulators. The average power rating of 9-3/16 in. rigid line at 53 MHz is 600 kW. This average rating is based on an allowable temperature rise (above 40°C ambient) of 23°C for the outer conductor and 62°C for the inner conductor. The maximum peak power for the line is 5.8 MW, which corresponds to a 24-kV peak.

The transmission line will be fixed at the cavity end and have a sliding section at the resonator end. The sliding section will be used to adjust line length.

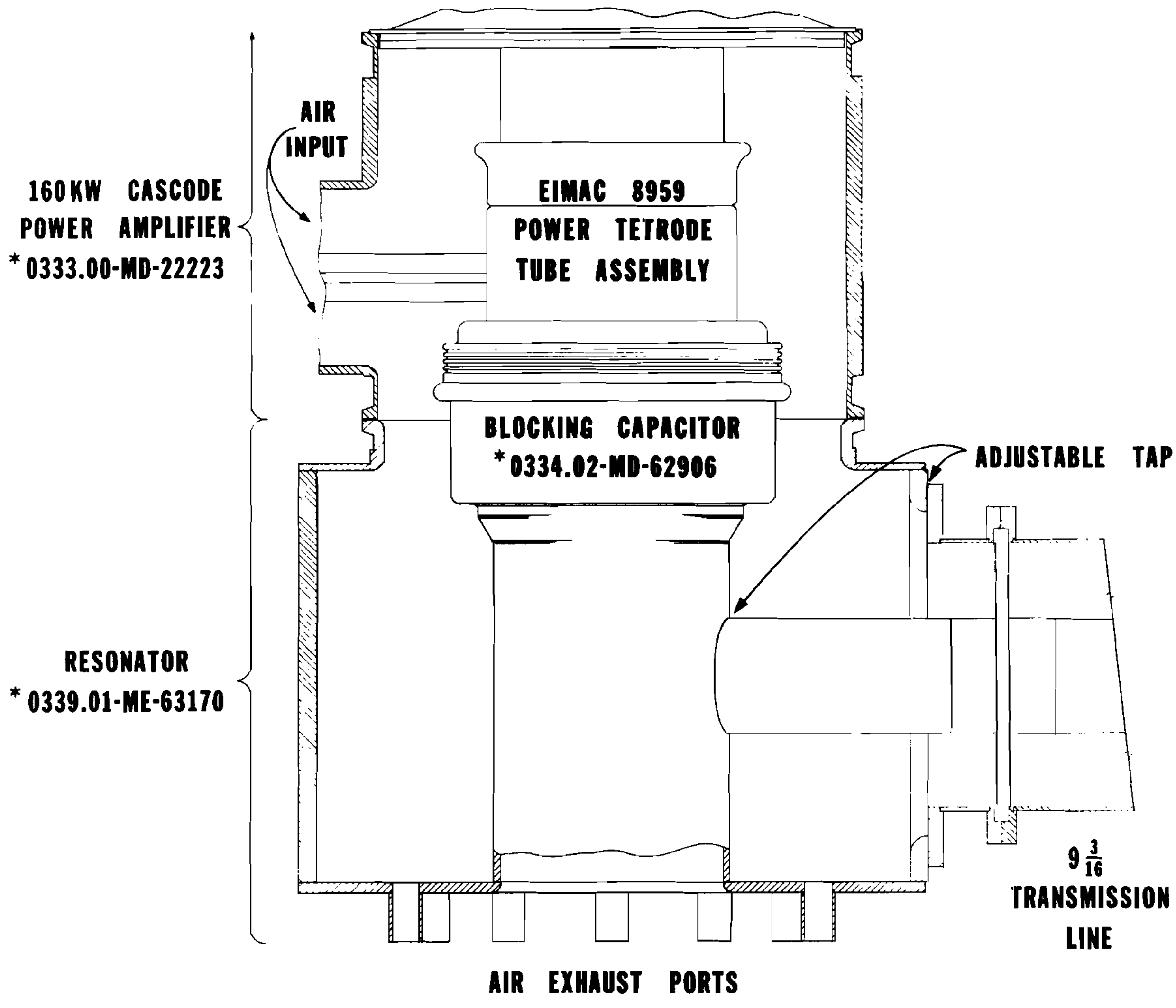

Fig. 9-5. RF power amplifier and resonator.

9.4.4 Modulators. Statements about the modulator suitability require some knowledge of the exact rf program intended. The Main-Ring modulators are presently being modified to operate at 30-kV output for operation with the modified cavities. They are capable of a regulated output current of 10 A as presently designed.

At 2.5×10^{13} intensity, the required PA power is 126 kW, with 57% efficiency. The power required from the modulator at (28 kV dc) is therefore 221 kW. The modulator current is 7.75 A, which, with a 5-kV series-tube drop, results in a modulator series-tube power dissipation of 38.8 kW. When power is being delivered to the beam, the rf voltage will remain high, so we will keep the series tube voltage drop near 5 kV. Present modulators are a good match to the 160-kW PA at 2.5×10^{13} ppp. During flattop, there is no real beam power, but there are reactive beam load and cavity power to be considered. Maximum dissipation occurs when the modulator output is approximately 16.5 kV. By careful programming of the voltage drop across the series tube, we can use the 15 A capability of the series tube.

Main-Ring rf modulators will be used initially as designed and later with modifications to deliver 15 A as beam intensity increases. To achieve 1×10^{14} ppp, a new modulator design will be required. One modulator will then be used to supply plate voltage to a higher-power PA.

9.4.5 Anode power supplies. Presently two anode power supplies across the road from the F0 RF Building supply dc voltage for Main-Ring modulators. These power supplies are each rated for 33 kV at 48 A average dc load. A series 20-Ω resistor is installed in the dc output of the supply to prevent overstressing the power transformer during crowbar operation.

If we run rf stations with two modulators on each anode supply, the resulting 30-A load current is well below the average rating of the supply. This assumes that we accelerate in the Main Ring only during the fall of the superconducting field. For a cycle requiring acceleration in the Main Ring during superconducting acceleration or flattop, as will be required for any colliding-beam mode, additional anode power-supply capability will be necessary for intensities greater than 2.5×10^{13}.

9.5 Cavity Design and Operation

9.5.1 Electrical design parameters. The cavity, shown in Fig. 9-6, is a coaxial resonator, 12 in. in diameter and 108-1/4 in. long, formed of copper 102 with ceramic rf windows. The characteristic impedance Z_o is approximately 70 Ω over most of its length, purposely lowered in the center section, and modified at each end by corona rings. Because the required frequency range Δf is a maximum of 2.271 kHz, the cavity is designed as a fixed-tuned two-gap structure of length $\ell \approx \beta\lambda/2$. The drift tube is actually 160° long electrically rather than 180°, so that $V_{effective} = V_{gap} \sin(160°/2) = 0.985\ V_{gap}$ is slightly less than the maximum achievable. The cavities' resultant mechanical length permits mounting them end-to-end at 180° electrical spacing if desirable.

The 160° drift tube is supported by ceramic rf windows and is capped by corona rings dimensioned to minimize the corona-ring gradient. At 200-kV peak gap voltage, the rf gradient is approximately 70 kV/cm. The corona-ring capacitance somewhat increases the skin loss. This design results in the parameters in Table 9-II.

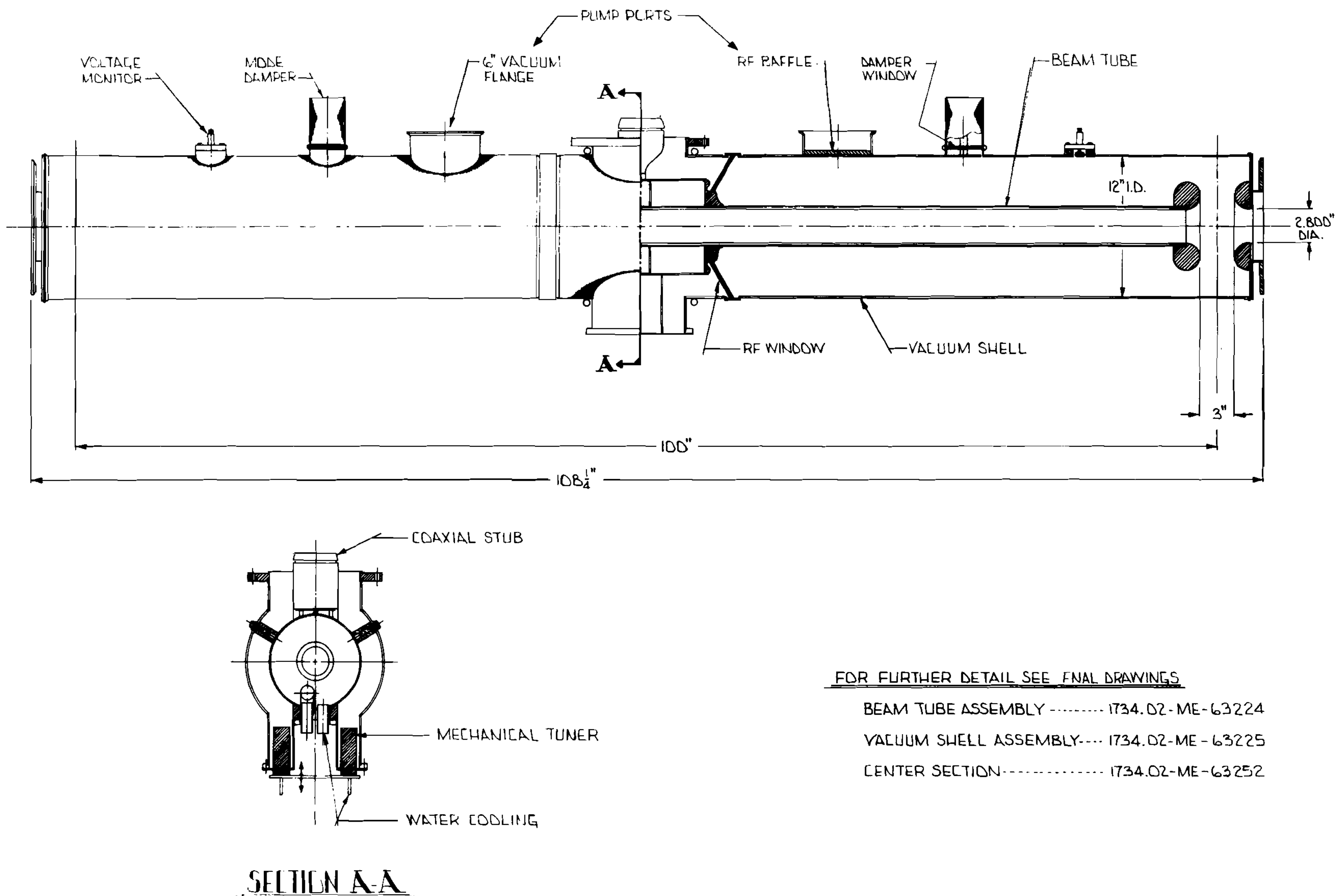

Fig. 9-6. RF cavity.

Table 9-II. RF Cavity Parameters.

Parameter	Unloaded Cavity	Cavity w/Beam Load (2.5×10^{13} ppp)	
Peak voltage	360	360	kV
Frequency	53	53	MHz
Z_o	70	70	Ω
Q	6,500	3,650	
Shunt impedance	1	0.56	MΩ
Time constant	39	22	μs
RF power required	64	114	kW
0.707 bandwidth	8	14	kHz
Stored energy	1.2	1.2	J

RF power is applied near the center of the cavity at a point tapped down on the drift tube where the 50-Ω drive line is impedance-matched at full load. At less than full load, the $3\lambda/2$ line will operate at the same rf voltage at the voltage maxima as with full load, but instead of operating as a flat line, will contain voltage minima. This scheme was chosen to minimize the possibility of line sparking. There will be spark-protection circuitry that interrupts rf drive and anode supply voltage for either cavity, coax line, or PA sparking.

It is expected that the cooling and spark protection will allow operation at 360-kV peak accelerating voltage per cavity (180-kV peak per gap).

Damping of obnoxious modes will be accomplished by resistors coupled through the side walls of the resonator, comparable to what has been successfully done on the present Main-Ring cavities.[1] At 1×10^{14} ppp, we will need the "stuntbox," which sends an antipulse through the PA to arrive at the cavity synchronously with the beam-loading perturbation.[2] This feed-forward technique is available to us in principle at any time, but we will have to construct additional low-level hardware for its implementation.

9.5.2 Mechanical design. The mechanical design is sketched in Fig. 9-6. The drift tube is cooled by internally circulating water; this cooling is necessary to minimize thermal detuning. The outer copper tank is also water-cooled and temperature-stabilized.

The rf windows are 99% Al_2O_3 ceramic cones, metallized and brazed to OFHC copper rings that are in turn heliarc-welded to the copper inner and outer coaxial conductors. Thus, the entire cavity structure is vacuum-tight with no organic vacuum seals and is completely bakeable to 250°C if needed in order to lower initial outgassing rates.

9.6 Bunch Reconfiguration in the Main Ring

For antiproton-proton colliding beams, it is necessary to rebunch the beam in the Main Ring to approximately 12 bunches, in order to concentrate more protons per bunch to increase luminosity.

The plan is to debunch the beam from the usual harmonic h = 1113 by reducing the rf voltage adiabatically, then turning on a low-harmonic cavity to relocate bunches in phase space. After one-fourth of a phase oscillation, the bunches will have roughly clustered in phase at the lower harmonic, with an increase in total energy spread. The bunches are then recaptured in h = 1113 buckets by turning on the ordinary rf system.

Recent storage studies in the Main Ring have indicated, at an intensity of 2×10^{13} protons in approximately 1066 of the 1113 buckets, some 90% of the beam is contained within bunches 3 ns long and appear to be matched to stationary buckets of 1.25 MV/turn. This corresponds to a bunch length $\Delta\phi$ of 0.5 radians and a bunch area of 0.19 eV-s per bucket.

If the rf voltage is reduced until the bucket area has shrunk to the bunch area, then turned off, dilution by a factor $\pi/2$ will occur, so that the debunched emittance will be 0.3 eV-s per bunch, corresponding to an energy spread of ±7.8 MeV or a phase-space density of 5.7×10^{10} protons/eV-s. In order to create bunches containing 10^{11} protons, a charge bunch occupying area 1.75 eV-s must be captured. To compensate for losses in extraction, injection, and acceleration, we take this area to be 2 eV-s.

The voltage to create a 150-GeV 2-eV-s bucket at h = 1113 is 226 kV, so that recapture will create no problems. The maximum energy spread corresponding to a 2-eV-s bucket is ±83 MeV, well within the observed useful momentum aperture at 150 GeV.

The low-harmonic cavity should keep the center of charge stationary with respect to h = 1113 buckets while rotating a set of bunches. Its harmonic number must therefore be a factor of 1113. Consider, for example, h = 21, corresponding to a frequency of 1.0019 MHz. This bucket covers the azimuthal region occupied by 53 bunches. Approximately 26 bunches can be rotated into a vertical strip 19 ns long using a voltage of 12.7 kV. The synchrotron period is 0.6 s, so rotation will require 150 ms.

If the same exercise is carried out at h = 53, f = 2.53 MHz, each bucket will encompass 21 of the original bunches. The required voltage is 32 kV, a little high. The problem of aligning the h = 1113 bunches vertically in this phase space also appears to be more difficult than at h = 21, because of synchrotron tune spread, so the h = 53 option looks less favorable.

The question of whether the Main-Ring beam can be debunched at 150 GeV without instability has been investigated in a recent storage study.

Main-Ring beam was debunched at 100 GeV in a manner close to that described above and was observed to have a beam-storage lifetime consistent with that observed for bunched beam. Attempts to measure the momentum spread of the debunched beam by Schottky-scan techniques were not successful, due possibly to insufficient detector sensitivity or magnet ripple. Further attempts to make such measurements are planned.

Actual study and verification of the parameters described above cannot be accomplished at present, because we do not have an rf cavity of sufficiently large voltage that can operate in the Main Ring below 5 MHz. Reconfiguration studies at frequencies that are not integral sub-harmonics of 1113 are nevertheless useful and should be pursued. To this end, a surplus low-frequency cavity from the PPA accelerator has been installed in the Main Ring and various bunch-reconfiguration experiments will be done in coming months to clarify the precise requirements.

The antiproton beam is expected to consist of 12 bunches of 2-ns width, each containing 10^{10} antiprotons with a bunch area of 0.08 eV-s. This will require a stationary bucket of 3.6 eV-s and a voltage of 120 kV/turn at 1000 GeV.

References

[1] Q. A. Kerns and H. W. Miller, IEEE Trans. Nucl. Sci. NS-24, 1704 (1977).

[2] Q. A. Kerns, Proton-Proton Colliding-Beam Storage Rings for the National Accelerator Laboratory, Design Study Section VI, 19 8.

10. INJECTION

10.1 Introduction

The beam-transfer system from the Main Ring to the superconducting ring for both normal and reverse directions is essentially the same as that reported previously.[1] In the vertical plane, two Lambertson magnets form a dogleg to lower the Main-Ring beam by 25.5 in. In the horizontal plane, one fast kicker is used to extract the beam from the Main Ring and another to inject it into the new ring. In addition to these, two bump magnets in the Main Ring are used to adjust the closed orbit. Similar adjustments of the superconducting-ring closed orbit during beam transfer will be made by the regular steering elements built into quadrupoles. Space is available between the rings to install one small quadrupole common to both directions, useful for fine matching of beam shapes. Steering dipoles of modest size may also be placed there if needed. Specifications for all these magnets are not terribly difficult, but some developmental work may be required to improve the fast-kicker system.

The design presented here takes into account the somewhat complicated relative geometry of the two rings.[2] In the long straight section, the beam in the new ring is inside the Main Ring, but crosses it near the downstream end. For beam transfer, which is planned to be at 150 GeV/c, the Main-Ring beam must have a momentum offset of +0.25% for synchronous transfer and this moves the Main-Ring beam even farther out. It has been decided that the beam transfer will be done in long straight section E for both directions. One advantage of this scheme compared with the previous design, in which two long straight sections were used, is that some magnets can be shared by the normal and reverse beam transfers. At the same time, the essential features of the design are not affected much by this choice.

There are a number of important factors dominating the design of the system: (i) beam characteristics, (ii) Main-Ring aperture at 8-GeV injection, (iii) superconducting-ring aperture for circulating and for single-passage beams, (iv) maximum fields of septum magnets, (v) maximum integrated field, rise and fall times, and field ripple of fast kickers. Depending on how one factor is weighed relative to others, many variations of the design are possible and, as more information becomes available, the present design will probably be modified. What is presented here is an example demonstrating that there are no fundamental difficulties in beam transfer in either direction.

10.2 Beam Characteristics

10.2.1 Injection energy. The beam line is 25.5 in. below the Main-Ring beam line and the beam must be brought down in less than 50 m, the length of a long straight section. The upper limit of the beam momentum is then dictated by the bend fields achievable in septum magnets and the strengths of fast kickers. The lower limit is determined by the field quality of the superconducting magnets. Measurements indicate poor field quality at an excitation current of 200 A (45 GeV/c). Even at 500 A (113 GeV), the relative sextupole component of dipole magnets is 50% larger than at higher currents (see Fig. 3-11). Beyond 1,000 A (226 GeV/c), the field quality is essentially independent of the excitation currents. It is therefore assumed here that the transfer momentum is 150 GeV/c, which corresponds to 660 A. More careful design of septum magnets and kickers may show a possibility of using higher momentum values. Below 1,000 A, the magnetic field is modified by hysteretic magnetization that is produced by persistent current in superconducting filaments. The resulting field distortion in dipoles is mostly sextupole field and its magnitude depends strongly on the ramp history. In operation, the ramp current should be cycled to 500 A or lower to set the magnet fields on the proper side of the hysteresis loop. The possibility of introducing harmonic corrections for half-integer and third-integer resonances during beam transfer should not be excluded in the overall design.

10.2.2 Longitudinal emittance. A measurement[3] at 125 GeV/c gives 0.37 eV-s (90% of the beam, bunch spreader off) when the intensity is 2×10^{13}. There are reasons to believe that this value could be reduced by improvements in the Main-Ring injection phase-lock and in transition crossing. The value used here is 0.25 eV-s. At approximately 1 MV/turn in the Main Ring, the beam injected into the new ring is expected to have a momentum spread of $\pm0.25\times10^{-3}$. The contribution to beam size arising from dispersion is then less than ±1 mm in the long straight section. The beam will be transferred into stationary rf buckets with constant magnetic field, so there will be no mismatch and the momentum spread of the beam may be reduced by reducing the Main-Ring rf voltage. There may be a limit to the minimum value of the momentum spread one can achieve; too-small values might induce microwave instabilities. If the beam were transferred to accelerating rf buckets, say 50 GeV/s, with a synchronous phase = 133°, there would be a mismatch and the momentum spread of the circulating beam would increase to $\pm 0.33 \times 10^{-3}$ or more, depending on the Main-Ring rf voltage at the time of transfer. Any error in the phasing would contribute to a further increase in the spread and in the emittance. It is desirable to limit this error to within $\pm 5°$.

10.2.3 Transverse emittance. For single-turn injection of H^+ to the Booster, the emittance measured in the 8-GeV transport line is (1.0 to 1.2)π mm-mr. If there are no dilutions caused by mismatching or nonlinear fields, the emittance at 150 GeV/c will be 0.07π mm-mr. As a more realistic value, 0.15π mm-mr (95%) is assumed for the design. There are very few data available for multi-turn H^- injection into the Booster, but it is generally believed that the emittance is the same or only slightly larger.

10.3 Apertures

The radial offset of the ring relative to the Main Ring in the long straight section is shown schematically in Fig. 10-1. In order to make pp collisions of $(150 \text{ to } 200 \text{ GeV/c})_{MR} \times (1{,}000 \text{ GeV/c})$ possible, the path length is designed to be longer by a factor 7.0×10^{-6} compared with the Main Ring. As a consequence, the Main-Ring beam must have a momentum offset of +0.25% during beam transfer if the beam is to be injected with zero momentum offset in the superconducting ring. The septum magnets should not be too close to the beam axes, although how much space is really needed is not well defined. Larger space would certainly make operation easier. In the present design, the kicker in the Main Ring for normal transfer is placed at station 48 immediately upstream of the septum magnet in order to prevent a large beam excursion at that point. In the new ring the falloff of the design

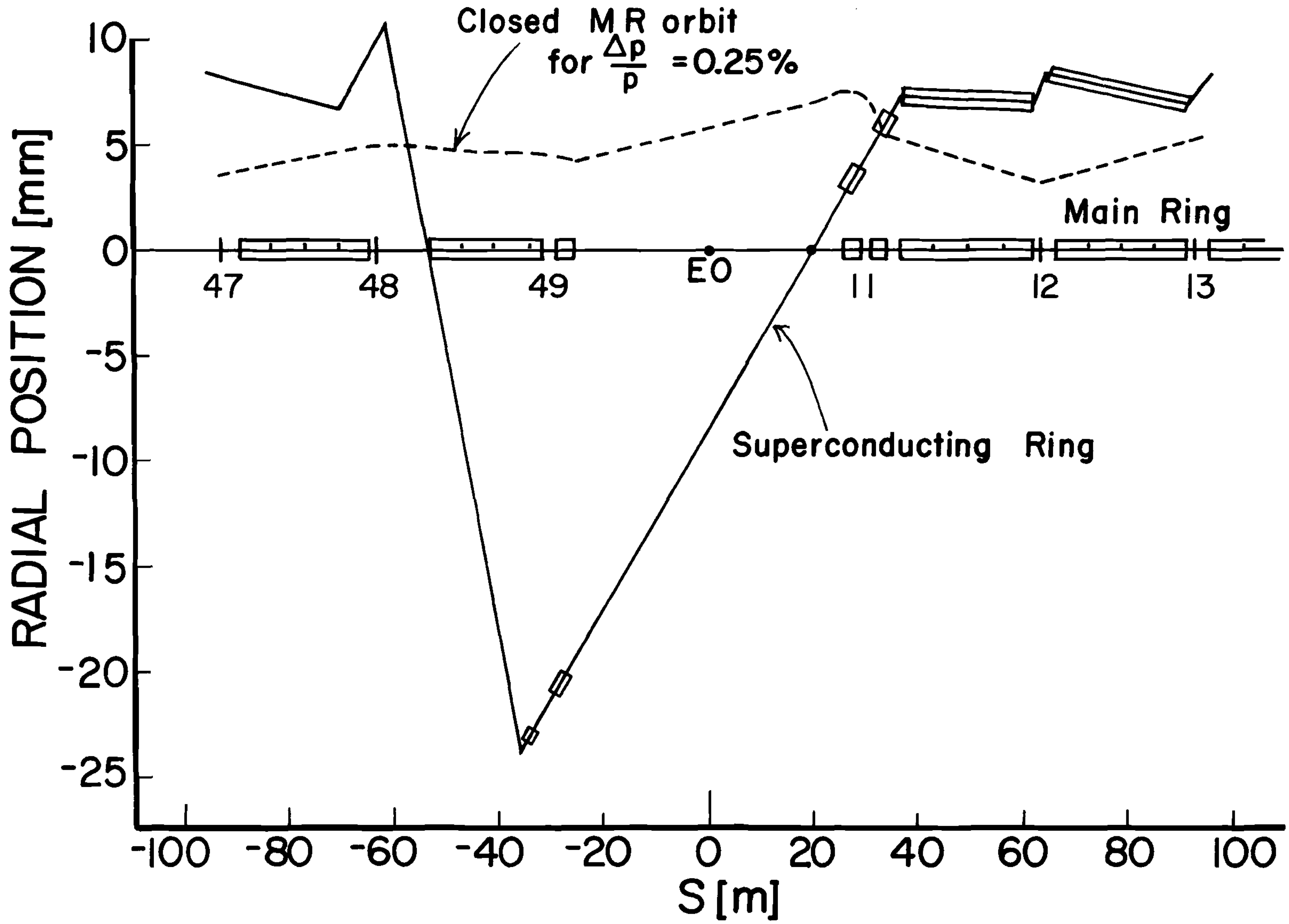

Fig. 10-1. Radial positions of the off-momentum closed MR orbit and the Superconducting Ring relative to the Main Ring.

field in the bending magnets starts at ±20 mm and has dropped to a $\Delta B/B$ of 10^{-3} at ±28 mm. Thus it would be best if circulating beams could be kept within 20 mm and single-pass beams within 28 mm of the magnet centers. This criterion is not satisfied in the case of reverse injection and further detailed study of the effects of the magnetic-field variation with radius on the injected beam is necessary. Quadrupole magnets have a much larger good-field aperture and are not expected to have a degrading effect on the beam.

10.4 Description of the System

A layout of straight section E is shown in Fig. 10-2. One important restriction in the design of the transfer system is the limited choice of kicker location in the new ring. Kickers must be placed only at warm places, which are at stations 17 and 48. In the Main Ring, all stations are in principle available, except where there are already major devices such as extraction and abort elements. Except at 48 and 17, where one and two dipoles are missing, respectively, the available space for a kicker or a bump magnet is not much more than 1 m. One feature that is a special advantage is that there is no need to do a major matching of the beam shape in the transverse phase space using many quadrupoles. The new lattice, even with various modifications, is still quite similar to the Main-Ring lattice as far as focusing characteristics are concerned and one weak quadrupole, $B'\ell = 18$ kG, is sufficient for both horizontal and vertical matching. By means of changes in polarity, the quadrupole can be used for injection in either direction. Without this matching, the expected dilution in emittance is approximately 30%. The location of this matching quadrupole is shown in Fig. 10-3.

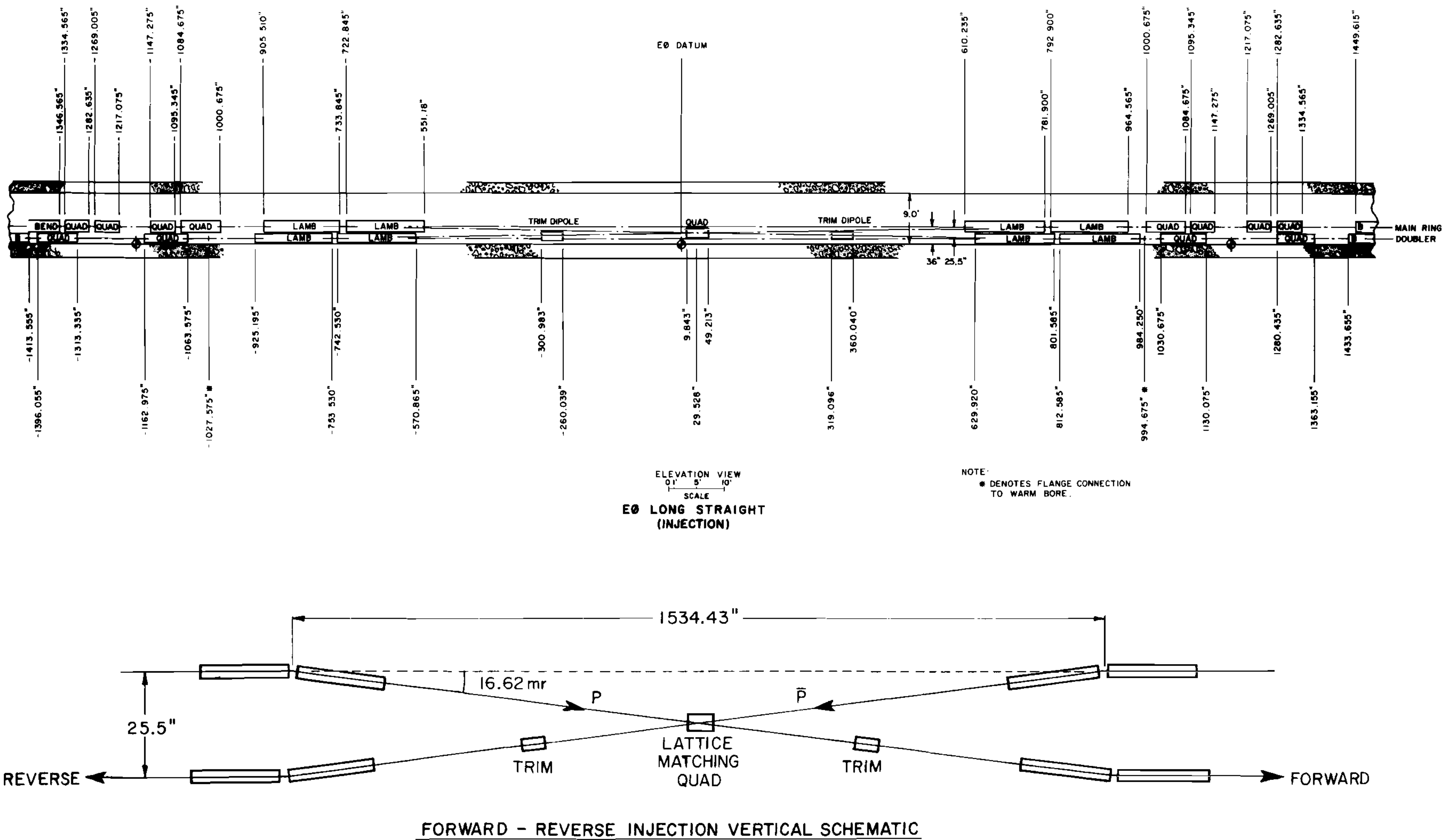

Fig. 10-2. Layout of E0 long straight section.

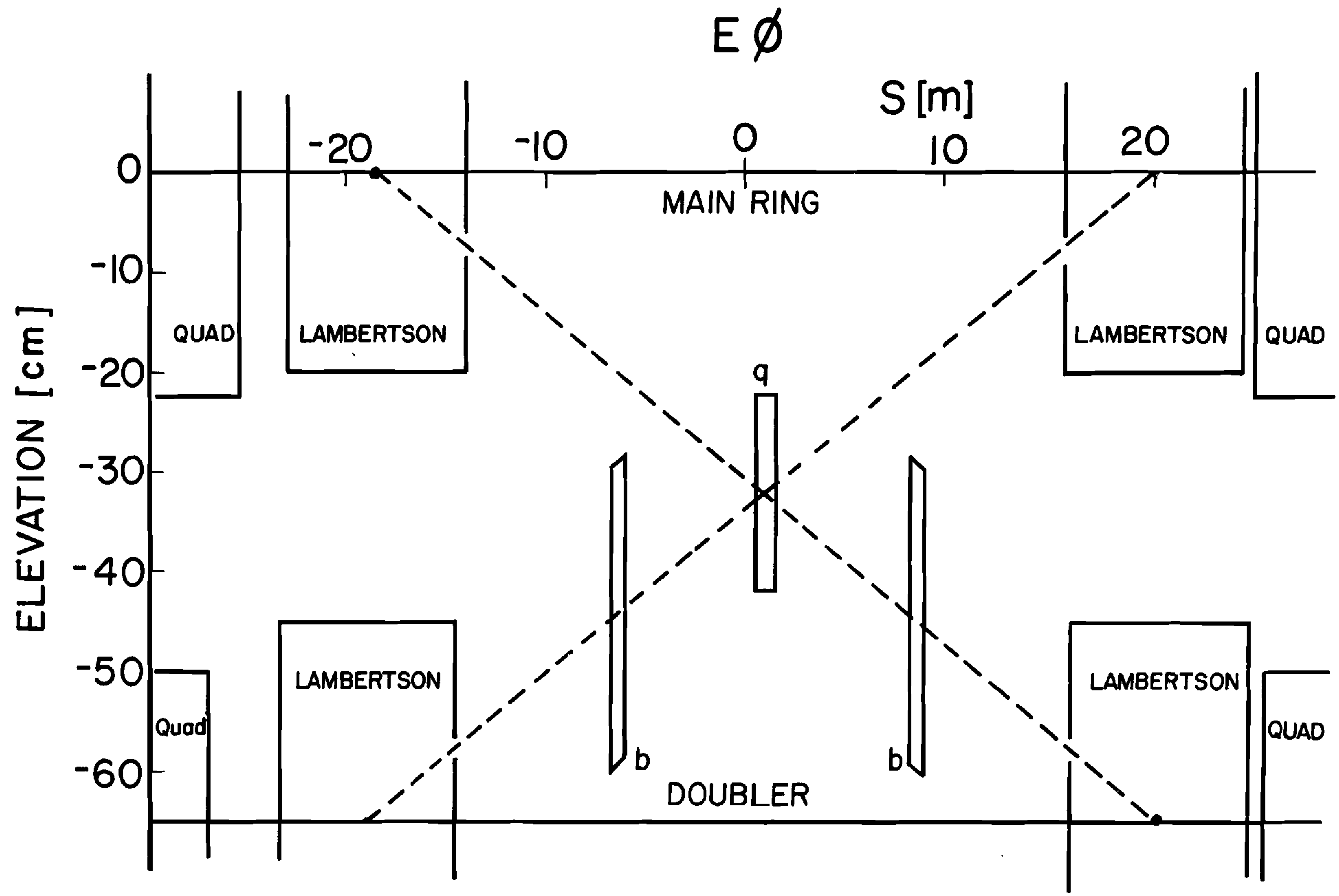

Fig. 10-3. Beam-transfer matching magnets.

Vertically, the system is two simple doglegs, each with two Lambertson magnets. In order to ease problems in the radial direction, the bend centers of those near station 49 are 7 and 8 m away from the upstream quadrupole, while the downstream ones are 5.3 and 5.0 m from the downstream quadrupole. The center-to-center distance of two magnets is approximately 39 m.

Radial positions of the beam center are shown in Fig. 10-4a for the normal-direction transfer and in Fig. 10-4b for the reverse direction. For the normal direction, the closed orbit is a combination of the natural closed orbit for $\Delta p/p = +0.25\%$ and a local bump between D46 and E17. The bump is not completely local, but the maximum perturbation outside is less than ±2 mm. In Fig. 10-4a, the beam is kicked outward by the kicker at D48 and this produces a separation of 15 mm at the septum magnet. The beam size there is ±3 mm (H) × ±4 mm (V). A three-magnet bump (D48, E11, E13) in the new ring gives a separation of 17 mm between the injected beam and the circulating beam. The kicker is at E17 and there are uncomfortable radial excursions of the beam between the Lambertson and the kicker. It may be necessary to introduce another local orbit bump (E13, E15, E17) if the excursion at 22.5 mm at E15 is too large. Steering coils in quadrupoles are strong enough to scan the entire aperture at injection.

In Fig. 10-4b, the Main-Ring kicker is at E13 and the other kicker at D48. Lambertson magnets are rotated to make small radial kicks. Specifications for the various elements are given in Table 10-I. The local closed orbit in the Main Ring between D46 and E17 is identical to the one for the normal beam transfer.

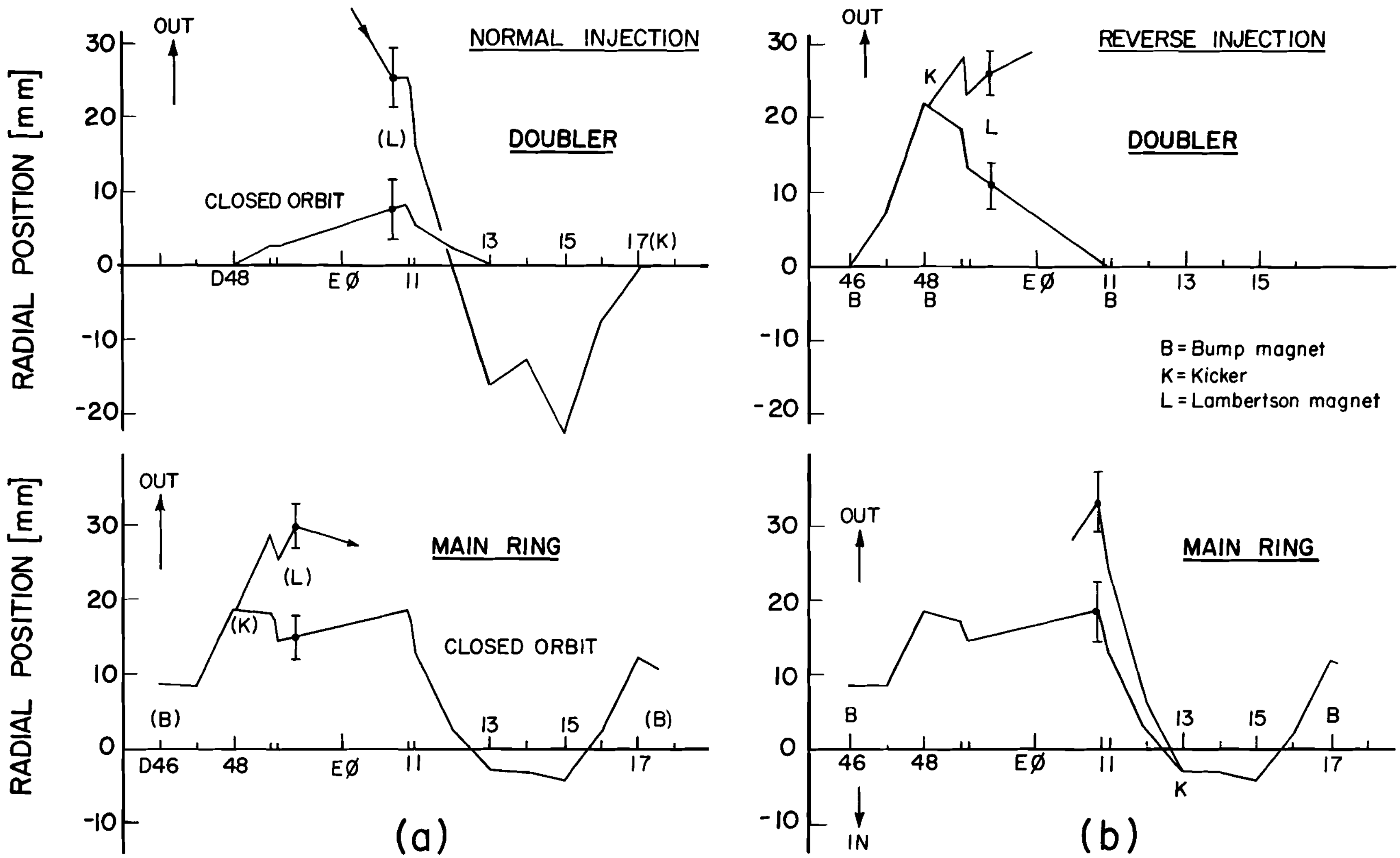

Fig. 10-4. Radial position of beam center during normal and reverse injection.

All needed spaces in the Main Ring are free of major elements. If necessary, short correction magnets can be relocated elsewhere. Since the abort system is entirely confined to long straight section C, large radial excursions of the beam exist in the superconducting ring only during slow extraction. These excursions are not excessive in E0 and there should be no problem with interference of the injection Lambertson with the extracted beam (see Fig. 8-2).

10.5 Discussion

(i) Lambertsons and fast kickers are in a way complementary. If, for example, one can use stronger Lambertsons, they can be moved towards the center (E0) to ease the requirements on kicker strength. This will have the advantage of reducing the radial beam position near the quadrupoles at both ends of the long straight section.

(ii) Steering in both radial and vertical directions must be provided. In the radial direction, local bumps in both rings can be used with a proper ratio to obtain either position-only or angle-only changes. It is easy to introduce a vertical local bump in the new ring, D47-E11-E14 for the normal transfer and D47-D49-E12 for the reverse transfer. The latter produces an almost pure position change. One probably needs vertical steering magnets between the two Lambertsons to make an orthogonal set together with these orbit bumps. One can see from the elevation view of Fig. 10-3 that there is enough space to install two steering dipoles of the vernier type 4-4-30 in addition to the matching quadrupole in the center. This dipole can produce a 0.8 mrad kick at 150 GeV/c.

(iii) Some phase-space dilution will occur during the injection process. If we require less than 25% dilution in both momentum and transverse phase space, then errors in the injection magnetic field should be less than approximately 10^{-4} and errors in position (angles) about 1 mm (10 μrad). Such position errors would be hard to obtain by dead reckoning; beam-detector readouts of the first few turns will be available for analysis and minimization of injection coherent oscillations. If the tune spread of the beam can be held to $\Delta\nu < 0.002$ by use of the chromaticity-correction sextupoles, then dampers that work over less than 50 turns can be effective.[4] The kickers alone are expected to have 2% peak-to-peak ripple over the injection time and short-duration rise-or fall-time tails and reflections of about 5% (or $2\frac{1}{4}$ mm at maximum beta positions). A damper capable of reducing these oscillations would be 3 m long, have a 6-cm gap, deflection plate voltage of ±4 kV, and a bandwidth of 5 MHz. It could produce a maximum of 1.3-μrad deflection per turn.

(iv) Since the entire injection system is confined to a relatively short distance, any perturbation in the phase advance should not affect the overall performance of the system. For example, if a low-beta insertion is introduced for colliding and if it is desirable to inject beam with the insertion on, the phase advance in a sector may change 30 degrees or more. It is easy to readjust local orbit bumps to compensate for this.

(v) The usefulness of the ring as a fixed-target accelerator will be enhanced considerably if the intensity can be increased to 10^{14}. With single-turn beam transfer, the intensity will be less than approximately

4×10^{13}. Furthermore, the beam quality certainly deteriorates as the intensity is increased in the Main Ring and this may make clean beam transfer very difficult. It would be much better if one could transfer ten turns of 1×10^{13} each; stacking in momentum space seems to be the only possibility for realizing this. Since one must avoid even a very small beam loss, it is essential that the dispersion at the kicker position (E17) be large. A high-dispersion insertion to raise η at E17 to almost 10 m has been worked out.[5] It requires different excitation of the main quadrupoles from E11 to E26. The largest change in excitations is at E11, where the amount required is $B'\ell = 55$ kG or 19% of this focussing quad strength. This change can be excited by shunt supplies with 200-A leads. Simultaneous correction of the injected and stacked beams is another problem one must solve. Nevertheless, it seems possible to think about momentum stacking and an example was included in an earlier report.[1] For stacking, the momentum offset of the beam should be +0.05% in the Main Ring and -0.20% in the new ring. The negative offset is natural because the beam comes from inside at the kicker position, E17, as shown in Fig. 10-4.

The magnet elements needed for beam transfer are summarized in Table 10-I on the next page.

10.6 Injection Kickers and Beam Synchronization

The operation of the kickers is different for injection of p's for fixed-target physics or pp colliding beams and the injection of p's and $\overline{p}$'s for colliding beams. In the first case, 12/13 of the Main Ring will be filled with beam and transferred to the superconducting ring in a single turn. Thus

Table 10-I. Magnets and Kickers for Beam Transfer.

Beam momentum and momentum offset: 150 GeV/c, +0.25% (Main Ring) / 0 (superconducting ring)
Beam emittance longitudinal: 0.25 eV-s
transverse: 0.15π mm-mr

A. Elements common to both directions

1. Two bump magnets in the main ring, at D46 (1.4 m from the quadrupole) and at E17 (12 m from the quadrupole).

$$B\ell = \pm 0.84 \text{ kG-m}$$

2. A quadrupole between two pairs of Lambertson magnets. (See Fig. 10-1)

normal direction: horizontal focus $B'\ell$ = 18 kG
reverse direction: vertical focus = 18 kG

B. Normal direction (see Fig. 10-3).

Main Ring

1. kicker at D48 (3 m from the quadrupole)
$B\ell$ = 1.97 kG-m
2. Lambertson (center at 7 m from the quadrupole.)
$B\ell$ = 9 m × 9.2 kG, rotated by 2.6°

Superconducting Ring

1. bump magnets (standard trim dipoles built in main quadrupole cryostats)
D48: 0.44 kG-m, E11: -0.24 kG-m, E13: 0.40 kG-m
2. kicker at E17 (4 m from the quadrupole)
$B\ell$ = 1.33 kG-m
3. Lambertson (center at 5.3 m from the quadrupole),
$B\ell$ = 9 m × 9.2 kG, rotated by 2.2°

C. Reverse direction (see Fig. 10-4).

Main Ring

1. kicker at E13 (1.3 m from the quadrupole)
$B\ell$ = 0.75 kG-m
2. Lambertson (center at 5 m from the quadrupole),
$B\ell$ = 9 m × 9.2 kG, rotated by 1.3°

Superconducting Ring

1. bump magnets (standard trim dipoles built into main quadrupoles cryostats)
D46 & E11: 1.2 kG-m, D48: -1.0 kG-m
2. kicker at D48 (4 m from the quadrupole)
$B\ell$ = 2.13 kG-m
3. Lambertson (center at 8 m from the quadrupole).
$B\ell$ = 9 m × 9.2 kG

there will be 19.0 μs of beam and a gap of 1.9 μs. This long gap is necessary to accommodate the rise time of the abort kicker, which is discussed in Section 11. No problem is expected in meeting or exceeding this specification for rise time of the p excitation kicker from the Main Ring or for the fall time of the p injection kicker.

For $\bar{p}p$ colliding-beam operation, individual rf buckets of p's ($\bar{p}$'s) spaced approximately 1 μs apart will be injected one at a time into the superconducting ring. By injecting single pulses, exact spacing of a specific number of rf buckets can be obtained independent of the rebunching spacing of protons in the Main Ring. For two interaction regions, a spacing of 62 buckets or 1.17 μs is required.

Once the protons are injected, individual $\bar{p}$ bunches can be injected between them. The optimal timing is for $\bar{p}$'s to pass through the injection kicker when the two nearest p bunches are equally spaced from the kicker. This equalizes kicker rise- and fall-time requirements. Once all bunches have been injected (usually twelve of each), the azimuthal position of the crossing can be adjusted to coincide with the center of the interaction region. The two orthogonal rf systems discussed in Section 9.2 will be run at slightly different frequencies until the proper azimuthal relationship of p's and $\bar{p}$'s has been obtained.

There are a total of four magnet systems. The kicker specifications are given in Table 10-II. The p extraction kickers and injection kickers are to be used in both fixed-target and $\bar{p}$ colliding-beam operation. Three of the systems will require matched lumped-element transmission-line

Table 10-II. Kicker Specifications.

	p Extraction fixed target	p Extraction $\bar{p}p$ mode	p Injection fixed target	p Injection $\bar{p}p$ mode	$\bar{p}$ Extraction	$\bar{p}$ Injection
B × ℓ	1.97	1.97	1.33	1.33	0.75	2.13 kG-m
Pulse Length	20.0	0.01	20.	0.01	40	0.01 μs
Rise Time 0-100%	0.4 n	0.4	-	0.4	20	0.5 μs
Fall Time 100-0%	-	0.4	0.4	0.4	20	0.5 μs
Magnet Impedance	25 Ω	25 Ω	12.5 Ω	12.5 Ω	5.625 μH	12.5 Ω
# Modules	5	5	1	1	1	1
PFN Impedance	8.3 Ω & 12.5 Ω	8.3 Ω & 12.5 Ω	12.5 Ω	12.5 Ω	45μf	12.5 Ω
Magnet Module Length	1.0	1.0	2	2	1.5	3.5 m
Field	400	400	670	670	500	600 G
Gap (V × H)	2 × 6	2 × 6	2 × 2	2 × 2	2 × 6	2 × 2 in.^{2}
Charging Voltage	80	80	67	67	1.5	60 kV

magnets, because beam will circulate through their aperture after the kicker is fired. The rise and fall time of 0.5 μs should be more than adequate for any colliding-beam operation. The only system exempt from these requirements is the $\bar{p}$ extraction kicker. It can be a simple 40 μs half-sine-wave device because we plan to have only one $\bar{p}$ bucket at a time in the Main Ring.

Electronic schematics for the four kickers are given in Figs. 10-5 to 10-8. The p extraction kicker is composed of two parallel sections and can produce either short or long pulses. In the case of the long pulse both the cable and the lumped delay lines are charged, and both the main and long-pulse thyratrons fired. For the short pulse, only the front-end PFN's need be charged and only the main thyratrons need be fired.

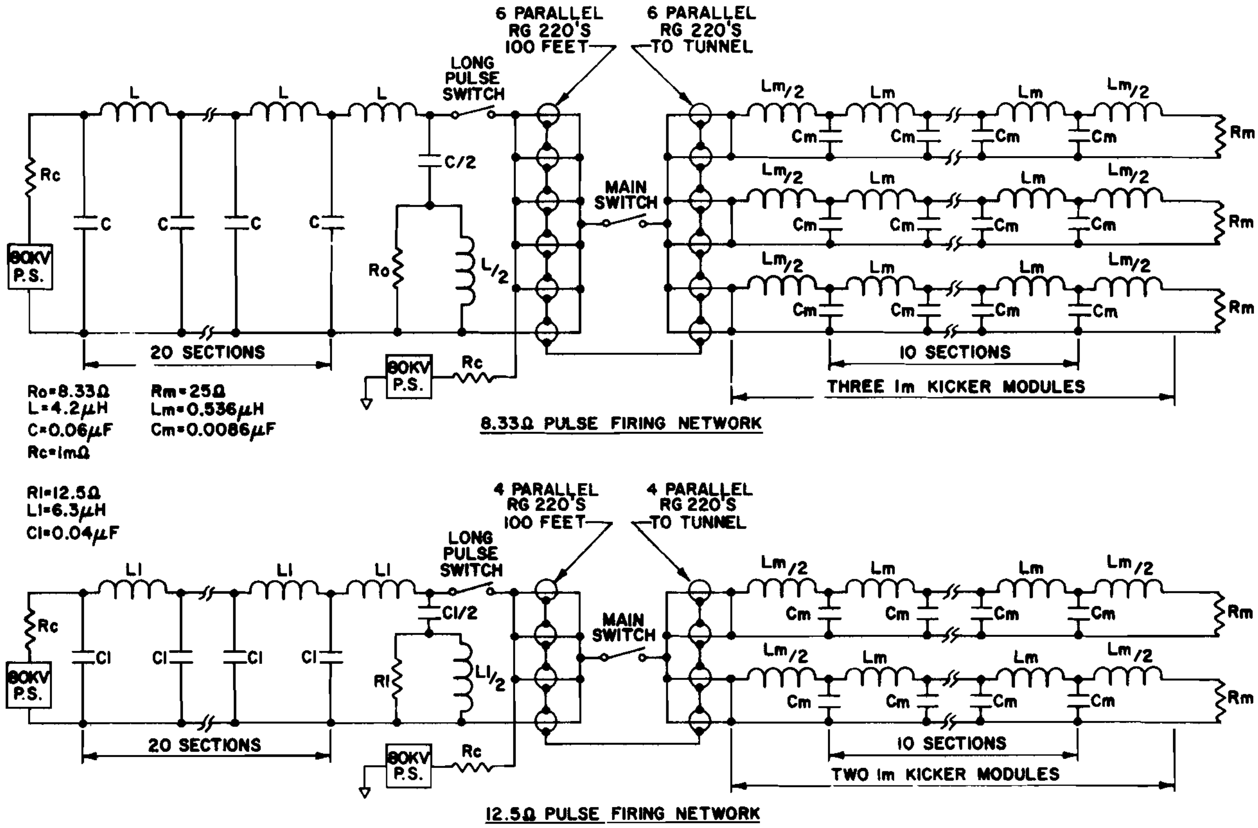

Fig. 10-5. Proton extraction kicker.

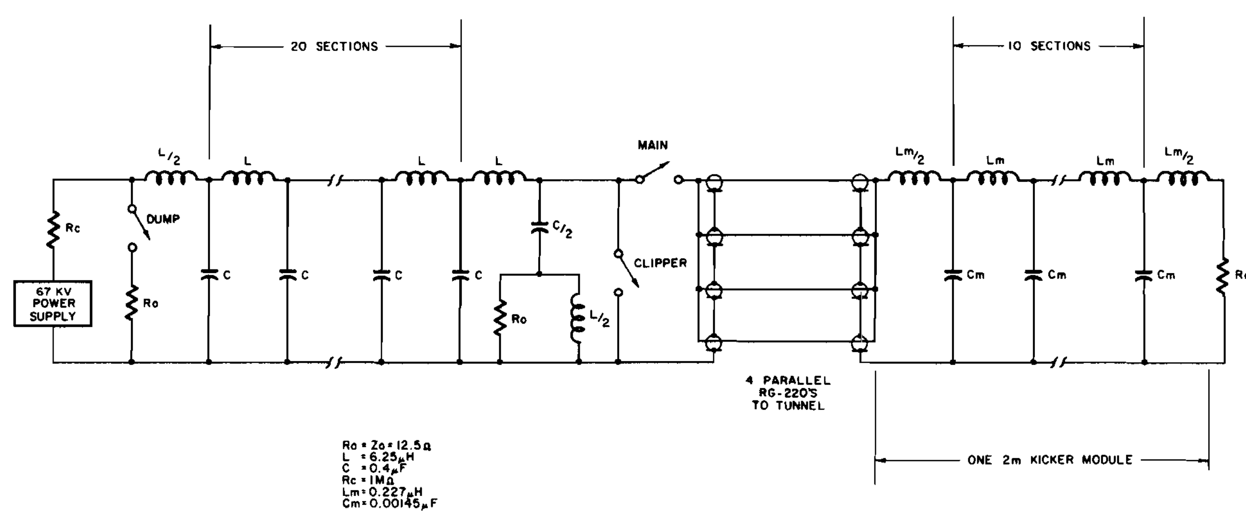

Fig. 10-6. Proton injection kicker.

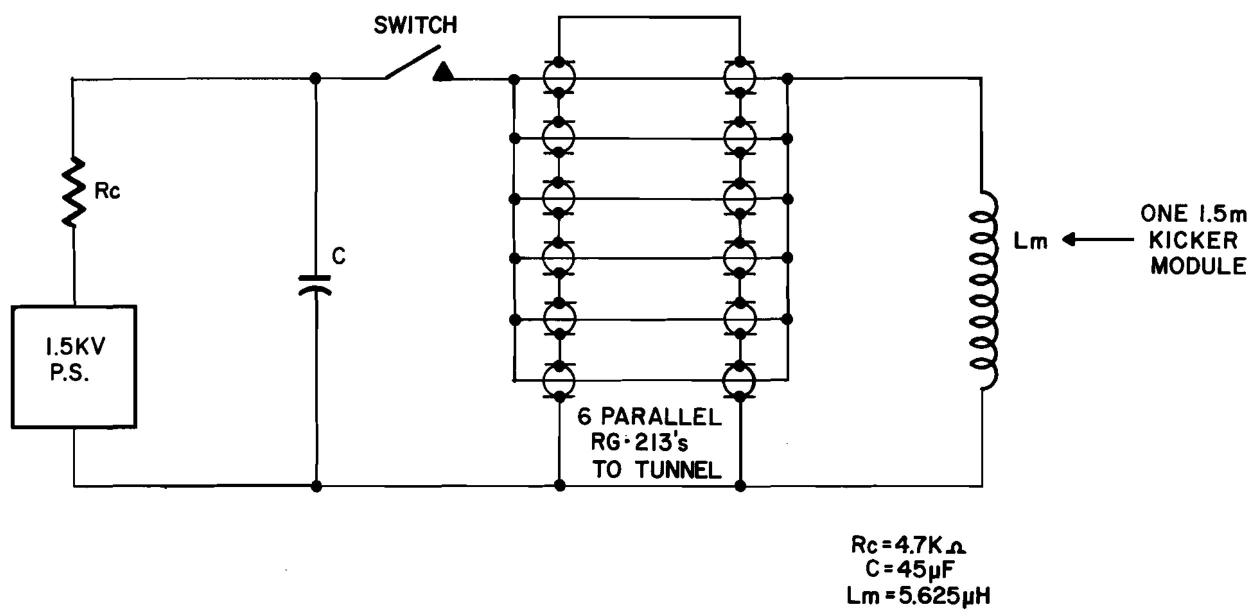

Fig. 10-7. Antiproton extraction kicker.

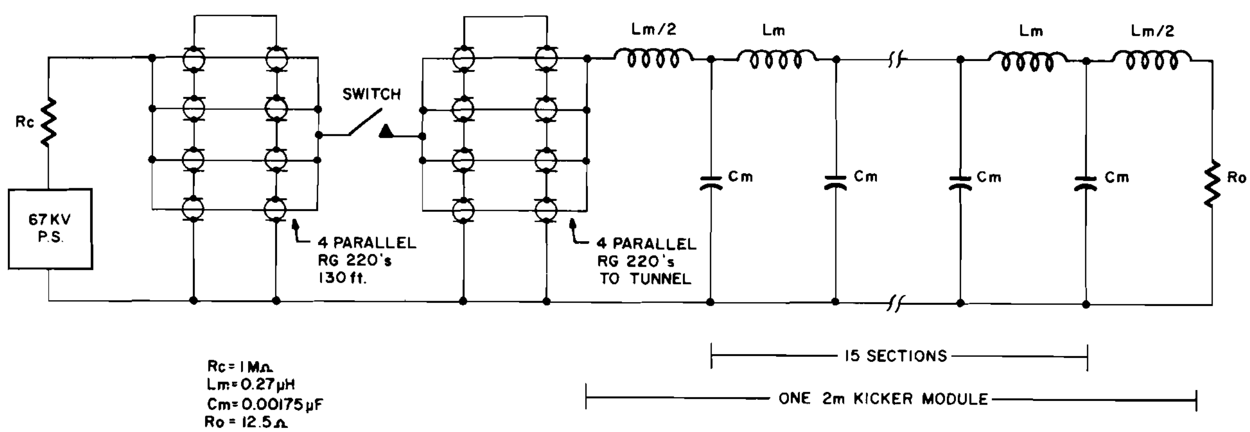

Fig. 10-8. Antiproton injection kicker.

In order to produce the fast fall time for the p injection kicker, two additional thyratrons are needed, one to act as a clipper to generate the fast fall time and one as a dump to terminate reflections from the clipper. These are shown in Fig. 10-6. This system can be used also to produce the short pulse for p injection for colliding beams by appropriately timing the clipper and dump switches relative to the main switch.

The $\overline{p}$ extraction kicker is a simple SCR device similar to the Main-Ring pingers.

Figure 10-8 shows the proposed $\overline{p}$ injection kicker. A lumped delay line is not necessary because of the short pulse length.

References

[1] S. Ohnuma, Beam Transfer - Normal and Reverse Directions, Fermi National Accelerator Laboratory Report UPC No. 19, December 4, 1978 (Revised January 11, 1979).

[2] T. L. Collins, The Great Doubler Shift, Fermi National Accelerator Laboratory Internal Report TM-874, April 1979 (also UPC No. 96).

[3] H. Miller, Fermi National Accelerator Laboratory Internal Report EXP-87, March 21, 1978.

[4] H. Miller, Transverse Active Dampers for the Tevatron, Fermi National Accelerator Laboratory Report UPC No. 36, January 17, 1979.

[5] T. L. Collins, High Eta for Stacking, Fermi National Accelerator Laboratory Report UPC No. 23, December 13, 1978.

11. BEAM-ABORT SYSTEM

11.1 Requirements and General Design

Detailed studies have shown that if even a tiny fraction of the 2×10^{13} protons circulating in the ring interact in the nearby solid material, for example, in the vacuum-chamber wall or injection or extraction devices, then a disruptive quench of one or more of the superconducting magnets will likely result. It is therefore imperative that a beam-abort system exist that can anticipate the imminent occurrence of such quench-inducing losses and cleanly dispose of the beam before they are allowed to happen.

Clearly the most effective strategy is one of prompt single-turn extraction to an external beam dump. The basic elements of the abort system will therefore consist of a fast-rise full-aperture kicker followed by a Lambertson septum magnet and a magnetic beam channel to an external dump. The elements of the abort system are intermeshed with elements of a straight-section bump (discussed in Section 13) used for radiation protection of the downstream superconducting magnets. The effect of beam lost on the magnetic septum and collimators inside the magnets is reduced in this way. Estimates indicate that a few times 10^{11} protons can be lost on the septum. Then the extraction inefficiency of the abort system should be less than 1%. For operation in the $\bar{p}p$ collider mode, an abort for the backward moving $\bar{p}$'s is also required. Since the expected number of $\bar{p}$'s is less than 1×10^{11}, a considerably larger inefficiency can be tolerated; a fast kick into the face of a dump block placed several centimeters from the closed orbit will suffice.

The signal to trigger the beam abort will be generated by any one of the following devices: loss monitors viewing aperture stops at various locations around the ring; fast beam-position and beam-size detectors; power-supply malfunction detectors; magnet quench detectors. The circulating beam will have a gap to accommodate the rise time of the kicker; only 12 Booster batches will be injected into the Main Ring, giving a 1.9-μs gap Once an abort condition is recognized by a detector somewhere around the ring, complete beam disposal can be accomplished in less than 60 μs.

In a previous report[1] two possible solutions for the forward abort geometry were proposed. Further study has shown a solution grouping the elements closely to be very desirable. The geometry described here places the entire forward and backward abort systems as close as possible to the same long straight section. This system has the advantages that the beam does not travel as far during abort and that it conserves valuable long straight-section space. It also allows more flexibility in $\bar{p}$ and p bunch distributions and in the arrangement of functions in the long straight sections. The use of fast kickers with peak fields of 3 kG allows efficient long straight-section design. A conceptual design of a 3-kG kicker and pulsing system is described in this section.

The location of the p and $\bar{p}$ abort systems in long straight-section C is shown in the layout sketch of Fig. 1-2. In Fig. 11-1 we show the location of all the elements of the abort system and the calculated abort orbit. A plan of straight-section C itself is given in Fig. 11-2.

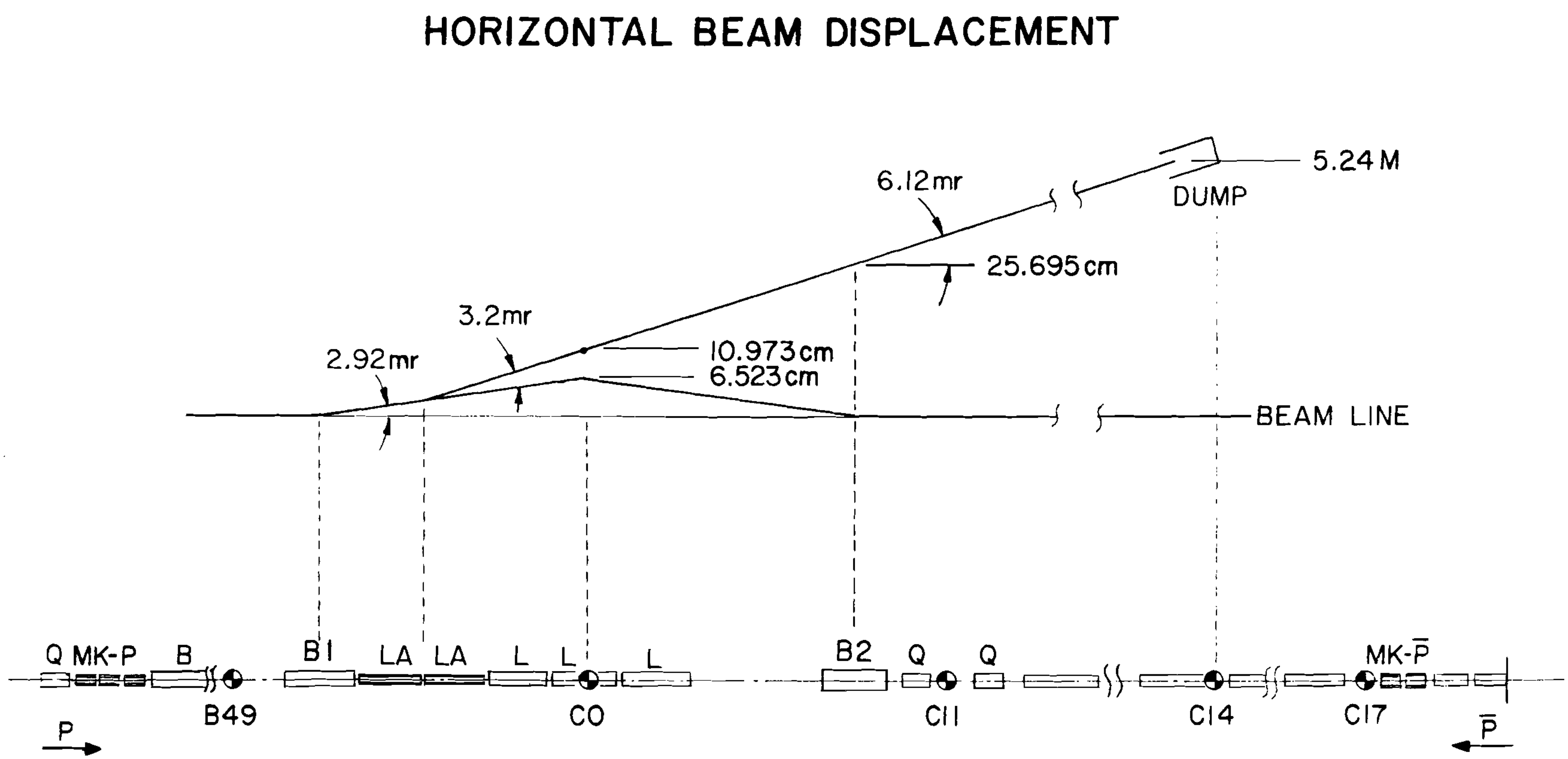

Fig. 11-1. Location of abort-system elements and displacement of aborted beam.

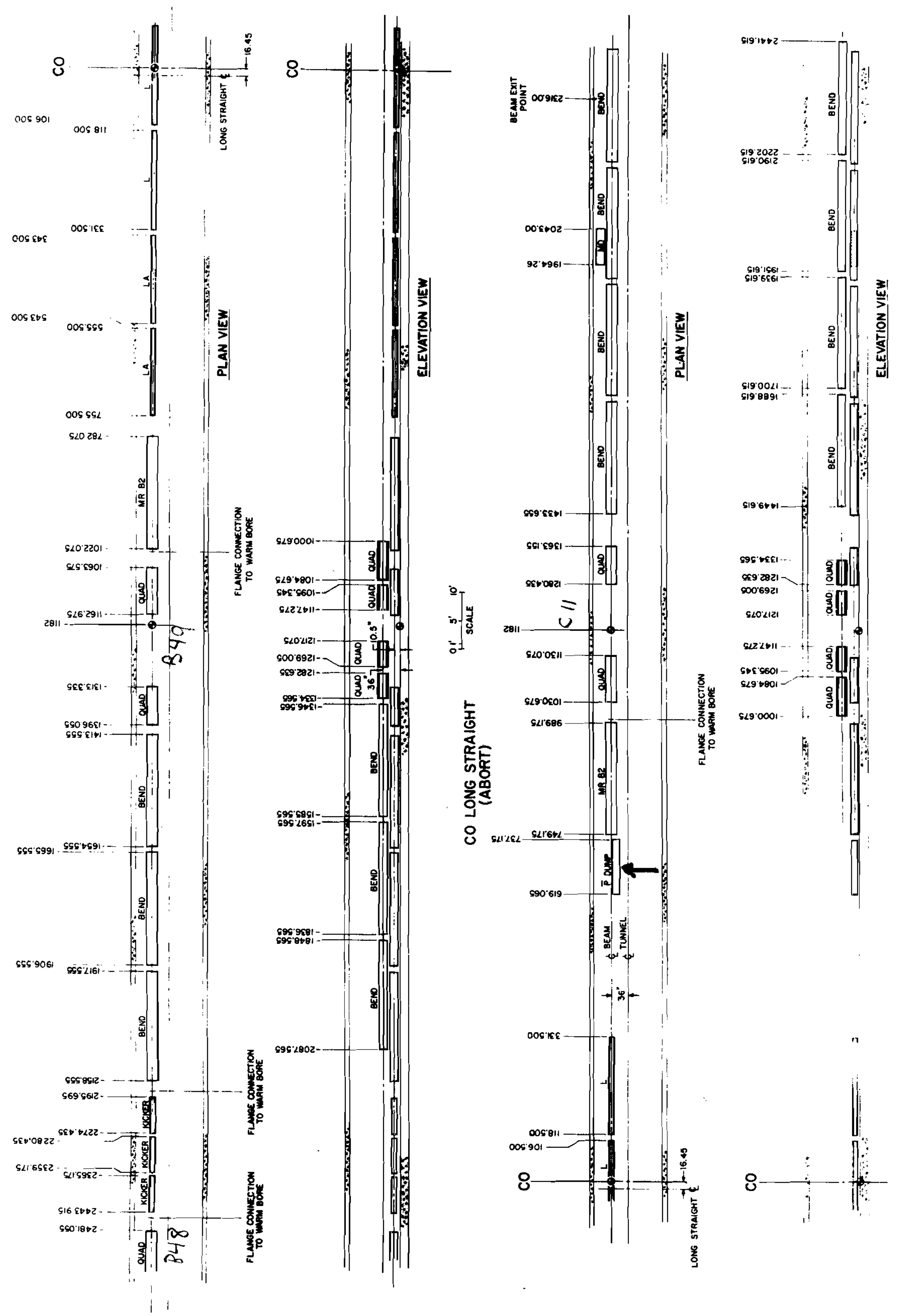

Fig. 11-2. Layout of C0 long straight section.

11.2 The Forward Abort

For the forward proton abort, a 6-m long, 3-kG kicker is placed at the B48 location, 60 m upstream of C0. It deflects the beam downward by 0.54 mrad, resulting in a -20.5 mm displacement and -0.03 mrad slope at the entrance to the long straight section. The closed orbit through the long straight section has a kink of amplitude 6.5cm created by the three horizontally-bending magnets, B1-L-B2. The abort Lambertson magnet, LA, which immediately follows B1, is positioned with its septum centered at -10 mm vertically; LA bends the kicked beam horizontally through +3.2 mrad, providing a +24 cm displacement at the upstream face of B2. Magnet L is a Lambertson which bends only the main beam; in order to increase the vertical separation between the aborted beam and the closed orbit at L (and hence have higher field), LA is rotated by 5° around the beam direction, resulting in a 0.28 mrad downward deflection of the aborted beam. The extracted beam passes through a hole in the return yoke of B2, exits through the wall of the Main-Ring tunnel, and on to a beam dump 120 m downstream of C0. At the dump the extracted beam is 4.4 m from the outside wall of the Main Ring tunnel, as shown in Fig. 11-2. The Lambertson L is 16.2 m in length and will necessarily be made up of three or four modules; a 1-m gap between modules can be arranged in the vicinity of C0 in order to allow for an internal target and utilization of the existing spectrometer room at the Internal Target Area.

The basic parameters of the magnets are listed in Table 11-I. Another magnet, MD, is placed just downstream of magnet B2; the purpose of MD is to sweep the beam vertically in order to increase the effective beam area at the beam dump. MD is a single-turn picture-frame dipole with a half-sine-wave pulse 70 μs long; the field rises from 0 to 4 kG during the 19 μs of beam passage, resulting in an angular sweep of 0.24 mrad.

Table 11-I. Forward Abort Magnet Parameters.

	MK-p	MK-$\bar{p}$	LA	MD	L	B1, B2
Type	1-mil Fe	1-mil Fe	Fe	Fe	Fe	Fe
$\Delta\theta$	0.56 mrad	0.34	3.2	0-0.24	5.84	2.92
Length	3 × 2 m	2 × 2	10.2	2.0	16.2	6.1
Field	3.0 kG	2.8	10.5	5.0	12.0	16.0
Aperture HXV	5 × 5 cm	5 × 5	-	3 × 3	-	10 × 5
Rise Time (95%)	1.5 μs	1.5	Ramped	35	Ramped	Ramped

A cross section of the Abort Lambertson magnet (LA) at the upstream end is shown in Fig. 11-3. In addition to the 10-kG dipole field (at 1000 GeV), it has a gradient of 0.5 kG/cm (horizontally defocusing), which is used to increase the horizontal beam size at the dump. At the center of the long straight section the beam size at 150 GeV is ±3.0 mm. At 1 TeV the main beam is ±1.2 mm, but during slow extraction it has horizontal "wings" extending ±3.4 mm on either side. The abort Lambertson and magnets B1, L, B2 are ramped to track the beam energy.

Without the vertical sweeping action of MD or the focusing action of the abort Lambertson, the 1-TeV beam spot size (2σ) at the beam dump would be ±3.3 mm horizontally by ±2.1 mm vertically. A beam of 2×10^{13} protons with this size would cause physical damage to practically any solid material used in the beam dump. For the most readily available material, aluminum, the beam area should approach 1000 mm^2 to avoid damage. From

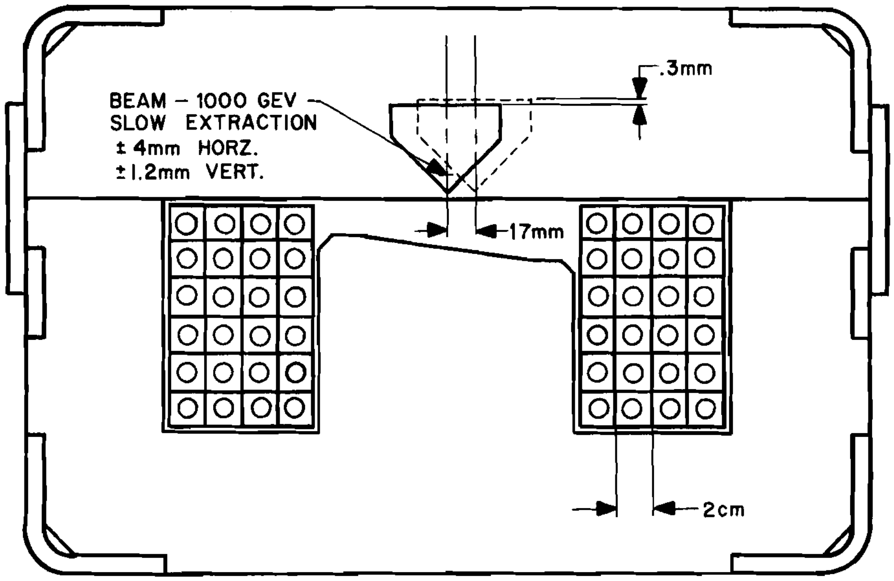

LAMBERTSON CROSS SECTION

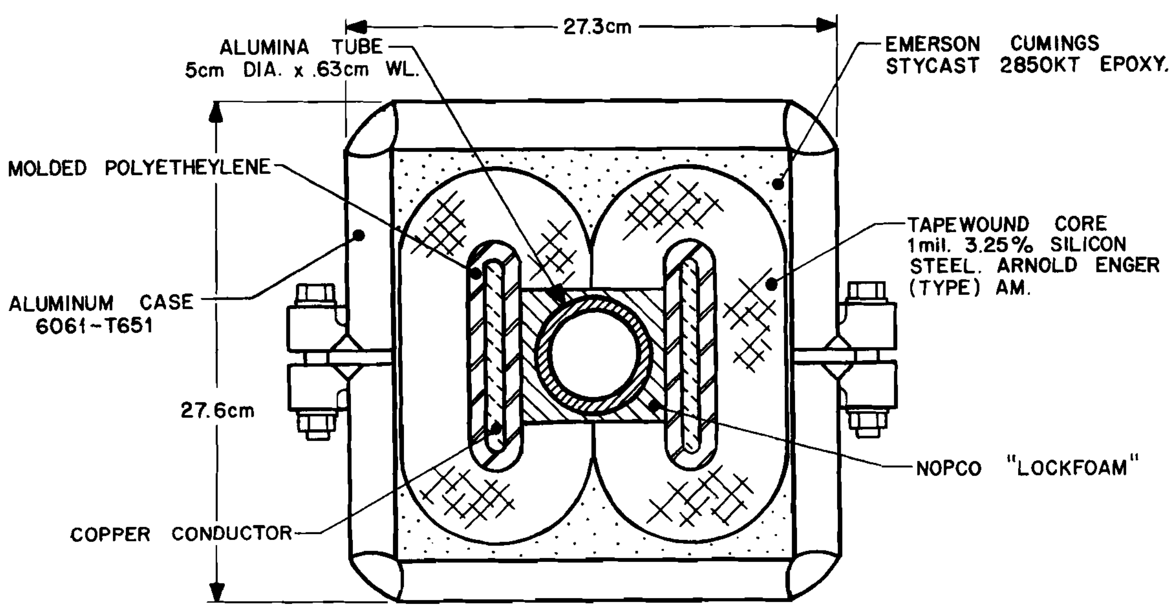

3 KG KICKER MAGNET

Fig. 11-3. Lambertson and kicker magnets of the abort system.

the lens action of the gradient Lambertson, the horizontal spot size at the dump becomes ±16 mm; the vertical sweep of MD yields a vertical motion of 2 cm, resulting in an effective area of 900 mm^2. A calculation using the CASIM program indicates that a 1-TeV beam of 2×10^{13} protons and this effective area will give a peak temperature rise of the order of 250° C in an aluminum absorber; the peak occurs about 85 cm into the absorber.

11.3 The Backward Abort ($\bar{p}$)

A 4-m long fast kicker similar to that used at B48 for the forward abort is placed at the C17 location, 214 m downstream from C0. A +0.34 mrad horizontal kick at this point results in a -22.0 mm displacement of the $\bar{p}$ beam as it enters the C0 straight section. The $\bar{p}$'s will be absorbed in a 3-m long steel dump block just beyond the magnet B2, as can be seen in Fig. 11-2 placed with its vertical edge at -20 mm. As with the forward abort, the kink in the closed orbit is very effective in preventing the radiation that escapes the dump block from impinging on the downstream superconducting magnets.

In order to achieve a "clean" abort in the $\bar{p}p$ collider mode, there must not be any beam between the two fast kickers, i. e., between B48 and C17, when they turn on. The distance is equivalent to a flight time of 0.92 μs. The ring must be filled in a way that leaves a 2.42 μs gap (0.92 μs plus the 1.5 μs risetime of the kickers) in both the $\bar{p}$ and p beams and these gaps must "collide" at C0. The presence of these gaps implies that up to 77% of the azimuth of the ring can be utilized for $\bar{p}p$ collisions at any given interaction region.

11.4 3-kG Fast Kicker Magnet and Pulsing System

A cross-section view of the kicker magnet is shown in Fig. 11-3. During slow beam extraction, the beam at the B48 location has horizontal wings that extend out to ±17 mm. To accommodate these wings the beam tube through the kicker consists of a 5-cm i.d. ceramic tube, resulting in a 7-cm square gap for the magnet aperture. The magnet core is made with 1-mil tapewound cores of 3.25% silicon steel. Pulse tests carried out on these cores show that a risetime of 1.5 μs (0-95%) is readily obtained. The basic specification for MK-p and MK-$\bar{p}$ are listed in Table 11-I; additional requirements include: 21 μs pulse length, tracking of the ring ramp, and repetition rate of 2 cycles/min. (11s ramp risetime).

The overall system consists of a charging supply, a pulse line for energy storage, a switch, matched impedance cables, terminating resistors and lumped-element kicker magnets in a series circuit, as shown in Fig. 11-4. In order to achieve the L/R time-constant of 0.5 μs with a reasonable supply voltage (<90 kV), the kickers will be constructed out of 2-m long sections. The pulse line and switch will be located above ground in a service building, approximately 110 m distant from the kicker magnets in the tunnel. Each of the 2 m long kicker modules is fed by a separate 2.5 Ω line. The important design specifications of the subunits of Fig. 11-4 are :

a) Kicker magnet:

$L = \mu_0 \ell = 2.51\ \mu\text{H}$ (for $\ell = 2$ m)

$I_{max} = Bd/\mu_0 = 16.7$ ka (for B = 3 kG)

Stored energy = 351 J ($\equiv$ E)

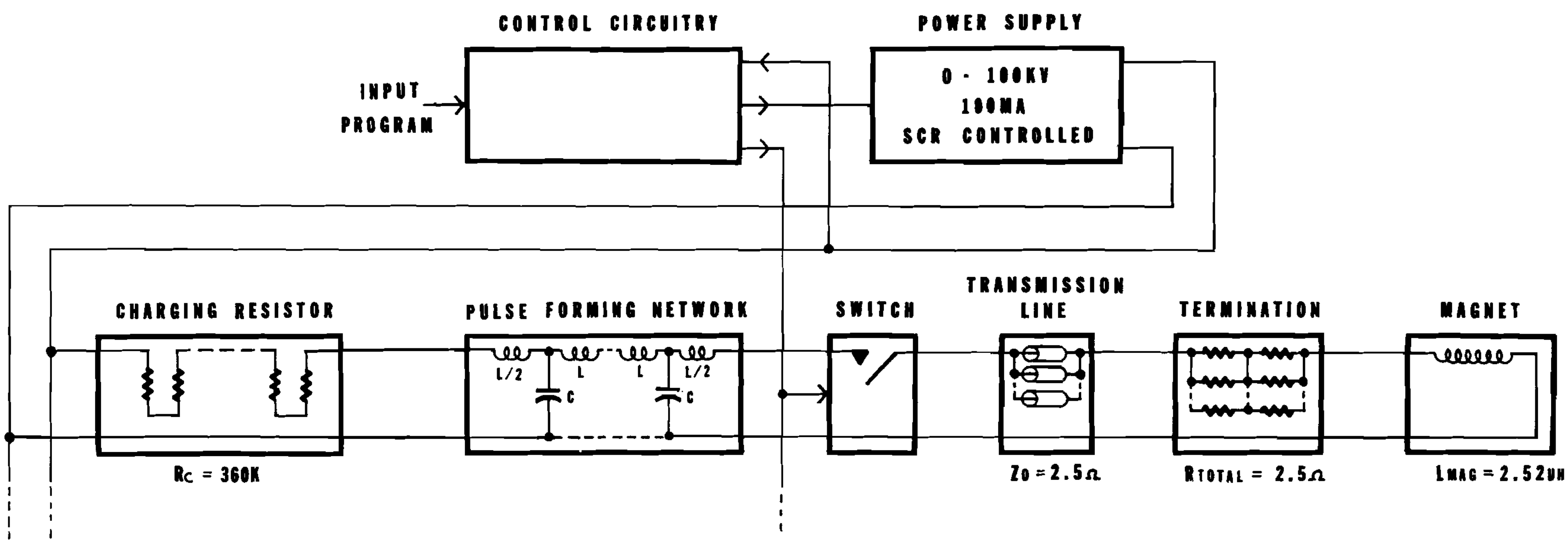

Fig. 11-4. Fast-kicker power supply.

b) Termination resistor:

$Z_0 = L/2\tau = 2.51\,\Omega$

Energy dissipated/pulse = 14.7 kJ

Average power = 489 W (for 2 cycles/min)

To minimize the instantaneous heating of the termination, we have chosen 80-50 Ω ceramic low inductive-power resistors. Each will dissipate 183 J per pulse, giving a temperature rise of 0.92°C after each pulse. If the basic architecture of two resistors in series is adopted, each resistor will have a peak voltage of 20.9 kV and a peak current of 418 A.

c) Transmission line:

Twenty RG220 coax cables (Z_0 = 50Ω) in parallel will be used to transmit the pulse energy to each 2-m magnet in the tunnel.

d) Switch

We are currently planning to use a deuterium-filled ceramic thyratron (English Electric Valve 1192B) as the switch between the transmission line and the pulse-forming network (PFN). The characteristics of the device are:

Required	1192B Rating (crowbar service)
I_{max} = 17 kA	60 kA
I × T = 0.36 A-s	2 A-s
V_{max} = 83.6 kV	90 kV
V_{min} = 12.5 kV	7 kV
dI/dt = 34 ka/μs	100 kA/μs
Rep rate = 2 cycles/min	6 cycles/min

e) **Pulse** forming network:

$Z_0 = 2.5\ \Omega$, N = 20 sections

$T_s = T/2N = 0.53\ \mu s$

$C_s = T_s/Z_0 = 0.21\ \mu F$; $L_s = Z_0 T_s = 1.33\ \mu H$

Stored energy = ET/τ = 14.7 kJ

f) **Power** supply and charging resistor:

A single power supply and 3 charging resistors will be used to track the ramp energy. If the maximum voltage on the pulse line corresponding to 1 TeV, is 83.6 kV, the minimum voltage is 12.5 kV, corresponding to 150 GeV. The minimum acceleration time is 11 sec with a period of about 30 sec. Then $\Delta V/\Delta T$ of the pulse line must be 6.46 kV/s. Assuming approximately 10 kV across the charging resistor, the characteristics of the power supply and charging resistor are:

I_{peak} = 81.4 mA; I_{AV} = 35 mA

P_{peak} = 7.7 kW; P_{AV} = 1.81 kW

$P_{peak,\ R}$ = 814 W; $P_{AV,\ R}$ = 350 W

An oil circulation and heat-exchanger system will be used for the supply, charging resistor, PFN, and switch.

11.5 Beam Dump

A possible plan for the beam dump is shown in Fig. 11-5. It is designed to take 3.5×10^{17} protons per year at 1 TeV; at that level it will use up 20% of the Laboratory annual limit for tritium contamination of the ground water. It is intended that this dump will be a common facility to

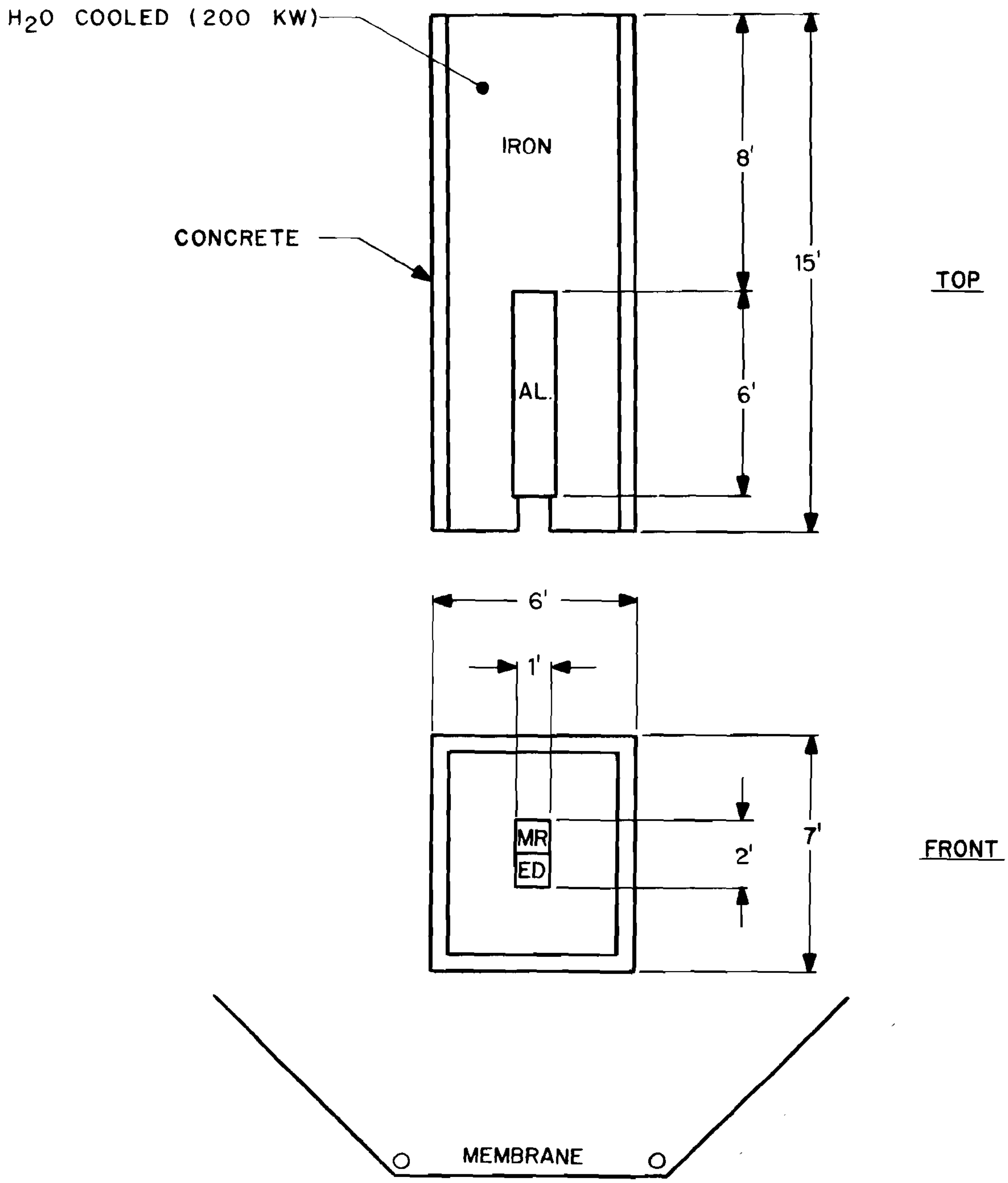

Fig. 11-5. Beam dump.

both the Main Ring and the superconducting ring. The beam impinges on a 6-ft long block of aluminum followed by 8 ft of steel. The membrane shown is a barrier to prevent activation produced above it from passing into the ground water.

Reference

[1]F. Turkot, Energy Doubler Beam Abort System, Fermi National Accelerator Laboratory UPC No. 20, December 7, 1978 (Revised January 1, 1979).

12. CONTROLS

12.1 Control Requirements

In this section we will discuss the nature of the system we are trying to control, how it differs from the present Main-Ring system and what controls might fulfill the necessary functions. Certainly, as ideas become engineering realities and details implemented in hardware or software, the present concepts may be modified or destroyed by hard realities.

The superconducting accelerator-collider is a very different animal from the present Main Ring, where, if one does not know what went wrong, one can try again in a few seconds. Present measurements indicate that it may take half an hour to recover from a full-field quench, which could make for dull and unproductive knob twiddling. We must have information recorded on the pulse that went astray so that we can diagnose the problem and minimize the chance of recurrence.

The refrigeration system is very large, with many components working in parallel and series. Control must be set up to balance the satellite and central systems for stable operation, monitoring for failure of individual components, and automatic adjustment and compensation for such failure.

The magnet power supply system must at all times monitor the operational integrity of the magnets, as discussed in Section 6. It is also likely that as refrigeration capabilities change or beam-loss problems arise, changes in ramp rate, peak energy, flat-top time and cycle time will need to be made. The whole system should make it possible to make these changes easily and quickly.

Accumulating enough $\bar{p}$'s for injection into the collider is expected to take three hours. They must be injected correctly and manipulations performed on the stored beam in a properly sequenced and coordinated fashion. Coordination of the operation of the Linac, Cooling Ring, Booster, Main Ring, and Superconducting Ring over long times is also imperative. Operation will not be as repetitive as now and emphasis will be put on setting up a sequenced operation and requiring that it be initiated at a specific time and carried through.

In the following sections, we shall discuss in detail only the basic systems necessary for fixed-target operation and tuneup.

12.2 System Architecture

The control system for the superconducting ring will make use of the central computer system of the present accelerator control system. But the special requirements of a superconducting accelerator, discussed in Section 12.1 above, will mean that additions to the system will be needed.

The interface electronics for providing control, monitoring, and diagnostic facilities will use modular packaging for each of the major subsystems (vacuum system, correction element waveform generators, etc.) of the accelerator. Most monitoring and control of the individual subsystems will be done at the local level, using interface electronics that incorporate both microprocessor-based intelligence and local memory.

The orchestration and coordination of the distributed-subsystem electronics is provided by communication with the central computer system.

The local subsystem electronics will be supported from a CAMAC crate system (ANSI/IEEE Standard 583), which provides a powerful data-architecture for device interface. Communication between one or more CAMAC crates located in each service building and the central computer system will be via high-speed serial data links that will utilize existing dedicated, direct-buried coaxial cables. The protocol of the serial links will be modeled to ANSI/IEEE Standard 595 (Serial Highway Interface System) protocols to the extent possible or desirable.

The new ring will require diagnostic facilities that will involve the transmission of large blocks of data from the local electronics to the central system when unusual conditions arise (magnet quenches, etc.). The desirable aspects of the standard Serial Highway Interface System will be supplemented by block-transfer facilities, which provide an efficient method for transferring significant quantities of data from the local electronics to the central system. Correlation, analysis, and presentation of these data to the main control room will use the software facilities of the central system.

12.3 General-Purpose Multiplexed Analog-to-Digital Converter (MADC)

Each service building will have a general-purpose MADC and associated CAMAC-based controller making available digital representations of varied analog system process parameters. The MADC will have 12-bit resolution (0.025% of full scale) and will provide for up to 64 differential analog inputs. The MADC controller will contain on the order of 2K words of memory for storage of digitized data. These data will be transmitted to the central computer upon demand for correlation and analysis.

The MADC and its associated controller will provide three distinct modes of data collection:

(i) Self-Scanning Mode: The MADC will automatically digitize all channels at a predetermined or programmed rate, perhaps 10 Hz and store results as files in a pseudo-circulating memory. 1K of RAM would provide storage for 15 files. This feature will provide the necessary snapshot data in the event of a quench or abort. Provision will be made via block-transfer facilities for the central computer to read the most recent or all of the 64-word files.

(ii) Plotting Mode: This mode of the MADC will provide for plotting of up to four different channels at a user-programmed frequency. Continuous data are required for such plots and the associated memory for this function would therefore be in two sections, so that the central computer could read one section while the other was being loaded. The time resolution of such a plotting facility is expected to be 1 ms or better. Maximum time resolution will be ultimately determined by saturation of block-transfer and graphics-output facilities.

(iii) Transient-Analyzer Mode: This mode is similar to the plotting mode and could provide up to 10 to 20-μs resolution of any single analog input. This mode is an operational alternate to the plotting mode and would use the same memory. Up to four channels could be plotted at a sample frequency specified by the operator. Sampling would be triggered externally and would stop when the allocated memory was filled. Data would be returned to the host via block-transfer facilities.

The various modes of operation of the digitizer make it a general-purpose instrument that can be used for a variety of applications. For example, detailed measurements and studies of power-supply ripple can be made by digitizing power-supply readbacks at selected locations while simultaneously digitizing the output of a beam-sensitive detector in the extraction channel.

12.4 Local Control Terminal

A local intelligent, interactive, stand-alone terminal is desirable. Such a terminal will be portable and will interact with service-building devices by connection to the CAMAC system. It will be of particular use in turn-on and adjustment of the satellite refrigerators, where local adjustments of engines may always be necessary, but it will also aid in testing and development of other systems. The hardware configuration will include a floppy-disk system, a keyboard, an alphanumeric display monitor, and a video-graphics monitor as input-output devices. The processing power that is required at the local terminal is not particularly great and the local terminal will be packaged so that it can be moved easily from one service building to another.

12.5 Cryogenic System

The cryogenic system will require a number of closed-loop servo systems for process regulation. There are three independent major subsystems controlling

(i) the compressor suction and high-pressure gas systems,

(ii) the 24 satellite helium system (11 control points per satellite),

(iii) the liquid-nitrogen system.

The cryogenic system utilizes four compressors in each of six buildings with pressure regulation at each building and a master loop to balance the ring. The suction-pressure regulation must be done by a high-pressure kickback valve to the central system. This valve will control the gas inventory in the entire ring system.

Figure 12-1 is a schematic of the satellite system with the process variables labeled as letters and the control points labeled as numbers. Control of the satellite during normal operation is described below.

The amount of liquid used from the CHL is adjusted by valve (6) and is servoed from the return-gas temperature measured at point B between heat exchangers III and IV. The wet-engine speed (4) is controlled by the pressure at the refrigerator output (point C). The JT valves at the ends of the individual magnet strings (7, 8) are controlled by pressure sensors and helium vapor pressure thermometers at points D and E. The JT valves are set such that the temperatures at D and E are 0.1K above the two-phase boundary temperature to insure maximum magnet cooling. Cooling for the nitrogen shields of the magnets is maintained by constant-temperature control at the nitrogen outlets.

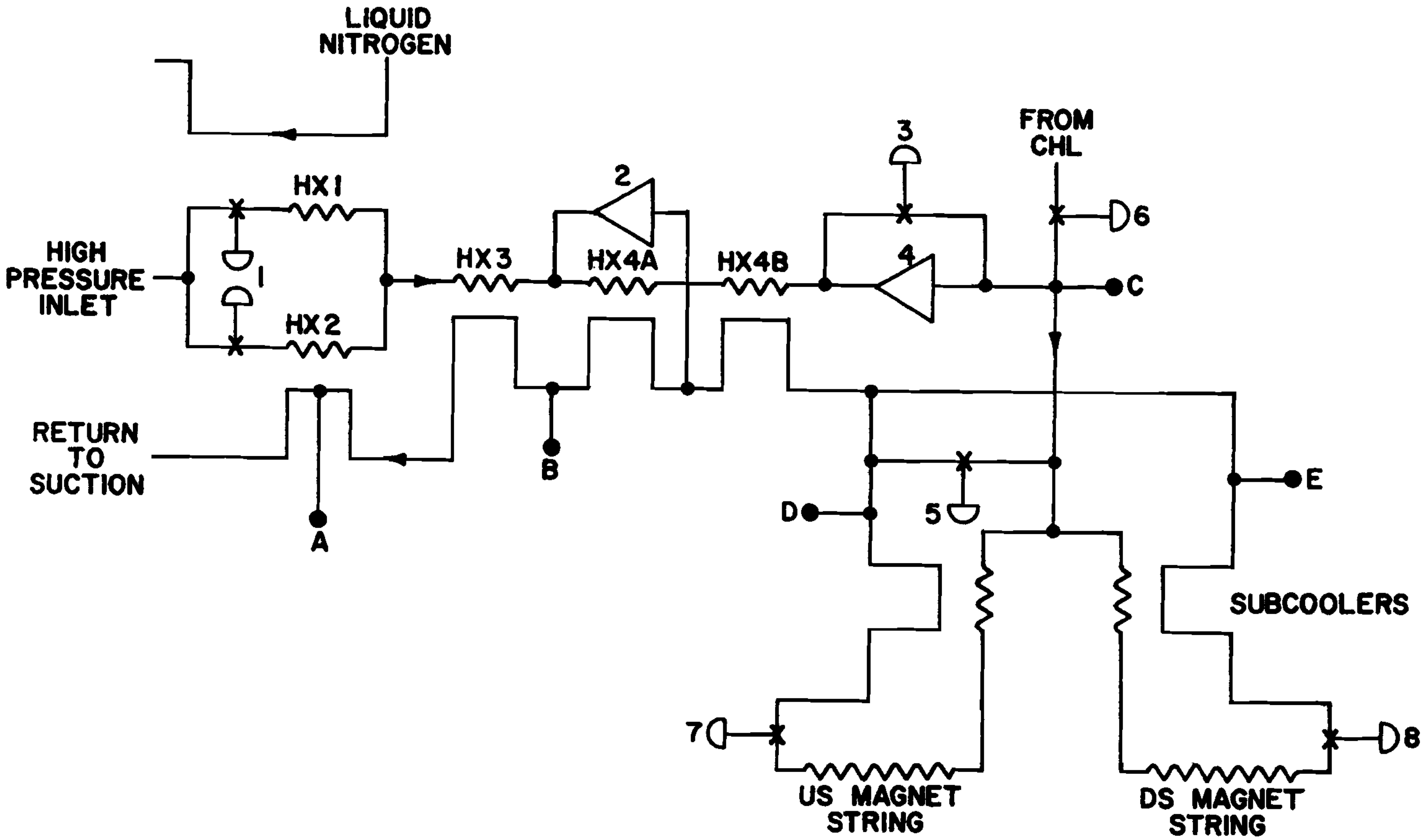

Fig. 12-1. Satellite system schematic showing process variables (letters) and control points (numbers).

When liquid from the CHL is not used, the percentage of helium flow through the liquid-nitrogen precooler (HX1) is adjusted by valves (1). The settings of these valves are controlled by the temperature of the return gas measured in the middle of HX2. The nitrogen level in HX1 is controlled by its own level detector. The gas-engine speed (2) is now servoed from the temperature at point B.

The primary JT valve (3) and bypass valve (5) can be controlled from point C. The JT is used primarily during failure of the wet engine and the bypass valve is used during cooldown or unstable operation.

The nitrogen system has three servo loops. The first maintains the liquid level in the first heat exchanger HX1. The other loops control the cooling in the nitrogen shield in the two magnet strings fed from one service building by maintaining a constant output temperature at the nitrogen outlet.

Most routine control, adjustment and monitoring will be done from the main control room using the general-purpose serial CAMAC facilities. The refrigeration system will also require the development of flexible closed-loop control that is local to a given satellite and development of the interactive local control station for use in the initial debugging and in performing operational adjustments.

Experience thus far has indicated that it is desirable to implement the closed loops using a dedicated intelligence module housed in the local CAMAC crate. The present scheme calls for monitoring about 60 channels of analog information and control of as many as 11 closed loops. This system could easily be extended to provide local generation of tolerance alarms, resulting in a significant reduction in the number of devices that the main system would be required to scan.

12.6 Vacuum Monitor and Control

A CAMAC-based vacuum controller will be implemented at each of the 24 service buildings to collect vacuum data and to exercise control of valves and pumps associated with insulating vacuum and section valves in the bore tube. The controller will continuously scan all its local transducers and calculate the average vacuum readings at the service building. During normal operations, the average reading and the local high and low will be sent to the central system. This scheme will greatly reduce the communications workload that exists in the current Main-Ring system, where each individual reading is returned to the central computer for house-average calculation. Any out-of-tolerance readings will be flagged to allow localizing trouble conditions. Upon request of an operator, all individual readings will be made available via block-transfer facilities for display.

The controller will be able to sequence events to establish and maintain desired insulating vacuum and to operate the electropneumatic section gate valves in the beam tube. In the event of a partial or catastrophic vacuum loss, the controller should respond immediately to prevent propagation of the problem.

An interlock will be supplied to the refrigeration system to indicate sufficient vacuum for start of cooldown and a beam permit will be generated to indicate that all section gate valves in the bore tube are in the full-open position. A temperature input is desirable to allow turning off appropriate pump stations once cryopumping dominates.

A manual control panel in the service buildings will allow local readings of individual transducers and operation of individual pumps and valves. The controller will respond to a manual operation if established vacuum is not jeopardized. Any illogical request will generate a warning and will be performed only if a separate manual override is set.

12.7 Quench Detection and Snapshot

If possible, it is best to detect a beam problem and fire the abort before the magnets quench, so that recovery time can be minimized. In order to detect such problems continuous monitoring of various beam parameters is necessary. For instance, beam position and tune should be kept within allowable limits and beam losses kept below the level sufficient to trigger a quench. Local continuous monitoring of all beam-position detectors could generate an abort trigger if any signal exceeded the allowable limit. If all the position information is stored in a local memory that is frozen at the time of the abort trigger, then in effect a "snapshot" is taken. The information can be recalled to the central computer and analyzed in terms of necessary corrections to the trim-dipole wave forms before another pulse of beam is attempted. Note that corrections are used throughout the acceleration cycle and must be set properly at every level of excitation.

There will also be instances when a quench occurs but no previous indication of malfunction or mistuning has been detected. In this case, the cause of the quench may have occurred considerably earlier in time and the snapshot of various quantities must be monitored over sufficient time to give an indication of cause, be it caused by beam, insufficient refrigeration or a weak magnet.

Thus the time from the initiation of a quench to its detection is the fundamental time constant of the system. Presently two control techniques are being investigated. The first technique calls for data from all pertinent devices to be collected for a time extending backward from the time the quench is detected to the time of the start of a quench. A second scheme that anticipates quench propagation calls for collection of data both before and after a quench or abort.

Accommodation of one or both techniques demands an accelerator-wide philosophy of data collection that can yield analytically coherent snapshot information. Questions remain as to what is a realistic time constant for each of the various subsystems and also as to what rate of sampling is required within this time constant.

The quench-detection interface module should have a circular buffer capable of storing half-cell voltages for a period of 1 s prior to a quench to 10 s after. The data can be used to reconstruct primary and secondary quenches for analysis and to cross-check the quench-detection monitor itself.

12.8 Abort Trigger

The abort trigger system consists of an input panel in each service building that accepts triggers from a large number of different types of control units, for example, power supplies, quench detectors, beam-position detectors, loss monitors, and so on. Each trigger input and its time of occurrence will be recorded in a digital status module. The information can then be transferred to the central system to determine which alarm or alarms generated the abort, and their order of occurrence.

An or-ed output of all activated triggers is used as an input to the abort-trigger-system communications link. This link makes use of a dedicated cable which runs from service building to service building around the ring. A circulating pulse on this cable is used as a "heart beat" or "keep-alive" signal to the abort kicker; when the heart-beat pulse disappears, the abort kicker is fired. The use of a dedicated abort-trigger system communications link results in a delay of only a few turns before the information to trigger a beam abort is transmitted from any service building to the abort kicker at C 0.

12.9 Correction and Adjustment Elements

The present correction element package consists of 180 trim dipoles, quadrupoles, sextupoles, and a large number of skew quadrupoles and octopoles. The dipoles are independently powered and require 180 independently driven but synchronized waveforms. The other correction elements will be powered in series strings utilizing up to eight power supplies per type of correction element; they also demand up to an order of magnitude higher precision. The description of the dipole function generators will consequently emphasize the potential operational problems in using so large a number of independent waveform generators.

12.9.1 Dipole function generators. The correction-element power supplies require a versatile ramp generator. The detailed shapes of the time-varying excitation currents of the dipoles are not known a priori, but must be determined during commissioning and operation. On the other hand, the basic functional service provided by the correction elements is relatively straightforward and well-defined and the associated waveforms are not expected to be unduly complex.

The design of the waveform generators has been guided by the following design requirements, operational characteristics, and viewpoints:

(i) It is desirable and possible to characterize each of the 180 waveforms by a small number of parameters. Specifically, each waveform can be parameterized by a sequence of thirty-two (or fewer) piecewise linear segments.

(ii) User-oriented software facilities, available at a control-room console, will be used to set up, generate, validate, and manipulate the parameters of the various waveforms. These parameters will then be downloaded to the local function generators, which will develop the required waveforms without further interaction with the main control room until a modification is required.

(iii) Continuous diagnostic and monitoring features are necessary to ensure the reliable operation of the waveform generators and power supplies. These features will be provided by incorporating self-checking facilities into the design of the function generators. These continuously active, self-checking features should allow the central control system and the control-room operator to ignore the normal operation of the correction-element package, but should provide the operator with information on abnormal or out-of-tolerance conditions.

(iv) The waveform generators should provide facilities for accommodation of changes in the main-supply excitation curve and facilities for entering and leaving the storage mode and for tuning the elements while in that mode. A B-dot clock with a frequency controlled by the main guide field could possibly be used in conjunction with the ramp generators to ease the complexity of changing ramp times and flat-top lengths. The first-order field dependence of the correction could then be removed explicitly from the waveform curves. The relative merits of the real-time clock vs. B-dot clock are yet to be assessed and the following discussion uses a a real-time clock for simplicity of description.

(v) A temperature-stable, bipolar, 12-bit digital-to-analog converter (11 bits + sign) is adequate for providing the required accuracy and tolerance.

These functional characteristics of the waveform generators could be realized with a design technique using either random logic or microprocessor-based local intelligence. The two techniques would be comparable in performance and flexibility; the preferred implementation technique in this case would undoubtedly be determined by the economics of specific designs.

The function generators will be packaged as CAMAC modules and be housed in new CAMAC crates located in each service building.

12.9.2 Quadrupole, sextupole, and octopole generators. The description of the quadrupole and octopole power-supply systems in Section 7 summarizes the rigid tolerances that are required for these elements. The use of high-precision A-to-D and D-to-A converters is mandatory; greater attention to noise and isolation protection is necessary. For these reasons, it is clearly desirable to package the A-to-D and D-to-A converters with the power supply.

With this modification, the function generators for the dipoles, described above, would also be adequate for the quadrupole, sextupole, and octopole power supplies. The use of totally digital techniques both to parameterize the waveforms and to generate the required voltage set-point is easily extended to the required 16-bit precision.

12.10 Position Detectors

A horizontal position detector is located at the upstream end of each horizontally focusing quadrupole and a vertical detector at each vertically focusing quadrupole. These detectors are electrostatic.

The electronics of the system consists primarily of an rf multiplexer to switch among signal input pairs, and a beam-position processor unit which uses amplitude-to-phase conversion and phase comparison to obtain the position information independent of intensity. A trigger box senses when beam is present, especially for first-turn information and an interface module will contain memory to store the information as a function of detector and time. Typically, signals from nine detectors come to each building. Extra channels are available for test signals and additional detectors. Provision will be made so that a special single-bucket processor can be inserted between the multiplexer and position processor. In the $\bar{p}p$ mode, the single-bucket processor will be necessary in order to produce appropriate oscillating signals for the position processes. It may utilize gating of p and $\bar{p}$ buckets and shock-excited ringing circuitry.

The beam monitors will have two modes of operation, single-turn and closed-orbit. The single-turn operation will be used at injection time to measure position and intensity on the first turn as a function of azimuthal location. Information from a few successive turns will be helpful in minimizing coherent oscillations produced by injection errors. A minimum of one detector per house can be measured on each beam pulse. Minimum intensity requirements are approximately 5×10^9 protons over a 0.6-μs time. If a full turn of beam is injected, it appears to be possible to read as many as five detectors per house by rapid switching of the multiplex channels. Thus a full set of horizontal or vertical position information might be obtained in a single beam pulse. Here intensities of the order of 10^{11} protons are necessary. In either case, information on subsequent turns could also be read. At the conclusion of single-turn data taking, the beam-position detector (BPD) will revert to the multiturn mode of operation. Sequential scan of all detectors in a house will be established, with data averaged over 10 turns per channel and a full scan every 2 ms.

Data from the single-turn and closed-orbit modes will be stored separately in a local memory in the interface module. Fixed space will be allotted for the single-turn data and circular memory for the closed-orbit information. Memory size will be sufficiently large to permit meaningful snapshotting of the system data in the event of an abort or magnet quench. In event of an abort or quench, updating of the local memory will cease and all stored information will be transferred on command to the central computer for analysis.

The BPD will provide programmable discrimination capabilities to sense large position errors and provide alarms and abort-triggers. In addition, BPD information can be used to make single-turn plots, closed-orbit plots, and real-time position plots available to the operator, as in the present Main Ring system.

12.11 Loss Monitors

Loss monitors will be installed at all quadrupoles and other special locations to monitor time-dependent losses throughout the cycle. The magnets are more susceptible to quenching from losses at higher energies and abort discrimination levels of the monitors should therefore be weighted as a function of magnet excitation (possibly by use of a B-dot clock). Loss-monitor signals will be integrated over two distinct time intervals. The first will be of the order of 1 ms to detect fast losses and the second of the order of 100 ms, to detect slow or quasi-dc losses. The two times are necessary because the superconducting magnets have different sensitivities to losses with different time dependences (see Section 13). The integrated outputs will be compared against differently weighted discrimination thresholds and, as with the position detectors, an alarm or abort trigger can be generated. During extraction, it is possible that the extraction rate could be slowed if too high a loss level is sensed.

There will be approximately 10 loss-monitor inputs per service building. Inputs will not be multiplexed but rather will go directly into the processor unit, which will provide integration, sampling, digital conversion and alarm discrimination.

The loss-monitor processor (LMP) is almost identical in concept to the beam-position detector interface module. Sufficient memory should be available to store loss-monitor history preceding aborts or magnet quenches, as well as provision for transfer of information to the central computer at its request.

13. MEASURES FOR RADIATION PROTECTION

13.1 Beam Loss in Superconducting Magnets

A basic problem of superconducting accelerators and storage rings is the extent to which the magnet system must be shielded from beam losses. Relatively small fractions of the total beam can cause superconducting magnets to quench. The recovery time required is not negligible.

Conventional accelerators and storage rings do lose beam, as attested to by the residual radioactivity of their magnet systems and by experimental observation of both slow and catastrophic intensity reductions through failure of equipment, beam blowup or in the course of tune-up procedures. Certain processes, such as resonant extraction and beam scraping to clean up phase space are inherently lossy and can be described reasonably accurately. Other processes, such as single-turn injection, single-turn extraction, acceleration and storage, are in principle "loss-free." Experience has proved these processes do not work perfectly, and one must try to minimize such accidental beam-loss effects on the superconducting magnet system.

13.2 Tolerable Level of Energy Deposition

Primary beam protons or their secondary shower products that hit and interact with the superconducting coils will cause local energy deposition in the conductor through ionization loss. This energy, if not removed, will heat the superconductor to the normal transition temperature and thus cause the magnet to quench. The temperature allowed above the nominal operating point of 4.6 K is related to the product of magnetic field and current in the conductor. At high excitation, near quench limit, only fractions of a degree K temperature difference can be tolerated, whereas at the zero-current field limit, the conductor must be elevated to approximately 10 K in order to reach the normal domain. The critical field B_c and current density J_c are related to the temperature by $(J_c \cdot B_c)^{\frac{1}{2}} \propto (10^\circ - T)$. For a particular magnet that at 4.6 K has a maximum current and field operating point of $I_{max} B_{max}$, the allowable temperature difference is then related to the operating point by

$$\Delta T(^\circ K) \simeq (10^\circ - 4.6^\circ) \left[1 - \left(\frac{I \cdot B}{I_{max} \cdot B_{max}} \right)^{\frac{1}{2}} \right].$$

The temperature change resulting from energy deposition is related to the time dependence of the loss. At one extreme, an instantaneous loss ΔE will result in a temperature change given by the integral of the specific heat of the conductor

$$\Delta E = \int_{4.6^\circ}^{T_{final}} C_p(T) dT.$$

At the other extreme, for a slow (> 100 ms) uniform loss, the conductor-helium system will be in equilibrium, with heat transfer taking place from the conductor through the cable insulation to the helium, which is assumed in this limiting case to be boiling. For loss times of the order of a millisecond, an intermediate condition exists where very high heat transfers to the helium inside the insulation might exist for a short time. The amount of energy deposition that can be tolerated according to models[1] for these different time domains is shown in Fig. 13-1, together with experimental results of measurements on magnets,[2,3] interpreted with the help of shower calculations. As expected, at peak excitation the allowable energy deposition

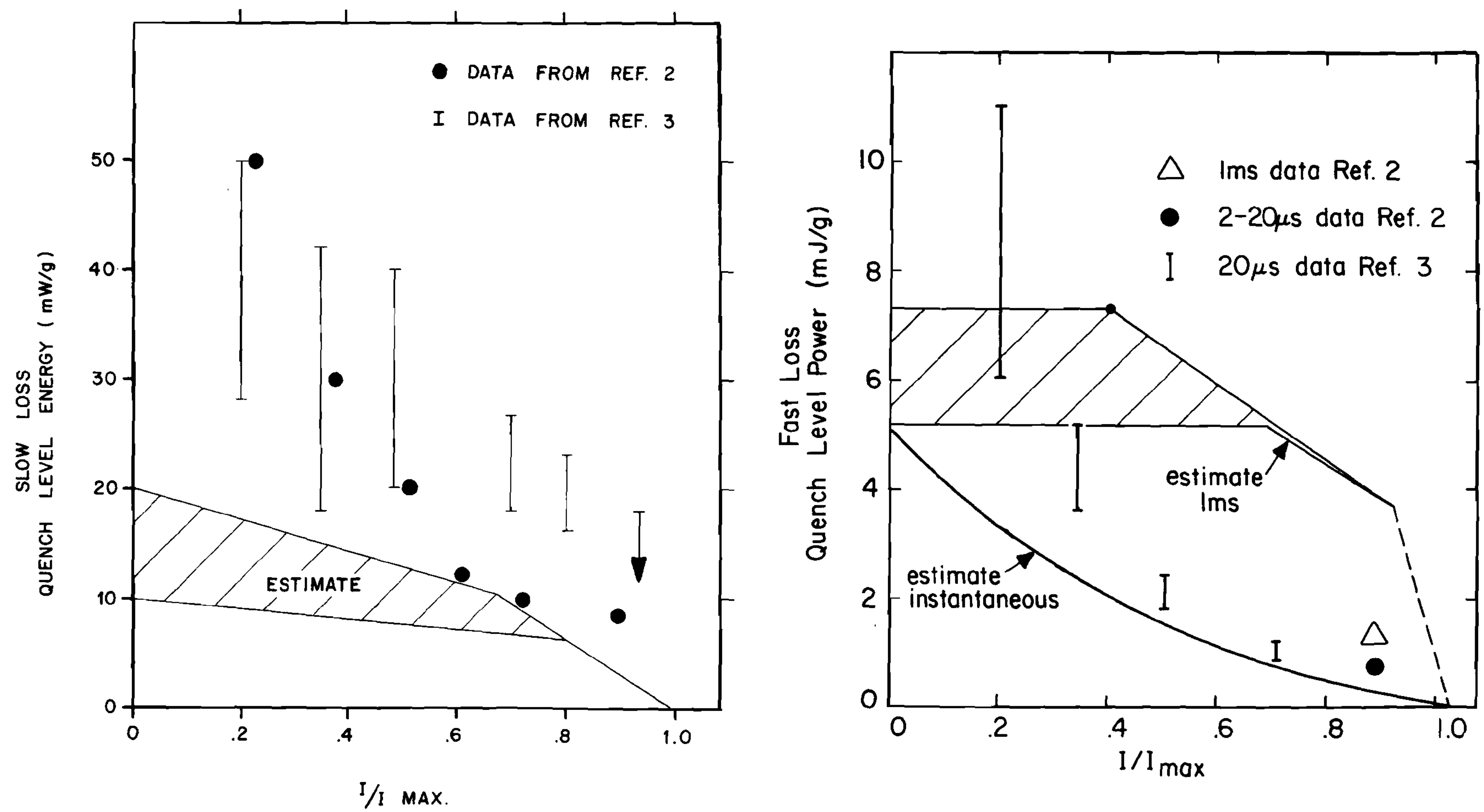

Fig. 13-1. Tolerable energy deposition in superconducting coils.

is small, especially for instantaneous loss. Design limits at 90% of maximum excitation have thus been chosen. They are listed in Table 13-I below.

Table 13-I. Energy Deposition Design Limits

slow loss (DC)	8 mW/g
fast loss (1 ms)	1 mJ/g/pulse
fast loss (20 μs)	$\frac{1}{2}$ mJ/g/pulse

For the present, it is convenient to adopt a single overall limit of 1 mJ/g. It is a proper choice for the abort or 1-ms resonant extraction. It is slightly conservative for slow losses, but here the total heat load in the cryogenic system must also be considered.

With this limit, the need for protection of the superconducting magnets is clear. The average density of the NbTi-Cu wire is approximately 8 g/cm^3, so 1 mJ/g is equivalent to 5×10^7 GeV/cm^3. If a shower produced by a single interacting primary particle deposits on the average 5×10^{-3} GeV/cm^3, to take a typical figure near the shower maximum, then 10^{10} interacting primaries will result in deposition of energy at the design limit. This situation corresponds to the loss of only 0.05% of the circulating beam.

13.3 Loss Mechanisms and Protective Measures

The kinds of loss can be categorized as:

(i) Resonant-extraction loss

a) Beam hits electrostatic septum wires

b) Beam hits extraction-channel Lambertson magnets

(ii) Abort loss; beam hits abort-channel Lambertson magnets

[similar to (i)b]

(iii) Injection first-turns loss; beam is mis-steered into magnets

(iv) Betatron-space blow-up; beam hits scraper system

(v) Off-momentum loss; beam hits momentum scraper system

The possible protective measures can be categorized as:

(i) Scraper system

a) Beam scraper and collimator system in long straight sections with conventional bending magnets and momentum analysis

b) Beam scraper systems in medium straight sections for off-momentum loss

c) Plugs in specific superconducting magnets downstream of bad loss points

d) Beam scrapers in superconducting magnets throughout the accelerator

(ii) Electronic - alarms and abort

a) Position detectors, alarms

b) Loss monitors, alarms

c) Tune and coherent-oscillation detectors

d) Device-failure alarms

e) Abort

13.4 The Extraction-Loss Problem

In the resonant-extraction process, individual-particle amplitudes grow at a rate that increases with amplitude. For efficient extraction the final step size, when particles pass through the field region of the electrostatic septum, is of the order of the septum wire-to-cathode gap and the probability that any particle hits the septum wires is approximately $2W/\Delta$, where W is the wire thickness (approx. 2 mils) and Δ is the two-turn step size or wire-cathode spacing (approx. 400 mils). It is expected that 1 to 2% of the beam will hit septum wires during extraction. These wires are 2-mil tungsten spaced every 0.1 in. along the length of the septum (two modules, each 12 ft long). Particles that hit the septum wires at D0 can be considered as a uniform parallel beam perfectly aligned with the septum wires. As they proceed along the septum, they can either undergo nuclear interactions, multiply scatter out, or pass through all wires. Typical angles for multiple Coulomb scattering and coherent nuclear elastic scattering are 40 μrad and these particles will propagate around to the extraction channel at A0, where they will either be (a) extracted, (b) hit the Lambertson septum, (c) continue around the accelerator and be extracted two turns later or (d) be lost in the accelerator. Those lost in the accelerator or in the Lambertson will shower and produce radiation in the downstream superconducting magnets.

Protons that undergo nuclear interactions in the electrostatic septum will similarly produce radiation in the magnets downstream of the straight section. For the present purposes this radiation can be characterized by three components:

(1) high-energy protons with energies above 500 GeV

(2) neutral secondaries from π^0 decay

(3) low-energy (< 500 GeV) charged secondaries.

If shielding is not placed between the septum and the superconducting magnets, the three components have the following effects:

(1) High-energy protons will continue quite a way in the aperture of the superconducting magnets before being bent into the inside wall. They carry substantial energy and produce substantial energy deposition over considerable distance.

(2) Neutrals proceed straight ahead as the magnets bend away from them horizontally and, because they are reasonably well collimated, tend to produce a peak in the energy density roughly where they intersect the vacuum wall.

(3) Charged secondaries are bent into the magnets quickly in the first few meters.

(4) There is a sharp peak at the front of the magnet string from any particles with large enough angle to hit the magnet's front face.

Figure 13-2 illustrates these components.

Significant reduction in energy deposition can be made by incorporating an orbit-bump magnetic analyzer and collimator scheme with the electrostatic septum in the D0 straight section. Figure 13-3 illustrates this scheme. Four conventional (perhaps Main-Ring) bending magnets are arranged to produce a vertical orbit kink. Inside these magnets are placed collimators of dimensions determined by the injected beam emittance, the resonant-extracted horizontal beam size, and the relative betatron-amplitude functions at the various magnet locations. Care is taken to ensure that under normal operation the upstream collimators are the aperture stops and that

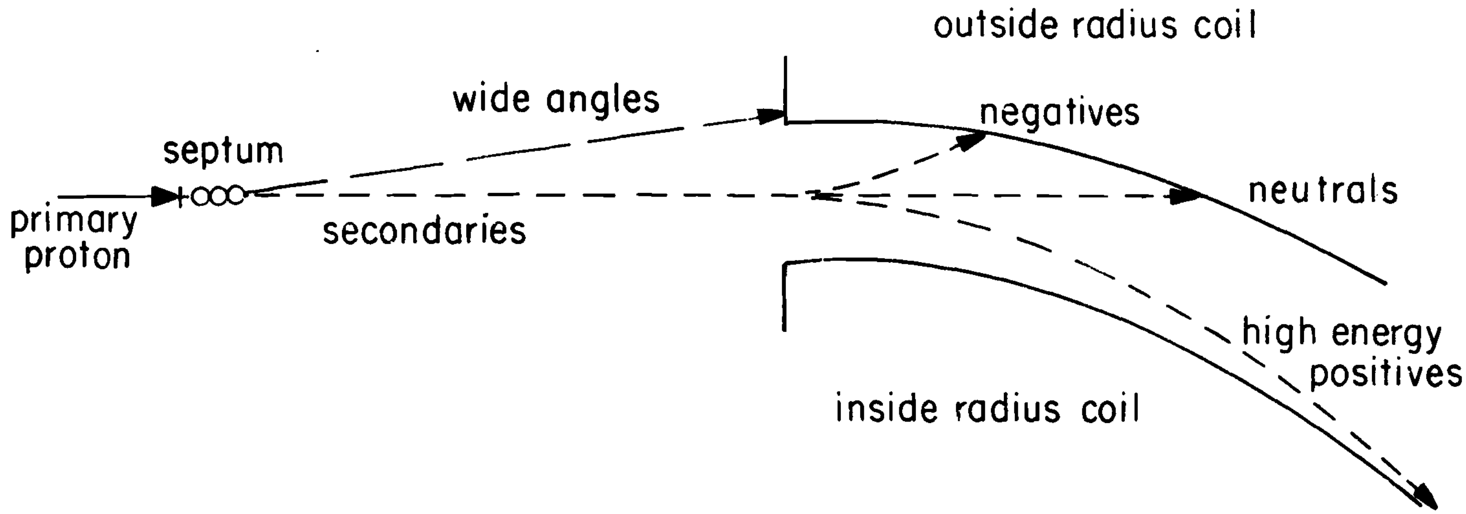

Fig. 13-2. Radiation components from nuclear interactions.

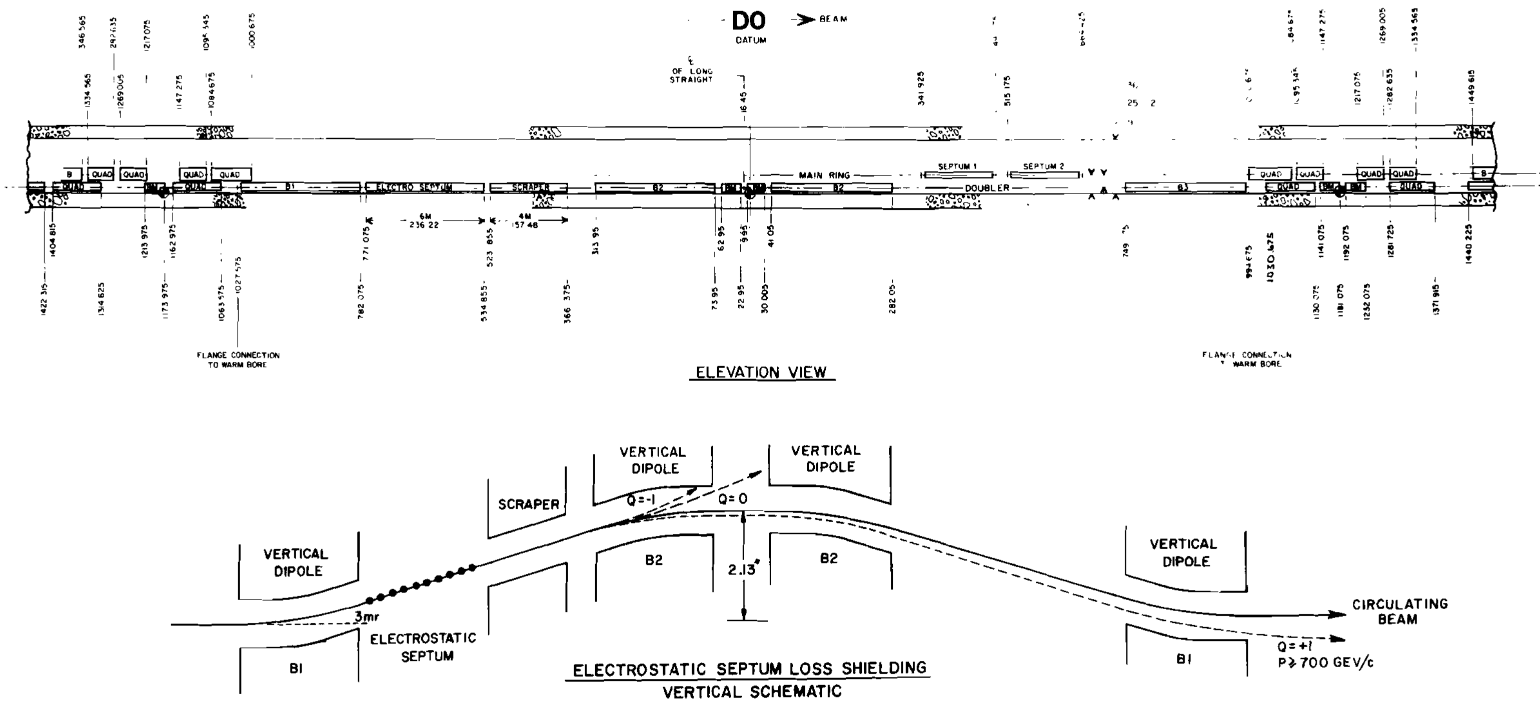

Fig. 13-3. Layout of D0 long straight section.

primary beam never scrapes on the downstream collimators or superconducting-magnet beam plugs. With each conventional magnet bending by 3 mrad and with collimator sizes as given in Table 13-II, it is possible to intercept all neutral and negative particles and positive-charged particles with energies below approximately 75% of the beam energy. Calculations of shower energy density in the superconducting magnets indicate that reductions of factors of 20 to 50 are gained by this collimator scheme which should be sufficient for 1-ms resonant extraction of 2 to 5 $\times 10^{13}$ per pulse. That is, with 2% of 2 to 5 $\times 10^{13}$ protons hitting the septum wires, 1 mJ/g of heating will be produced in the superconducting magnets.

Table 13-II. Collimator Sizes

(Full Width in cm)

	B1	B2	B3	Quad Plug	Bend Plug
Horiz.	7.5	5.0	3.4	4.0	5.0
Vertical	1.6	2.2	4.0	6.0	4.0

Multiply scattered particles from the septum that proceed around half the accelerator and strike the extraction-channel Lambertson septa behave in two different ways. Those that strike the front surface of the first magnet septum have good probability of showering extensively in the septum steel and considerable energy is absorbed before the shower products reach the superconducting elements. Because of the lattice optics, however, the beam is horizontally converging and some particles may graze the long side of the magnetic septum with an angle of approximately 30 μrad. These produce 10 times more radiation in the downstream superconducting string. The radiation protection measures planned in A0 are:

(i) a 2-m collimator at the downstream end of the straight section.

(ii) the Lambertson magnet septa, built wider at the upstream end to reduce the number of particles that can hit with grazing incidence.

It should be possible for 10^{11} particles to hit the Lambertson without exceeding the 1 mJ/g limit in downstream magnets. A plug or thick-walled vacuum chamber placed within the downstream superconducting magnets will further raise this limit.

13.5 The Abort Problem

The abort extraction channel incorporates a magnetic analyzer-collimator system similar to that at D0. Detailed calculations of this geometry have not been done, but we expect that a few times 10^{11} to 10^{12} protons can be lost at C0 in the abort process without quenching the nearby magnets. Here the particles hitting the septum are those that have grown to a large phase space before the kicker is fired and thus hit the septum at the abort time.

Beam scrapers at the upstream ends of C0 and D0 straight sections will be used in conjunction with the orbit kinks in these straight sections to act as limiting aperture restrictions for large betatron oscillations and for halo scrapers during colliding-beam experiments.

13.6 Calculations of Energy Deposition in Magnets

A study is in progress to calculate the distribution of energy deposition in the superconducting magnets for the various complicated geometries of the accelerator system. The program CASIM[4] has been modified to include the geometry of the magnet configurations and the presence of the electric and magnetic fields of septa and magnets.

The calculations are not complete, but a number of configurations have been analyzed.[5] They have been made only for 1000-GeV protons and the only material considered so far for scrapers, collimators, and plugs has been iron. We give some examples for illustrative purposes of energy deposited in the median plane of the superconducting magnets. Figure 13-4 shows the bin subdivision of the coils used in the calculations. Here we only display data from the cross-hatched region. Inward and outward regions in the ring are specified at "inside radius" and "outside radius", as shown in Figure 13-2.

In Fig. 13-5, results are given for a simplified geometry of the D0 straight section that does not include superconducting quadrupoles at the upstream end of the superconducting bend string. The curves show energy deposition in the median-plane coil regions of the superconducting bends as a function of distance along the bends per proton incident on the electrostatic-septum wires. The different conditions of the curves are:

(i) No shielding; no conventional bend magnets.

(ii) Septum upstream of four bend magnets. The first magnet bends horizontally inward. Collimators in the magnets are $5.6 \times 2\ cm^2$. (h xv)

(iii) Septum is downstream of the first bend magnet, which bends inward. The momentum difference Δp from the primary momentum, which gets through the conventional system, should be about half that of (ii).

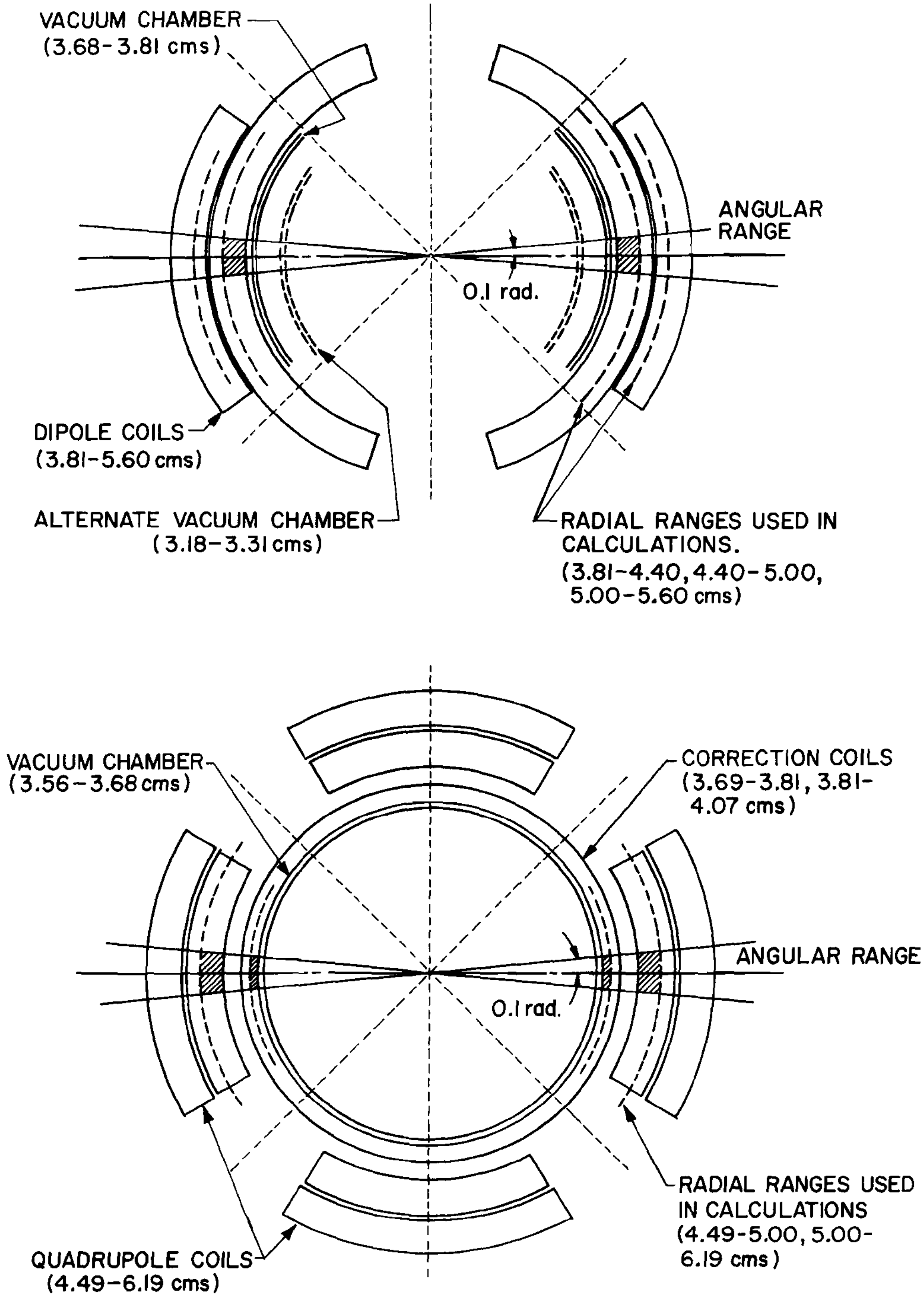

Fig. 13-4. Dipole and quadrupole coil geometry used for energy deposition calculations. Crosshatching indicates regions discussed here.

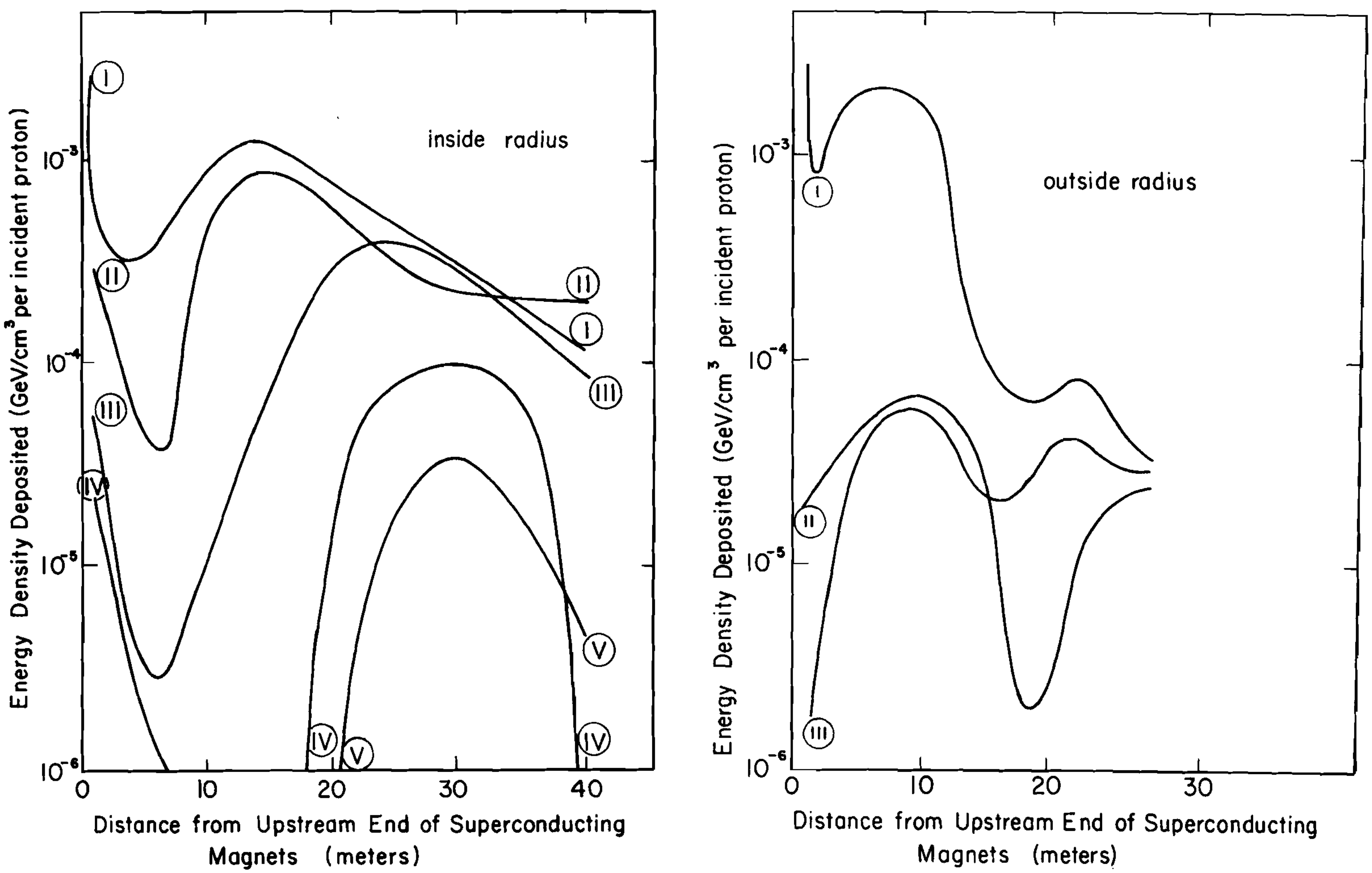

Fig. 13-5. Energy deposition downstream of the D0 septum.

(iv) The septum is downstream of the first bend, which now bends vertically. The momentum difference cutoff is further reduced because the vertical aperture of the collimator is smaller than its horizontal aperture.

(v) A plug (5 $\times$3 cm) has been put in the superconducting magnets. It extends to the coil surface. A further small reduction in in energy density is achieved.

It appears that a reduction of a factor 50 has been obtained and curves of energy density on the inside-radius coil surface clearly show effects of increasingly better momentum selection. The energy deposition on the outside-radius coil surface is greatly reduced by a beam bump and does not present a problem. In the case of the vertical bump, care must be taken in the way the results are interpreted because we no longer have up-down symmetry. The inside-radius coil at the midplane may not be the location of the energy-density maximum; this location is expected to vary with distance along the magnets. Further investigation indicates that the maximum energy density may exceed that at the inside median plane by as much as a factor of two.

We have also investigated a more realistic geometry including the superconducting quadrupoles and collimators of size given in Table 13-II. Results are very similar to the above. Further calculations are required to optimize the plug geometry.

Figure 13-6 illustrates the energy deposition in a medium straight section from a scraper downstream of the quadrupole for cases with no

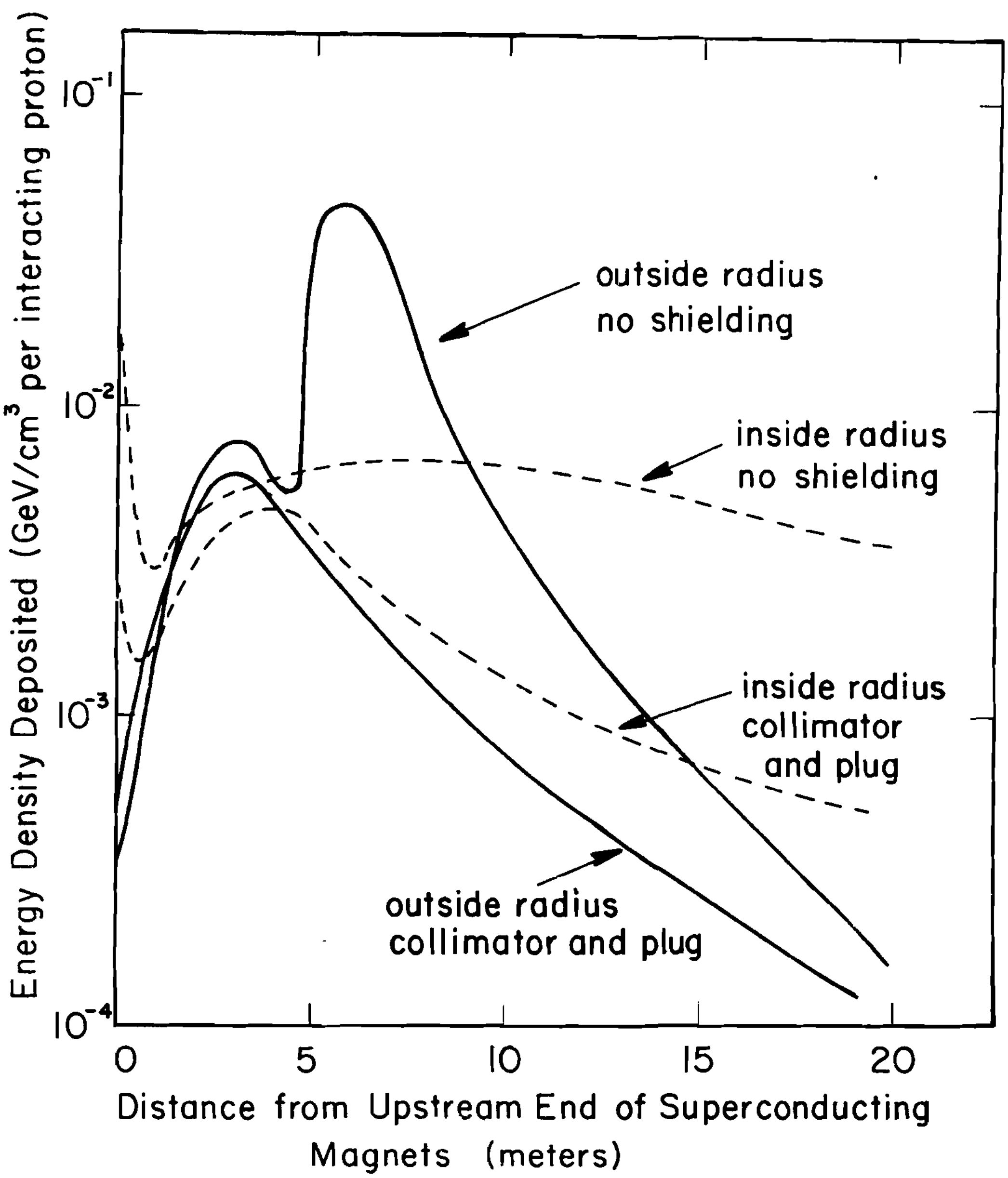

Fig. 13-6. Energy deposition in magnets downstream of a scraper in a medium straight section.

shielding and with a 2-m collimator upstream and a plug in the superconducting magnets, both with 5 $\times$3 cm aperture. The absorption of the neutral peak by the plug is clearly illustrated; the reduction of energy from charged particles is smaller, but can still be seen.

We have also considered the case of beam striking a Lambertson magnet in a long straight section. With a parallel incident beam uniformly distributed over the septum region for a height of ± 1 mm, we find peak energy densities of 4×10^{-4} GeV/cm^3 per incident particle in the downstream superconducting bending magnet. If the incident particle strikes the side with a glancing angle of 30 μrad, energy densities of 3×10^{-3}GeV/cm^3 result. There is no magnet plug included in these calculations.

Other cases are being considered in this work, but have not yet been completed.

13.7 Status of Shielding Design

Simulation of the process of a particle circulating in a synchrotron until it hits the edge of a scraper and produces a shower is a complicated problem involving both particle dynamics in an accelerator and the multiple-scattering, nuclear-interaction and shower-development processes of a particle near the edge of an absorber.

An attempt to model the behavior described above is in progress in order to determine the amount of energy characteristically absorbed in the scraper, as opposed to that deposited in downstream superconducting magnets. A conservative design that does not rely on this analysis assumes that the scraper acts only as a source in which nuclear interactions occur and does not in itself absorb or develop the shower. It is clear under these guidelines that scraper systems are best implemented in long straight sections C0 and D0, where the conventional bumps can provide shields, as discussed above. Using the electrostatic-septum calculations as a guide, we would guess that at least 2×10^{11} particles could interact in a scraper without exceeding 1 mJ/g energy deposition in the superconducting magnets.

Off-momentum protons may not hit the scrapers in the long straight sections because the dispersion function η is one-third its maximum value at these locations. At medium straight sections, (Locations 17) η is a maximum and scrapers can be installed. There is not, however, sufficient space for magnetic shields as used in C0 and D0, so that the scraper acts mainly as a source for interactions and the downstream drift space allows the secondary beam to diffuse. Calculations indicate that 10^{10} interactions will produce 1 mJ/g of heating.

The effects of beam hitting the superconducting - magnet vacuum - chamber itself are reduced by certain simple measures. For instance, if the vacuum chamber wall is moved away from the superconducting coils, energy density is reduced because the shower can diffuse in the distance it must travel between the vacuum wall and the coil. Of the order of 10^{8} 1000-GeV particles must hit at one point in a bending magnet to deposit a peak of 1 mJ/g in energy. Figure 13-7 illustrates this reduction, as well as that gained by a plug in the magnet.

Further reduction of magnet sensitivity seems possible if collimator arrangements are located in the quadrupole assemblies as indicated in

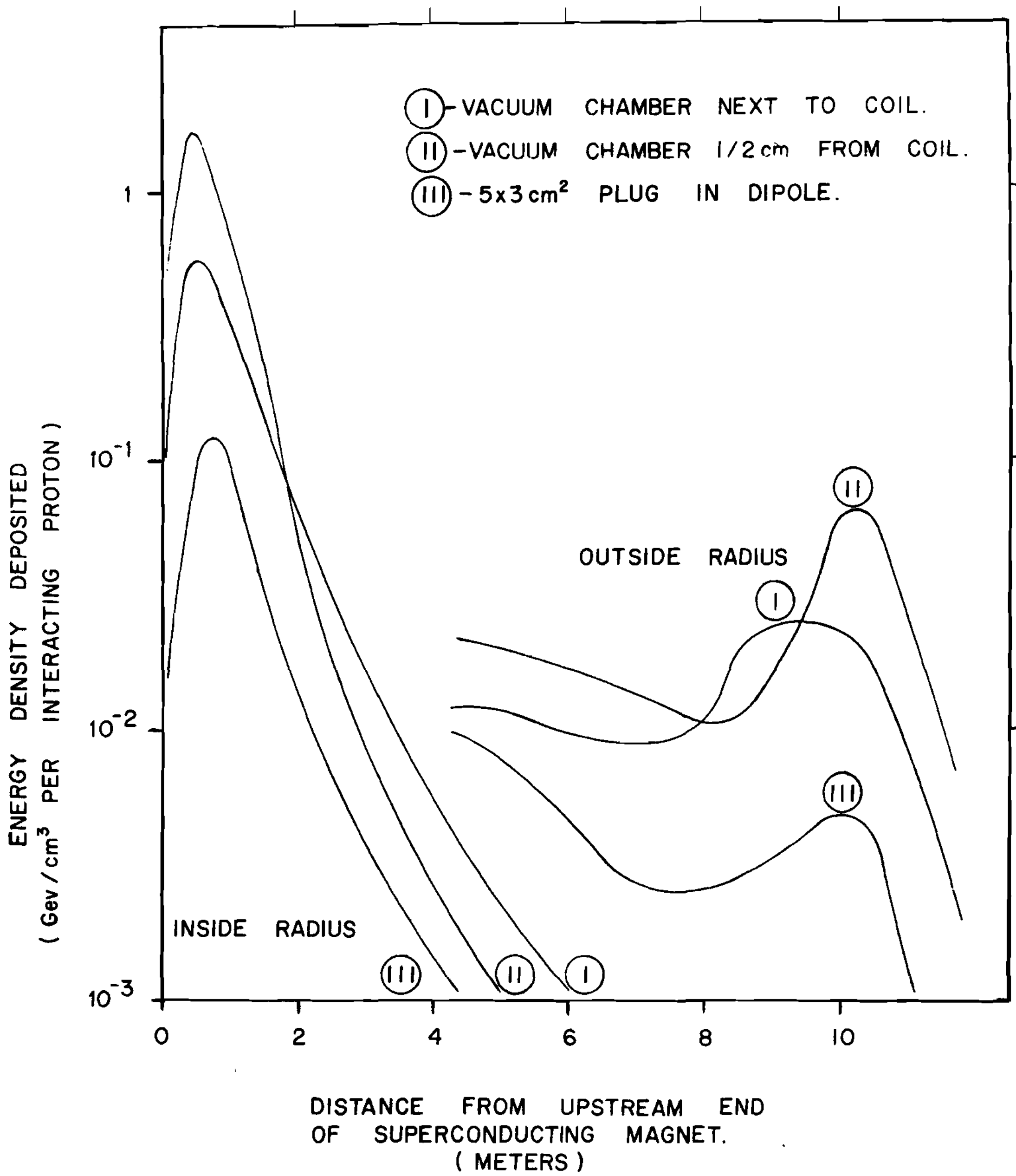

Fig. 13-7. Effects of different vacuum-chamber positions on energy deposition. The incident proton hits the upstream end of the dipole vacuum chamber or plug on the inside radius.

Fig. 13-8. Results for this case are shown in Fig. 13-9. A short primary scraper upstream of the quadrupole followed by a longer one between the quadrupole and bending magnet reduces the peak energy deposited in the dipole by a factor of 10 from that given above. The quadrupole itself can tolerate 5×10^8 particles for 1 mJ/g. The quadrupole magnets are not run as near the short sample limit as the dipoles and can tolerate a larger energy density before quenching. The correction coils inside the quadrupoles receive the most heating, but it is less of a problem if the correction coils quench than if the main magnets quench. The determination of optimum shielding arrangements of this type has not yet been made.

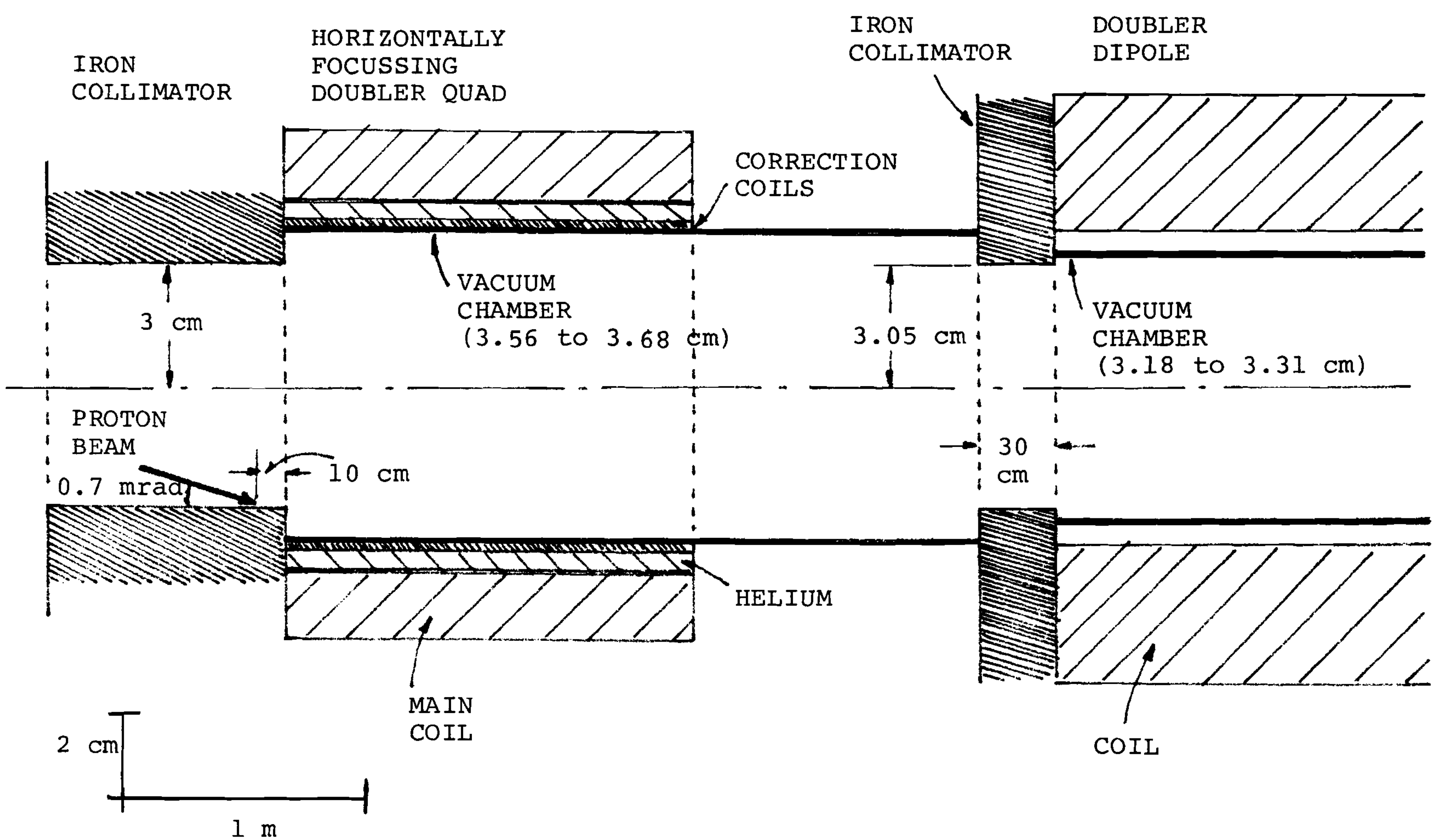

Fig. 13-8. Collimator geometry in quadrupole assembly used in calculations of Fig. 13-9.

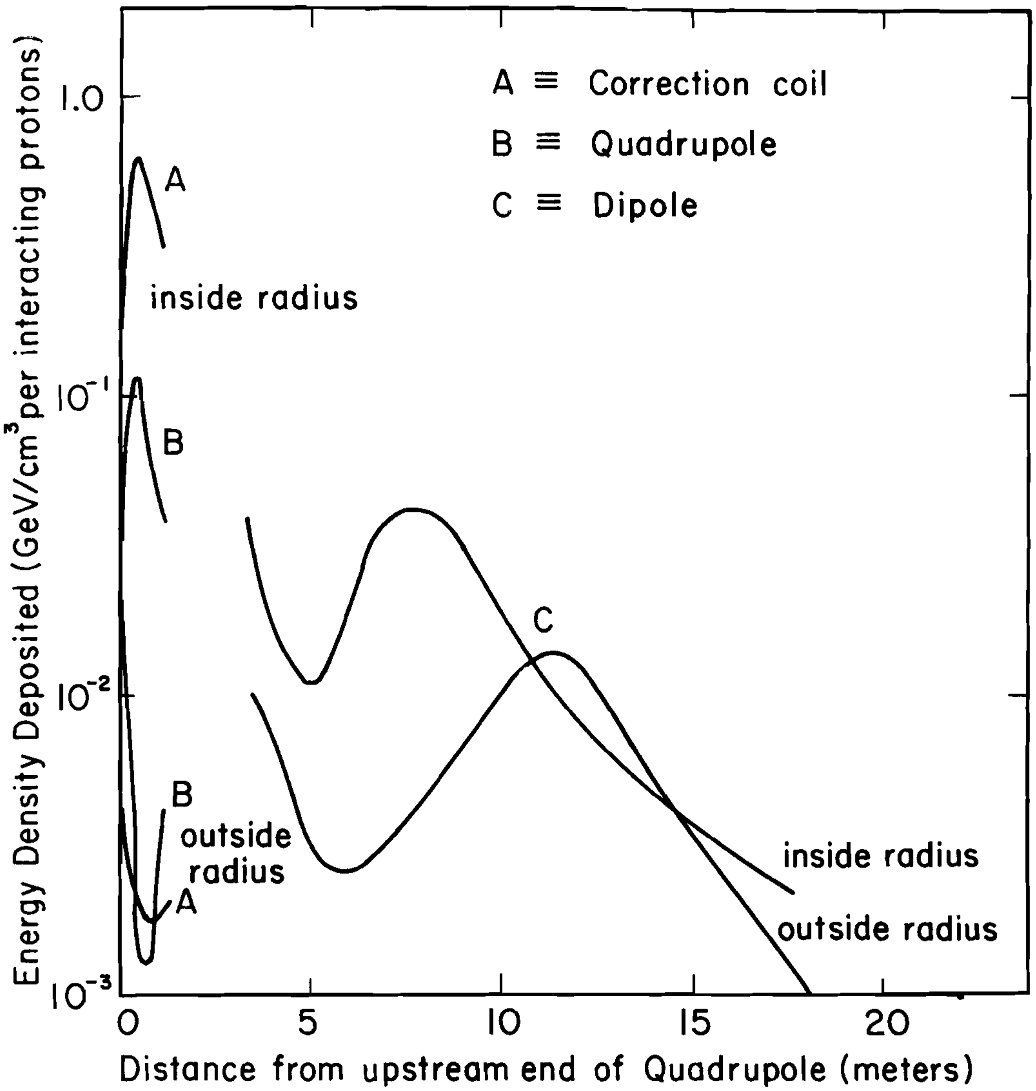

Fig. 13-9. Energy deposition in a quadrupole and dipole with collimator geometry of Fig. 13-8. Protons hit scraper upstream of quadrupole on the inside radius.

References

[1] H. Edwards, paper submitted to the HEPAP Committee, Woods Hole Meeting, June 1977.

[2] B. Cox, P. O. Mazur, and A. Van Ginneken, Sensitivity of an Energy Doubler Dipole to Beam-Induced Quenches, Fermi National Accelerator Laboratory Internal Report TM-828-A, November 1978.

[3] H. Edwards, C. Rode, and J. McCarthy, IEEE Trans. Magn. **1**, 666 (1977).

[4] A. Van Ginneken, CASIM - Program to Simulate Hadronic Cascades in Bulk Matter, Fermi National Accelerator Laboratory Report FN-272, January 1975.

[5] H. Edwards, S. Mori, and A. Van Ginneken, Studies on Radiation Shielding of Energy Doubler Magnets (1), Fermi National Accelerator Laboratory UPC No. 30, December 27, 1978.

H. Edwards, S. Mori, and A. Van Ginneken, Supplement to UPC 30, Fermi National Accelerator Laboratory UPC No. 40, January 12, 1979.

H. Edwards, S. Mori, and A. Van Ginneken, Supplement 2, of UPC No. 40, February 1979.

14. $\bar{p}p$ COLLIDING BEAMS

14.1. Performance

It will be assumed here that the present Main-Ring proton intensity of 2×10^{13} can be debunched at 150 GeV and that about 10% can be recaptured into 21 bunches. The rf details of how this relocation is to be done are discussed in Section 9.6.

In the superconducting ring, a single bunch will cause a $\Delta\nu = 2 \times 10^{-3}$ tune shift per crossing for the antiprotons, within acceptable limits. Collision of a single proton bunch with a single bunch of 6×10^{9} antiprotons will yield a luminosity of 5×10^{28} cm^{-2} s^{-1}.

Development of higher-luminosity schemes will primarily use more antiprotons and more bunches. For modest luminosity schemes in which there is no high-momentum precooler or accumulator ring, it is necessary to accelerate the antiprotons in single bunches from the 200-MeV cooling ring through the Booster and Main Ring. For more than about 10^{10} particles per bunch, serious deterioration of transmission and beam quality occurs in the Booster. The luminosity per bunch is therefore limited to about 10^{29} cm^{-2} s^{-1}. Optimistic estimates of antiproton collection rates would limit the total number to about 3 to 4×10^{10} for a reasonable collection time, so there might be 6 bunches of protons and antiprotons, with a total luminosity of approximately 5×10^{29}, assuming the interaction β could be reduced to about 1.5 m.

Addition of a high-momentum precooling ring or accumulator ring would allow more rapid collection of antiprotons, and also the possibility of rebunching at higher momentum, removing the restriction on single-bunch intensities imposed by the Booster. As an example, if 6×10^{11} antiprotons were collected at 200 MeV in a Booster-length cooling ring, they could be rebunched at 30 MHz, accelerated through the Booster with approximately 10^{10}/bunch, reinjected into the precooler and rebunched with 12 bunches. These bunches would be individually extracted, accelerated to 150 GeV and placed in proper location in the superconducting ring. The luminosity would be in the high 10^{30} range. The bunches in each beam would be separated by about 1 μs, which is adequate for kicker rise and fall times (approx. 0.8 μs) and desirable for experimental instrumentation. About one-fourth of the ring would be left vacant to accommodate the abort system.

At this luminosity, there is on the average almost one interaction per crossing. Higher luminosity schemes must then employ more bunches. This conflicts with single-bunch kicker rise and fall times and it will be necessary to regroup the larger number of bunches into about one-third the circumference of the Main Ring and to transfer all the bunches of protons or antiprotons at a single time. This scheme, although not worked out in detail, is compatible with abort and kicker capabilities.

14.2. Specific needs for Antiproton Collisions

(i) Injection kicker. The schemes described above are within the present abilities of kicker systems. Details are described in Section 10.

(ii) Low-beta section. The correction package for the ring (Section 7) will be influenced by the need to compensate for the low-β section. The tune shift caused by the insertion should be minimal and, as in Case E of Table 2-II, the momentum dispersion should be compensated, so that retuning for low β can be done locally.

(iii) Radio-Frequency systems. These systems are described in Section 9.6. Here we emphasize again that a low-frequency system is needed in the Main Ring. In addition, it may be necessary to employ a high-frequency Landau cavity to maintain the stability of these bunches. In order to reverse-accelerate antiprotons in the Main Ring, the cavities must be rephased at a low power level.

The rf system should be capable of independent acceleration of protons and antiprotons. This can be achieved by proper cavity spacing, as described in Section 9.2. It appears possible to perform the necessary steps with 6 cavities. If high-frequency cavities are necessary for the stability of the proton bunches, then two must be employed in order to cancel out the antiproton acceleration by these cavities.

(iv) Electrostatic Beam Separators. Measurement of collision parameters and luminosity calibration can be achieved by an electrostatic system to separate the beams at the collision point. This is most easily done by placing deflection plates at quadrature points of betatron phase from the intersection point, at, for example, approximately 7 m from the center of adjacent long straight sections. In order to reduce the interaction rate to about 1% of the undeflected rate (for Gaussian profiles), an electric field-length product of approximately 20 MV is required at each quadrature point ($\beta \simeq 68$ m). If a 5-MV/m field can be sustained over the 2-cm aperture, 4 m of electrode is required. In principle systems should exist for separating both the horizontal and vertical directions.

A discussion of antiproton production is given in Reference 1. A discussion of proton-proton collisions is given in Reference 2.

References

[1] F. E. Mills and D. E. Young, A Scenario to Achieve a Luminosity of Approximately 5×10^{29} $cm^{-2}s^{-1}$ for $\bar{p}p$ **Collisions** in the Fermilab Energy Doubler. Fermilab report UPC-73 (unpublished) Nov. 11, 1978.

[2] D. Ayres et al., Kissing Magnet Design for the pp Collider. Fermilab report UPC-76 (unpublished) Nov. 8, 1978, revised Dec. 21, 1978.

APPENDIX I. SUMMARY OF ACCELERATOR PARAMETERS

A. Fixed-Target Accelerator

Peak Energy	800 - 1000 GeV
Intensity	$>2 \times 10^{13}$ ppp
Rep rate	1 - 2 cyc/min
Injection	150 GeV, single turn
Injection phase space	$< 0.2\,\pi$ mm-mr ($2\,\sigma$)
Injection $\Delta p/p$	$< \pm 0.3 \times 10^{-3}$ (<0.3 eV-s)
Ramp Rate	50 - 75 GeV/s
Main Power Supplies	6 @ 2 kV, 4500 A each - Ramping 1 @150 V, 4500 A - Holding
RF	53 MHz (Main-Ring frequency)
Harmonic number	1113 (same as Main Ring)
RF Voltage	250-380 kV/cavity, 6 cavities
Bend-Field current at 1000 GeV	44 kG @ 4400 A
Number of dipoles	774
Number of quadrupoles	216
Good-field aperture	±0.8 in. horiz., ±0.6 in. vert.
Lattice	Modified Main Ring, -FODO, -antisymmetric long straight section High β for extraction, 2 straight sections Low β for colliding beams, 1 straight section
Radius	0.7 cm radius increase from Main Ring (1 km)
Amplitude functions	
Normal cell	
β_{max}	99.5 m
β_{min}	28.6 m
η_{max}	6.0 m
Long Straight Sections	
β_{max} - Normal	110.3 m
β_{max} - High-β	243.4 m
Tune	19.4 horiz. and vert.
Flattop time	Variable to dc
Correction magnets	Superconducting, ramped to full excitation. Dipole, quadrupole, sextupole at each main quad. Skew quadrupole, octopole, skew sextupole as needed.
Extraction	Slow resonant (1 to 10 s) Fast resonant (1 ms)
Abort System	Single-turn beam extracted.

Cryogenics

Heat leak/magnet	Dipole dc < 7 w at 4.6 K 22 w at 80 K Dipole ac <500 J/cyc at 4.6 K Quadrupole dc < 7 w at 4.6 K 13 w at 80 K
Heat leak and helium usage for leads	Power leads, correction leads, end boxes etc., total 350 ℓ/h + 550 w
Central Helium Liquefier	> 4000 ℓ/h
Nitrogen Reliquefier	2550 ℓ/h (54 ton/day)
Satellite Refrigerators	24 units each 966 w max. @ 4.6 K with 129 ℓ/h helium input

B. $\bar{p}$ - p Collider

Interaction region	one[1]
β^*	1 - 10 m (horiz. and vert.)
Space for detector	12 - 40 m
Number of filled rf buckets	1, possibly going to 12[2]
Spacing between filled buckets	1 μs (approx)
Number of p's/bucket	$2 \times 10^{10} - 10^{11}$
Number of $\bar{p}$'s/bucket	$6 \times 10^{9} - 10^{10}$
Luminosity/bucket	$10^{28} - 8 \times 10^{28}$ cm^{-2} s^{-1}
Injection	Forward and backward single bucket
Abort	Forward and backward dumps
RF	2 sets of orthogonal cavities total of 6 (4p - 2$\bar{p}$)
Vacuum in straight sections	$<10^{-8}$ Torr
Storage time needed	> 3 h
Longitudinal Emittance	p: 2 eV-s $\bar{p}$: 0.08 eV-s
Beam tune shift/crossing	2×10^{-3}

Interaction region (for a β^* of 2 meters) (triplets adjacent to interaction region)

η^*	0.4 m
β max	380 m
η max	9.5 m
$\Delta\nu$	0.3
Space for detector	14 m
Chromaticity	1.1 times normal
Number of separate quad power supplies	5
Number of quads separately powered	10

1) A second interaction region could be developed if the extraction septum and related shielding were removed during colliding-beam operation.

2) More than one bucket will come with development of high-momentum pre-cooler or accumulator.

C. p-p Collider (minimal system)

Main Ring

Energy	150 - 200 GeV
Intensity	2×10^{13} (full ring)
β^*	5 m (approx.)
Storage Time Needed	1/2 h

Superconducting Ring

Energy	800 - 1000 GeV
Intensity	2×10^{13} p (full ring)
β^*	10 m
Storage Time Needed	1/2 hour

Luminosity	2×10^{30} cm^2 sec^{-1}
Injection	Backward injection and acceleration in Main Ring required
Abort	Backward MR abort required.
Radius	Superconducting Ring at 0.7 cm larger radius than Main Ring
Space for Detector	12 m
Interaction Region	Kissing magnets (Beams come together and then apart in one straight section). Main-Ring magnets must be lowered near interaction straight section.

APPENDIX II. LATTICE FUNCTIONS AND GEOMETRY

The ring has two-fold symmetry. Thus the accompanying SYNCH printout covers only three sectors explicitly. Stations are listed at the left of the elements.

The drawings show the relationships between the layout of the two rings. All numbers are in inches. Numbers in square parentheses indicate the radial offset of the superconducting ring relative to the Main Ring. Outside dipoles, the angle is always 0.4298 mrad. Neither the longitudinal nor the radial scale is linear.

SYNCH RUN DOUBLER LATTICE

```
==========================================================================================

               DOUBLER LATTICE USING TWO SHELL NORMAL QUADS AND SPECIAL
               LENGTH MATCHING QUADS. ALL QUADS RUN AT SAME EXCITATION
               CORRESPONDING TO THE 35 TURN DIPOLE.

               21 FOOT DIPOLES

               LATTICE WITH COLLINS HIGH BETA IN SECTS. D & A

               ALL QUANTITIES GIVEN AT THE END OF THE ELEMENT.
               ALL QUANTITIES IN UNITS OF M.KG.KG/M.KG-M.

               11 APRIL 79 DE JOHNSON

*** BRHO   =          //  33387.702
*** BZ     =          //  44.27664
*** GF     =          //  760.32056  = 19.31214 KG/in
*** GD     =          //  -760.32056
*** BL     =          //  6.1214          241"                Bend length
*** QL     =          //  1.67894         66.1                Normal Quad length
*** QLS    =          //  0.8146          32.07               48 Location Quad length straight section C, E, F
*** O      DRF        //  0.2794          11                  Bend to Bend drift
*** OO     DRF        //  2.29616         90.4                Normal Mini straight drift
*** OOO    DRF        //  0.4445          17.5                Drift just ahead of standard cell quads
               NORMAL CELL
*** B      MAG        //  BL       0.       BRHO   BZ    $
*** QF     MAG        //  QL       GF       BRHO
*** QD     MAG        //  QL       GD       BRHO
               HALF CELL
*** .HC    BML        //  OO   B   O   B   O   B   O   B   OOO
*** HC     MMM        //  .HC
               MEDIUM STRAIGHT
*** MS1    DRF        //  14.67866        577.90   48.158     17 location straight length
*** MS2    DRF        //  0.8636          34                  Drift just ahead of 18 location Quad
               REGULAR LATTICE
*** QFS    MAG        //  QLS      GF       BRHO
*** QDS    MAG        //  QLS      GD       BRHO
*** .NC    BML        //  2( HC  QD  HC  QF   ) MS1  B  O  B  MS2  12(
 *                    //  QD  HC  QF  HC   )
               LONG STRAIGHT at C0 E0 F0
*** QL1    =          //  2.1011          82.72"              Outside Quad of Doublet
*** QL2    =          //  2.5248          99.40               Inside Quad of Doublet
*** D1     DRF        //  8.1915          322.5    26.875'    48 Location Straight length
*** D2     DRF        //  3.8191          150.35   12.53      Drift Space between doublet
*** D3     DRF        //  1.7907          70.5                Mini straight length downstream of 11 location doublet
*** LS     DRF        //  26.5970         1047.12  87.26      Long straight half length
*** Q1     MAG        //  QL1      GF       BRHO
*** Q2     MAG        //  QL2      GD       BRHO
*** -Q1    MAG        //  QL1      GD       BRHO
*** -Q2    MAG        //  QL2      GF       BRHO
               LONG STRAIGHT LATTICE
*** .LSS   BML        //  QFS  D1   B   O    B   O  B  OOO  Q1  D2  Q2  LS
 *                    //  LS   -Q2  D2  -Q1  D3  B  O  B    O   B   O   B
 *                    //  OOO  QDS  HC

               HIGH BETA LONG STRAIGHT D & A
*** QHL1   =          //  0.6477          25.5                F48 Quad
*** QHL2   =          //  2.2908          90.19               Outside Quad of doublet
*** QHL3   =          //  2.5248          99.40               Inside Quad of doublet
```

```
***  QH1    MAG        //  QHL1     GF        BRHO
***  QH2    MAG        //  QHL2     GD        BRHO
***  QH3    MAG        //  QHL3     GF        BRHO
***  -QH3   MAG        //  QHL3     GD        BRHO
***  -QH2   MAG        //  QHL2     GF        BRHO
***  -QH1   MAG        //  QHL1     GD        BRHO
***  DH1    DRF        //  8.1359          320.31    26.69     48 location straight length
***  DH2    DRF        //  3.8519          151.65    12.637    Drift length between doublet
***  DH3    DRF        //  1.7351           68.31              Mini straightlength down stream of Sta 11 doublet
***  LSD    DRF        //  26.5970        1047.12    87.26     Long straight half length

***  .LSD   BML        //  QH1  DH1  B    0    B    0    B    000  QH2  DH2  QH3  LSD
  *                    //  LSD  -QH3 DH2  -QH2 DH3  B    0    B    0    B    0    B
  *                    //  000  -QH1 HC

***         PAGE       //
```

*** RING CYC 2 // 2(.NC QD HC .LSS QF) .NC QD HC .LSD QF

	POS		S	PSIX	BETAX	ALPHAX	XEQ	DXEQ	PSIY	BETAY	ALPHAY	YEQ	DYEQ
A13	0		0.0000	0.00000	97.994218	1.87497	2.071389	-.03395	0.00000	28.891693	-.57695	0.00000	0.00000
	1	HC	28.0645	.08816	29.047159	.58179	1.544133	-.00148	.08863	97.537839	-1.86792	0.00000	0.00000
A14	2	QD	66.1(29.7434	.09746	29.046426	-.58134	1.591447	.05814	.09134	97.543759	1.86447	0.00000	0.00000
	3	HC	57.8079	.18564	97.955299	-1.87406	3.648766	.09061	.17980	28.992169	.57739	0.00000	0.00000
A15	4	QF	59.4868	.18834	97.954846	1.87432	3.682794	-.05030	.18912	29.002981	-.58397	0.00000	0.00000
	5	HC	87.5513	.27653	29.039269	.58132	2.696855	-.01782	.27727	98.124526	-1.87783	0.00000	0.00000
A16	6	QD	89.2302	.28584	29.039652	-.58155	2.753629	.08582	.27996	98.125748	1.87712	0.00000	0.00000
	7	HC	117.2947	.37402	97.975178	-1.87480	5.587604	.11829	.36807	29.029470	.58414	0.00000	0.00000
A17	8	QF	118.9736	.37671	97.975915	1.87437	5.605704	-.09684	.37738	29.019685	-.57619	0.00000	0.00000
	9	MS1	133.6523	.40940	52.874714	1.19820	4.184170	-.09684	.43675	55.900645	-1.25310	0.00000	0.00000
	10	B	139.7737	.43067	39.931670	.91622	3.616204	-.08873	.45203	72.960881	-1.53379	0.00000	0.00000
	11	O	140.0531	.43179	39.423284	.90335	3.591419	-.08873	.45263	73.821547	-1.54662	0.00000	0.00000
	12	B	146.1745	.46022	30.089993	.62137	3.073141	-.08061	.46431	94.472861	-1.82689	0.00000	0.00000
	13	MS2	147.0381	.46487	29.051122	.58159	3.003528	-.08061	.46574	97.662508	-1.86654	0.00000	0.00000
A18	14	QD	148.7170	.47418	29.051319	-.58171	2.963658	.03286	.46845	97.655859	1.87042	0.00000	0.00000
	15	HC	176.7815	.56233	97.985879	-1.87461	4.311409	.06533	.55699	28.908159	.57843	0.00000	0.00000
A19	16	QF	178.4604	.56503	97.985299	1.87495	4.282285	-.09984	.56634	28.910335	-.57975	0.00000	0.00000
	17	HC	206.5249	.65320	29.042179	.58167	1.906000	-.06737	.65482	97.778468	-1.87302	0.00000	0.00000
A21	18	QD	208.2038	.66250	29.041535	-.58128	1.853185	.00412	.65752	97.785911	1.86866	0.00000	0.00000
	19	HC	236.2683	.75069	97.951095	-1.87415	2.394259	.03659	.74579	29.034822	.58028	0.00000	0.00000
A22	20	QF	237.9472	.75339	97.951198	1.87409	2.378595	-.05515	.75509	29.038446	-.58249	0.00000	0.00000
	21	HC	266.0117	.84158	29.043156	.58129	1.256542	-.02267	.84325	97.985377	-1.87309	0.00000	0.00000
A23	22	QD	267.6906	.85088	29.043880	-.58173	1.258610	.02515	.84595	97.979792	1.87535	0.00000	0.00000
	23	HC	295.7551	.93905	97.989614	-1.87499	2.390041	.05762	.93425	28.957659	.58227	0.00000	0.00000
A24	24	QF	297.4340	.94175	97.990046	1.87474	2.409453	-.03462	.94358	28.949850	-.57751	0.00000	0.00000
	25	HC	325.4985	1.02990	29.050703	.58175	1.863387	-.00215	1.03210	97.572277	-1.86651	0.00000	0.00000
A25	26	QD	327.1774	1.03920	29.050313	-.58151	1.919865	.06979	1.03481	97.571305	1.86707	0.00000	0.00000
	27	HC	355.2419	1.12737	97.969347	-1.87425	4.304003	.10226	1.12334	28.941806	.57756	0.00000	0.00000
A26	28	QF	356.9208	1.13007	97.968626	1.87467	4.336456	-.06381	1.13267	28.946971	-.58192	0.00000	0.00000
	29	HC	384.9853	1.21825	29.038940	.58147	2.971333	-.03134	1.22100	97.958619	-1.87589	0.00000	0.00000
A27	30	QD	386.6642	1.22756	29.038774	-.58137	3.014036	.08248	1.22370	97.954048	1.87273	0.00000	0.00000
	31	HC	414.7287	1.31575	97.959793	-1.87446	5.754267	.11495	1.31186	29.041740	.58233	0.00000	0.00000
A28	32	QF	416.4076	1.31845	97.960391	1.87411	5.761497	-.10638	1.32116	29.038829	-.58056	0.00000	0.00000
	33	HC	444.4721	1.40662	29.048205	.58141	3.201568	-.07391	1.40940	97.816896	-1.86900	0.00000	0.00000
A29	34	QD	446.1510	1.41592	29.048832	-.58179	3.179453	.04743	1.41211	97.808521	1.87388	0.00000	0.00000
	35	HC	474.2155	1.50408	97.993714	-1.87490	4.936015	.07990	1.50057	28.914088	.58019	0.00000	0.00000
A32	36	QF	475.8944	1.50677	97.993581	1.87497	4.911148	-.10936	1.50991	28.910664	-.57810	0.00000	0.00000
	37	HC	503.9589	1.59493	29.046727	.58178	2.267570	-.07689	1.59847	97.634081	-1.86951	0.00000	0.00000
A33	38	QD	505.6378	1.60424	29.045996	-.58134	2.210259	.00826	1.60117	97.639134	1.86657	0.00000	0.00000
	39	HC	533.7023	1.69242	97.954789	-1.87406	2.667542	.04073	1.68957	28.997474	.57650	0.00000	0.00000
A34	40	QF	535.3812	1.69511	97.954382	1.87430	2.843646	-.06904	1.69889	29.004864	-.58299	0.00000	0.00000
	41	HC	563.4457	1.78331	29.039575	.58131	1.331677	-.03657	1.78708	98.038343	-1.87567	0.00000	0.00000
A35	42	QD	565.1246	1.79261	29.039991	-.58157	1.312592	.01371	1.78978	98.037917	1.87592	0.00000	0.00000
	43	HC	593.1891	1.88079	97.976499	-1.87482	2.123011	.04618	1.87796	29.005376	.58307	0.00000	0.00000
A36	44	QF	594.8680	1.88349	97.977214	1.87440	2.131948	-.03559	1.88728	28.997749	-.57643	0.00000	0.00000
	45	HC	622.9325	1.97165	29.051274	.58161	1.558584	-.00312	1.97568	97.640600	-1.86632	0.00000	0.00000
A37	46	QD	624.6114	1.98095	29.051409	-.58169	1.603576	.05701	1.97839	97.634615	1.86961	0.00000	0.00000

	47	HC	652.6759	2.06910	97.984397	-1.87457	3.628972	.08948	2.06694	28.910642	.57819	0.00000	0.00000
A38	48	GF	654.3548	2.07180	97.983782	1.87493	3.661743	-.05065	2.07629	28.913766	-.58009	0.00000	0.00000
	49	HC	682.4193	2.15998	29.041705	.58165	2.665912	-.01818	2.16475	97.807534	-1.87359	0.00000	0.00000
A39	50	GD	684.0982	2.16928	29.041095	-.58128	2.721090	.08426	2.16745	97.815011	1.86524	0.00000	0.00000
	51	HC	712.1627	2.25747	97.951400	-1.87417	5.511295	.11673	2.25569	29.038786	.58062	0.00000	0.00000
A42	52	GF	713.8416	2.26017	97.951563	1.87407	5.529240	-.09547	2.26500	29.041488	-.58227	0.00000	0.00000
	53	HC	741.9061	2.34835	29.043681	.58129	3.275617	-.06300	2.35316	97.965544	-1.87250	0.00000	0.00000
A43	54	GD	743.5850	2.35766	29.044418	-.58174	3.274419	.06155	2.35586	97.959247	1.87617	0.00000	0.00000
	55	HC	771.6495	2.44582	97.990661	-1.87499	5.427474	.09403	2.44418	28.949493	.58201	0.00000	0.00000
A44	56	QF	773.3284	2.44852	97.991042	1.87477	5.410385	-.11427	2.45352	28.942051	-.57748	0.00000	0.00000
	57	HC	801.3929	2.53667	29.050426	.58176	2.628937	-.08180	2.54205	97.571693	-1.86680	0.00000	0.00000
A45	58	GD	803.0718	2.54598	29.049983	-.58149	2.574951	.01715	2.54476	97.571714	1.86678	0.00000	0.00000
	59	HC	831.1363	2.63414	97.967546	-1.87422	3.481823	.04962	2.63328	28.949582	.57759	0.00000	0.00000
A46	60	QF	832.8152	2.63684	97.966838	1.87463	3.453090	-.08367	2.64261	28.957130	-.58218	0.00000	0.00000
	61	HC	860.8797	2.72503	29.038811	.58145	1.530649	-.05119	2.73091	97.979290	-1.87608	0.00000	0.00000
A47	62	GD	862.5586	2.73433	29.038707	-.58139	1.493165	.00630	2.73361	97.984011	1.87333	0.00000	0.00000
	63	HC	890.6231	2.82252	97.961320	-1.87450	2.095656	.03878	2.82176	29.038747	.58255	0.00000	0.00000
A48	64	GFS	891.4377	2.82383	99.542135	-.05632	2.111349	-.00029	2.82628	28.551847	.01817	0.00000	0.00000
	65	D1	899.6292	2.83684	101.140996	-.13887	2.108934	-.00029	2.87097	30.605054	-.26882	0.00000	0.00000
	66	B	905.7506	2.84638	103.218748	-.20056	2.131974	.00782	2.90082	35.206904	-.48292	0.00000	0.00000
	67	O	906.0300	2.84681	103.331607	-.20337	2.134160	.00782	2.90208	35.479493	-.49270	0.00000	0.00000
	68	B	912.1514	2.85612	106.199089	-.26506	2.206893	.01594	2.92718	42.821564	-.70667	0.00000	0.00000
	69	O	912.4308	2.85653	106.347985	-.26788	2.211347	.01594	2.92821	43.219183	-.71645	0.00000	0.00000
	70	B	918.5522	2.86555	110.005180	-.32957	2.333772	.02406	2.94856	53.299452	-.93022	0.00000	0.00000
	71	OOO	918.9967	2.86619	110.300159	-.33405	2.344466	.02406	2.94988	54.133333	-.94578	0.00000	0.00000
A49	72	Q1	921.0978	2.86931	100.932680	4.64201	2.277310	-.08745	2.95565	64.156153	-3.98821	0.00000	0.00000
	73	D2	924.9169	2.87661	68.734502	3.78882	1.943343	-.08745	2.96330	98.471704	-4.99442	0.00000	0.00000
	74	G2	927.4417	2.88304	59.660897	-.02279	1.859945	.02059	2.96708	109.304249	.91361	0.00000	0.00000
B0	75	LS	954.0387	2.94918	72.736582	-.46883	2.407480	.02059	3.01534	72.579453	.46718	0.00000	0.00000
	76	LS	980.6357	2.99734	109.538627	-.91486	2.955016	.02059	3.08160	59.602246	.02074	0.00000	0.00000
	77	-Q2	983.1605	3.00111	98.679312	5.00576	2.793842	-.14671	3.08804	68.678404	-3.78783	0.00000	0.00000
B11	78	D2	986.9796	3.00874	64.295840	3.99727	2.233541	-.14671	3.09534	100.870081	-4.64129	0.00000	0.00000
	79	-Q1	989.0807	3.01450	54.238511	.94876	2.033311	-.04548	3.09846	110.241163	.33168	0.00000	0.00000
	80	D3	990.8714	3.01992	50.552944	.88603	1.951873	-.04548	3.10106	109.085568	.31365	0.00000	0.00000
	81	B	996.9928	3.04119	41.418293	.67158	1.698330	-.03736	3.11014	105.615844	.25315	0.00000	0.00000
	82	O	997.2722	3.04227	41.045749	.66179	1.687892	-.03736	3.11056	105.475170	.25033	0.00000	0.00000
	83	B	1003.3936	3.06837	34.256379	.44734	1.484041	-.02924	3.11993	102.781052	.18977	0.00000	0.00000
	84	O	1003.6730	3.06967	34.009139	.43755	1.475871	-.02924	3.12036	102.675798	.18695	0.00000	0.00000
	85	B	1009.7944	3.10038	29.965050	.22310	1.321712	-.02112	3.12994	100.758029	.12633	0.00000	0.00000
	86	O	1010.0738	3.10187	29.643115	.21331	1.315810	-.02112	3.13038	100.688224	.12351	0.00000	0.00000
	87	E	1016.1952	3.13550	28.544306	-.00114	1.211343	-.01301	3.14012	99.547332	.06286	0.00000	0.00000
	88	OOO	1016.6397	3.13798	28.552238	-.01671	1.205561	-.01301	3.14083	99.493443	.05838	0.00000	0.00000
B12	89	QDS	1017.4543	3.14249	29.036736	-.58105	1.204059	.00931	3.14214	97.910043	1.87560	0.00000	0.00000
	90	HC	1045.5187	3.23070	97.932173	-1.87387	1.891046	.04179	3.23052	28.933318	.58140	0.00000	0.00000
B13	91	QF	1047.1977	3.23340	97.932580	1.87363	1.900083	-.03108	3.23986	28.926951	-.57753	0.00000	0.00000
	92	HC	1075.2621	3.32159	29.043157	.58107	1.453471	.00139	3.32841	97.579543	-1.86757	0.00000	0.00000
B14	93	GD	1076.9411	3.33090	29.044601	-.58195	1.502736	.05761	3.33112	97.581624	1.86635	0.00000	0.00000
	94	HC	1105.0055	3.41905	98.009199	-1.87543	3.544976	.09008	3.41960	28.966942	.57775	0.00000	0.00000
B15	95	QF	1106.6845	3.42175	98.009860	1.87505	3.581425	-.04689	3.42893	28.974994	-.58265	0.00000	0.00000
	96	HC	1134.7489	3.50989	29.055021	.58199	2.691067	-.01442	3.51718	98.015975	-1.87628	0.00000	0.00000
B16	97	GD	1136.4279	3.51919	29.054088	-.58142	2.753434	.08911	3.51988	98.019007	1.87451	0.00000	0.00000
	98	HC	1164.4923	3.60735	97.960301	-1.87389	5.679798	.12158	3.60803	29.029999	.58293	0.00000	0.00000

B17	99	QF	1166.1713	3.61005	97.958950	1.87467	5.700422	-.09714	3.61734	29.024363	-.57950	0.00000	0.00000
	100	MS1	1180.8499	3.64275	52.853112	1.19821	4.274480	-.09714	3.67668	55.953388	-1.25507	0.00000	0.00000
	101	B	1186.9713	3.66402	39.910617	.91611	3.704676	-.08903	3.69194	73.039366	-1.53603	0.00000	0.00000
	102	B	1187.2507	3.66514	39.402291	.90324	3.679802	-.08903	3.69255	73.901288	-1.54688	0.00000	0.00000
	103	B	1193.3721	3.69360	30.071078	.62114	3.159690	-.08091	3.70421	94.581839	-1.82941	0.00000	0.00000
	104	MS2	1194.2357	3.69825	29.032617	.58134	3.089817	-.08091	3.70564	97.775880	-1.86910	0.00000	0.00000
B18	105	GD	1195.9147	3.70756	29.032520	-.58128	3.052222	.03588	3.70834	97.770474	1.87225	0.00000	0.00000
	106	HC	1223.5791	3.79576	97.953263	-1.87454	4.484853	.06836	3.79679	28.932421	.57981	0.00000	0.00000
B19	107	GF	1225.6581	3.79846	97.954554	1.87379	4.455216	-.10347	3.80613	28.931402	-.57919	0.00000	0.00000
	108	HC	1253.7225	3.88663	29.052880	.58135	1.976982	-.07100	3.89460	97.723603	-1.87088	0.00000	0.00000
B21	109	GD	1255.4015	3.89593	29.053974	-.58202	1.920292	.00311	3.89731	97.727455	1.86864	0.00000	0.00000
	110	HC	1283.4659	3.98407	98.012609	-1.87516	2.433107	.03558	3.98566	28.999291	.57951	0.00000	0.00000
B22	111	GF	1285.1449	3.98676	98.012127	1.87544	2.414531	-.05759	3.99498	29.003355	-.58198	0.00000	0.00000
	112	HC	1313.2093	4.07491	29.046375	.58199	1.223880	-.02512	4.08321	97.950231	-1.87359	0.00000	0.00000
B23	113	GD	1314.8883	4.08422	29.044909	-.58110	1.220747	.02137	4.08591	97.948560	1.87457	0.00000	0.00000
	114	HC	1342.9527	4.17241	97.934339	-1.87361	2.245946	.05384	4.17418	28.984254	.58199	0.00000	0.00000
B24	115	GF	1344.6317	4.17511	97.933736	1.87396	2.263671	-.03284	4.18350	28.979010	-.57880	0.00000	0.00000
	116	HC	1372.6961	4.26332	29.035409	.58107	1.767730	-.00036	4.27192	97.677049	-1.86792	0.00000	0.00000
B25	117	GD	1374.3751	4.27262	29.036410	-.58167	1.824152	.06794	4.27462	97.674051	1.86967	0.00000	0.00000
	118	HC	1402.4395	4.36080	97.986856	-1.87521	4.156288	.10041	4.36311	28.938974	.57873	0.00000	0.00000
B26	119	GF	1404.1185	4.36350	97.988198	1.87443	4.190379	-.06001	4.37245	28.942019	-.58058	0.00000	0.00000
	120	HC	1432.1829	4.45164	29.057586	.58175	2.931722	-.02754	4.46084	97.842736	-1.87336	0.00000	0.00000
B27	121	GD	1433.8619	4.46094	29.057621	-.58177	2.979585	.08486	4.46354	97.847166	1.87077	0.00000	0.00000
	122	HC	1461.9263	4.54909	97.990069	-1.87447	5.786759	.11733	4.55180	29.019042	.58094	0.00000	0.00000
B28	123	GF	1463.6053	4.55178	97.988753	1.87524	5.796914	-.10530	4.56111	29.019487	-.58121	0.00000	0.00000
	124	HC	1491.6697	4.63996	29.036857	.58170	3.267298	-.07283	4.64936	97.877976	-1.87122	0.00000	0.00000
B29	125	GD	1493.3487	4.64927	29.035805	-.58106	3.249138	.05108	4.65206	97.873066	1.87409	0.00000	0.00000
	126	HC	1521.4131	4.73748	97.932959	-1.87393	5.108276	.08355	4.74042	28.949347	.58103	0.00000	0.00000
B32	127	GF	1523.0921	4.74018	97.933498	1.87361	5.083983	-.11234	4.74976	28.945226	-.57852	0.00000	0.00000
	126	HC	1551.1565	4.82837	29.044306	.58109	2.356842	-.07987	4.83824	97.661682	-1.86885	0.00000	0.00000
B33	129	GD	1552.8355	4.83767	29.045773	-.58198	2.297359	.00863	4.84094	97.662757	1.86822	0.00000	0.00000
	130	HC	1580.8999	4.92583	98.011366	-1.87544	2.965199	.04110	4.92938	28.969368	.57869	0.00000	0.00000
B34	131	GF	1582.5789	4.92852	98.011912	1.87512	2.938811	-.07237	4.93871	28.974403	-.58175	0.00000	0.00000
	132	HC	1610.6433	5.01656	29.054389	.58201	1.333393	-.03990	5.02700	97.937060	-1.87439	0.00000	0.00000
B35	133	GD	1612.3223	5.02596	29.053344	-.58138	1.308713	.01034	5.02970	97.938881	1.87333	0.00000	0.00000
	134	HC	1640.3867	5.11413	97.956418	-1.87382	2.024530	.04281	5.11793	29.010311	.58196	0.00000	0.00000
B36	135	GF	1642.0657	5.11683	97.955099	1.87459	2.031012	-.03513	5.12724	29.006763	-.57980	0.00000	0.00000
	136	HC	1670.1301	5.20503	29.032529	.58130	1.470609	-.00266	5.21557	97.757885	-1.86881	0.00000	0.00000
B37	137	GD	1671.8091	5.21434	29.032556	-.58132	1.513546	.05408	5.21827	97.752650	1.87185	0.00000	0.00000
	138	HC	1699.8735	5.30254	97.956542	-1.87462	3.456910	.08655	5.30673	28.931492	.57960	0.00000	0.00000
B38	139	GF	1701.5525	5.30524	97.957881	1.87384	3.490319	-.04697	5.31607	28.931114	-.57937	0.00000	0.00000
	140	HC	1729.6169	5.39340	29.053688	.58139	2.597728	-.01450	5.40454	97.739619	-1.87129	0.00000	0.00000
B39	141	GD	1731.2959	5.40270	29.054695	-.58201	2.656948	.08542	5.40724	97.743970	1.86887	0.00000	0.00000
	142	HC	1759.3603	5.49084	98.011313	-1.87510	5.479779	.11789	5.49558	29.003743	.57971	0.00000	0.00000
B42	143	GF	1761.0393	5.49354	98.010718	1.87544	5.500661	-.09315	5.50489	29.007393	-.58193	0.00000	0.00000
	144	HC	1789.1037	5.58169	29.045308	.58197	3.312078	-.06068	5.59312	97.944939	-1.87331	0.00000	0.00000
B43	145	GD	1790.7827	5.59099	29.043842	-.58108	3.315984	.06536	5.59582	97.942666	1.87464	0.00000	0.00000
	146	HC	1818.8471	5.67919	97.932912	-1.87362	5.575725	.09783	5.68410	28.978804	.58191	0.00000	0.00000
B44	147	GF	1820.5261	5.68189	97.932422	1.87390	5.560216	-.11620	5.69343	28.973498	-.57868	0.00000	0.00000
	148	HC	1848.5905	5.77009	29.036126	.58105	2.724668	-.08373	5.78186	97.668433	-1.86792	0.00000	0.00000
B45	149	GD	1850.2695	5.77940	29.037214	-.58172	2.670500	.01886	5.78457	97.666000	1.86934	0.00000	0.00000

	150	HC	1878.3339	5.86758	97.990191	-1.87526	3.625346	.05133	5.87305	28.942367	.57864	0.00000	0.00000
B46	151	QF	1880.0129	5.87027	97.991484	1.87450	3.594870	-.08744	5.88238	28.945896	-.58079	0.00000	0.00000
	152	HC	1908.0773	5.95842	29.057629	.58179	1.566516	-.05497	5.97076	97.860401	-1.87363	0.00000	0.00000
B47	153	QD	1909.7563	5.96772	29.057539	-.58173	1.523785	.00379	5.97346	97.854623	1.87117	0.00000	0.00000
	154	HC	1937.8207	6.05586	97.986730	-1.87439	2.055841	.03627	6.06171	29.019631	.58114	0.00000	0.00000
B48	155	QFS	1938.6353	6.05717	99.566977	-.05573	2.069795	-.00205	6.06623	28.534754	.01709	0.00000	0.00000
	156	Q1	1946.8266	6.07017	101.156035	-.13826	2.053011	-.00205	6.11093	30.606978	-.27006	0.00000	0.00000
	157	B	1952.9482	6.07971	103.226183	-.19993	2.065314	.00607	6.14078	35.224760	-.48428	0.00000	0.00000
	158	O	1953.2276	6.08014	103.338690	-.20274	2.067010	.00607	6.14203	35.498111	-.49407	0.00000	0.00000
	159	P	1959.3490	6.08945	106.198311	-.26441	2.129005	.01419	6.16712	42.957649	-.70815	0.00000	0.00000
	160	O	1959.6284	6.08987	106.346852	-.26723	2.132969	.01419	6.16815	43.258101	-.71794	0.00000	0.00000
	161	B	1965.7498	6.09888	109.995946	-.32890	2.244657	.02230	6.18848	53.355367	-.93183	0.00000	0.00000
	162	OOO	1966.1943	6.09952	110.290328	-.33358	2.254571	.02230	6.18980	54.190685	-.94740	0.00000	0.00000
	163	Q1	1968.2954	6.10264	100.921150	4.64211	2.188272	-.08488	6.19556	64.236829	-3.99314	0.00000	0.00000
B49	164	D2	1972.1145	6.10994	68.722659	3.78880	1.864092	-.08488	6.20320	98.584767	-5.00059	0.00000	0.00000
	165	Q2	1974.6393	6.11637	59.647637	-.02218	1.781501	.01867	6.20698	109.431848	.91430	0.00000	0.00000
C0	166	LS	2001.2363	6.18255	72.692920	-.46830	2.278063	.01867	6.25518	72.664660	.46808	0.00000	0.00000
	167	LS	2027.8333	6.23073	109.469180	-.91442	2.774626	.01867	6.32138	59.633675	.02186	0.00000	0.00000
	168	-Q2	2030.3581	6.23451	98.617469	5.00245	2.621666	-.13837	6.32781	68.708359	-3.78834	0.00000	0.00000
C11	169	D2	2034.1772	6.24215	64.256769	3.99462	2.093229	-.13837	6.33512	100.903295	-4.64164	0.00000	0.00000
	170	-Q1	2036.2783	6.24791	54.206532	.94793	1.903713	-.04354	6.33823	110.272334	.33297	0.00000	0.00000
	171	D3	2038.0690	6.25333	50.923912	.88521	1.825749	-.04354	6.34083	109.112146	.31493	0.00000	0.00000
	172	B	2044.1904	6.27462	41.398932	.67082	1.584080	-.03542	6.34991	105.626958	.25440	0.00000	0.00000
	173	O	2044.4698	6.27570	41.026814	.66103	1.574184	-.03542	6.35033	105.485587	.25158	0.00000	0.00000
	174	B	2050.5912	6.30180	34.246456	.44663	1.382207	-.02730	6.35970	102.776391	.19098	0.00000	0.00000
	175	O	2050.8706	6.30311	33.999613	.43684	1.374579	-.02730	6.36013	102.670457	.18816	0.00000	0.00000
	176	B	2056.9920	6.33382	29.963878	.22245	1.232294	-.01919	6.36971	100.738000	.12751	0.00000	0.00000
	177	O	2057.2714	6.33531	29.842310	.21266	1.226934	-.01919	6.37016	100.567533	.12470	0.00000	0.00000
	178	B	2063.3928	6.36893	28.551198	-.00174	1.134342	-.01107	6.37990	99.512346	.06401	0.00000	0.00000
	179	OOO	2063.8373	6.37141	28.559665	-.01731	1.129422	-.01107	6.38061	99.457434	.05953	0.00000	0.00000
C12	180	QDS	2064.6519	6.37592	29.045256	-.58180	1.128929	.00985	6.38192	97.872724	1.87605	0.00000	0.00000
	181	HC	2092.7164	6.46408	97.995770	-1.87598	1.831028	.04232	6.47037	28.898234	.58067	0.00000	0.00000
C13	182	QF	2094.3953	6.46678	97.996127	1.87488	1.842876	-.02829	6.47972	28.891523	-.57679	0.00000	0.00000
	183	HC	2122.4598	6.55495	29.050892	.58182	1.474607	.00418	6.56836	97.523943	-1.86759	0.00000	0.00000
C14	184	QD	2124.1387	6.56423	29.050277	-.58145	1.529290	.06130	6.57107	97.529660	1.86426	0.00000	0.00000
	185	HC	2152.2032	6.65240	97.963471	-1.87411	3.675323	.09378	6.65955	28.988788	.57722	0.00000	0.00000
C15	186	QF	2153.8821	6.65510	97.962659	1.87458	3.713754	-.04824	6.66887	28.999974	-.58403	0.00000	0.00000
	187	HC	2181.9466	6.74329	29.037462	.58140	2.785505	-.01577	6.75702	98.130210	-1.87808	0.00000	0.00000
C16	188	QD	2183.6255	6.75260	29.037451	-.58139	2.848628	.09137	6.75971	98.131910	1.87709	0.00000	0.00000
	189	HC	2211.6900	6.84079	97.962038	-1.87457	5.838296	.12384	6.84780	29.033993	.56423	0.00000	0.00000
C17	190	QF	2213.3689	6.84349	97.962842	1.87410	5.857607	-.10096	6.85711	29.024202	-.57827	0.00000	0.00000
	191	MS1	2228.0476	6.87618	52.868718	1.19799	4.375715	-.10096	6.91647	55.906635	-1.25313	0.00000	0.00000
	192	B	2234.1690	6.89745	39.928080	.91603	3.782579	-.09284	6.93175	72.966976	-1.53378	0.00000	0.00000
	193	O	2234.4484	6.89857	39.419796	.90317	3.756640	-.09284	6.93236	73.827641	-1.54662	0.00000	0.00000
	194	B	2240.5698	6.92701	30.088577	.62121	3.213195	-.08472	6.94403	94.478747	-1.82686	0.00000	0.00000
	195	MS2	2241.4334	6.93166	29.049972	.58143	3.140031	-.08472	6.94546	97.668341	-1.86651	0.00000	0.00000
C18	196	QD	2243.1123	6.94096	29.050616	-.58163	3.097568	.03389	6.94817	97.661210	1.87066	0.00000	0.00000
	197	HC	2271.1768	7.02911	97.996488	-1.87490	4.474254	.06636	7.03672	28.905073	.57848	0.00000	0.00000
C19	198	QF	2272.8557	7.03181	97.996172	1.87508	4.441644	-.10500	7.04607	28.906885	-.57958	0.00000	0.00000
	199	HC	2300.9202	7.11997	29.045630	.58181	1.920482	-.07253	7.13456	97.764496	-1.87262	0.00000	0.00000
C21	200	QD	2302.5991	7.12927	29.044742	-.58127	1.859374	-.00065	7.13726	97.772154	1.86835	0.00000	0.00000
	201	HC	2330.6636	7.21745	97.949075	-1.87397	2.266602	.03182	7.22553	29.034753	.58012	0.00000	0.00000

C22	202	0F	2332.3425	7.22015	97.948735	1.87417	2.247092	-.05493	7.23484	29.038907	-.58265	0.00000	0.00000
	203	HC	2360.4070	7.30835	29.039376	.58125	1.130980	-.02246	7.32299	97.999676	-1.87342	0.00000	0.00000
C23	204	QD	2362.0859	7.31765	29.040000	-.58163	1.129355	.02052	7.32569	97.994265	1.87658	0.00000	0.00000
	205	HC	2390.1504	7.40583	97.981895	-1.87495	2.130746	.05299	7.41397	28.950873	.58244	0.00000	0.00000
C24	206	0F	2391.8293	7.40853	97.982697	1.87448	2.150740	-.02930	7.42331	28.952659	-.57745	0.00000	0.00000
	207	HC	2419.8938	7.49668	29.052656	.58167	1.754041	.00317	7.51182	97.555780	-1.86624	0.00000	0.00000
C25	208	GD	2421.5727	7.50598	29.052651	-.58167	1.816022	.07106	7.51453	97.564348	1.86708	0.00000	0.00000
	209	HC	2449.6372	7.59414	97.982402	-1.87448	4.235757	.10353	7.60307	28.937292	.57747	0.00000	0.00000
C26	210	0F	2451.3161	7.59684	97.981596	1.87495	4.272496	-.06000	7.61241	28.944497	-.58185	0.00000	0.00000
	211	HC	2479.3806	7.68501	29.039930	.58162	3.014281	-.02753	7.70074	97.953715	-1.87595	0.00000	0.00000
C27	212	QD	2481.0595	7.69432	29.039313	-.58125	3.064834	.08807	7.70344	97.959638	1.87250	0.00000	0.00000
	213	HC	2509.1240	7.78251	97.948857	-1.87418	5.961999	.12054	7.79160	29.045037	.58229	0.00000	0.00000
C28	214	GF	2510.8029	7.78521	97.949207	1.87397	5.971887	-.10883	7.80091	29.042466	-.58073	0.00000	0.00000
	215	HC	2538.8674	7.87339	29.044838	.58127	3.343362	-.07635	7.88913	97.830500	-1.86919	0.00000	0.00000
C29	216	QD	2540.5463	7.88270	29.045725	-.58181	3.321676	.05038	7.89184	97.821882	1.87421	0.00000	0.00000
	217	HC	2568.6108	7.97086	97.996292	-1.87508	5.161208	.08285	7.98029	28.913886	.58034	0.00000	0.00000
C32	218	0F	2570.2897	7.97356	97.996598	1.87490	5.134062	-.11502	7.98964	28.909935	-.57794	0.00000	0.00000
	219	HC	2598.3542	8.06171	29.050550	.58183	2.331752	-.08255	8.07820	97.619514	-1.86919	0.00000	0.00000
C33	220	GD	2600.0331	8.07101	29.049899	-.58143	2.266914	.00490	8.08090	97.624423	1.86633	0.00000	0.00000
	221	HC	2628.0976	8.15918	97.962044	-1.87409	2.829948	.03737	8.16932	28.994486	.57832	0.00000	0.00000
C34	222	0F	2629.7765	8.16188	97.961257	1.87455	2.801675	-.07087	8.17864	29.002292	-.58307	0.00000	0.00000
	223	HC	2657.8410	8.25007	29.037478	.58139	1.238373	-.03840	8.26683	98.045725	-1.87595	0.00000	0.00000
C35	224	GD	2659.5199	8.25937	29.037521	-.58141	1.213174	.00822	8.26952	98.045749	1.87593	0.00000	0.00000
	225	HC	2687.5844	8.34756	97.963556	-1.87460	1.869414	.04069	8.35770	29.005888	.58317	0.00000	0.00000
C36	226	0F	2689.2633	8.35026	97.964375	1.87412	1.877322	-.03132	8.36701	29.002190	-.57849	0.00000	0.00000
	227	HC	2717.3278	8.43843	29.050448	.58146	1.423909	.00115	8.45541	97.544632	-1.86624	0.00000	0.00000
C37	228	GD	2719.0067	8.44773	29.051037	-.58182	1.471808	.05621	8.45811	97.638145	1.87003	0.00000	0.00000
	229	HC	2747.0712	8.53588	97.995643	-1.87486	3.474968	.08868	8.54667	28.907169	.57822	0.00000	0.00000
C38	230	GF	2748.7501	8.53858	97.995260	1.87508	3.511339	-.04559	8.55602	28.909980	-.57993	0.00000	0.00000
	231	HC	2776.8146	8.62674	29.044984	.58180	2.657465	-.01312	8.64449	97.794428	-1.87342	0.00000	0.00000
C39	232	GD	2778.4935	8.63604	29.044099	-.58126	2.720954	.08915	8.64719	97.802176	1.86891	0.00000	0.00000
	233	HC	2806.5580	8.72423	97.948273	-1.87398	5.648537	.12162	8.73544	29.039281	.58048	0.00000	0.00000
C42	234	0F	2808.2369	8.72693	97.948002	1.87414	5.670231	-.09592	8.74475	29.042505	-.58244	0.00000	0.00000
	235	HC	2836.3014	8.81512	29.039823	.58124	3.403911	-.06345	8.83250	97.980401	-1.87282	0.00000	0.00000
C43	236	QD	2837.9803	8.82443	29.040499	-.58165	3.406080	.06605	8.83560	97.974216	1.87642	0.00000	0.00000
	237	HC	2866.0448	8.91260	97.983887	-1.87498	5.685168	.09852	8.92391	28.952275	.58219	0.00000	0.00000
C44	238	0F	2867.7237	8.91530	97.984658	1.87453	5.667311	-.11967	8.93324	28.944397	-.57740	0.00000	0.00000
	239	HC	2895.7882	9.00345	29.052663	.58170	2.734313	-.08723	9.02177	97.553531	-1.86651	0.00000	0.00000
C45	240	QD	2897.4671	9.01276	29.052562	-.58165	2.674563	.01565	9.02448	97.563119	1.86675	0.00000	0.00000
	241	HC	2925.5316	9.10091	97.980359	-1.87443	3.539275	.04812	9.11301	28.945112	.57748	0.00000	0.00000
C46	242	0F	2927.2105	9.10361	97.979528	1.87491	3.506212	-.08729	9.12235	28.952764	-.58213	0.00000	0.00000
	243	HC	2955.2750	9.19179	29.039473	.58160	1.481970	-.05482	9.21065	97.376222	-1.87617	0.00000	0.00000
C47	244	GD	2956.9539	9.20109	29.038913	-.58126	1.436759	.00068	9.21335	97.981452	1.87313	0.00000	0.00000
	245	HC	2985.0184	9.28929	97.949787	-1.87421	1.881369	.03315	9.30151	29.042405	.58253	0.00000	0.00000
C48	246	0H1	2985.6661	9.29033	99.448699	-.43262	1.893826	.00529	9.30509	28.580721	.13254	0.00000	0.00000
	247	DH1	2993.6020	9.30288	107.278369	-.52974	1.936831	.00529	9.35087	28.780754	-.15713	0.00000	0.00000
	248	B	2999.9234	9.31169	114.211116	-.60281	1.994033	.01340	9.38317	32.036558	-.37473	0.00000	0.00000
	249	0	3000.2028	9.31207	114.548900	-.60615	1.997778	.01340	9.38456	32.248736	-.38468	0.00000	0.00000
	250	E	3006.3242	9.32031	122.417086	-.67922	2.104672	.02152	9.41242	38.289854	-.60218	0.00000	0.00000
	251	0	3006.6036	9.32067	122.797567	-.68256	2.110665	.02152	9.41358	38.629129	-.61212	0.00000	0.00000
	252	B	3012.7250	9.32833	131.601192	-.75563	2.267272	.02964	9.43641	47.453897	-.82946	0.00000	0.00000
	253	000	3013.1695	9.32887	132.275306	-.76094	2.280446	.02964	9.43789	48.198313	-.84527	0.00000	0.00000

	POS		S	PSIX	BETAX	ALPHAX	XEQ	DXEQ	PSIY	BETAY	ALPHAY	YEQ	DYEQ
	254	QH2	3015.4603	9.33149	152.558575	-8.44322	2.487329	.15278	9.44545	46.415008	1.59247	0.00000	0.00000
C49	255	DH2	3019.3122	9.33480	224.633856	-10.26840	3.075807	.15278	9.46062	35.277229	1.29903	0.00000	0.00000
	256	QH3	3021.8370	9.33648	243.426535	3.18886	3.231709	-.03078	9.47253	33.947424	-.74709	0.00000	0.00000
D0	257	LSD	3048.4340	9.36292	106.254923	1.96855	2.413107	-.03078	9.54558	106.156863	-1.96786	0.00000	0.00000
	258	LSD	3075.0310	9.43588	33.996956	.74823	1.594506	-.03078	9.57204	243.303822	-3.18863	0.00000	0.00000
	259	-QH3	3077.5558	9.44777	35.327881	-1.30063	1.632045	.06087	9.57372	224.527121	10.26214	0.00000	0.00000
D11	260	DH2	3081.4077	9.46292	46.478128	-1.59411	1.866521	.06087	9.57703	152.494901	8.43830	0.00000	0.00000
	261	-QH2	3083.6985	9.47047	48.261137	.84703	1.892785	-.03817	9.57965	132.226208	.75924	0.00000	0.00000
	262	DH3	3085.4336	9.47637	45.428916	.78528	1.826553	-.03817	9.58176	129.627374	.73856	0.00000	0.00000
	263	B	3091.5550	9.50017	37.148434	.56744	1.617737	-.03005	9.58954	121.023874	.66688	0.00000	0.00000
	264	O	3091.8344	9.50137	36.834125	.55750	1.609340	-.03005	9.58991	120.552156	.66354	0.00000	0.00000
	265	B	3097.9558	9.53020	31.342293	.33966	1.450216	-.02194	9.59826	112.968195	.59168	0.00000	0.00000
	266	O	3098.2352	9.53163	31.155268	.32972	1.444087	-.02194	9.59865	112.636498	.58834	0.00000	0.00000
	267	B	3104.3566	9.56458	28.452086	.11188	1.334656	-.01382	9.60758	105.976195	.51632	0.00000	0.00000
	268	O	3104.6360	9.56615	28.392345	.10194	1.330795	-.01382	9.60800	105.588609	.51298	0.00000	0.00000
	269	B	3110.7574	9.60068	28.477814	-.11590	1.271056	-.00570	9.61750	99.749829	.44982	0.00000	0.00000
	270	COO	3111.2019	9.60316	28.587881	-.13172	1.268522	-.00570	9.61821	99.360305	.43550	0.00000	0.00000
D12	271	-QH1	3111.8496	9.60674	29.048557	-.58179	1.270888	.01701	9.61925	97.858543	1.87572	0.00000	0.00000
	272	HC	3139.9140	9.69490	97.994307	-1.87492	2.061656	.04548	9.70771	28.897875	.58071	0.00000	0.00000
D13	273	GF	3141.5930	9.69760	97.994218	1.87497	2.071389	-.03395	9.71707	28.891693	-.57635	0.00000	0.00000

R=1000.00010 TGAM=(18.73603, 0.00000) THETA= 6.28318501 QX= 19.39519 QY= 19.43413

MAXIMA BETAX(256)= 243.42654 XEQ=(214)= 5.97189 BETAY(258)= 243.30382 YEQ(273)= 0.00000
MINIMA BETAX(268)= 28.39235 XEQ=(180)= 1.12893 BETAY(155)= 28.53475 YEQ(273)= 0.00000
CONTRIBUTIONS TO CHROMATICITY (DNU/(DP/P)) FROM MAGNETS EXPLICITLY IN RING CHRX = -22.5125, CHRY = -22.4846

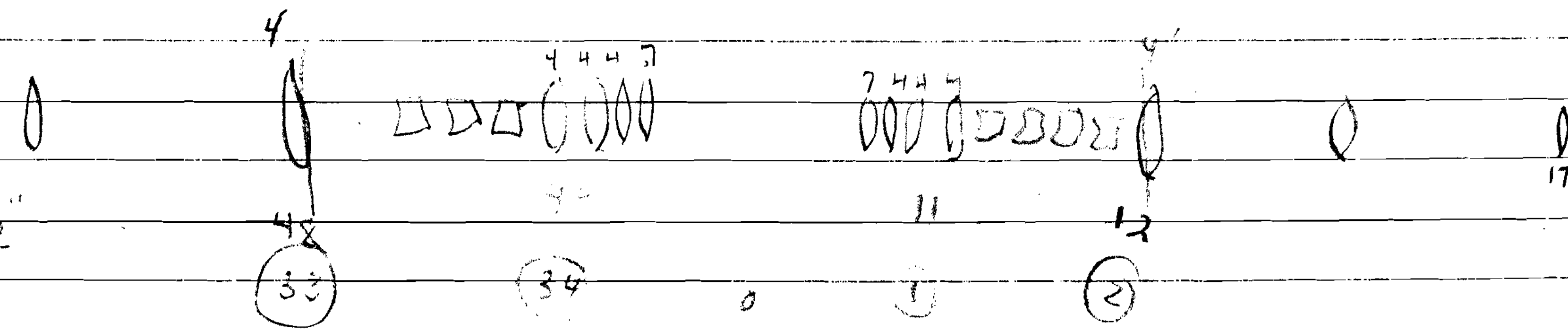

129
6
774

210" stations

11 - 19   21 - 29   32 - 39   42 - 49

Sect. has A0 to B0 : 2 pre-straights = 7 dipole , 3 ...
1 medium st.   2   1
30 normal cells = 120 / 129   30 / 34

-A12-

ΔΔΔ 18

62 9/16 iron length (Quad)

Regular Cell

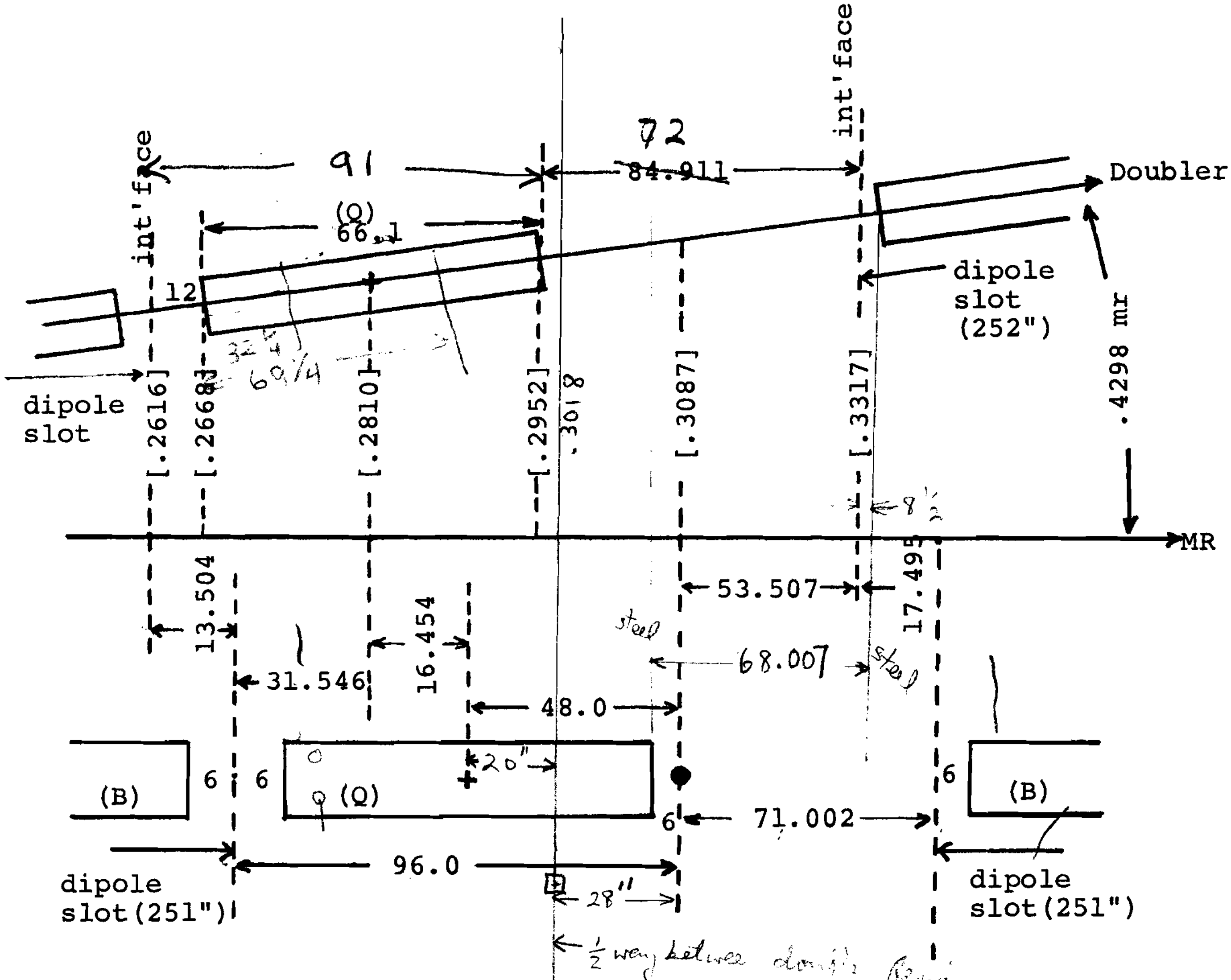

Interface to interface = 163.011" (on MR axis)

97.583'

2.1178105 mr/dipole

32.471242 mr/cell

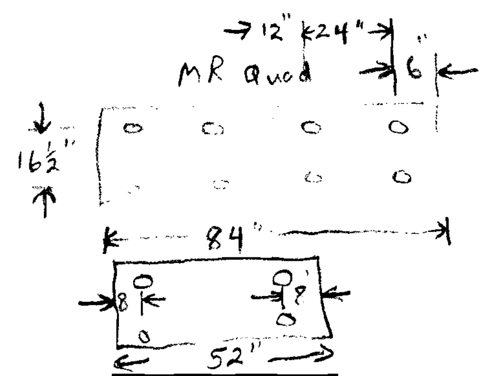

<u>Medium Straight</u> (upstream)

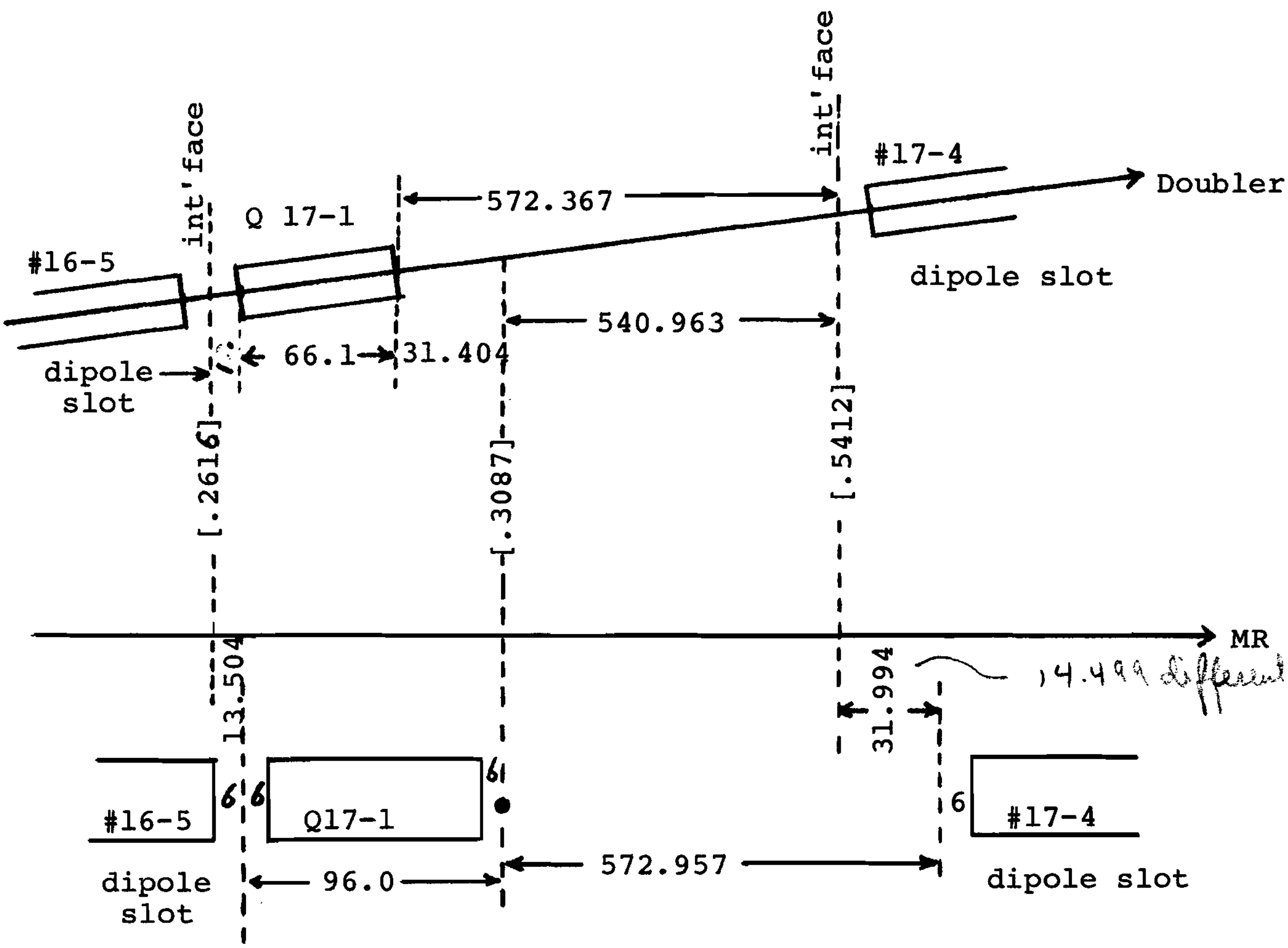

Medium Straight (downstream)

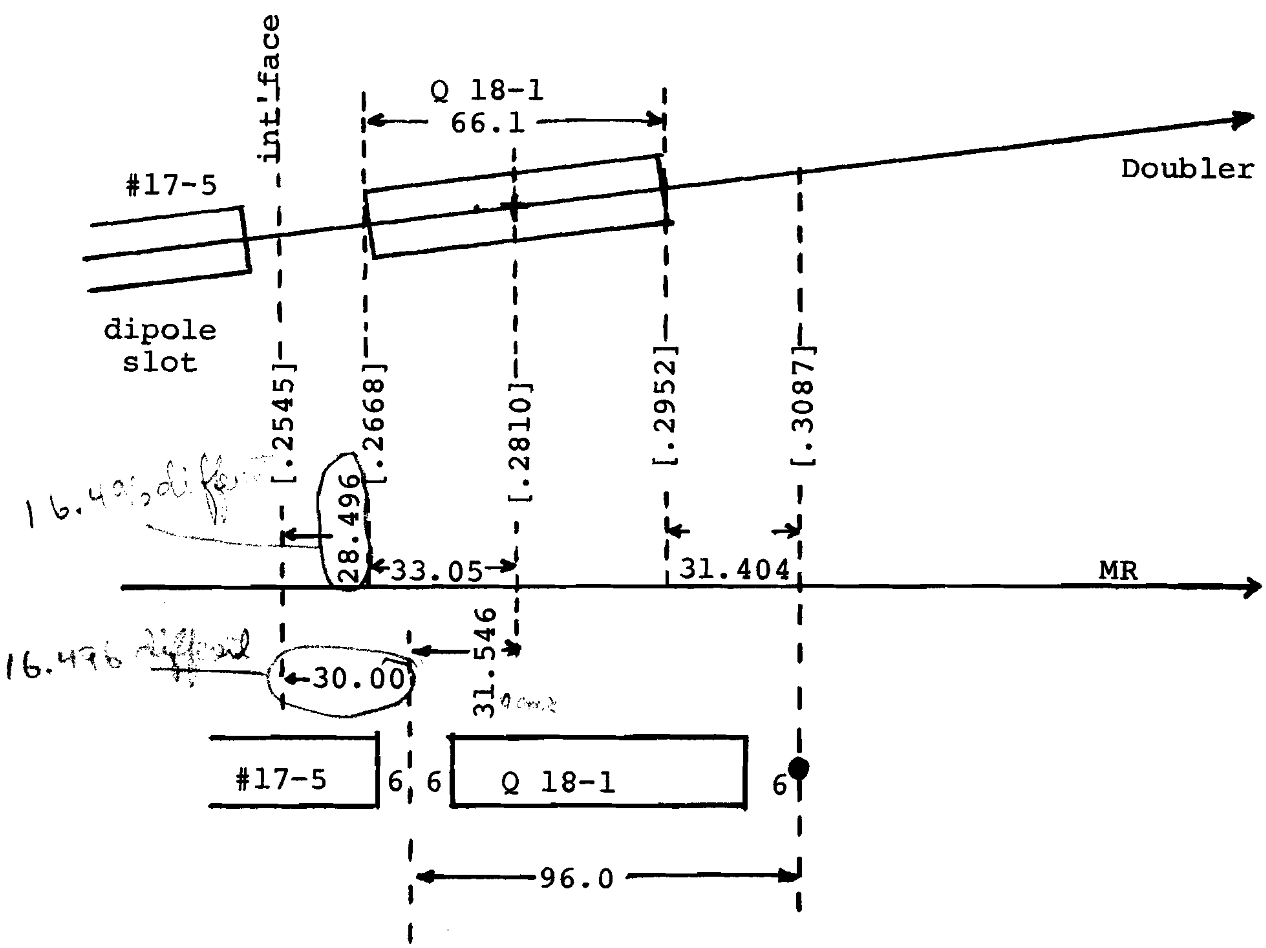

$$S = a + b + c$$

$$S - L \cong \left(a + b + \frac{c}{3}\right)\frac{\theta^2}{8}$$

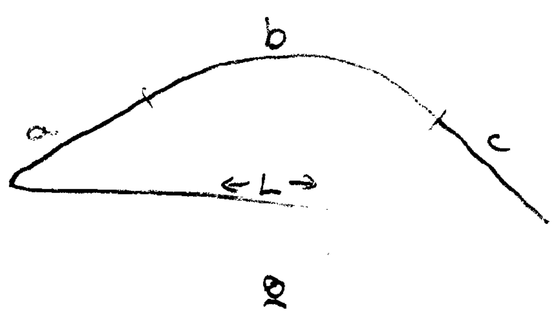

<u>Long Straight</u>, upstream of BØ, CØ, EØ and FØ

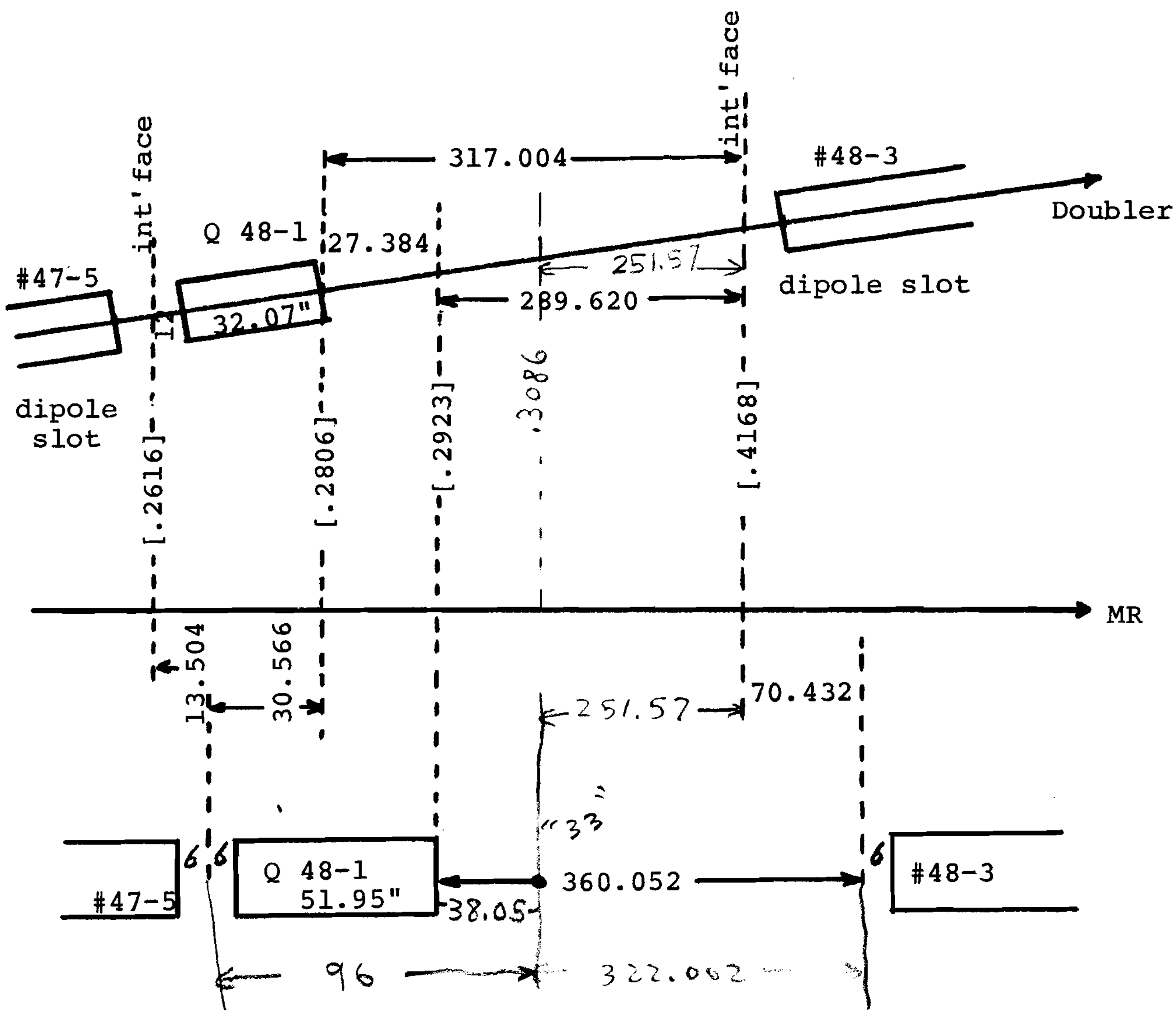

48

NB: Arc [illegible] from S48 to S49 = 1233.614 / 1233.627 } depending on whether M48-5 to S49 = { 158.612 / 158.625 }

Formula on p. A15 ⇒ need 152.616 [illegible] chord = 1233.564 (all agree on that)

Long Straight, BØ, CØ, EØ and FØ

(1428.155)
1428.148 sho

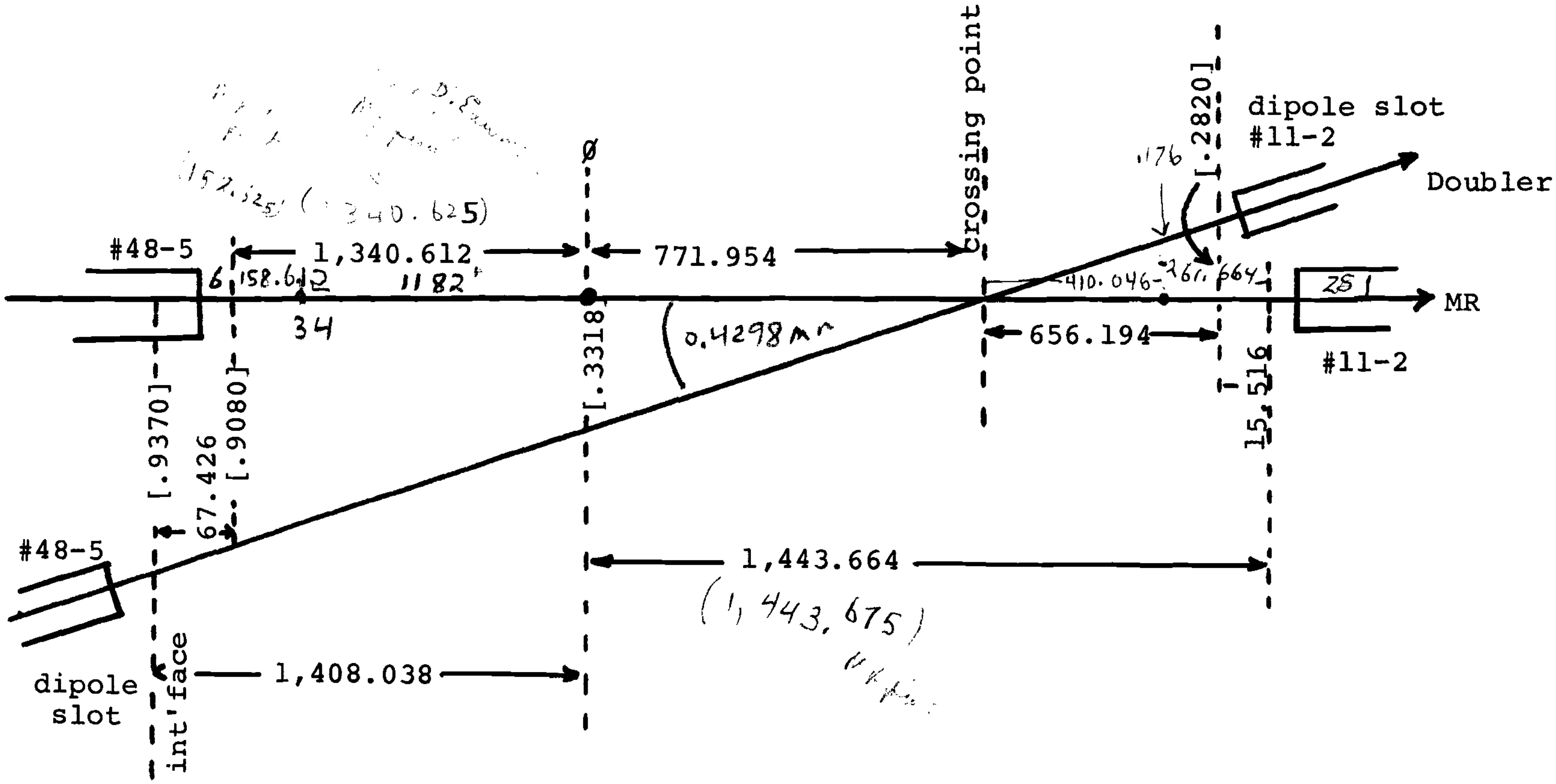

Long Straight, downstream of BØ, CØ, EØ and FØ

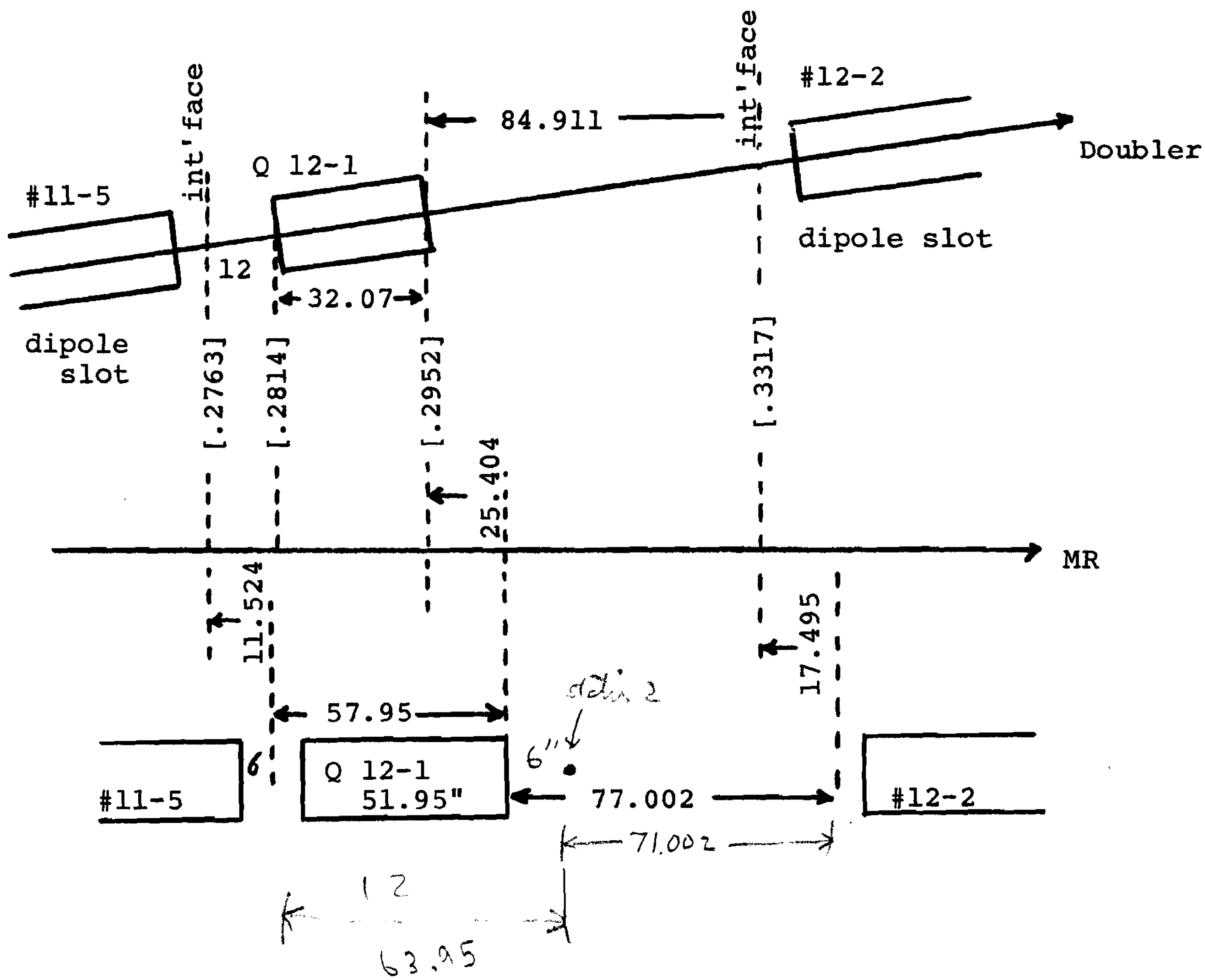

Long Straight, upstream of AØ and DØ

(High-Beta Insertion)

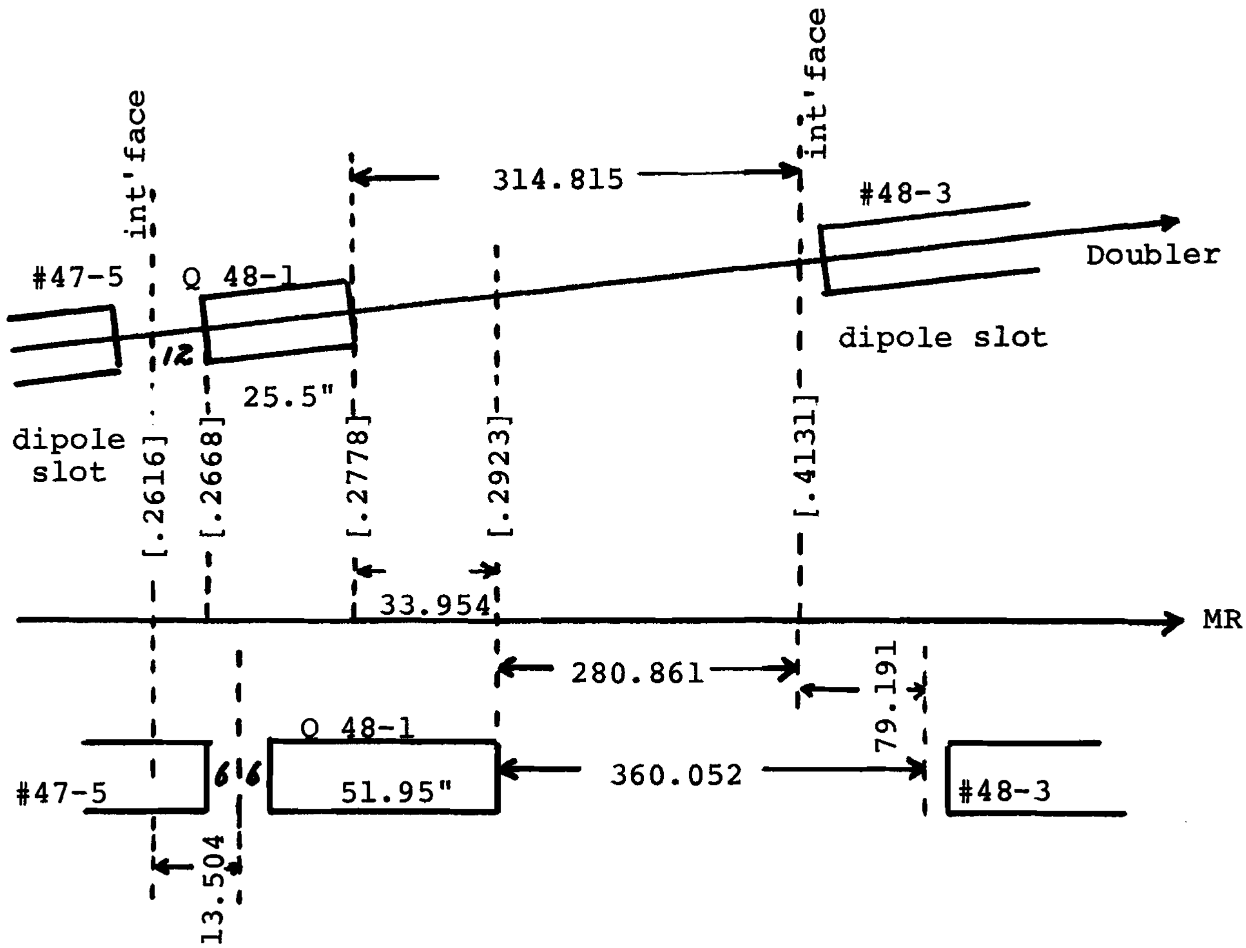

Long Straight, AØ and DØ (High-Beta Insertion)

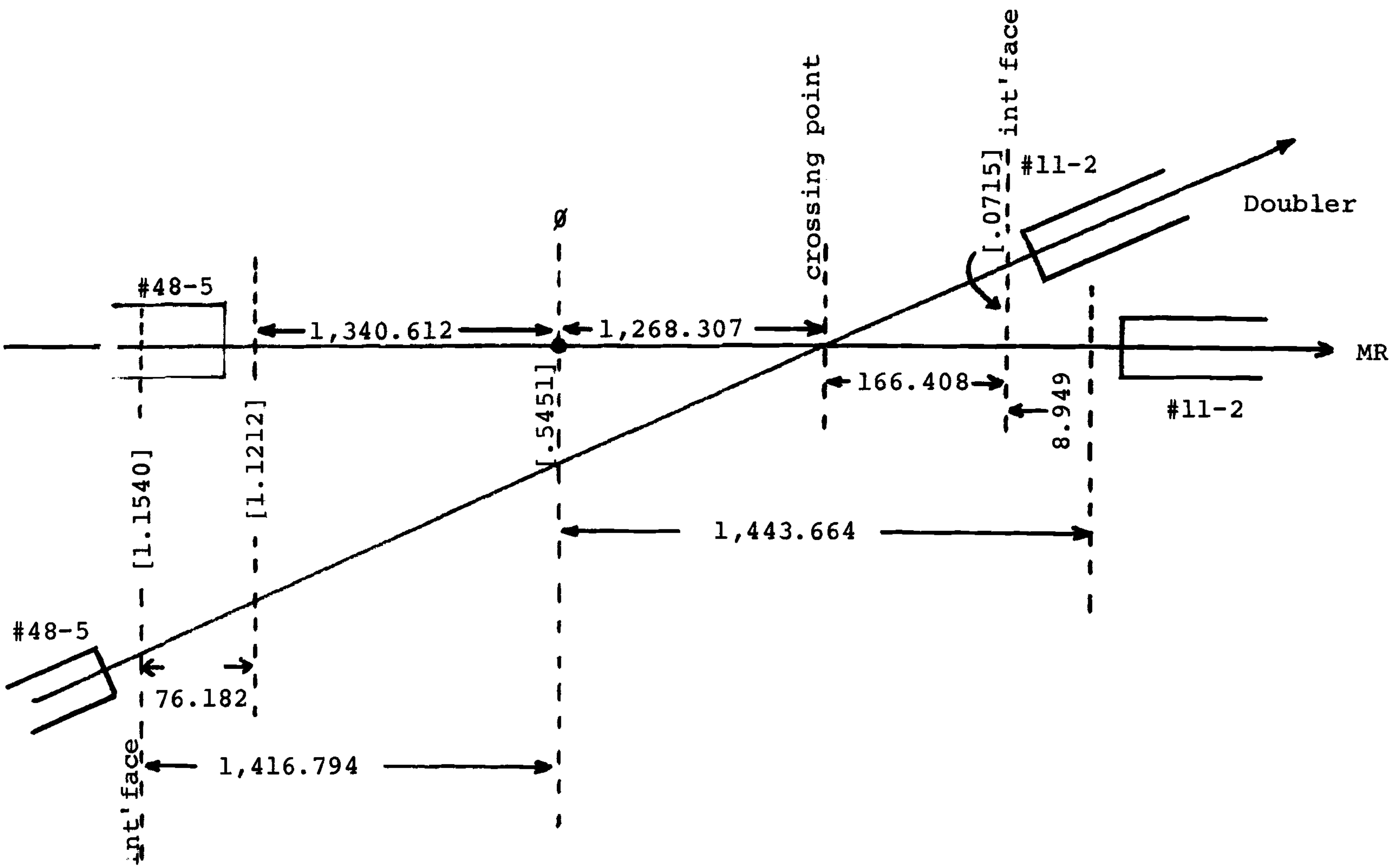

<u>Long Straight</u>, downstream of AØ and DØ
(High-Beta Insertion)

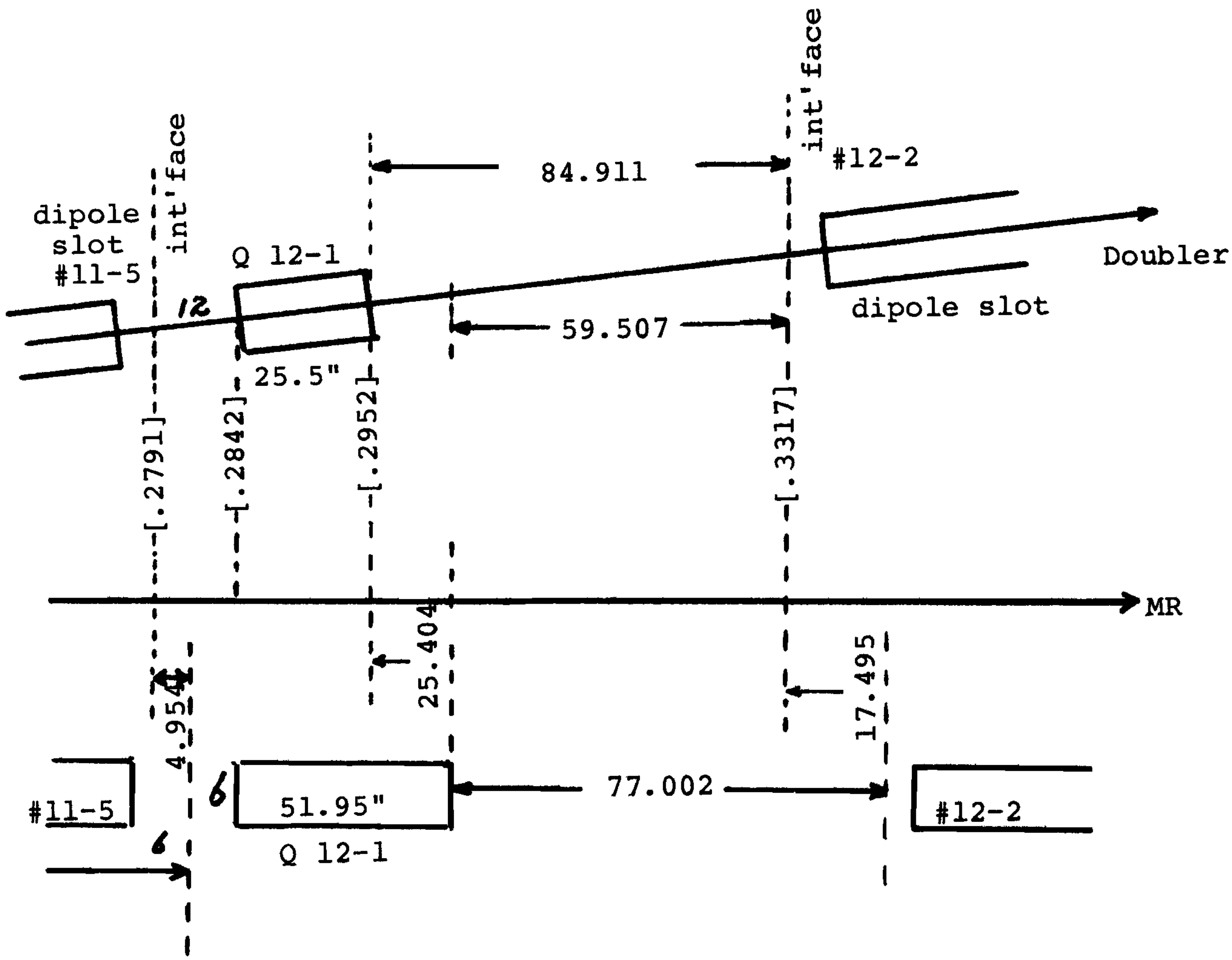

APPENDIX III. COMPUTED MAGNET DATA

The computer output reproduced on the following pages shows a variety of data on the dipole and quadrupole designs. The four pages for each type of magnet present:

1. Fields integrated throughout the magnet for a shield of infinite length.
2. Specification of dimensions for each turn in the coil.
3. Body fields.
4. Fields and flux at inner surface of iron shield.

All dimensions and fields are stated at room temperature. See drawing 1620-MB-103657A for the dipole, and drawing 1620-MB-103690A for the quadrupole.

INTEGRATED MULTIPOLE STRUCTURE OF E-SERIES DIPOLE(091878 KEYSTONED) ENDEM 041979-1030

ORDER OF POLE	= 1	CALCULATIONAL MODE	= 1	NUMBER OF LAYERS	= 3
HIGHEST MULTIPOLE ORDER	= 19	CONDUCTOR CURRENT(A)	= 4526.0000	REFERENCE RADIUS(IN)	= 1.0000
INNER IRON RADIUS(IN)	= 3.7500	HORIZONTAL INCREMENT(IN)	= .1000		

LAYER	TURNS	FAC (IN)	WIDTH (IN)	HGTMAX (IN)	HGTMIN (IN)	CURDEN (KA/IN/IN)	THETAS (DEG)	THETAF (DEG)	SPACER (IN)	RINNER (IN)	ROUTER (IN)	LENGTH (IN)	WRAP (IN)
1	35.0	0.000	.3070	.0550	.0440	297.832	.1729	72.9436	.0018148	1.5000	1.8140	239.9190	.0035
2	1.0	0.000	.3070	.0550	.0440	297.832	.1438	2.4157	.0112433	1.8350	2.1490	238.3870	.0035
3	20.0	0.000	.3070	.0550	.0440	297.832	2.4157	36.3483	.0012433	1.8350	2.1490	238.3870	.0035

MULTIPOLE COEFFICIENTS OF FIELD AT REFERENCE RADIUS

N	NET FIELD HY(KG-IN)	NET FIELD HX(KG-IN)	AIR FIELD HY(KG-IN)	AIR FIELD HX(KG-IN)	IRON CONTR. HY(KG-IN)	IRON CONTR. HX(KG-IN)	NORMALIZED FIELD HY/HY0	NORMALIZED FIELD HX/HY0
1	10907.858440	0.000000	8874.741362	0.000000	2033.127078	0.000000	1.000000	0.000000
3	.042123	0.000000	-6.568599	0.000000	6.610712	0.000000	.000004	0.000000
5	1.131406	0.000000	1.142892	0.000000	-.011486	0.000000	.000104	0.000000
7	4.838068	0.000000	4.839956	0.000000	-.001889	0.000000	.000444	0.000000
9	-13.186246	0.000000	-13.186220	0.000000	-.000026	0.000000	-.001209	0.000000
11	3.963744	0.000000	3.963744	0.000000	.000000	0.000000	.000363	0.000000
13	-.896261	0.000000	-.896261	0.000000	.000000	0.000000	-.000082	0.000000
15	.075775	0.000000	.075775	0.000000	-.000000	0.000000	.000007	0.000000
17	.034208	0.000000	.034208	0.000000	-.000000	0.000000	.000003	0.000000
19	-.047799	0.000000	-.047799	0.000000	-.000000	0.000000	-.000004	0.000000

MEDIAN PLANE FIELD VERSUS DISTANCE

X(IN)	NET FIELD HY(KG-IN)	NET FIELD HX(KG-IN)	AIR FIELD HY(KG-IN)	AIR FIELD HX(KG-IN)	IRON CONTR. HY(KG-IN)	IRON CONTR. HX(KG-IN)	NORMALIZED FIELD HY/HY0	NORMALIZED FIELD HX/HY0
.000	10907.868	0.000	8874.741	0.000	2033.127	0.000	1.000000	0.000000
.100	10907.869	0.000	8874.676	0.000	2033.193	0.000	1.000000	0.000000
.200	10907.872	0.000	8874.481	0.000	2033.391	0.000	1.000000	0.000000
.300	10907.884	0.000	8874.162	0.000	2033.722	0.000	1.000001	0.000000
.400	10907.916	0.000	8873.731	0.000	2034.184	0.000	1.000004	0.000000
.500	10907.977	0.000	8873.198	0.000	2034.779	0.000	1.000010	0.000000
.600	10908.057	0.000	8872.551	0.000	2035.505	0.000	1.000017	0.000000
.700	10908.070	0.000	8871.707	0.000	2036.363	0.000	1.000018	0.000000
.800	10907.782	0.000	8870.430	0.000	2037.353	0.000	.999992	0.000000
.900	10906.685	0.000	8868.212	0.000	2038.473	0.000	.999892	0.000000
1.000	10903.823	0.000	8864.099	0.000	2039.724	0.000	.999629	0.000000
1.100	10897.528	0.000	8856.422	0.000	2041.105	0.000	.999052	0.000000
1.200	10884.907	0.000	8842.290	0.000	2042.617	0.000	.997895	0.000000
1.300	10860.606	0.000	8816.349	0.000	2044.257	0.000	.995667	0.000000
1.400	10813.431	0.000	8767.406	0.000	2046.025	0.000	.991342	0.000000
1.500	10717.082	0.000	8669.161	0.000	2047.921	0.000	.982509	0.000000

END TO END COIL LENGTH

```
  1  OUTSIDE LENGTH(IN)=
                   245.115   244.974   244.834   244.694   244.556   244.414   244.273   244.133   243.993   243.853
                   243.713   243.572   243.432   243.292   243.152   243.012   242.871   242.731   242.591   242.451
                   242.311   242.170   242.030   241.890   241.755   241.437   241.124   240.811   240.498   240.185
                   239.872   239.559   239.246   238.933   238.620
  1  INSIDE LENGTH(IN) =
                   244.994   244.854   244.714   244.574   244.434   244.293   244.153   244.013   243.873   243.733
                   243.592   243.452   243.312   243.172   243.032   242.891   242.751   242.611   242.471   242.331
                   242.190   242.050   241.910   241.770   241.630   241.317   241.004   240.691   240.379   240.065
                   239.752   239.439   239.126   238.813   238.500
  2  OUTSIDE LENGTH(IN)=
                   244.635
  2  INSIDE LENGTH(IN) =
                   244.477
  3  OUTSIDE LENGTH(IN)=
                   244.477   244.325   244.173   244.022   243.870   243.718   243.566   243.414   243.262   243.110
                   242.959   242.807   242.655   242.503   242.351   242.199   242.047   241.895   241.744   241.592
  3  INSIDE LENGTH(IN) =
                   244.359   244.207   244.055   243.904   243.752   243.600   243.448   243.295   243.144   242.992
                   242.841   242.689   242.537   242.385   242.233   242.081   241.929   241.778   241.626   241.474
```

RADIAL DISTANCES IN DEVELOPED COIL

```
  1  OUTSIDE RADIUS(IN)=
                    2.5978    2.5377    2.4776    2.4174    2.3573    2.2972    2.2370    2.1769    2.1168    2.0566
                    1.9965    1.9364    1.8763    1.8161    1.7560    1.6959    1.6357    1.5756    1.5155    1.4553
                    1.3952    1.3351    1.2750    1.2148    1.1547    1.0946    1.0344     .9743     .9142     .8541
                     .7939     .7338     .6737     .6135     .5534
  1  INSIDE RADIUS(IN) =
                    2.5377    2.4776    2.4174    2.3573    2.2972    2.2370    2.1769    2.1168    2.0566    1.9965
                    1.9364    1.8763    1.8161    1.7560    1.6959    1.6357    1.5756    1.5155    1.4553    1.3952
                    1.3351    1.2750    1.2148    1.1547    1.0946    1.0344     .9743     .9142     .8541     .7939
                     .7338     .6737     .6135     .5534     .4933
  2  OUTSIDE RADIUS(IN)=
                    3.1240
  2  INSIDE RADIUS(IN) =
                    3.0450
  3  OUTSIDE RADIUS(IN)=
                    3.0450    2.9861    2.9271    2.8681    2.8091    2.7501    2.6911    2.6321    2.5731    2.5142
                    2.4552    2.3952    2.3372    2.2782    2.2192    2.1602    2.1013    2.0423    1.9833    1.9243
  3  INSIDE RADIUS(IN) =
                    2.9861    2.9271    2.8681    2.8091    2.7501    2.6911    2.6321    2.5731    2.5142    2.4552
                    2.3962    2.3372    2.2782    2.2192    2.1502    2.1013    2.0423    1.9833    1.9243    1.8653
```

INTEGRATED MULTIPOLE STRUCTURE OF E-SERIES DIPOLE(091878 KEYSTONED) ENDEM 041979-1030

ORDER OF POLE	= 1	CALCULATIONAL MODE	= 0	NUMBER OF LAYERS	= 3
HIGHEST MULTIPOLE ORDER	= 19	CONDUCTOR CURRENT(A)	= 4526.0000	REFERENCE RADIUS(IN)	= 1.0000
INNER IRON RADIUS(IN)	= 3.7500	HORIZONTAL INCREMENT(IN)	= .1000		

LAYER	TURNS	FBC (IN)	WIDTH (IN)	HGTMAX (IN)	HGTMIN (IN)	CURDEN (KA/IN/IN)	THETAS (DEG)	THETAF (DEG)	SPACER (IN)	RINNER (IN)	ROUTER (IN)	LENGTH (IN)	WRAP (IN)
1	35.0	0.000	.3070	.0550	.0440	297.832	.1729	72.9435	.0018148	1.5000	1.8140	1.0000	.0035
2	1.0	0.000	.3070	.0550	.0440	297.832	.1438	2.4157	.0112433	1.8350	2.1490	1.0000	.0035
3	20.0	0.000	.3070	.0550	.0440	297.832	2.4157	36.3483	.0012433	1.8350	2.1490	1.0000	.0035

MULTIPOLE COEFFICIENTS OF FIELD AT REFERENCE RADIUS

N	NET FIELD HY(KG-IN)	NET FIELD HX(KG-IN)	AIR FIELD HY(KG-IN)	AIR FIELD HX(KG-IN)	IRON CONTR. HY(KG-IN)	IRON CONTR. HX(KG-IN)	NORMALIZED FIELD HY/HYO	NORMALIZED FIELD HX/HYO
1	45.001719	0.000000	36.613812	0.000000	8.387907	0.000000	1.000000	0.000000
3	.035119	0.000000	.007083	0.000000	.028035	0.000000	.000780	0.000000
5	.014433	0.000000	.014478	0.000000	-.000040	0.000000	.000321	0.000000
7	.021176	0.000000	.021184	0.000000	-.000008	0.000000	.000471	0.000000
9	-.055024	0.000000	-.055023	0.000000	-.000000	0.000000	-.001223	0.000000
11	.016757	0.000000	.016757	0.000000	.000000	0.000000	.000372	0.000000
13	-.003746	0.000000	-.003746	0.000000	.000000	0.000000	-.000083	0.000000
15	.000326	0.000000	.000326	0.000000	-.000000	0.000000	.000007	0.000000
17	.000147	0.000000	.000147	0.000000	-.000000	0.000000	.000003	0.000000
19	-.000200	0.000000	-.000200	0.000000	-.000000	0.000000	-.000004	0.000000

MEDIAN PLANE FIELD VERSUS DISTANCE

X(IN)	NET FIELD HY(KG-IN)	NET FIELD HX(KG-IN)	AIR FIELD HY(KG-IN)	AIR FIELD HX(KG-IN)	IRON CONTR. HY(KG-IN)	IRON CONTR. HX(KG-IN)	NORMALIZED FIELD HY/HYO	NORMALIZED FIELD HX/HYO
.000	45.002	0.000	36.614	0.000	8.388	0.000	1.000000	0.000000
.100	45.002	0.000	36.614	0.000	8.388	0.000	1.000008	0.000000
.200	45.003	0.000	36.614	0.000	8.389	0.000	1.000032	0.000000
.300	45.005	0.000	36.615	0.000	8.390	0.000	1.000073	0.000000
.400	45.008	0.000	36.615	0.000	8.392	0.000	1.000134	0.000000
.500	45.012	0.000	36.617	0.000	8.395	0.000	1.000218	0.000000
.600	45.016	0.000	36.618	0.000	8.398	0.000	1.000326	0.000000
.700	45.022	0.000	36.621	0.000	8.402	0.000	1.000454	0.000000
.800	45.028	0.000	36.622	0.000	8.406	0.000	1.000584	0.000000
.900	45.032	0.000	36.621	0.000	8.411	0.000	1.000674	0.000000
1.000	45.031	0.000	36.615	0.000	8.416	0.000	1.000644	0.000000
1.100	45.017	0.000	36.596	0.000	8.422	0.000	1.000349	0.000000
1.200	44.981	0.000	36.553	0.000	8.428	0.000	.999535	0.000000
1.300	44.900	0.000	36.464	0.000	8.435	0.000	.997730	0.000000
1.400	44.729	0.000	36.286	0.000	8.443	0.000	.993933	0.000000
1.500	44.362	0.000	35.911	0.000	8.451	0.000	.985774	0.000000

MAX. FIELD ON IRON(KG) = 16.0055 FLUX IN IRON(KG-IN) = 63.8569

FIELD AND FLUX ON INNER IRON SURFACE

ANGLE(RAD)	BN(KG)	FLUX(KG-IN)
0.00000	0.00000	0.00000
.03491	.65274	.04273
.06981	1.30472	.17085
.10472	1.95514	.38423
.13963	2.60312	.68250
.17453	3.24770	1.06558
.20944	3.88775	1.53265
.24435	4.52203	2.08314
.27925	5.14914	2.71620
.31416	5.76756	3.43090
.34907	6.37561	4.22559
.38397	6.97154	5.09940
.41888	7.55355	6.05023
.45379	8.11990	7.07623
.48869	8.66953	8.17522
.52360	9.19808	9.34431
.55851	9.70698	10.58237
.59341	10.19401	11.88513
.62832	10.65823	13.25016
.66323	11.09903	14.67443
.69813	11.51617	16.15495
.73304	11.90970	17.68932
.76794	12.28000	19.27179
.80285	12.62768	20.90223
.83776	12.95334	22.57675
.87266	13.25951	24.29255
.90757	13.54356	26.04695
.94248	13.80953	27.83742
.97738	14.05790	29.66153
1.01229	14.29876	31.51699
1.04720	14.50331	33.40160
1.08210	14.70209	35.31326
1.11701	14.88563	37.24974
1.15192	15.05437	39.20967
1.18682	15.20865	41.19053
1.22173	15.34874	43.19056
1.25664	15.47497	45.20822
1.29154	15.58723	47.24137
1.32645	15.68596	49.28835
1.36136	15.77121	51.34736
1.39626	15.84310	53.41666
1.43117	15.90174	55.49450
1.46608	15.94724	57.57915
1.50098	15.97967	59.66370
1.53589	15.99910	61.76205
1.57080	16.00557	63.85699

INTEGRATED MULTIPOLE STRUCTURE OF 2-SHELL SECTOR QUAD(100577 WIRE) ENDEM 042179-1345

ORDER OF POLE	= 2	CALCULATIONAL MODE	= 1	NUMBER OF LAYERS	= 4
HIGHEST MULTIPOLE ORDER	= 26	CONDUCTOR CURRENT(A)	= 4526.0000	REFERENCE RADIUS(IN)	= 1.0000
INNER IRON RADIUS(IN)	= 4.0000	HORIZONTAL INCREMENT(IN)	= .1000		

LAYER	TURNS	FBC (IN)	WIDTH (IN)	HGTMAX (IN)	HGTMIN (IN)	CURDEN (KA/IN/IN)	THETAS (DEG)	THETAF (DEG)	SPACER (IN)	RINNER (IN)	ROUTER (IN)	LENGTH (IN)	WRAP (IN)
1	8.0	0.000	.3070	.0550	.0440	297.832	.1501	14.4403	0.0000000	1.7500	2.0670	64.8390	.0050
2	6.0	0.000	.3070	.0550	.0440	297.832	19.4018	30.1194	0.0000000	1.7500	2.0570	65.1440	.0050
3	1.0	0.000	.3070	.0550	.0440	297.832	.1275	1.9511	.0060000	2.0880	2.4050	64.5770	.0050
4	19.0	0.000	.3070	.0550	.0440	297.832	1.9511	30.7839	0.0000000	2.0880	2.4050	64.5770	.0050

MULTIPOLE COEFFICIENTS OF FIELD AT REFERENCE RADIUS

	NET FIELD		AIR FIELD		IRON CONTR.		NORMALIZED FIELD	
N	HY(KG-IN)	HX(KG-IN)	HY(KG-IN)	HX(KG-IN)	HY(KG-IN)	HX(KG-IN)	HY/XGYO	HX/XGYO
2	1307.840989	0.000000	1215.330666	0.000000	92.510322	0.000000	1.000000	0.000000
6	-.034810	0.000000	-.033659	0.000000	-.001151	0.000000	-.000027	0.000000
10	-.270267	0.000000	-.270265	0.000000	-.000002	0.000000	-.000207	0.000000
14	.093808	0.000000	.093808	0.000000	.000000	0.000000	.000072	0.000000
18	-.003726	0.000000	-.003725	0.000000	-.000000	0.000000	-.000003	0.000000
22	-.000734	0.000000	-.000734	0.000000	-.000000	0.000000	-.000001	0.000000
26	.000011	0.000000	.000011	0.000000	.000000	0.000000	.000000	0.000000

MEDIAN PLANE FIELD VERSUS DISTANCE

	NET FIELD		AIR FIELD		IRON CONTR.		NORMALIZED FIELD	
X(IN)	HY(KG-IN)	HX(KG-IN)	HY(KG-IN)	HX(KG-IN)	HY(KG-IN)	HX(KG-IN)	HY/XGYO	HX/XGYO
.000	.000	0.000	.000	0.000	.000	0.000	1.000000	0.000000
.100	130.784	0.000	121.533	0.000	9.251	0.000	1.000000	0.000000
.200	261.568	0.000	243.066	0.000	18.502	0.000	1.000000	0.000000
.300	392.352	0.000	364.599	0.000	27.753	0.000	1.000000	0.000000
.400	523.136	0.000	486.132	0.000	37.004	0.000	.999999	0.000000
.500	653.919	0.000	607.664	0.000	46.255	0.000	.999998	0.000000
.600	784.699	0.000	729.193	0.000	55.506	0.000	.999993	0.000000
.700	915.473	0.000	850.716	0.000	64.757	0.000	.999983	0.000000
.800	1046.230	0.000	972.222	0.000	74.008	0.000	.999959	0.000000
.900	1176.955	0.000	1093.696	0.000	83.259	0.000	.999913	0.000000
1.000	1307.625	0.000	1215.116	0.000	92.509	0.000	.999835	0.000000
1.100	1438.231	0.000	1336.472	0.000	101.759	0.000	.999726	0.000000
1.200	1568.816	0.000	1457.807	0.000	111.010	0.000	.999622	0.000000
1.300	1699.544	0.000	1579.284	0.000	120.259	0.000	.999618	0.000000
1.400	1830.707	0.000	1701.199	0.000	129.508	0.000	.999852	0.000000
1.500	1962.318	0.000	1823.561	0.000	138.757	0.000	1.000283	0.000000
1.600	2092.092	0.000	1944.087	0.000	148.004	0.000	.999783	0.000000
1.700	2208.667	0.000	2051.416	0.000	157.251	0.000	.993405	0.000000

```
                                        END TO END COIL LENGTH
 1  OUTSIDE LENGTH(IN)=
                       67.827    67.703    67.580    67.457    67.333    67.210    67.086    66.963
 1  INSIDE LENGTH(IN) =
                       67.708    67.594    67.461    67.338    67.214    67.091    66.967    66.844
 2  OUTSIDE LENGTH(IN)=
                       66.849    66.550    66.251    65.952    65.653    65.354
 2  INSIDE LENGTH(IN) =
                       66.730    66.431    65.132    65.833    65.534    65.235
 3  OUTSIDE LENGTH(IN)=
                       68.096
 3  INSIDE LENGTH(IN) =
                       67.953
 4  OUTSIDE LENGTH(IN)=
                       67.953    67.809    67.664    67.520    67.376    67.232    67.088    66.943    66.799    66.655
                       66.511    66.367    66.222    66.078    65.779    65.480    65.181    64.882    64.583
 4  INSIDE LENGTH(IN) =
                       67.834    67.690    67.545    67.401    67.257    67.113    66.969    66.824    66.680    66.536
                       65.392    66.248    65.103    65.959    65.560    65.361    65.062    64.763    54.464


                                        RADIAL DISTANCES IN DEVELOPED COIL
 1  OUTSIDE RADIUS(IN)=
                       1.4939    1.4344    1.3749    1.3154    1.2559    1.1964    1.1369    1.0774
 1  INSIDE RADIUS(IN) =
                       1.4344    1.3749    1.3154    1.2559    1.1964    1.1369    1.0774    1.0179
 2  OUTSIDE RADIUS(IN)=
                        .8527     .7932     .7337     .6742     .6147     .5552
 2  INSIDE RADIUS(IN) =
                        .7932     .7337     .6742     .6147     .5552     .4957
 3  OUTSIDE RADIUS(IN)=
                       1.7594
 3  INSIDE RADIUS(IN) =
                       1.6879
 4  OUTSIDE RADIUS(IN)=
                       1.6879    1.6284    1.5689    1.5094    1.4499    1.3904    1.3309    1.2714    1.2119    1.1524
                       1.0929    1.0334     .9739     .9144     .8549     .7954     .7359     .6764     .6169
 4  INSIDE RADIUS(IN) =
                       1.6284    1.5689    1.5094    1.4499    1.3904    1.3309    1.2714    1.2119    1.1524    1.0929
                       1.0334     .9739     .9144     .8549     .7954     .7359     .6764     .6169     .5574
```

INTEGRATED MULTIPOLE STRUCTURE OF 2-SHELL SECTOR QUAD(100577 WIRE) ENDEM 042/79-1345

ORDER OF POLE	=	2	CALCULATIONAL MODE	=	0	NUMBER OF LAYERS	= 4
HIGHEST MULTIPOLE ORDER	=	26	CONDUCTOR CURRENT(A)	=	4526.0000	REFERENCE RADIUS(IN)	= 1.0000
INNER IRON RADIUS(IN)	=	4.0000	HORIZONTAL INCREMENT(IN)	=	.1000		

LAYER	TURNS	FBC (IN)	WIDTH (IN)	HGTMAX (IN)	HGTMIN (IN)	CURDEN (KA/IN/IN)	THETAS (DEG)	THETAF (DEG)	SPACER (IN)	RINNER (IN)	ROUTER (IN)	LENGTH (IN)	WRAP (IN)
1	8.0	0.000	.3070	.0550	.0440	297.832	.1501	14.4403	0.0000000	1.7500	2.0670	1.0000	.0050
2	6.0	0.000	.3070	.0550	.0440	297.832	19.4018	30.1194	0.0000000	1.7500	2.0670	1.0000	.0050
3	1.0	0.000	.3070	.0550	.0440	297.832	.1275	1.9511	.0060000	2.0880	2.4050	1.0000	.0050
4	19.0	0.000	.3070	.0550	.0440	297.832	1.9511	30.7839	0.0000000	2.0880	2.4050	1.0000	.0050

MULTIPOLE COEFFICIENTS OF FIELD AT REFERENCE RADIUS

	NET FIELD		AIR FIELD		IRON CONTR.		NORMALIZED FIELD	
N	HY(KG-IN)	HX(KG-IN)	HY(KG-IN)	HX(KG-IN)	HY(KG-IN)	HX(KG-IN)	HY/XGYO	HX/XGYO
2	19.672351	0.000000	18.280039	0.000000	1.392263	0.000000	1.000000	0.000000
6	.006082	0.000000	.006097	0.000000	-.000015	0.000000	.000309	0.000000
10	-.003950	0.000000	-.003950	0.000000	-.000000	0.000000	-.000201	0.000000
14	.001458	0.000000	.001458	0.000000	.000000	0.000000	.000074	0.000000
18	-.000056	0.000000	-.000056	0.000000	-.000000	0.000000	-.000003	0.000000
22	-.000011	0.000000	-.000011	0.000000	-.000000	0.000000	-.000001	0.000000
26	.000000	0.000000	.000000	0.000000	.000000	0.000000	.000000	0.000000

MEDIAN PLANE FIELD VERSUS DISTANCE

	NET FIELD		AIR FIELD		IRON CONTR.		NORMALIZED FIELD	
X(IN)	HY(KG-IN)	HX(KG-IN)	HY(KG-IN)	HX(KG-IN)	HY(KG-IN)	HX(KG-IN)	HY/XGYO	HX/XGYO
.000	.000	0.000	.000	0.000	.000	0.000	1.000000	0.000000
.100	1.967	0.000	1.828	0.000	.139	0.000	1.000000	0.000000
.200	3.934	0.000	3.656	0.000	.278	0.000	1.000000	0.000000
.300	5.902	0.000	5.484	0.000	.418	0.000	1.000002	0.000000
.400	7.869	0.000	7.312	0.000	.557	0.000	1.000008	0.000000
.500	9.836	0.000	9.140	0.000	.696	0.000	1.000019	0.000000
.600	11.804	0.000	10.968	0.000	.835	0.000	1.000037	0.000000
.700	13.772	0.000	12.797	0.000	.975	0.000	1.000064	0.000000
.800	15.739	0.000	14.626	0.000	1.114	0.000	1.000098	0.000000
.900	17.708	0.000	16.455	0.000	1.253	0.000	1.000137	0.000000
1.000	19.676	0.000	18.284	0.000	1.392	0.000	1.000179	0.000000
1.100	21.645	0.000	20.113	0.000	1.531	0.000	1.000238	0.000000
1.200	23.615	0.000	21.945	0.000	1.671	0.000	1.000354	0.000000
1.300	25.591	0.000	23.782	0.000	1.810	0.000	1.000678	0.000000
1.400	27.579	0.000	25.630	0.000	1.949	0.000	1.001355	0.000000
1.500	29.580	0.000	27.491	0.000	2.088	0.000	1.002413	0.000000
1.600	31.564	0.000	29.337	0.000	2.227	0.000	1.002810	0.000000
1.700	33.367	0.000	31.000	0.000	2.367	0.000	.997721	0.000000

MAX. FIELD ON IRON(KG) = 11.1507 FLUX IN IRON(KG-IN) = 22.2502

FIELD AND FLUX ON INNER IRON SURFACE

ANGLE(RAD)	BN(KG)	FLUX(KG-IN)
0.00000	0.00000	0.00000
.01745	.38312	.01337
.03491	.76537	.05349
.05236	1.14787	.12029
.06981	1.52875	.21373
.08727	1.90812	.33371
.10472	2.28560	.48011
.12217	2.66030	.65279
.13963	3.03331	.85157
.15708	3.40274	1.07625
.17453	3.75866	1.32660
.19199	4.13064	1.60236
.20944	4.48826	1.90324
.22689	4.84103	2.22833
.24435	5.18863	2.57906
.26180	5.53047	2.95325
.27925	5.86613	3.35112
.29671	6.19514	3.77218
.31416	6.51724	4.21575
.33161	6.83134	4.68195
.34907	7.13759	5.16960
.36652	7.43532	5.67835
.38397	7.72406	6.20755
.40143	8.00338	6.75661
.41888	8.27234	7.32492
.43633	8.53203	7.91148
.45379	8.73054	8.51535
.47124	9.01802	9.13722
.48869	9.24411	9.77475
.50615	9.45851	10.42766
.52360	9.66091	11.09513
.54105	9.85107	11.77630
.55851	10.02876	12.47031
.57596	10.19379	13.17628
.59341	10.34597	13.89333
.61087	10.48524	14.62055
.62832	10.61142	15.35704
.64577	10.72445	16.10199
.66323	10.82426	16.85415
.68068	10.91082	17.61292
.69813	10.98410	18.37728
.71558	11.04405	19.14628
.73304	11.09070	19.91901
.75049	11.12402	20.69453
.76794	11.14402	21.47191
.78540	11.15068	22.25022

☆ U.S. GOVERNMENT PRINTING OFFICE: 1979—652-104

Tooling, Joslien, Carl Koepke, Don Edwards, Sho Ohnuma,
Mike Harrison, Al Russel, Frank Cole, Bob Shafer

Larry Sauer Eng.

Will Hanson - Conv. magnets